PETROLOGICAL STUDIES OF DEVONIAN ROCKS IN SCOTLAND AND CRETACEOUS ROCKS IN CANADA

Girish C. Saigal

A Thesis Submitted for the Degree of PhD
at the
University of St Andrews

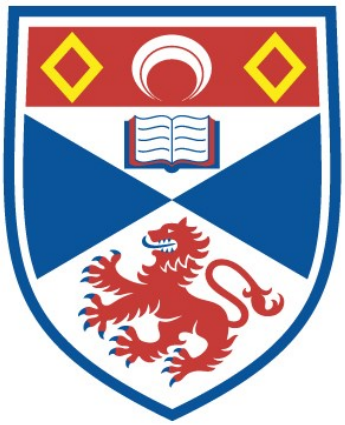

1985

PETROLOGICAL STUDIES OF DEVONIAN ROCKS IN SCOTLAND AND CRETACEOUS ROCKS IN CANADA

A dissertation submitted for the degree of Ph.D. at the University of St Andrews, February 1985.

Girish C. Saigal

ProQuest LLC.
789 East Eisenhower Parkway
P.O. Box 1346
Ann Arbor, MI 48106 – 1346

A267

UNIVERSITY OF ST. ANDREWS

Thesis Copyright Declaration Form.

A UNRESTRICTED

"In submitting this thesis to the University of St. Andrews I understand that I am giving permission for it to be made available for public use in accordance with the regulations of the University Library for the time being in force, subject to any copyright vested in the work not being affected thereby. I also understand that the title and abstract will be published, and that a copy of the work may be made and supplied to any bona fide library or research worker."

B RESTRICTED

"In submitting this thesis to the University of St. Andrews I wish access to it to be subject to the following conditions:

for a period of TWO years [maximum 5] from the date of submission the thesis shall be

~~a)~~ withheld from public use.

b) made available for public use only with consent of the head or chairman of the department in which the work was carried out.

I understand, however, that the title and abstract of the thesis will be published during this period of restricted access; and that after the expiry of this period the thesis will be made available for public use in accordance with the regulations of the University Library for the time being in force, subject to any copyright in the work not being affected thereby, and a copy of the work may be made and supplied to any bona fide library or research worker."

Declaration

I wish to exercise option Ba [i.e. A, Ba or Bb] of the above options.

Signature

Date 9th April 198

ACKNOWLEDGEMENTS

I take this opportunity to express my gratitude to Professor E.K. Walton, my supervisor for his suggestions, and encouragement and critial reveiw of the manuscript.

Open discussions with my wife, Dr Neeta Saigal on this project was a constant source of ideas and criticisms: I am grateful to her for her patience and encouragement throught this study.

It is my pleasure to record sincere appreciation for my parents and other family members for their constant encouragement throughout my studies.

Thanks are also due to the technical staff at St Andrews, particularly Jim Allan, Andy Mackie and Sandy Edwards for their efforts over the last three years. I am also thankful to Mrs J. Galloway for general help.

I also express my gratitude to every member of this department for their help and co-operation during the day-to-day work.

Sincere thanks are due to Dr M.S. Shawa for supplying core samples, Dr P.J. Hill of the Grant Institute of Geology, Edinburgh, for electron microprobe analyses and Dr A.E. Fallick, S.U.R.R.C., East Kilbride, for stable isotope analyses.

I owe a special thanks to Dr D.M. Banerjee, Delhi University, India for his constant encouragement throughout my studies.

I gratefully acknowledge the receipt of an Overseas Research Grant and Research Fellowships from St Andrews University, the Continental Oil Company and the Leckie Trust. I thank Marry for typing the manuscript.

CERTIFICATE

I herby certify that GIRISH C. SAIGAL has been engaged in research for nine terms at the University of St Andrews, that he has fulfilled the conditions of Ordinance No 12 and resolution of the University Court, 1967, No 1, and that he is qualified to submit the accompanying thesis in application for the degree of Doctor of Philosophy.

I certify that the following thesis is of my own composition, that it is based on the results of research carried out by me, and that it has not previously been presented in application for a higher degree.

ABSTRACT

Sedimentological, petrological and geochemical studies have been carried out to analyse the process of calcretization and to understand the influence of environment of deposition on sandstone diagenesis. The sediments examined come from Lower Old Red Sandstones (Lr. Devonian) of eastern Scotland and hydrocarbon bearing Viking, Cardium and Belly River Formations (Cretaceous) of southcentral Canada.

Some scepticism has been expressed regarding the occurrence of displacive calcite but this type of growth has been found in the calcrete profiles in Lower Old Red Sandstones of Carnoustie, east Scotland. This thesis presents fresh petrographic evidence of expansion and isolation of clastic grains by growing calcite crystals. The morphology of calcite crystals observed under cathodoluminescence provide compelling evidence that they are not a passive pore filling cement but have grown in confined spaces from supersaturated solutions by displacing the constraining medium. Field relationships suggest that the calcite was generated within the vadose zone where crystallization was promoted by rapid surface evaporation leading to supersaturation. A two-water model based on petrological and geochemical criteria has been suggested to explain the mechanism of growth of displacive calcite crystals (Chapter - IV). The recognition of displacive calcite is highly significant as it offers insight into paleoclimatic conditions and diagenetic

history.

Crystal morphologies observed under cathodoluminescence and microprobe data suggests that the displacive calcite was originally low Mg-calcite and grew from rapidly evaporating fresh pore waters with extremely low Mg/Ca ratios. The growth of originally low Mg-calcite and absence of palygorskite, sepiolite and dolomite in the Carnoustie calcretes is considered significant and it has been emphasized that no one process applies to all calcretes and the chemistry of pore waters and micro-environmental conditions within the pores are major significant factors controlling process of calcretization.

The comparisons drawn between the diagenetic products observed in the Lower Old Red Sandstone and the Viking, Cardium and Belly River Formations suggest that the detrital mineralogy and aqueous solutions migrating through the pore system of sandstones are the two major factors that accomplish all the complex chemical reactions during diagenesis. In general, the Viking, Cardium and Belly River sediments show large variations in their pre-burial early diagenetic histories within small areas (even between adjoining wells) while the Lr. Old Red Sandstone show a monotonous paragenetic sequence over the entire area. This is compatible with the expected variations in the pore-fluid chemistry and micro-environmental conditions within the pores deduced from the depositional environments of these sediments. Hence it has been concluded that the pre-burial early diagenetic processes and products in clastic sediments are controlled by their environment of deposition which subsequently could influence the course of late stage diagenesis as well.

CONTENTS

Page

LIST OF FIGURES

LIST OF TABLES

LIST OF APPENDICES

CHAPTER I

1.1 Introduction and Aims of Study

Diagenesis of sandstones is of fundamental importance to the petroleum industry and has been attracting an ever-increasing amount of attention in recent years. It is particularly important to locate and exploit subtle diagenetically controlled stratigraphic traps and reservoirs as they are the prospects of the future. Detailed information of the textural and mineralogical modification is essential to predict the regional diagenetic response, which partly controls hydrocarbon recovery programmes. Significant contributions have been made in the field of sandstone diagenesis in last few years primarily due to improvements in laboratory instrumentation and the search for petroleum (See eg. Scholle and Schluger, 1979; Parker and Sellwood, 1983 and McDonald and Surdam, 1984).

Diagenesis is also important from a purely academic point of view as it includes all processes that start operating immediately from the time of sediment deposition and lasting until the resulting rock moves into the realm of metamorphism. Sedimentologists have studied diagenesis in sediments from many different view points and regard it as a very complex field which has great potential for future research. Although all the controls on diagenesis are not yet fully known and understood, a few important ones that are believed to programme the course of sandstone diagenesis to a degree are:

1) Tectonic setting

2) Provenance and

3) Depositional Environment

To understand the influence of these factors, diagenetic studies were carried out on sandstones of different depositional environment, composition, age and geographic distribution. The sediments examined come from Lower Old Red Sandstones (Lr. Devonian) of eastern Scotland and hydrocarbon bearing Viking, Cardium and Belly River Formations (Cretaceous) of southcentral Canada.

Another objective of the present studies was to understand the process of calcretization and its influence on later diagenesis as calcretes with displacive growth of calcite were found in the Lower Old Red Sandstones during present studies.

1.2 Approach

In view of the above objectives an integrated sedimentological, petrological, mineralogical and geochemical approach was applied to understand the diagenesis and process of calcretization in the Lower Old Red Sandstones. The diagenetic histories of the Viking, Cardium and Belly River Formations were built up from the data obtained by thin section and SEM examinations.

1.3 Techniques

Various techniques used during present investigations include SEM, microprobe, cathodoluminescence and mass spectrometery in addition to standard petrographic techniques. Out of these, the emphasis was on the SEM studies as it provides sigificant information on the mineralogical and textual modifications which occurred during diagenesis. In particular, the SEM studies were carried out to gather information on the clay minerals which otherwise cannot be studied under ordinary optical microscope.

1.4 Areas of investigation

The Lower Old Red Sandstone described in this thesis are exposed on the east coast of Scotland. The area extends for approximately 10 km between Arbroath in the northeast and Carnoustie in the southwest (Fig 1.1). This region lies within the sheet no. 49 (Arbroath) of the one inch geological map of Scotland.

The specimens representing Viking, Cardium and Belly River Formations come from wells located in southcentral Alberta (Canada), directly adjacent to the foothills. The area extends from Township 31 through to Township 46 and from Range 25 west of the 4th Meridian to the disturbed belt on the west side. It covers a surface area of approximately 13,478 sq. km. (Fig. 1.2).

1.5 Stratigraphy and tectonic setting of the Lower Old Red Sandstone

According to the stratigraphical classification set up by Armstrong and Paterson (1970), the sediments described in this thesis lie within the 1525 m thick Garvock Group, towards the top of Lower Old Red Sandstone and are approximately Siegenian in age (Table 1.1). These sediments are composed largely of sandstone formations and represent the southeastern limb of Sidlaw Anticline (Fig. 1.1). The oldest subdivision of the Lower Old Red Sandstone (the Stonehaven Group) lies unconformably on Cambro-Ordovician rocks and is considered to be Infra-Gedinnian (topmost Silurian) in age (Mykura, 1983). On the basis of Rb-Sr dating of lavas (Arbuthnott Group), Thirlwall (1981 and 1983) suggested that a substantial part of the Lr. Old Red Sandstone could be of Silurian age. Westoll (1977), considering the spore content of the youngest subdivision (Strathmore Group), ascribed a middle Emsian age whereas plant remains such as *Psilophyton princeps*, *P. goldschmidti* and *Arthrostigma gracile* suggest a late Siegenian date (Mykura, 1983). The Strathmore Group is overlain unconformably by Upper Old Red Sandstone.

The Lower Old Red Sandstone comprising approximately 9.5 km (Armstrong and Paterson, 1970) thick sequence of red beds were deposited during the Caledonian orogenic cycle as continental facies. It is a conglomerate-litharenite assemblage, partly interstratified with acid to basic volcanic rocks. The sediments examined were deposited in Strathmore basin which was filled longitudinally from the northeast and had its axis parallel to the Highland Boundary Fault (Fig. 1.1). Conglomerates were deposited in aprons of coalescing fans (bajada) along active fault escarpments at or close to the Highland Boundary faults

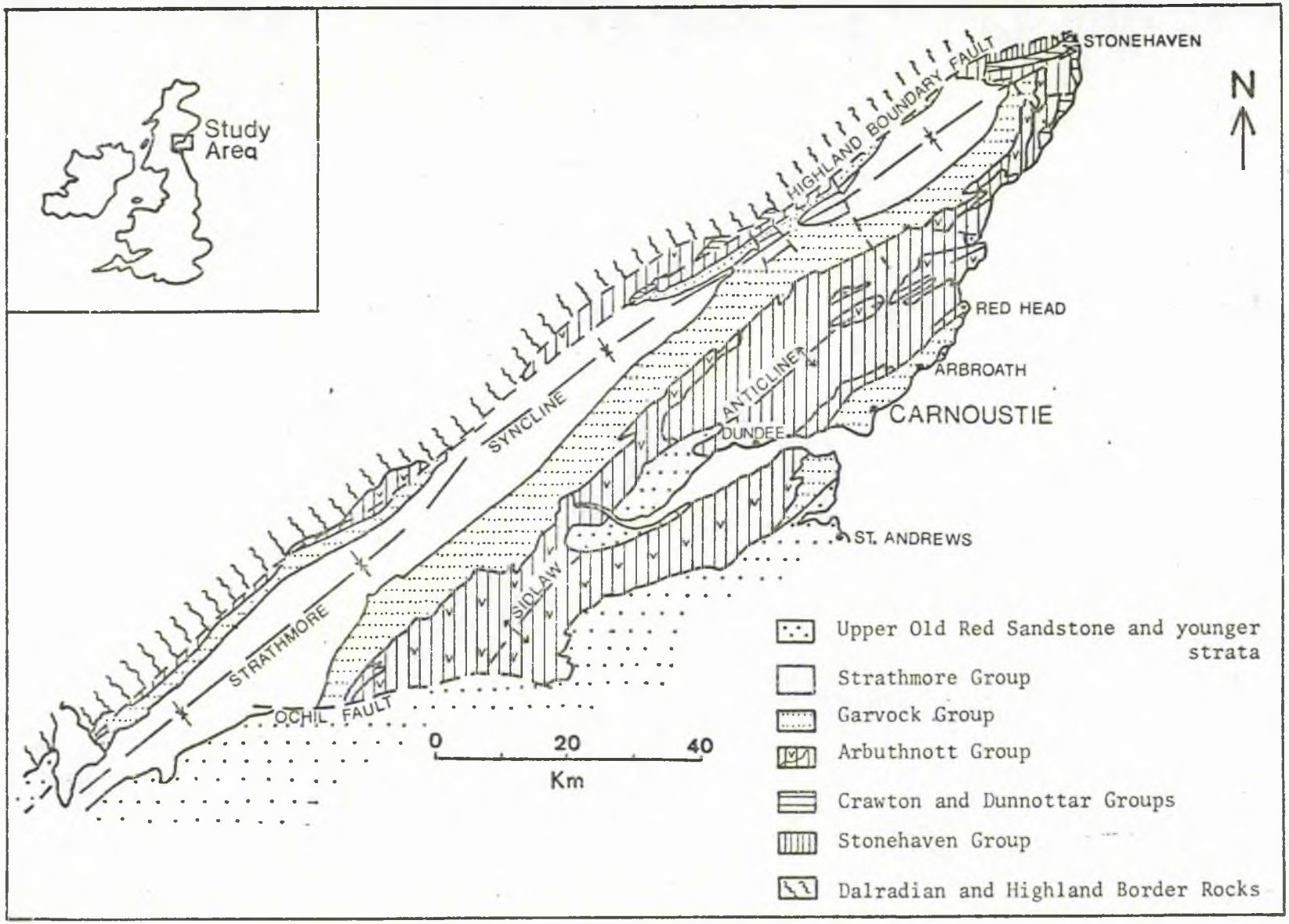

Fig. 1.1 Location and sketch map of the Lower Old Red Sandstone of the Strathmore basin (after Armstrong and Paterson, 1970).

Table 1.1 Lower Old Red Sandstone of the Strathmore region (after Armstrong and Paterson, 1970 and Mykura, 1983).

Major Divisions	Lithology	Probable Stages and Chrono-stratigraphy
Strathmore Group (2000 m)	Mudstone, sandstone, conglomerate	Emsian
		373 m y
Garvock Group (1525 m)	Sandstone, conglomerate, shale, lava	Siegenian
Arbuthnott Group (2100 m)	Sandstone, shale and flagstone, conglomerate, lava, pyroclastic rocks	388 m y
Crawton Group (670 m)	Conglomerate, sandstone, lava, ignimbrite	Gedinnian
Dunnottar Group (1660 m)	Conglomerate, sandstone, lava, pyroclastic rocks	395 m y
Stonehaven Group (1550 m)	Sandstone, shale, conglomerate, lava	Infra-Gedinnian (Silurian)
	U-N-C-O-N-F-O-R-M-I-T-Y	
Highland Border Rocks	Volcanic and metamorphic rocks	Cambro-Ordovician

whereas the sandstones are of fluvial origin (Mykura, 1983). The provenance of these sediments (Highland Border Rocks - Upper Cambrian?) is believed to be mixed volcanic and metamorphic rocks.

1.6 Stratigraphy and tectonic setting of the Viking, Cardium and Belly River Formations

The Viking Formation (200 ft) of south-central Alberta represents the Lr. Cretaceous rocks which extend from the Lower Manniville or Cadomin Conglomerate to the base of the Fish Scale zone (Table 1.2). Upper Cretaceous rocks lie conformably over Lower Cretaceous and extend from the Fish Scale zone to the base of the Paskapoo. These are here represented by Cardium (200 ft) and Belly River (900 ft) formations (Table 1.2).

During Columbian and Laramide orogenies, the Cordilleran miogeosyncline underwent major deformation, regional metamorphism, granitic intrusions and uplift producing the Cordilleran Uplift (Fig. 1.2). A large volume of sediments was eroded during Cretaceous time from the Cordilleran Uplift, in the west, and deposited on the interior platform which was covered with shallow seas (Fig. 1.2). Most of these sediments are continental grading eastward into marine sands and shales. Both Lower and Upper Cretaceous sediments form sedimentary wedges in Alberta that thin out eastward. The volcanic activity that prevailed near the end of Lower Cretaceous and continued into the Upper Cretaceous influenced in part the mineralogy of some Cretaceous sediments. Although most of the Cretaceous sediments were derived from the Cordilleran Uplift, tectonic features such as the Peace River - Athabasca High, the Canadian Shield, and the

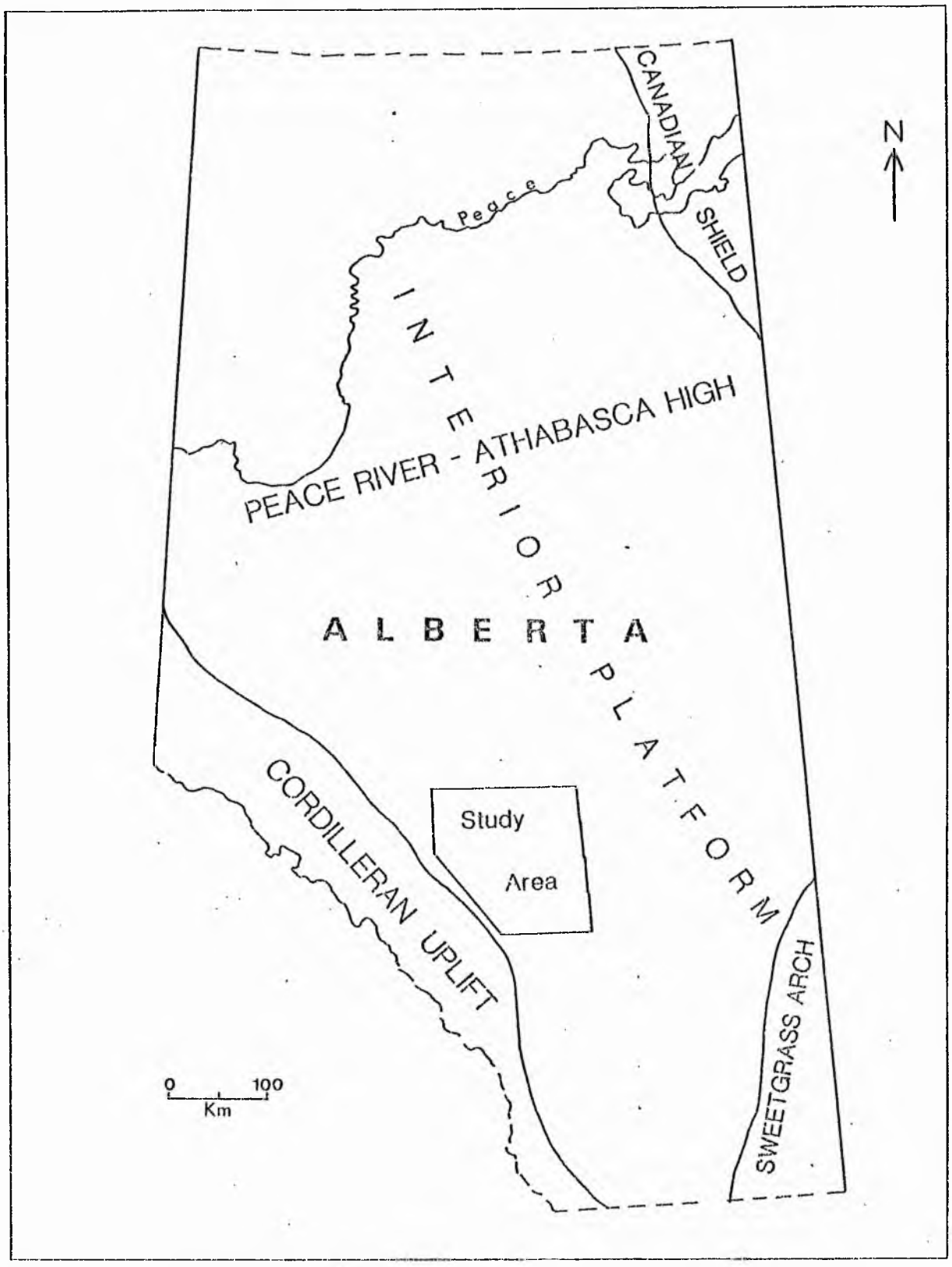

Fig. 1.2 Location map of the study area with tectonic elements.

Table 1.2 Cretaceous Formations of southern and central Alberta (Shawa et al., 1984).

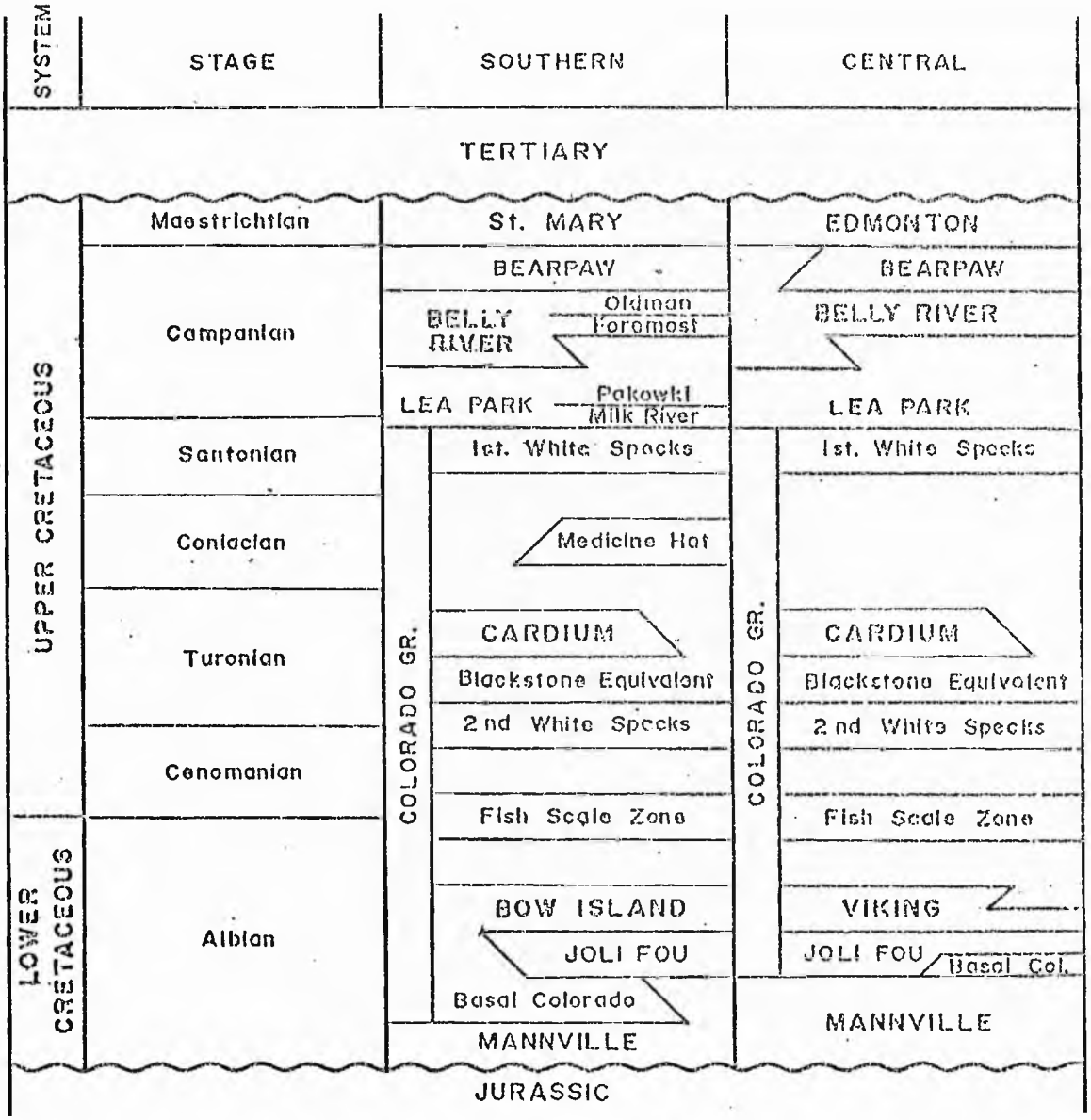

Sweetgrass Arch (Fig. 1.2) are believed to have influenced the sedimentation in Alberta almost throughout geological time (Shawa et al, 1984).

1.7 Presentation of the data

The results of the present investigations are presented in two separate sections. Section I deals with the Lower Old Red Sandstone and Section II is on the Viking, Cardium ad Belly River Formations.

SECTION - I

CHAPTER II

Environment of deposition of Lower Old Red Sandstone

Lithologs were prepared along five section lines (Fig. 2.1) between Carnoustie and Arbroath to recognize and analyse vertical and lateral facies variations in the area. These five lines were chosen because they offered continuous exposures and thick sequences. It has been possible to assign these sediments an origin in braided streams. Development of calcretes with displacive growth of calcite was also recognized; this is discussed in Chapter III.

2.1 An outline description of the lithofacies and their associations

A spectrum of siltstone, fine to very coarse grained sandstones, pebbly sandstones and conglomerates is present in these sediments. Lithologs (Fig 2.2) permit the recognition and analysis of vertical and lateral facies changes in the area.

This account concentrates on the description and analysis of six lithofacies (Table 2.1) and their interrelationships. Lithostratigraphic correlation is hampered by the frequent lateral and vertical variations of lithofacies and absence of regional marker horizons. An individual lithounit can only be traced for a few tens of metre. Lithofacies P being massive and hard stands out more prominently than other highly weathered facies and helps in local correlation. Like other facies, it normally extends for a few tens of metre and only rarely can be traced for nearly 150-200m. Most of these facies normally occur

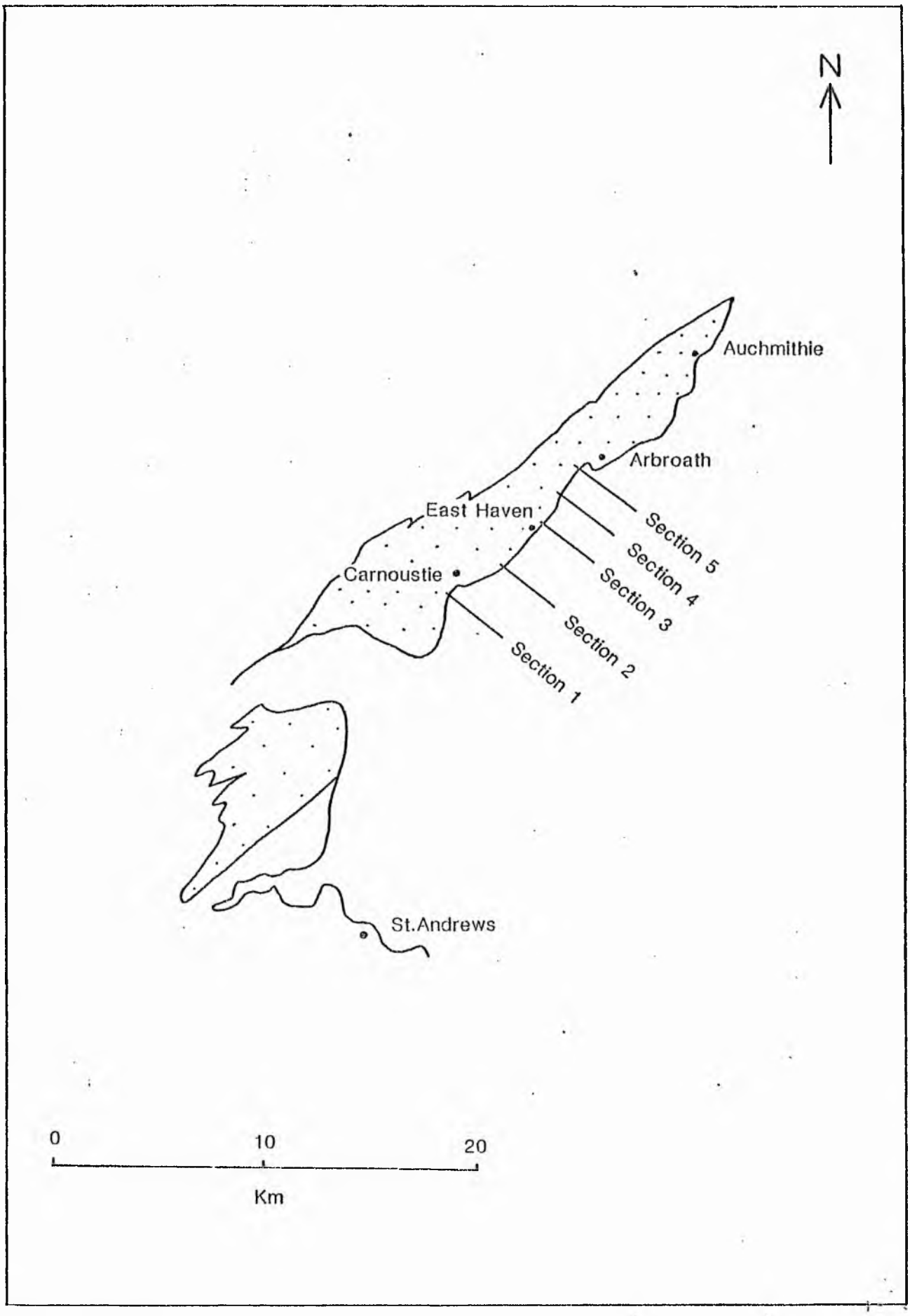

Fig. 2.1 Location map

Fig. 2.2 Successions in the Lr.Old Red Sandstone of Carnoustie.

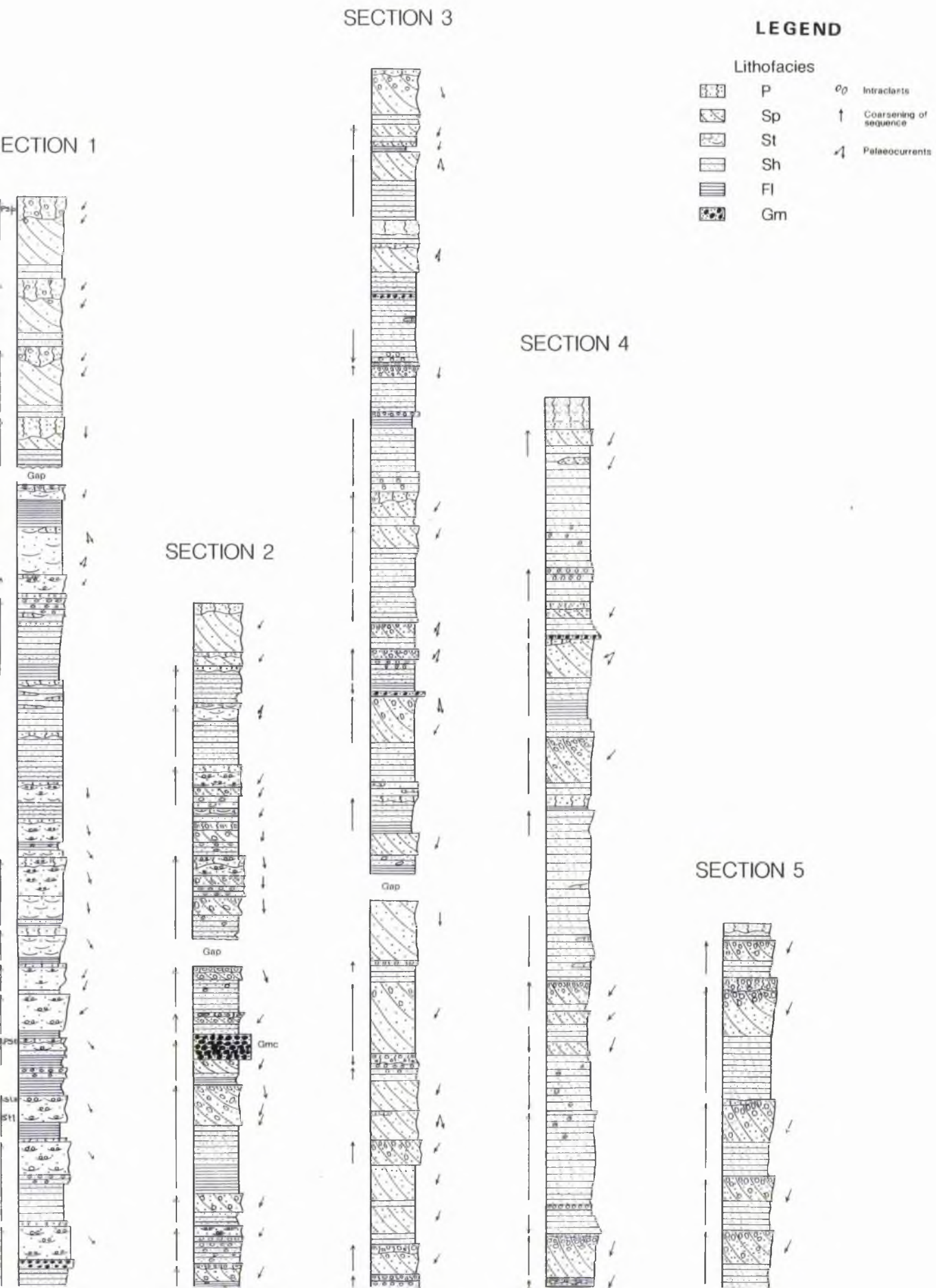

as tabular bodies frequently disappearing laterally into other units.

The overall clast compostion of the pebble mode does not vary with lithofacies and comprises carbonate, quartzite, vein quartz and acidic and basic igneous rocks. Normally the clasts are subspherical and more abundant in the north-east area. Only carbonate clasts show a distinct but gradual increase in amount towards south-west where they dominate above all others. They are believed to be locally derived by erosion of carbonates formed in adjacent pools during periods of channel abandonment. The carbonate clasts are more frequently cracked and commonly show honeycomb surface texture formed probably by wave action in recent times.

The term 'profile' used further in the text represents net accumulation of sediments during a single fluvial cycle. The upper decimetres of sediment in these profiles have been calcretized and are grey, massive and cracked. The calcretization is believed to have occurrred during periods of channel abandonment, hence, the calcretized sediments represent the top of profile. Calcretization is also associated with the gradual decoloration of the red sandstone into grey. Sandstones exposed north-east of Arbroath which are low stratigraphically are typically red in colour whereas near Carnoustie they are grey. The decoloration can often be even seen in a single profile, particularly in the centre of the area near East Haven. Here the sandstones are red near the base of the profile, becoming grey upwards. This gradual disappearence of red coloration is associated with an increase in carbonate content.

Beds showing a minimum degree of textural maturity (absence of matrix and clast size-sorting) and very poorly developed fabric are referred to as disorganized, while beds referred to as bimodal contain a fairly well sorted assemblage of clasts in a sand matrix which lacks clasts of an intermediate size (Steel and Thompson, 1983).

Miall's (1977 and 1978) letter code for facies nomenclature, which is popular because of its flexibility is used here. It is adopted with some further division of some of the facies on the basis of their pebble content, as described below: -

2.1.1 Lithofacies P: Massive, cracked calcretized sandstone

This is the most striking lithofacies of the area and is easily recognizable. Being hard and massive it stands out prominently as tabular sand bodies (Fig. 2.3) resembling hardpan calcretes. The important feature of this facies is the cementation of unimodal or polymodal sediments by displacively grown calcite (Chapter III). Calcretization has made it hard, massive and grey in colour and is believed to have formed during periods of emergence. Hence, this facies is a product of a pedogenic process. Thickness varies from a few centimetres to a few decimetres, depending upon the intensity of calcretization and rarely it is nearly 1 m thick.

Although this is hard, massive and cracked, still it often shows the faint impression of original sedimentary structures. Only when it is highly cracked and massive, does all sign of original sedimentary structures disappear. Various sedimentary

structures observed in the facies P include flat lamination, thin beds, planar and trough cross beds. This facies does not show any preference to any particular sedimentary structure . In fact it shows that whatever kind of lithofacies were exposed during periods of emergence were calcretized. At several places it can be observed that the sedimentary structures of the underlying lithofacies are continuing and preserved though faintly, in this facies. Where these sedimentary structures are recognizable, prefix P has been used to define a particular lithofacies that has been calcretized. For example near the base of column 1 (Fig. 2.2), cross-trough beds can be seen in facies P and hence it has been named as PSt. Similarly near the top it is PSp (calcretized planar cross beds) and the planar cross beds are shown by broken lines (Fig. 2.2).

Normally the top and base of faices P is very sharp (Fig. 2.4) but in some places the base is gradational into the underlying facies (Fig. 2.5). Facies P is found to be thickest (nearly 1 m) with gradual bottom contact when associated with planar cross beds. The cross beds probably acted as conduits and hence permitting the carbonate precipitating processes to penetrate into much deeper levels. Varying degrees of swelling and cracking are seen in this facies (Fig. 2.6). Several irregular calcite sheet-like bodies (1 to 4 m long and upto 1 m deep) are commonly present. Sometimes when the cracks are abundant and closely spaced, irregular prismatic columns have formed standing perpendicular to the bedding plane (Fig. 2.4). The cracks have been divided into two types.

1) Cracks associated with the calcretization process and

2) Cracks associated with the tectonic activity.

Cracks of the first type are irregular and do not show any particular orientation (Fig. 2.6). These are believed to have formed during calcretization either by displacive growth of calcite or simply as desiccation cracks in cohesive sediments. The cracks are often seen to be restricted to lithofacies P only and are often filled with calcite cement. The cracks of the second type are sharp and straight showing strong parallelism (Fig. 2.7). These are more like fine partings and can be classified into two or three subtypes depending on their orientation. In contrast to the first type, these are commonly seen to penetrate into underlying facies and filled with carbonate cement forming calcite sheets.

Calcretes occur most frequently (32.35% in section 1) in the south (near Carnoustie) and show a gradual decrease towards north (Table 2.1 and Fig. 2.8). They are absent near and north of Arbroath. As lithofacies P simply represents a calcretized part of other lithofacies, the paleocurrent directions obtained correspond to those of other facies. Commonly paleocurrent directions are obscure but overall the vector data obtained from this facies indicate unimodal transport from north to south with a low spread (Fig. 2.9).

2.1.2 Lithofacies Sp: Planar cross-bedded sandstone

Cross stratified sandstones are least common (11.45%) in section 1 near Carnoustie and show a gradual increase towards north to section line 3, (45.92%, see table 2.1 and Fig. 2.8).

Further north a gradual decrease is found with a corresponding increase in the horizontal plane beds. These planar cross beds are commonly small (< 1m, Fig. 2.5) but a few larger beds (1-2.5m) are also present. Individual sets vary in thickness from 3 cm to 30 cm and commonly show tangentional contact at base becoming steeper near top (Figs. 2.10 and 2.11). The large cross beds are common in section 3 and near the top of section 1. These thicker beds can sometimes be traced for nearly 100 m in the direction of transport but normally they disappear into other lithofacies after a few tens of metre.

Generally the planar cross beds are coarser than their horizontally stratified counterparts and show coarsening upwards (Figs. 2.11 and 2.12). Commonly the basal foresets are texturally more mature than those near the top. Basal foresets are either composed of only sand (medium to coarse) or show a bimodal assemblage with a few large clasts. Gradually the foresets become coarser (medium to very coarse) and immature towards the top where they show polymodal assemblages containing pebbles of all sizes varying from < 1 cm to as big as 20 cms. Less pebbly (< 10%) beds are referred to as Sp1 and more pebbly as Sp2. Normally the planar cross beds show a gradual change from Sp to Sp2 through Sp1 from the base towards the top. Pebbles are disorganised and they normally lie parallel to foresets. An interesting aspect observed in a few planar cross beds near Carnoustie is formation of alternate coarse and fine foresets. Coarser foresets are composed of fairly well sorted assemblage of clasts in a sand matrix where as finer foresets are of medium to coaarse grained sand. Commonly the clasts in

bimodal coarser foresets vary in size from 3 to 5 cm and are closely packed to form a clast supported framework of the foresets (Figs. 2.13 and 2.14). Compositionwise the clasts are predominantly of carbonate and also include a few quartzitic and igneous types.

Calcite sheets and cracks are commonly seen penetrating this lithofacies. Sometimes the calcite sheets penetrate right across from top to the base (Fig. 2.12). Commonly lithofacies Sp overlies lithofacies Sh and is overlain by lithofacies P, Sh or Fl (Table 2.2). Only at one place in section 2 it is overlain by lithofacies Gmc (Fig. 2.2). Near the base of section 3 it shows mulitistorey sequence (Fig. 2.2). In section 4 and north of the area near Arbroath lithofacies Sp alternates with lithofacies Sh. Their thickness varies from a few decimetres to more than a metre.

The paleocurrent data obtained from lithofacies Sp of the entire area show an unimodal transport from North to South (Fig. 2.9). In sections 1,2 and 3 it swings between due SE and SW, wheras in section 4 it varies between due WSW and SW. Further in the north in section 5 and near Arbroath paleocurrent data show an unimodal transport to SW.

2.1.3 Lithofacies St: Trough cross bedded sandstone

Medium to very coarse grained trough cross bedded sandstones are most abundant in section 1 and form approximately 33% of the total thickness. They are also present in section 2 though more rarely than their planar counterparts but it is completely absent

in the area north of section 2 (Table 2.1 and Fig. 2.2). It occurs most consistently near the base of section 1 and gradually disappears towards the top, where planar counterparts (Sp) dominates.

Like planar cross beds, these trough cross beds are normally small (< 1 m) but a few isolated large beds (1-2 m) are also present. Individual sets vary in thickness from 2 cm to 25 cm with trough width varying between 1 and 4 m. Coarsening upwards can also be commonly seen within these trough cross beds particularly in the thicker ones. Pebbles of different composition and size are commonly present and show an increase in number and size towards the top. Sometimes the opposite can also be seen. Less pebbly (<10%) beds are referred to as St 1 and more pebbly as St 2. Commonly a gradual change from St to St 2 is observed, particularly in thicker beds. These pebbles are disorganised and do not show any preferred fabric.

Like other lithofacies the trough cross beds can normally be traced for only a few tens of meters before they disappear into other lithofacies. Lithofacies St commonly lies above lithofacies Sh and Fl (Table 2.2) and top 5 to 30 cms is commonly calcretized to form lithofacies PSt (Fig.2.2). It is generally overlain by lithofacies Sh and rarely by lithofacies Fl. Calcite sheets and cracks are commonly seen to penetrate this lithofacies as well.

Paleocurrent data obtained from the trough cross beds also show an overall unimodal transport from north to south. When compared with the data of lithofacies Sp it shows rather more variation (Fig. 2.9). In section 1 it varies between due SE and

SW whereas in section 2 it is more consistent and is generally due south. Paleocurrent data show a maximum variation in section 1 where trough cross beds are most abundant (Fig. 2.2).

2.1.4 Lithofacies Sh: Horizontal bedded sandstone

Commonly Sh is medium grained but shows variation in grain size from fine to very coarse. Fine grained sandstones are present only in the section 1, whereas coarse to very coarse grained are more frequently present in the sections towards north. Lithofacies Sh occurs as tabular sandbodies which can be traced only for a few tens of metre in the southern part of the area, whereas in the north it sometimes extends for nearly 100-200 m before disappearing into other facies. Overall this lithofacies shows an appreciable increase from south to north. It forms 28.5%, 38%, 44% and 67% of the total thickness measured in sections 1,2,3 and 4 respectively. Further north in section 5 it shows a slight decrease (48%) with a corresponding increase in lithofacies Sp (Table 2.1 and Fig. 2.8). In the extreme north near Arbroath it again clearly dominates over all other lithofacies and constitutes nearly 80% of the total thickness, with a fall in lithofacies Sp.

Individual beds in lithofacies Sh vary in thickness from 2 cm to nearly 30 cm. They tend to be thinner (2-10 cm) in sections 1 and 2 than those found in the sections 3 and 4 (5-30 cm). Total thickness of lithofacies Sh varies from 0.15 m to 1.5 m in sections 1 and 2 whereas it is generally much thicker (0.3 to app. 4 m) in the northern part of the area. A few randomly

distributed clasts varying in size from < 1 cm to 10 cm can sometimes be present. Occasionally pebbles of all compositions and sizes are abundant as observed in other lithofacies. Less pebbly (<10%) beds are referred to as Sh1 whereas more pebbly as Sh2. Both coarsening and fining upwards sequences can be observed in this lithofacies but generally the pebbly ones tend to coarsen upwards (Fig. 2.2, sections 3 and 4).

Commonly it overlies lithofacies P and Fl and rarely Sp or St in sections 1 and 2 (Table 2.2). In section 2 it also overlies facies Gm once (Fig. 2.2). In the area north of section 3 lithofacies Sh generally overlies lithofacies Sp. In contrast to the variation observed in the underlying lithofacies, it is dominantly overlain by lithofacies Sp, except in the lower part of the section 1 where lithofacies St frequently lies over it (Fig. 2.2). Lithofacies Sh has at times been calcretized to form massive, hard and cracked rock (lithofacies P).

2.1.5 Lithofacies Fl: Flat laminated silt and sandstone

Lithofacies Fl defines thinly laminated siltstone and very fine to medium grained sandstones. Commonly these are interbedded wih bed thickness varying from <5 cm to 75 cms and laterally impersistent. The thickest bed (1.35m) occurs near the base of section 2 and can only be traced for nearly 5 m.

In contrast to lithofacies Sh it shows a gradual decrease from south to north and is very rare in the extreme north of the present area (Fig. 2.8). It comprises nearly 11.3%, 9.6%, 3.4% and 2.8% of the total succession measured in sections 1,2,3 and 4

respectively (Table 2.1). Commonly lithofacies Fl gradually changes upwards into lithofacies Sh (Table 2.2) with an increase in grain size, hence shows coarsening upwards. Sometimes lithofacies Fl is even directly overlain by other lithofacies such as lithofacies St (see section 1, Fig. 2.2) and Sp (see sections 2,3 and 4, Fig. 2.2). In fining upwards sequences it invariably forms the top and finer unit. Occasionally a few randomly distributed clasts (< 1 cm to 10 cm) can be seen in the lithofacies Fl which commonly is micaceous.

2.1.6 Lithofacies Gm: Horizontally - poorly stratified gravel

Gravel size particles occur quite frequently in the poorly sorted polymodal assemblages of the entire area. These assemblages are mostly dominated by pebbles and very rarely unimodal - well sorted gravel occurs as separate units. Mostly it occurs as crudely flat, thinly bedded units of 15 to 30 cm thickness. In the middle of section 3 and towards the top of section 4 it overlies planar cross bedded sandstone (lithofacies Sp) and forms coarsening upward sequences (Fig. 2.2). Near the base of section 1 it overlies lithofacies Sh and again forms coarsening upward sequence. Occasionally lithofacies Gm even shows coarsening upwards within itself as it is more pebbly towards the top. Less pebbly (<10%) beds are referred to as Gm 1 and more pebbly as Gm 2. Another subfacies (Gmc) has been found to occur only at one place in section 2 as a 75 cm thick unit. It is a horizontally-poorly stratified conglomerate and overlies lithofacies Sp forming a coarsening upwards sequence (Fig. 2.2).

Table 2.1 Facies assemblages in the Lower Old Red Sandstone of Carnoustie

Litho-facies Code	Outline description of Lithofacies	Percentage of succession at										Interpretation
		Section Line 1		Section Line 2		Section Line 3		Section Line 4		Section Line 5		
		Thick-ness	Frequ-ency	Thick-ness	Freq-ency	Thick-ness	Frequ-ency	Thick-ness	Frequ-ency	Thick-ness	Frequ-ency	
P	Massive-cracked calcretized sand-stone	14.86	32.35	12.18	24.44	6.33	22.22	6.92	19.14	6.85	15.38	Pedogenic feature formed during periods of stream abandonment-
Sp	Planar cross bed-ded sandstone	11.45	5.88	29.18	26.66	45.92	29.16	22.80	21.27	45.66	38.46	Sand waves, trans-verse and medial bars
St	Trough cross bed-ded sandstone	32.97	20.58	7.10	11.11	-	-	-	-	-	-	Migrating dunes
Sh	Horizontal bedded sandstone	28.48	25.00	38.07	28.88	43.94	40.27	66.92	51.06	47.95	46.15	Planar bed flow
Fl	Flat laminated silt and sand-stone	11.30	14.70	9.64	6.66	3.38	6.94	2.80	6.38	-	-	Channel pool/deposit waning current deposit
Gm	Horizontally-poorly stratified gravel	0.93	1.47	3.80	2.22	0.43	1.38	0.56	2.12	-	-	Medial bar (platform) deposits.

Table 2.2

Transition count matrix

	P	Sp	St	Sh	Fl	Gm	Sum
P	0	7	3	33	8	1	52
Sp	24	0	2	19	1	2	48
St	14	0	0	3	2	0	19
Sh	21	40	7	0	5	2	75
Fl	1	2	5	11	0	0	19
Gm	0	0	1	4	0	0	5
Total	60	49	18	70	16	5	218

Transition probability matrix

	P	Sp	St	Sh	Fl	Gm
P	0	.13	.06	.63	.15	.02
Sp	.5	0	.04	.39	.02	.04
St	.74	0	0	.16	.10	0
Sh	.28	.53	.09	0	.06	.03
Fl	.05	.10	.26	.58	0	0
Gm	0	0	.2	.8	0	0

Independent trials probability matrix

	P	Sp	St	Sh	Fl	Gm
P	0	.29	.10	.42	.09	.03
Sp	.35	0	.10	.41	.09	.03
St	.30	.24	0	.35	.08	.01
Sh	.42	.34	.12	0	.11	.03
Fl	.30	.24	.09	.35	0	.02
Gm	.28	.23	.08	.33	.07	0

Difference matrix

	P	Sp	St	Sh	Fl	Gm
P	0	-.16	-.04	.21	.06	-.01
Sp	.15	0	-.06	-.02	-.07	.01
St	.44	-.24	0	-.19	.02	-.01
Sh	-.14	.19	-.03	0	-.05	0
Fl	-.25	-.14	.15	.23	0	-.02
Gm	-.28	-.23	.12	.47	-.07	0

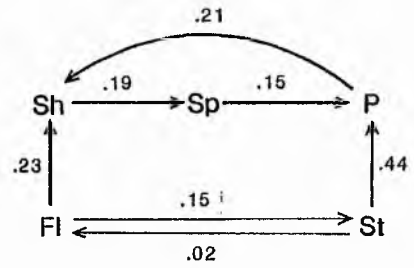

NB Transitions have been recorded from five sections (Fig. 2.2) and combined into one transition count matrix.

Lithofacies Gmc is of disorganized type in which the pebble/cobble assemblage is polymodal and is matrix supported. Clasts range in size from 6 cm to 41 cm and do not show any imbrication, due to the high roundness and to the clear dominance of spheroid shaped clasts. The clasts show a gradual but considerable decrease in their size and amount in the downcurrent direction and finally nearly after 12 m the conglomerate becomes pebbly sandstone (Fig. 2.15). This medium to coarse grained pebbly sandstone is flat and thinly bedded, hence is an equivalent of lithofacies Sh 2 described earlier. The matrix of the conglomerate is composed of medium to coarse grained sand.

Overall the bulk of sediments in the present area are composed of pebbly sandstones, but conglomerates increase in frequency to the north of Arbroath.

2.2 Fluvial pattern

The evidence considered together to assign a braided river origin for the Lower Old Red Sandstone are given below (following Collinson, 1978).

2.2.1 Thickness ratio of coarse to fine member:

The coarser member clearly dominates in the succession and shows a gradual increase towards the north. The member is represented mainly by coarse, gravelly and pebbly sandstones whereas siltstone and very fine to fine-grained sandstones constitutes the finer member. The total thickness in the overall

sequence of the finer member is approximately 7 % in section 1 and 4 whereas it is only 2 % and 3 % in sections 2 and 3 respectively. Futher north (near Arbroath) the finer sediments are even less than 2 %. The overall high coarse to fine member ratio probably reflects high angles of slope.

2.2.2 Palaeocurrent patterns:

Collinson (1978) drew attention to the importance of combination of variance within and between sections to determine the sinuosity of the stream. Hence palaeocurrent data gathered from different lithofacies (Appendix 2.1) occurring within the present area of study and further north of it has been compared to deduce the river pattern.

The paleocurrent data indicate unimodal transport from north to south with a low spread (Fig. 2.9). Although vector data of lithofacies Sp and St both show low variance, Sp (planar cross bedded sandstone) shows less variation than St (trough cross bedded sandstone) both within and between sections. This is probably due to the fact that St is believed to have formed by migrating dunes and is likely to show more variation than the planar cross beds of Sp produced probably by progradation of avalanche slopes of longitudinal bars or migrating sand waves.

It is believed that the overall low variance within and between sections with an areal spread of approximately 10 kms favours a braided river interpretation.

2.2.3 The internal organization of grain size and sedimentary structures:

This has been used most widely and has been the main criterion for channel reconstruction. Studies in the present area show an overall dominance of coarsening upward sequences (Fig. 2.2). The few fining upward sequences can be interpreted either as medial bars growing under conditions of waning flow (Bluck, 1979) or due to lateral wandering of the stream, rather than as point bars. Also the absence of epsilon cross bedding and lack of evidence that associated fine sediments were transported obliquely to the gravel mode, can be used to suggest the absence of point - bar deposits (Ricci-Luchi et al., 1981; Ori, 1982).

Lastly, the ubiquitous occurrence of large clasts (upto 15 cm) particularly in lithofacies P (representing the top of the sequence) favours the deposition under very high to high fluvial energy conditions. This further rules out the possibility of point bars as they are known to represent low fluvial energy conditions (Miall, 1977). Hence, all these features once again favour the braided-stream interpretation.

2.2.4 The shape of sand bodies:

It is difficult to determine precisely the three dimensional geometry of the sand bodies in the present area due to the unsuitable outcrops and frequent lateral variation. The outcrops are wrongly oriented and too small to identify any bar form in the field, which according to Bluck (1979) is a prerequisite to a

more certain identification of braided stream deposits. However, the observed frequent variations in lithofacies are consistent with a braided stream environment.

The utility of sand-body shape as a guide to channel type has been questioned (Collinson, 1978). Hence, the present interpretation of a braided stream is mainly based on the strength of the first three properties.

2.3 Mode of deposition

The processes that might have produced observed sequences in the present area have been interpreted separately for the generalized and specialized sequences mentioned below (based on work by Bluck, 1974, 76, 79; Cant, 1978; Collinson, 1978; Miall, 1970,78; Rust, 1978 and Smith, 1972).

2.3.1 Generalized sequences

Lateral variation is common but vertical variation is small. The profiles have been divided into two general types:

1) Flat stratified -> Trough-cross stratified sequences (Sh -> St) and

2) Flat stratifed -> Planar cross stratified sequences (Sh -> Sp)

1) Sh -> St sequences:

Sh-St sequences are present in the extreme southern part of the area (see sections 1 and 2 in Fig. 2.2) and vary in

thickness from less than 1 m to about 3 m. These sequences are particularly dominant in the bottom half of the section 1. The trough-cross bedded unit overlies the flat stratified unit and is generally coarser and more pebbly, hence, together they form a coarsening upwards sequence. The thickness of the cross-trough beds varies from 20 cm to app. 2 m and angle of dip is commonly $< 20^{o}$. Commonly the troughs are filled with varying amounts of pebbles and gravel. These features suggest that these trough-cross beds were formed during the migration of dunes under varying discharge conditions.

It is believed that the transition from flat stratified beds to trough-cross beds was perhaps dependent on the flow strength, grain size and ratio between suspended load to bed load (Allen, 1968 and Engelund and Fredsoe, 1974). Initially, the basal flat stratified beds were formed under higher flow velocity when there was more finer material and the ratio between suspended material to bed load was high. Later an increase in coarser material coupled with a decrease in the ratio between suspended material to bed load led to the formation of dunes (Allen, 1968 and Engelund and Fredsoe, 1974). Then on migration these dunes produced trough-cross beds and occasionally concentrated gravels and pebbles which later filled the troughs. Finally, during periods of abandonment, the top sediments were calcretized to form lithofacies P. Occasionally when lithofacies Fl overlies lithofacies St, it probably reflects waning of the current before abandonment, as commonly these were later calcretized.

2) Sh --> Sp sequences

These sequences dominate in the northern parts of the area and are generally thicker than the type 1 sequences (see base and top of section 1, Fig. 2.2). Their thickness varies largely from < 1 m to a maximum of app. 8 m. The sequences thicker than 4 m are generally composite and involve more than one unit of flat stratified and/or cross stratified beds (see middle of section 3). Overall, the grains in these sequences are coarser than the sequences of 1st type and vary from medium to very coarse. Similarly the pebbles are commonly bigger and more abundant. Like type 1, the pebble content in lithofacies Sh varies from meagre to considerable, suggesting deposition under conditions of varying discharge. Occasionally coarsening upwards can be seen within this unit reflecting an increase in the discharge.

The overlying planar cross beds show large textural and structural variations and hence are thought to have originated in different ways. These are discussed individually in the following pages:

a) Homogenous cross beds:

The tabular beds of this category mostly range in thickness from a few decimetre to a metre or more. These sets can normally be traced in the direction of flow for a few tens of meters or sometimes even up to nearly 100 m. These are composed of sand varying in size from medium to coarse and sometimes very coarse. Very rarely a few randomly distributed clasts upto 3 cm in size

may be included. Average angle of dip of the planar cross beds is about 30° and it varies from 25° to 40° . These planar beds normally show an angular contact with the underlying horizontal beds but sometimes tangential contacts are seen. A reactivation surface within these cross beds can rarely be seen.

These cross beds are believed to have formed by migrating sand waves under unidirectional flow. Places where cross beds are tangential to the bottom sets, the influence of other factors such as development of reverse eddies and/or abundant supply of suspended material is suggested (Harms et al, 1975). In those cases where reactivation surface is present, a pause in sedimentation is interpreted. The pause could have been due to a change in flow strength which began to modify sand wave profile, perhaps in the direction of becoming more dune-like. Then a shift back to the earlier flow intensity resumed sand wave migration (Harms et al., 1975).

Profiles where cross beds are overlain by lithofacies Sh or Fl. perhaps suggest waning of flow before stream changed its path. Later, during period of abandonment the top sediments were calcretized.

b) Heterogenous cross beds:

The tabular beds of this category are nearly similar in size and angle of dip with the above type but show a large variation in grain size and composition. Overall cross beds of this type dominate the area and generally show coarsening upwards. They are normally concave and show tangential contact with bottom sets

(Fig. 2.11) but sometimes planar beds with angular contacts are also seen. Pebble content varies from meagre at the base to considerable towards the top (Fig. 2.11).

These cross beds might have originated in the following possible ways:

I) Transverse bar model

This model shows how the lag grows into a transverse bar with an angle-of-repose producing cross stratification (Fig. 2.16). This was first proposed by Hein and Walker (1977) and is an extrapolation of Jopling's (1965) idea concerning the development of cross-stratification in sands. This model requires comparatively low rate of discharge than observed in diagonal and longitudinal bars. Under the low discharge, lag gets sufficient time to aggrade vertically rather than for most of the sediment to be swept on down stream (Fig. 2.16). On continuous supply of sediments the bar grows in height, gravel is rolled across the top and tends to avalanche down the foreset. Thus in this model slower rate of sediment discharge are more likely to result in vertical bar growth and deposition of cross-bedded gravels (cf. Hein and Walker, 1977). Hence, particularly thinner sequences would probably be better explained by this model. The vertical repetition of such sequences demands abandonment of entire portion of the braided stream and the renewed progradation. This is very well supported by the development of calcretes on the top of these sediments during periods of abandonment.

Sometimes these cross-stratified sand units resemble the cross-stratifed sand sheets of Bluck (1979, Fig. 2). They show a gradual increase in thickness in its growth direction (Fig. 2.17) and occasionally contain a few siltstone clasts lying on foresets. Bluck (1979) suggested that these commonly begin as sheets of ripples which by overtaking each other build up foresets that increase in thickness in the growth direction. Initially the siltstone-clay clasts perhaps formed as saucer shaped units infilling ripple troughs but subsequent erosion produced these clasts (c.f. Bluck 1979, Fig. 2). According to Bluck (1979) these cross-stratified sand sheets resemble the rippled sand bars of Williams and Rust (1969), sand wedges of Rust (1972), transverse bars of Smith (1972) and ripple-topped bars of Bluck (1974).

II) Medial bar model:

This model is particularly useful in explaining those sequences which are more pebbly and show pronounced coarsening upwards. Fig. 2.18 represents a profile found in the lower part of the section 2. Here cross bedded pebbly sand stone (Sp 1) is overlain by lithofacies Gmc and underlain by lithofacies Sh-Fl.

The two lithofacies Sp1 and Gmc represent the deposits of the bar platform and bar supra-platform respectively in Bluck's (1971,76) terminology. The superimposition of lithofacies Gmc over Sp 1 reflects the migration of the bar - head and bar tail deposits over the bar platform. The bar platform also migrates by lateral accretion across the subaqueous riffle face into the

channel pool (Fig. 2.19). The lithofacies Fl at the base of the sequence represents the deposits of channel pool. A few clasts found in lithofacies Fl might have rolled down from bar tops during fluctuating currents. The repetition of such sequences would need repeated bar migration and abandonment. Once again the development of calcretes in the top of sequence is an evidence of abandonment.

Occasional fining upward sequence could be explained by bar growth under waning current (Bluck, 1971,76).

2.3.2 Specialized sequences

Cross beds with alternating conglomeratic and sandy foresets

Figs. 2.13 and 2.14 show alternating conglomeratic and sandy foresets. The conglomeratic foresets are composed of fairly well sorted assemblage of clasts in a sand matrix whereas finer foresets are of medium to coarse grained sand. Commonly the clasts in bimodal coarser foresets vary in size from 3 to 5 cm and are closely packed. Compositionally the clasts are predominantly of carbonate and include a few quartzitic and igneous types. These characteristic cross beds are present only in one place near Carnoustie harbour. The angle of dip of these forsets is about 18°.

The formation of alternating coarse-fine laminations in the Platte river has been explained by avalanching of sediments previously sorted by small bed forms on the bar surface (Smith, 1972). A similar process is believed to have formed these alternating beds. Bed forms such as dunes or ripples must have

concentrated these pebbles on the top of migrating transverse or lateral bar, upstream from the slip face. As the bed form and its pebble filled scour pockets approached the edge of the bar, pebbles spilled over first and were followed by continuous avalanching of the finer material till the next trough reached the slip face (Fig. 2.20). These cross beds are slightly curved (Fig. 2.13) and resemble large scale cross-trough beds. This is probably due to slight sinuous shape of the bar slip face.

2.4 CONCLUSIONS

The Lower Old Red Sandstones of the present area were deposited by perennial, high energy and laterally wandering braided river. The sequence as a whole is believed to have formed part of a low relief alluvial plain.

The important factor responsible for overall distribution of various products was fluctuations in sediment discharge. Figure 2.21 and Table 2.1 show an inrease in the frequency of lithofacies Sh towards Arbroath whereas lithofacies Sp decreases to minimum near Carnoustie with a corresponding increase in lithofacies St. This relative distribution of facies suggest that in upstream areas, the high rate of discharge resulted in a dominance of lithofacies Sh, whereas in the downstream areas the lower rates of discharge caused diversity in the development of lithofacies. Similar relationships has been predicted and observed in other streams (Church and Gilbert, 1975; Bothroyd and Ashley, 1975 and Hein and Walker, 1977).

Braided streams are known to wander over the flood plain from one side to the other in quite a systematic way (Bluck, 1974, Fig. 14b). Development of calcretes (lithofacies P) on

the top of bars and other bed forms in the present area is an evidence of periodic exposure presumably resulting from lateral wandering of the stream. Calcretes are not observed further north of the present area.

Fig. 2.3. Hard and massive tabular sand bodies of lithofacies P resembling hardpan calcretes.

Fig. 2.4. Highly cracked lithofacies P showing sharp contact with underlying lithofacies Sh.

Fig. 2.5. Poorly developed lithofacies P with gradational base into the underlying lithofacies Sp.

Fig. 2.6. Swelling and irregular cracks (type 1) in lithofacies P.

Fig. 2.7. Sharp and straight cracks (type 2) showing strong parallelism in lithofacies P.

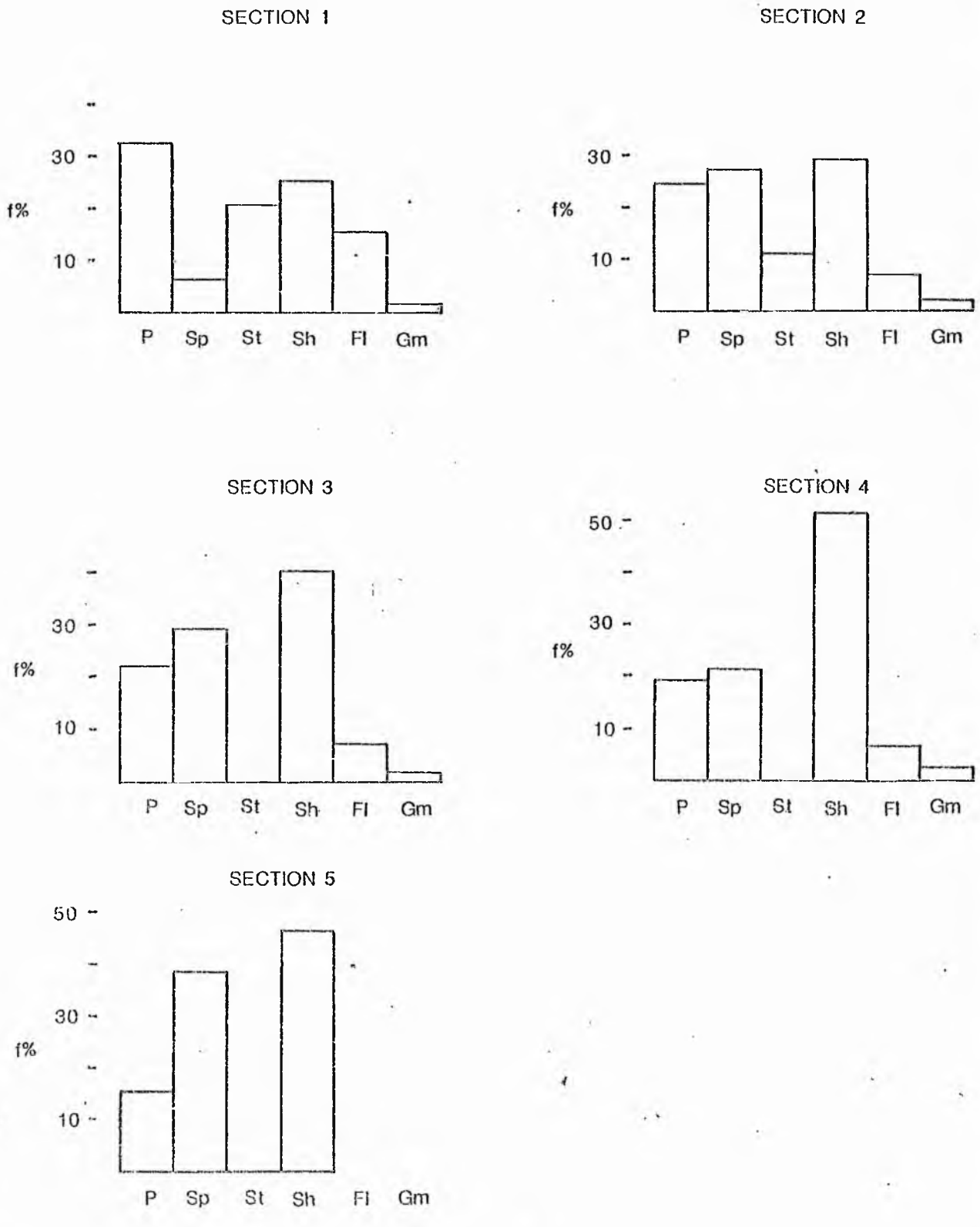

Fig. 2.8 Histograms showing distribution of lithofacies in the Lr. Old Red Sandstone of Carnoustie.

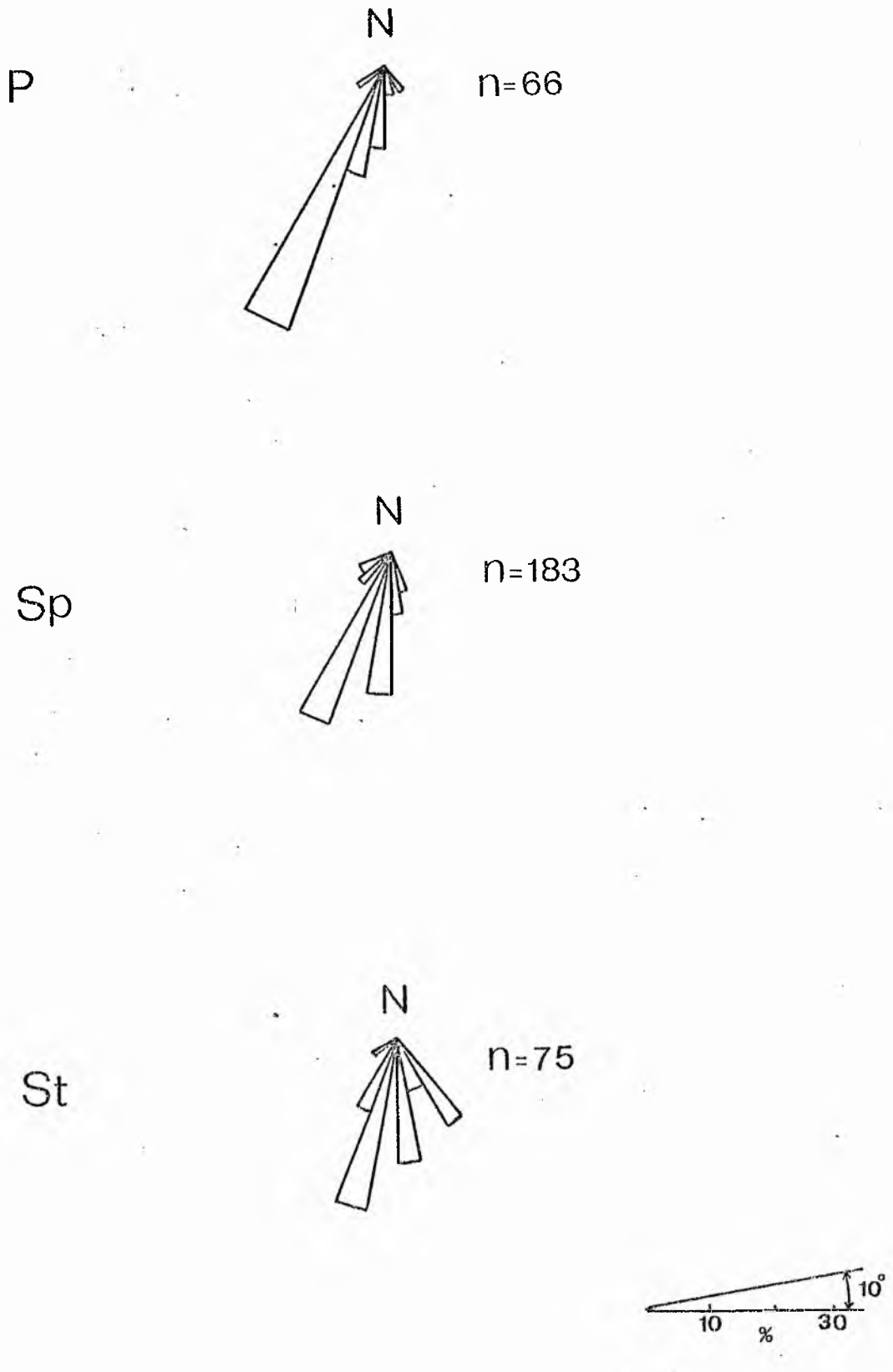

Fig. 2.9 Palaeocurrent pattern in lithofacies P, Sp and St.

Fig. 2.10. Planar cross-bedded sandstone (lithofacies Sp) showing tangentional contact at base becoming steeper near top.

Fig. 2.11. Planar cross-bedded sandstone (Sp) showing coarsening upwards. Note that the basal foresets are texturally more mature and show a bimodal assemblage with a few large clasts while the foresets towards the top show polymodal assemblages.

Fig. 2.12. Planar cross-bedded sandstone (Sp) showing coarsening upwards and calcite sheets penetrating right across from top to the base.

Fig. 2.13. Slightly curved alternating conglomeratic and sandy foresets. Hammer indicates current direction.

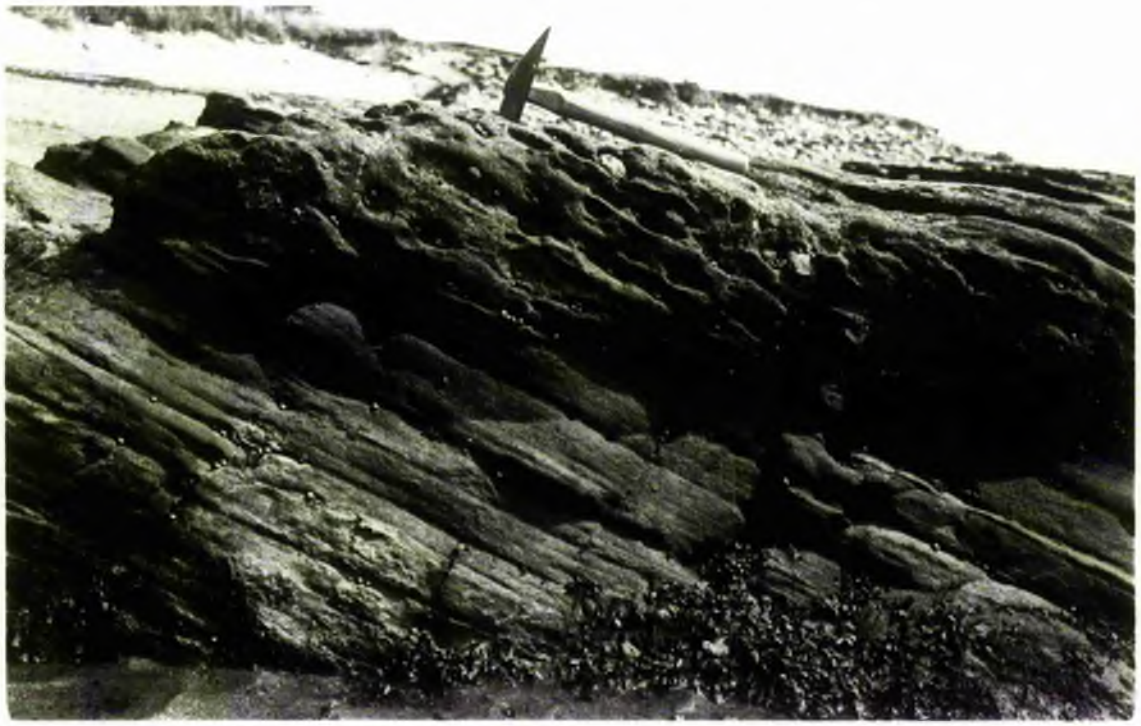

Fig. 2.14. Alternating conglomeratic and sandy foresets. Note that clasts in the conglomeratic foresets are closely packed to form a clast supported framework.

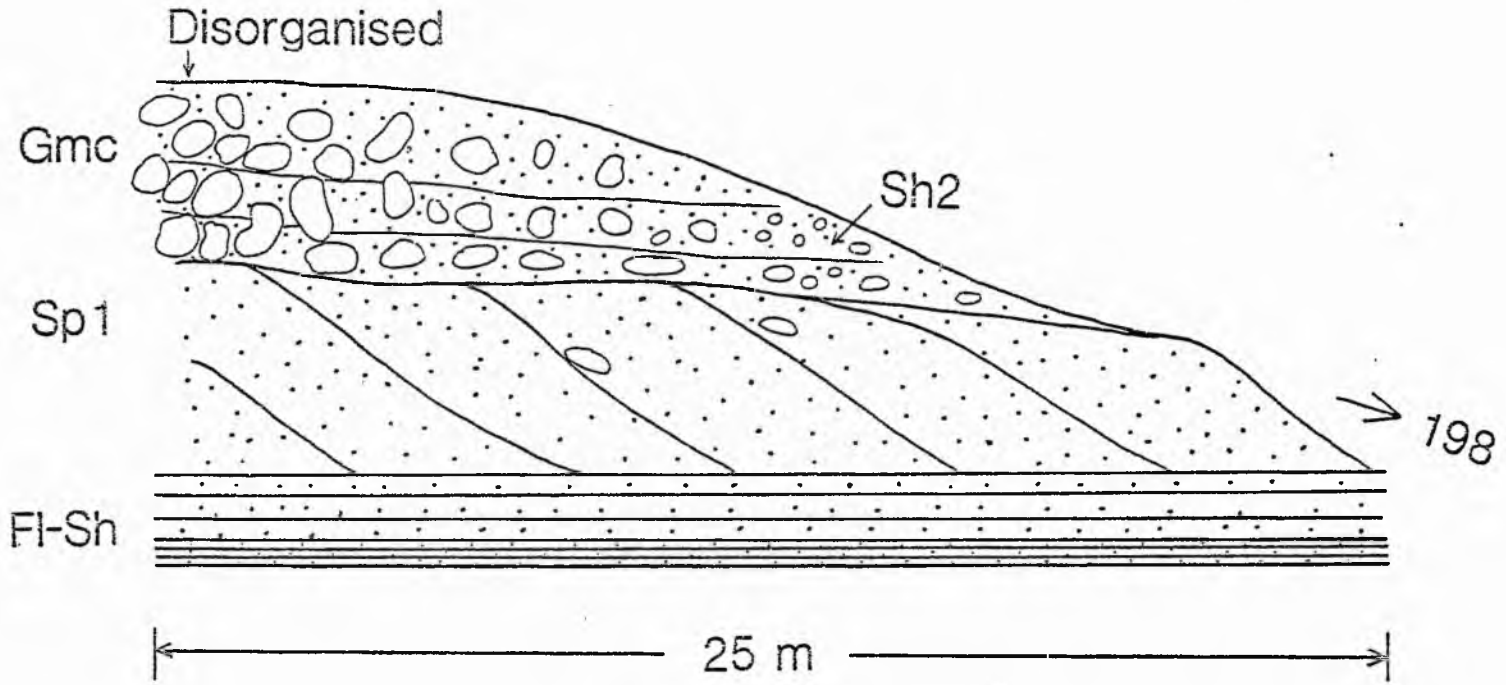

Fig. 2.15. Sketch showing association of lithofacies near the base of Section 1. Note lithofacies Gmc is passing laterally to pebbly sandstone (Sh2) in the down current direction.

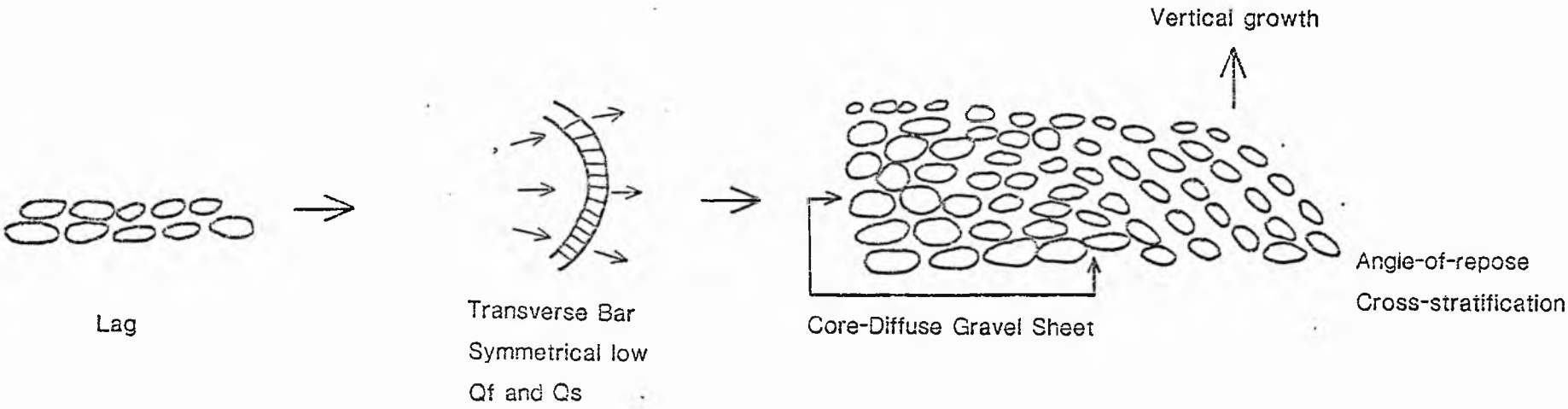

Fig. 2.16 Hein and Walker's (1977) model showing growth of diffuse gravel into transverse bar with an angle-of-repose producing cross stratification.

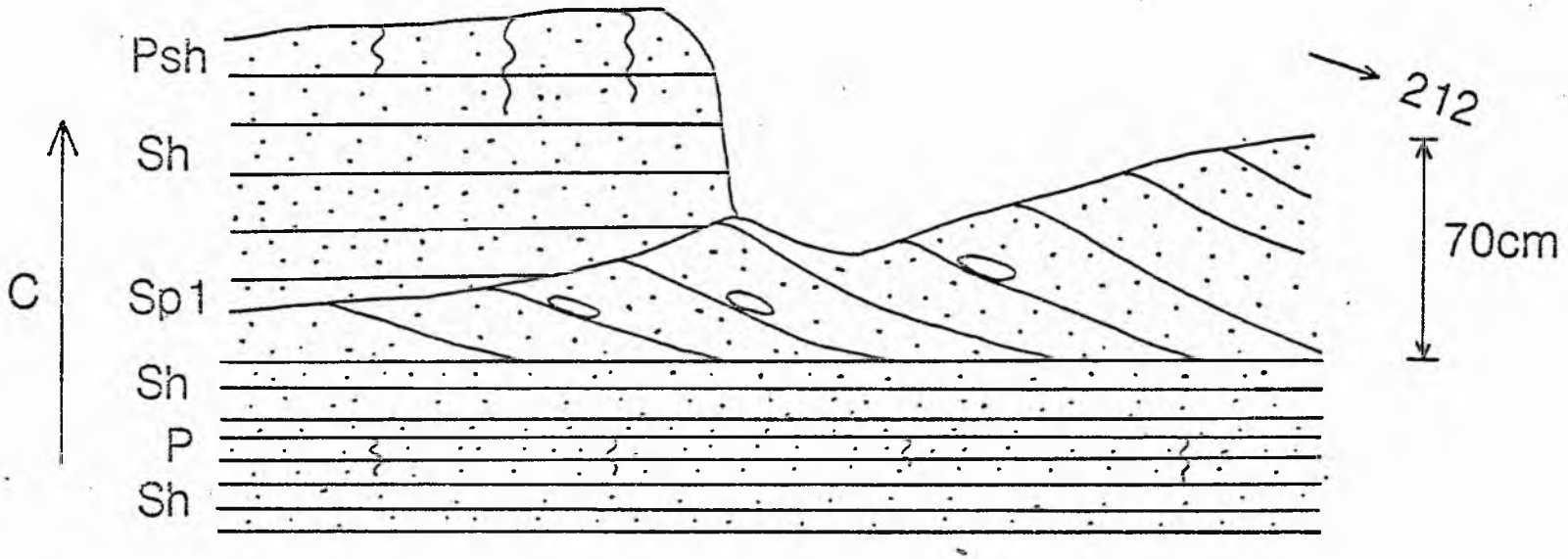

Fig. 2.17 Sketch showing gradual increase in thickness of lithofacies Sp in its growth direction.

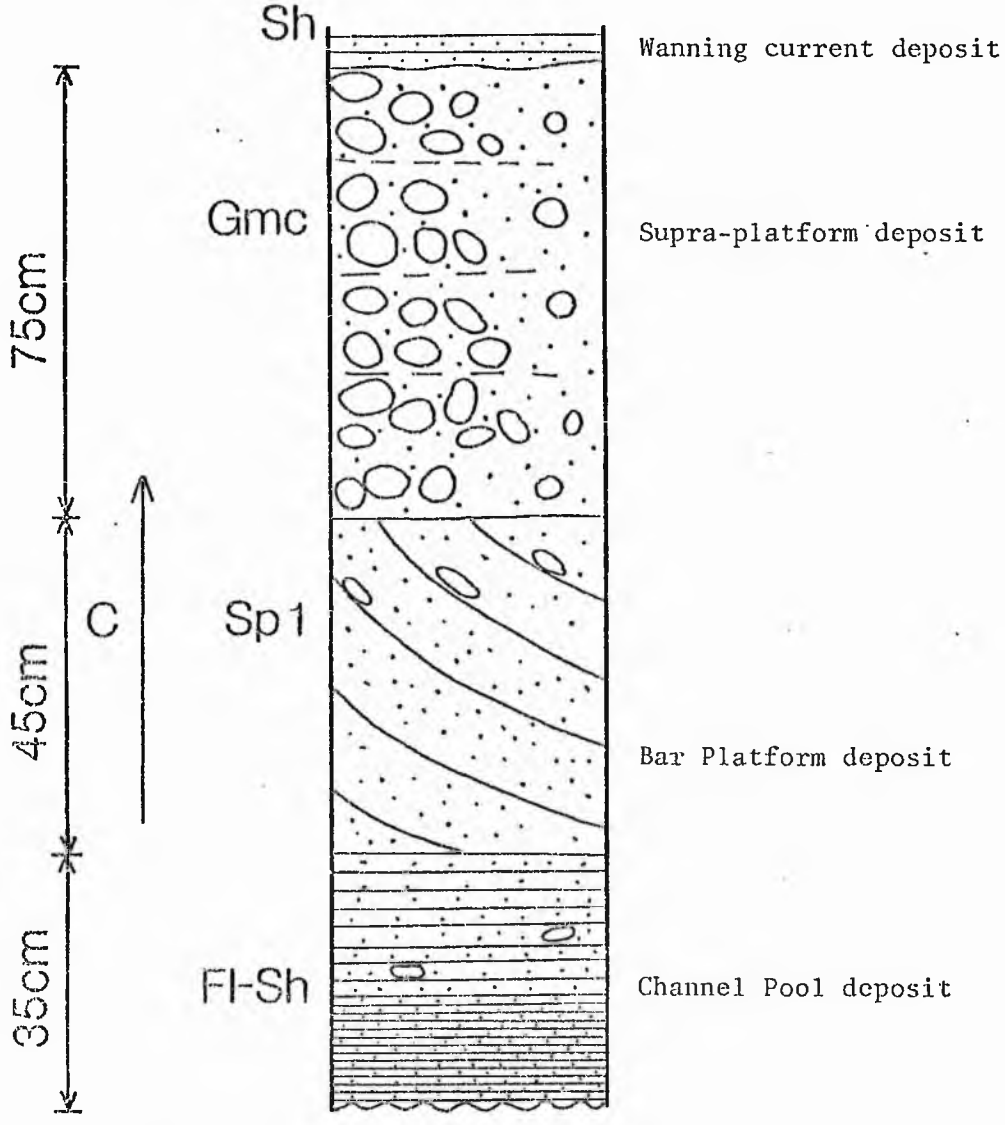

Fig. 2.18 Lithofacies interpretation using Bluck's (1971, 76) terminology.

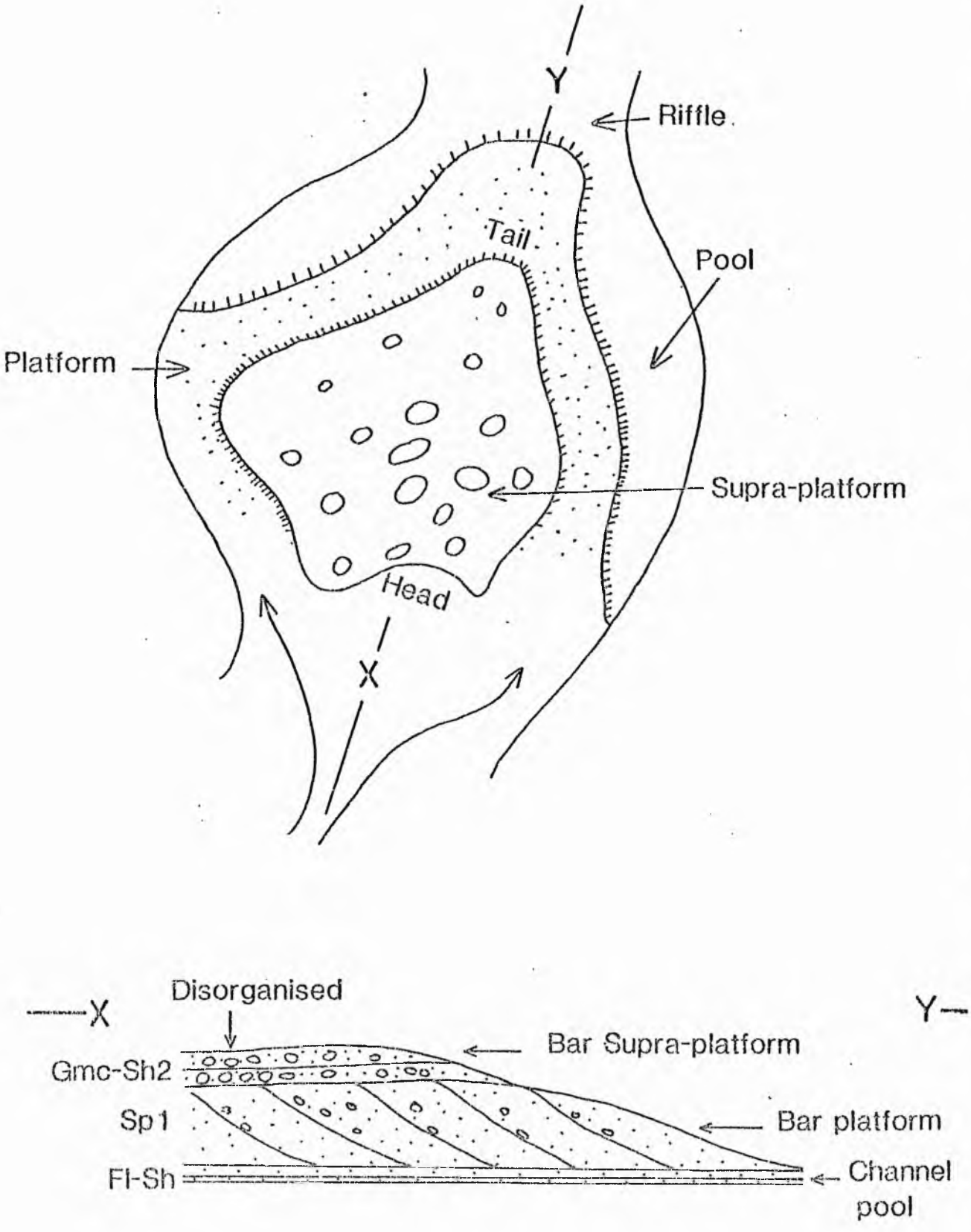

Fig. 2.19 Lithofacies relationship using the platform-supra-platform hypothesis of Bluck (1971, 76).

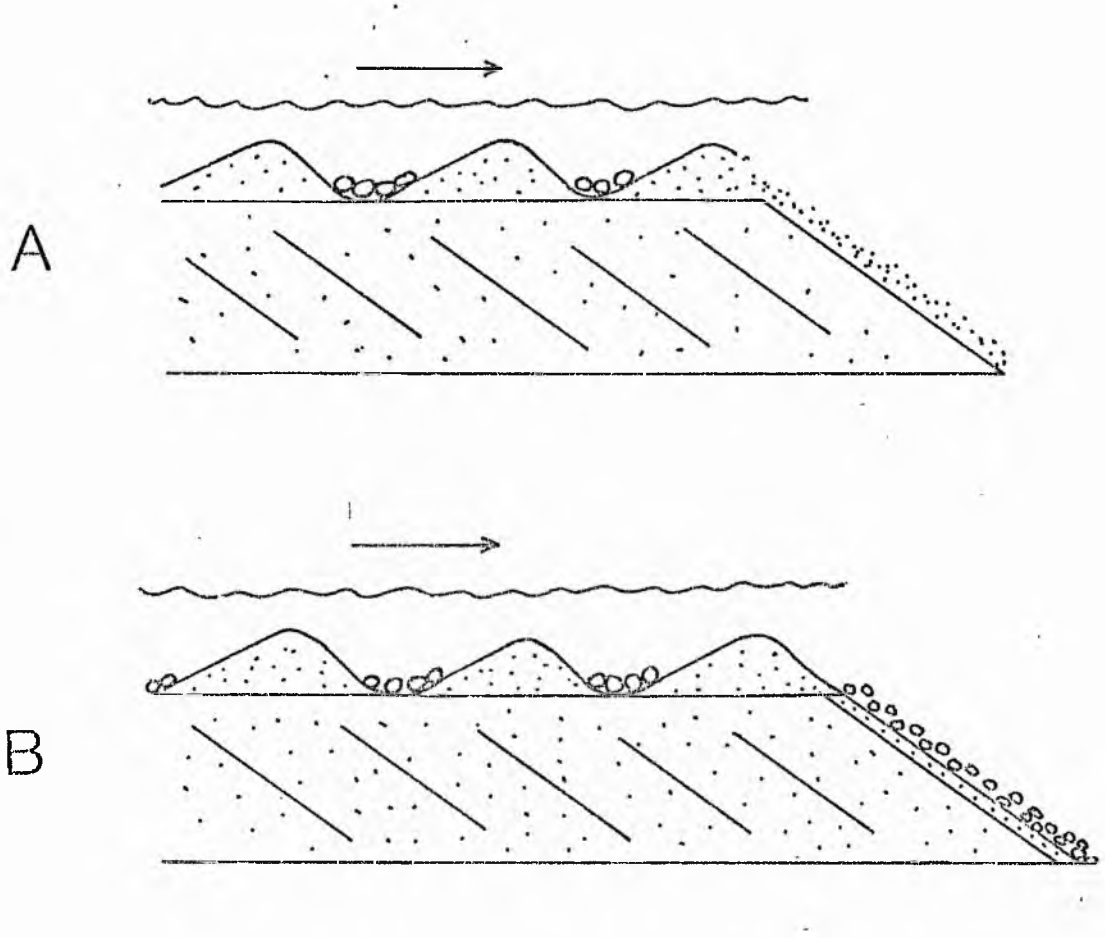

Fig. 2.20 Origin of coarse and fine foresets by continuous avalanching (Smith, 1972).

A - formation of finer forest

B - formation of coarser foreset.

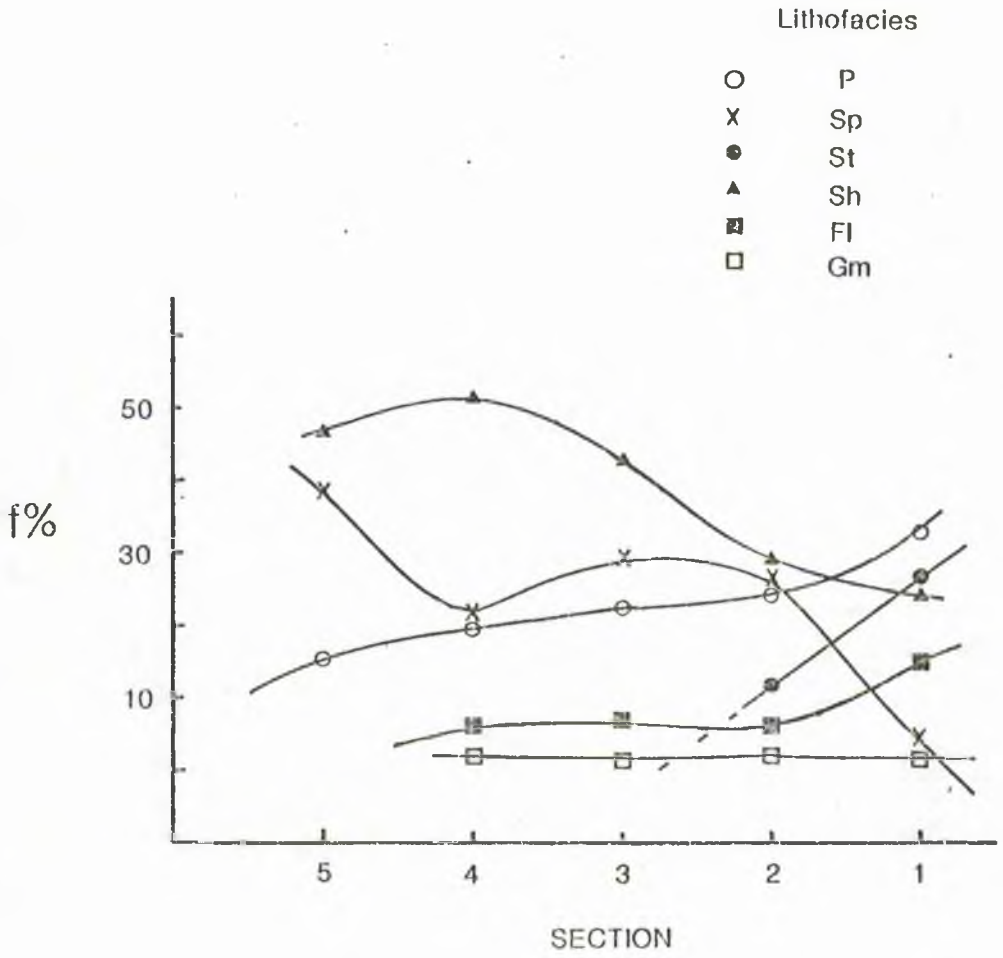

Fig. 2.21 Frequency distribution of lithofacies in the Lr. Old Red Sandstone of Carnoustie.

CHAPTER III

PETROLOGY

Introduction

A significant finding of the present investigations is the displacive growth of calcite in the calcretized sands (lithofacies P). The recognition of displacive calcite is important because it offers insight into paleoclimatic conditions and diagenetic history. This chapter gives an account of the petrology of calcretized and uncalcretized sands separately.

3.1 Petrology of calcretized sands (lithofacies P)

The sandstones are sublitharenites of fine to coarse grain size. The grains are subrounded to subangular and poorly sorted. The sandstone contains an average of 27% quartz (mono and polycrystalline with undulose extinction), 5% chert, 5% feldspars (dominantly orthoclase and microcline with some plagioclase), 10% rock fragments [carbonate (marl), micaceous quartzite, various acidic - basic lavas and intrusive igneous] and 5% micas (mainly biotite with some muscovite; Appendix 3.1). The proportion of calcite cement commonly varies between 35% and 60% (average 48%); and the indurdual grains show a large variation in size from micrite to spar (up to 85 μm). It is this calcite which is here argued to be displacive.

3.1.1 Displacive calcite (DC)

Displacive growth of naturally occurring minerals (eg. gypsum and halite) has long been known but the displacive growth of calcite is still in the realm of speculation. Many workers have been reluctant to accept displacive growth of calcite but the petrographic evidence found in these sediments suggest that calcite grew in this way. Displacive calcite has been described by only a few workers including Allen (1974), Read (1974) and Watts (1978) as micritic coats and fibrous crystals, but the present finding of displacive growth of well developed sparry calcite crystals is unique. Other textural and structural features reported by earlier workers to be related to displacive growth of calcite, such as (I) expansion and floating of clastic grains and (II) swelling and fracturing of host rock are also well preserved in these sediments (Chapter II). Fig. 3.1 represents a generalized section of calcrete profile with zone of displacive calcite at the top.

Sandstones below the lithofacies P are compacted while the sediments within lithofacies P show "floating" of clastic grains in a calcite groundmass (Fig. 3.2). Most of the micaceous grains and polymineralic rock fragments have been expanded to occupy several times their original space (Figs 3.3 to 3.6). Few feldspar and quartz grains have also been expanded, perhaps along fractures (Figs. 3.7 and 3.8). Normally the margins of these separated frements can be visually fitted back together, although due to the orientation of thin section and/or slight corrosion of margins, the visual fitting back is sometimes imperfect.

Under cathodoluminescence the calcite shows distinct growth

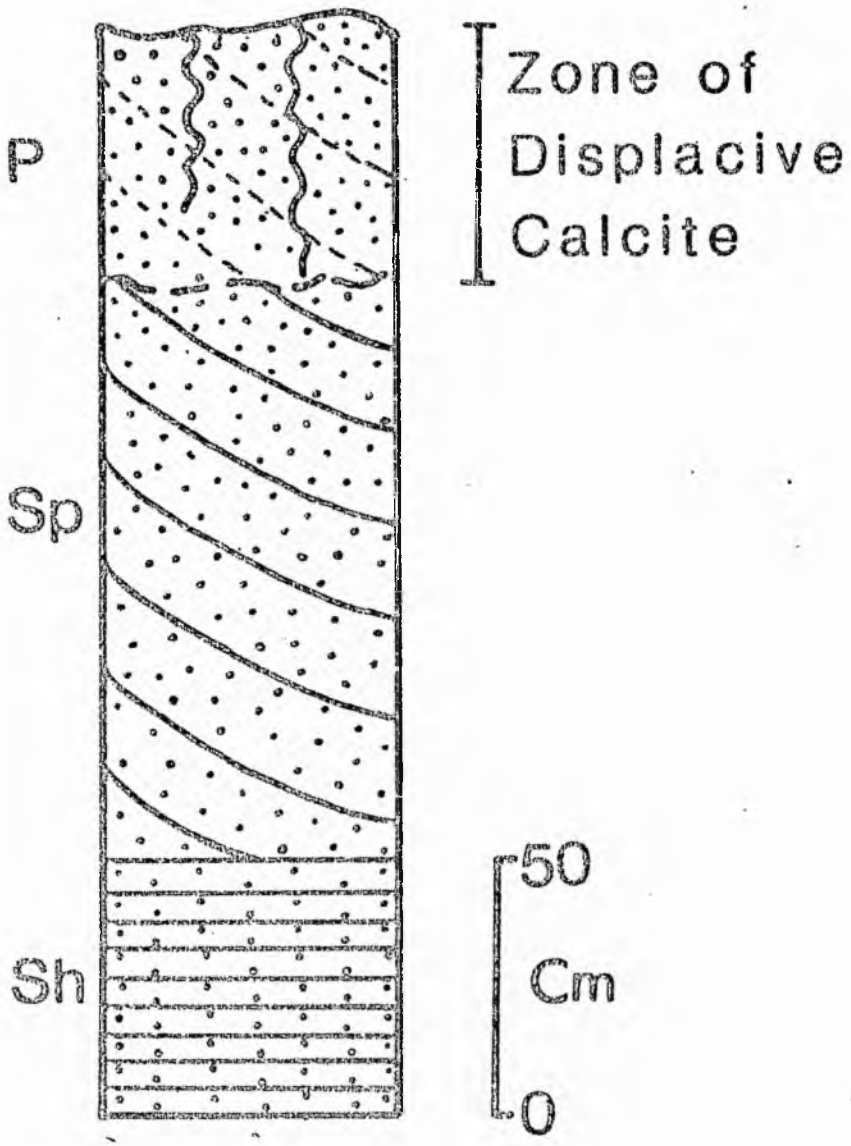

Fig. 3.1. Generalised section of calcrete profile.

bands which record the evolving shapes of calcite crystals. Although most of the crystals are well developed with planar crystal faces some variation in their shape can often be seen (Figs. 3.9 to 3.14). No fibrous crystals could be found. There are a few brighter patches associated with the calcite crystals (Fig. 3.9), filling mainly straight edged residual pores. These brighter patches do not show any growth bands and under plane polarized light are coarse sparry calcite. Brightly luminiscent halos around clastic grains (Fig. 3.15) can also be seen under cathodoluminescence. These halos may border the entire or a part of the grain and are generally seen to be connected with the bright patches described above (Fig. 3.15).

It might be argued that floating texture could be accomplished by replacement of grains but most of the grains are only slightly etched and similar in size to adjacent uncalcretized compacted sands. Hence, the floating texture and expansion of grains in particular is best explained by displacive growth of calcite pushing the grains apart. The visual fitting-back together of separated fragments also favours displacive origin. Besides these, the strongest, new evidence favouring displacive growth of calcite is the crystal morphologies observed under cathodoluminescence as they record the evolving shapes of calcite crystals suggesting that they have grown in confined spaces by displacing the constraining medium. Crystals show both simple (rhomb, lozenge, rectagular) and compound morphologies (Figs. 3.9 to 3.15). The ultimate form of crystals is believed to have been determined by the external forces resisting growth and the accessibility of the material

(Taber, 1916). Fig. 3.16 is a sketch showing successive stages of growth of a few simple and compound crystals as seen in Fig. 9. Crystal B in Fig. 3.16A clearly shows more pronounced growth towards the top (displacing biotite) and right while its growth towards left is much restricted. This is believed to be due to the forces exerted by simultaneously growing crystal A. The pressure exerted by crystal A in this case is transmitted through the fine biotite flake that separates the two crystals. Fig. 3.16B depicts various stages of growth of two crystals that had no barrier (eg. biotite as seen in Fig. 3.16A) between them. Their successive stages clearly demonstrate that during early stages both crystal A and B grew individually as simple rhombs. With increase in size both approached so close to each other that they coalesced along their contact (line C, Fig. 3.16B). Subsequently, both crystals grew together around each other pushing biotite and quartz grains apart. Similarly, if three or more crystals coalesce and grow together, they would eventually form a compound crystal as shown in Fig. 3.16C. The continuous growth by maintaining crystal faces suggests that calcite grew slowly enough to provide sufficient time for diffusion to supply new material to the crystal surfaces and pushed constraining grains out of its way (Taber, 1916). According to Taber (1916), during the growth of crystals, "the tendency is to produce that form which requires the least expenditure of energy, and if the resistance to growth were equal in all directions, the growing body would tend to become spherical; but usually the accessibility of material is an influential, if not the controlling, factor". Hence, the poorly developed crystals in

Figs. 3.11, 3.13 and 3.14 are believed to have grown under conditions where external forces resisting growth were acting from nearly all the directions and/or the accessibility of material was influential.

The fact that crystals can grow by displacing a solid constraint has long been known and was demonstrated experimentally by Becker and Day (1916) and Taber (1916). Recently, Plet-Lajoux et al (1971) have simulated floating texture by displacive gypsum growth. Weyl (1959) emphasized that displacive crystals can only grow from supersaturated solutions as the pressure exerted by growing crystals will cause dissolution due to increase in solubility, hence, there must be a rapid enough inward diffusion of solute towards the mineral to enable it to crystallise and counteract the increase in solubility. Weyl (1959) also calculated that calcite can exert a force of crystallisation "for a one percent supersaturation upto effective normal stress of 10 atmospheres. If supersaturation is high, the stresses against which crystals of calcite can grow will be proportionally higher".

Absence of compaction and excessive amount of calcite (35 to 60%) suggest that displacive cementation occurred during an early stage of diagenesis. The field relationships (Chapter II) suggest that it was generated at or close to the sediment surface. The most likely position for this vertically limited zone of displacive calcite is the vadose zone. Within this, during periods of channel abandonment, rapid surface evaporation on the exposed tops of bars and other bed forms provided the means by which supersaturation was achieved. This led to

nucleation within pores and microspaces such as cleavage planes in detrital micas, between component grains of rock fragments and fractures in clastic grains (Fig. 3.17A). Microspaces and pore throats in particular offer an unusually favourable environment for nucleation as less and less free energy is required (Berner, 1980). After nucleation, the calcite grew by its displacive force of crystallisation exerting an outward pressure causing expansion and dispersal of clastic grains (Fig. 3.17B). It is this displacive growth of calcite which also caused the overall swelling and cracking of the host rock leaving some residual straight edged pores and microspaces between the grain surfaces and surrounding displacive calcite. Taber (1916) also observed residual pores in his experimentally grown displacive copper sulphate crystals. Passively grown sparry calcite cement (PC) with a distinctive bright cathodoluminiscence then filled residual pores (Fig. 3.17B) and microspaces (fringes, Fig. 3.15) around grains. Their similar appearance suggests a single mode of origin although it is possible that some of the fringes represent slight replacement of quartz by calcite. This cement formed from fluids with much lower levels of saturation. The saturation levels remained low as the displacive calcite choked most of the pores and caused significant reduction in the rate of evaporation.

The process of expansion is complex and the precise mechanism controlling the size and geometry of displacive calcite is not wholly understood. Levels of supersaturation and differential stresses under which calcite was growing could have played an important role. Displacive crystals show both

complicated and simple morphologies (Figs. 3.14, 3.10 and 3.9) at times with little corrosion. Morphology is particularly complicated when crystals are smaller and numerous (Fig. 3.16C) whereas larger and fewer crystals tend to show simple geometry (Fig. 3.16A). It is possible that levels of supersaturation caused this difference as too many and tiny crystals would result from fluids with higher supersaturation levels whereas fewer and larger crystals would form from solutions with lesser degree of supersaturation, because it requires more energy to nucleate more crystals then to continue the growth (Berner, 1980). Hence, at places where crystals are few and have grown upto 85 μm, the supersaturation levels must have remained lower than those where calcite is micritic. What controlled this variation in levels of supersaturation is not fully known but it is believed that inhomogeneity within the sediments (eg. grain size, packing and fabric), relief and differential supply of ions could have influenced.

A rough estimate about the levels of supersaturation that existed in these sediments was attempted considering the displacive growth of a calcite crystal 40 cm below the surface. Depth of 40 cm was chosen to keep calculations simple and also as it is nearly the average thickness of the zone of displacive calcite.

Approximate overburden pressure at this depth would be 0.1 bar (taking pressure increase to be 1 bar/4m).

Assuming that calcite can exert a force of crystallization for a 1% supersaturation up to effective normal stress of 10 atmospheres (Weyl, 1959), it would require approximately only

0.1% level of supersaturation for calcite to grow displacively at this depth.

It seems very likely that the actual levels of supersaturation in these sediments might have had remained less than 0.1% as these calculations do not take into account other processes such as moisture swelling and thermal expansion which would reduce the effective stresses against which the calcite actually grew.

3.1.2 Significance of displacive calcite

The above described fabrics of displacive calcite are clearly different from the known fabrics of any cement and neomorphic calcite. Hence, the displacive calcite observed in these sediments is neither a cement nor does it have typical neomorphic characteristics. Watts (1978), described displacive calcite from Kalahari calcretes and asked for refinement in our ideas on the identification of cement and neomorphic calcite or to construct a new class of calcite texture, that is, displacive calcite. In view of the specialized set of conditions required for the displacive growth of calcite, such as supersaturated and near surface conditions, providing insight into depositional environment and diagenetic history, it is here suggested that a separate class of "Displacive Calcite" must be recognized.

Finally, the presence of displacive calcite in fluvial sediments, is strong evidence to support the view that the area lay near the Equator and experienced a dry hot climate, with intermittent wet periods.

3.1.3 Other textures associated with displacive calcite

Floating and brecciation of grains are the dominant textures present in the calcretized sands which have been attributed to the displacive growth of calcite as described above. Other less common textures seen in these sediments include (I) palisade of prismatic crystals and (II) syntaxial overgrowth of calcite.

(I) Palisade of prismatic crystals:

Palisades of prismatic crystals on isolated grains are composed of coarse spar and often associated with etching (Figs. 3.18 and 3.19). These prismatic crystals are oriented perpendicular to the grain surface and usually tend to be of constant thickness around each particular grain although some variation can often be seen (Fig. 3.18). Mostly (approximately 85%) the palisades are developed around basic igneous rock fragments but some quartz grains were also seen to show similar palisades. The palisades are not only more frequent but also clearly better developed around basic igneous rock fragments, whereas, around other grains such as quartz, they are rare and commonly developed only on a part of the grain surface (Fig. 3.19). This might suggest a relationship between calcite palisade growth and the surface properties of the host grain. Similar coats (or Calcitans) have been observed by earlier workers from other calcretes (eg. Jacka, 1974; Kahle, 1977; and Watts, 1977) and three possible modes of origin proposed:

1) Recrystallization of micrite to spar, perhaps triggered by the surface properties of the host grain.

2) Precipitation of spar in gaps around the grains

formed by repeated wetting and drying of the matrix of by displacive growth of calcite.

3) Etching of quartz by calcite produces spar which, with increasing distance from the quartz grain, breaks down to micrite. This hypothesis involves grain diminution (Orme and Brown, 1963) which, with the exception of Wardlaw (1962), has never been convincingly proved, and is, infact, kinetically extremely improbable (cf. Kahle, 1977).

The first two hypotheses are considered most probable but the first one is here preferred, because the palisades are frequently and better developed around possibly more reactive surfaces of basic igneous rock fragments. The second hypothesis would better explain the formation of palisades, particularly around quartz grains and was favoured by Watts (1977). It is here argued on the basis of cathodoluminescence studies that gaps or microspaces around grains were not filled by palisades but by passively grown sparry calcite (PC) forming bright fringes as discussed earlier (see displace calcite).

Randomly scattered patches of coarse calcite in micritic and microspar base are occasionally seen (Fig. 3.20). The coarse calcite has irregular interpenetrant grain boundaries and is considered to be neomorphic spar. This is thought to have formed after burial.

(II) Syntaxial Overgrowth

Syntaxial overgrowth of calcite on carbonate grains can sometimes be seen along with displacive growth of calcite (Fig. 3.21). The carbonate grains acting as substrates are randomly

scattered and thought to have been derived by the erosion of carbonate clasts from adjacent sediments.

The overgrowth is here taken to be cement that grew in lattice continuity with the substrate and hence differs from displacive calcite. The textural relationship shows that overgrowth is earlier than the displacive calcite. Earlier workers including Bathurst (1958,71) and Hatch et al (1938) also considered similar overgrowths to be cements and the use of the term "syntaxial" to indicate lattice continuity follows Goldman (1952).

Theoretically, the important principle is that cement crystals will grow on pre-existing crystals of the same species in the substrate where these exist, even where the nucleus crystal in the substrate is too small to be detected. This attachment of ions to an already existing host substrate as an overgrowth is a function of the free surface energies. According to Berner (1980) the formation of a crystal by precipitation from solution initially requires an increase in free energy and the seed crystals provide a considerable portion of this excess energy needed for nucleation. Hence, it is here believed that during early stages of evaporation, that is when sufficiently higher levels of supersaturation were not attained, the syntaxial overgrowth took place as a part of the required excess energy was provided by the carbonate substrates. Subsequently on rapid evaporation sufficient supersaturation levels were attained that initiated nucleation all over to be followed by displacive growth.

3.1.4 SEM analysis

SEM examination of calcretized sand reveals that displacive calcite crystals form interlocking texture (Fig. 3.22), occasionally leaving micro-lamellar pores between crystals (Fig. 3.22) and along detrital grain surfaces (Fig. 3.23). When these microspaces have been filled with passive calcite are believed to have formed bright fringes around grains observed under cathodoluminescence (see displacive calcite). Sometimes slight corrosion of grains can also be seen. Generally the porosity in calcretized sands is almost nil apart from microporosity just described and irregular fractures within calcite crystals (Fig. 3.24). Often, displacive calcite crystals show straight edged triangular · and/or rectangular pits of less than 10 μm size on their smooth surfaces (Fig. 3.24).

No authigenic clays were found towards the top of the zone of displacive calcite (facies P). Scattered development of smectite and/or illite have been found in samples near the base of lithofacies P. The clays occur in those profiles where the base of facies P is gradational into the underlying facies. Fig. 3.25 is a close up of a grain seen on the right side of figure 3.22 and shows flakes of illite bridging across the pore. No palygorskite or sepiolite was found.

A little silica overgrowth forming euhedral outlines on a few grains was also observed.

3.2 Petrology of uncalcretized sands (lithofacies Sp,St,Sh and Fl)

The uncalcretized sands differ significantly from calcretized in respect of their carbonate content, authigenic clays aud textural properties. In contrast to lithofacies P, these are slightly compacted (Fig. 3.26). Mineralogically they are sublitharenites of silt to coarse grain size. The grains are subangular to subrounded and poorly sorted. Sandstones contain on an average 52% quartz (mono and polycrystalline with undulose extinction), 6% chert, 7% feldspars (dominantly orthoclase with some plagioclase), 5% micas and 9% rock fragments (quartzitic, various acidic - basic lavas and intrusive igneous and carbonate; Appendix 3.2). Authigenic clays (dominantly smectite with some mixed layer smectite - illite form fringes around detrital grains and constitute approximately 4% of the rock. The proportion of calcite cement varies between 5% and 20%, depending upon the degree of dissolution. Secondary porosity formed dominantly by dissolution of calcite cement and some unstable grains varies from <5% to a maximum of 12%.

3.2.1 Authigenic silica

Authigenic silica occurs most commonly as overgrowths on some quartz and chert grains forming euhedral outlines (Fig. 3.27 and 3.28). It was also seen to be filling a few isolated reduced pores. Authigenic silica as overgrowths, although present in all lithofacies is volumetrically insignificant. The time of quartz overgrowth in these lithofacies can be established by reference to hematite coats.

3.2.2 Hematite coats

Hematite occurs as grain coatings and scattered blebs (Figs. 3.27 to 3.30). It is here taken to be of authigenic origin and the evidence for that comes from its physical relationship particularly with quartz and chert overgrowths. Hematite is clearly seen to be coating euhedral outlines of quartz and chert grains formed by authigenic overgrowths (Figs. 3.27 to 3.29). Also hematite is commonly absent at places of contact between grains (Fig. 3.28). Both these features imply that the hematite coatings were formed subsequent to silica overgrowths during early diagenesis. At times irregular scattered blebs of hematite partially filling the pores can also be seen (Figs. 3.28 and 3.30). The hematite gives these sediments their red colouration. The cause of its absence from the zone of displacive calcite is discussed later.

3.2.3 Authigenic clays

Authigenic clays start appearing near the base of lithofacies P but are best developed towards the base of the profile. Here they occur as poorly to very well developed rims of uniform thickness (app. 10 μm) and surround most of the grains (Fig. 3.27, 3.28 and 3.30). Only where the grains are in contact the clay rims are absent, eg. note the absence of both hematite and clay rim at the concavo-convex contact between a chert (right side) and quartz (left side) grain in the lower central part of figure 3.28. This suggests that both hematite and clay must be post-depositional and therfore authigenic.

That clay rims grew subsequent to the formation of hematite is evident from the fact that the clays can be seen growing on the hematite coatings (Figs. 3.27 and 3.30). Clay rims can even be seen enveloping hematitie bleb (top central area, Fig. 3.30).

The clay rims are composed wholly or dominantly of smectite: often some mixed layer smectite/illite is also present. Other authigenic clays are very rare but include illite, chlorite and kaolinite. No palygorskite or sepiolite was found.

3.2.4 Calcite cement

Sediments below the zone of displacive calcite are cemented with poikilitic calcite (Figs. 3.31 and 3.32). It fills all the residual pores left after the formation of clay fringes. Detrital grains have frequently been etched or partially replaced by the calcite, sometimes leaving a ghost of the grain (Fig. 3.32). Under cathodoluminescence the calcite is generally brightly luminescent (Fig. 3.33) but does show some variation. The variation in luminescence is random and sometimes can be observed even within a sparry calcite crystal (Fig. 3.34). In contrast to displacive calcite it does not show any zoning (Fig. 3.34). Random variation in luminescence is believed to be due to random distribution of Fe and/or Mn in the calcite. Texturally and luminescence-wise it resembles with passive calcite cement (PC) present in the zone of displacive calcite and is considered to be phreatic (P). It is possible that they may have genetic link.

3.2.5 Secondary porosity

The porosity present in these sediments is all secondary and has formed by dissolution of calcite cement and other unstable phases such as rock fragments and feldspars. It is commonly patchy, particularly in finer sediments although in coarser sediments it is sometimes uniform due to more extensive dissolution. Generally the pores are irregular and reduced (Fig. 3.27) with clay outlines and are not well connected. Scattered enlarged and vug-sized pores are also present in some coarser samples (Fig. 3.29). Clay fringes have also been either partly or completely removed in some places, particularly where pores are enlarged and vug sized (Fig. 3.29).

3.2.6 SEM analysis

SEM examination reveals that authigenic clays have developed diagenetically in a majority of the samples. Although they show random variation within and between profiles, generally they are more abundant towards the base and centre of the profiles. Sometimes lithofacies type seems to control their formation as they are commonly better developed in medium to coarse grained sediments. Smectite is most abundant and sometimes exclusive. It occurs as both grain coating and pore fillings, hence, has largely modified pore size and shape (Fig. 3.35). Smectite may occur with a little illite on detrital grains surfaces forming fringe of uniform thickness (app. 10 μm, Fig. 3.46). Such pore linings cause destruction of permeability by choking pore throats. Smectite normally occurs as wavy flakes showing smooth

fusing of adjacent arms forming honeycombed texture (Figs. 3.37 and 3.38). In figure 3.38 note that smectite is showing preferred orientation and increase in size towards the centre of the pore forming coarser boxwork texture in the centre. This preferred orientation and size variation is similar to that known from carbonate cements (Bathurst, 1975). Smectite is sometimes seen to be partially engulfed in quartz overgrown faces (Fig. 3.39). This suggests that some quartz overgrowth and smectite formation were going on simultaneously during early diagenesis.

Sometimes clay rims are composed of mixed layer smectite/illite (Fig. 3.40). They are very similar to smectite fringes both in size and in modifying pore geometry. In Figure 3.40, note that illite in the centre is bridging across the pore and causing almost complete choking of the pore throat. An authigenic feldspar crystal that grew after clay formation can also be seen in the top left corner. Illite flakes with wispy terminations have also been found to be abundant in a few samples (Fig. 3.41). Chlorite occurs as finely crystalline plates sometimes aggregated into rosette-like clusters (Fig. 3.42). It is also possible that these rosette-like clusters are of hematite as identification was not confirmed with EDX.

Authigenic feldspar (Fig. 3.43 and 3.44), quartz (Fig. 3.44) and kaolinite (Fig. 3.45) have also developed in some samples. Feldspar crystals vary in size from 5 μm - 20 μm and rest on smectite flakes (Fig. 3.43). Seldom feldspar crystals partially engulf smectite flakes (Fig. 3.44) suggesting their simultaneous growth. Quartz crystals vary in size from 2 μm to 10 μm (Figs. 3.44 and 3.46) and occur either within the

microspaces between smectite flakes (Fig. 3.44) or like feldspars rest on them (Fig. 3.46). Curved vermicular stacks of kaolinite succeeding smectite can sometimes be seen (Fig. 3.45).

Detrital feldspars occasionally show smooth (Fig. 3.47) and/or embayed (Fig. 3.48) V-shape pits on their surfaces. Feldspar grain in Fig. 3.48 shows alteration into clays and enlargement of pits during diagenesis.

3.2.7 X-ray diffration studies

Five selected samples from the base of different profiles were subjected to X.R.D. analysis. Procedure of analysis is given in Appendix 3.3. The X-ray diffraction patterns reveal that smectite is the chief mineral constituent with prominent reflection between 14 to 15 $\AA^{\circ}$ and a diffused tail down to 10 $\AA^{\circ}$ (Fig. 3.49). Reflection near 17 $\AA^{\circ}$ represents expansion of 001 with ethylene glycol. It is often taken that a 14 $\AA^{\circ}$ smectite belongs to the Ca varieties with two H20 molecules while Na varieties with one H20 molecule show 12 $\AA^{\circ}$ reflections (Thorez, 1976). The occurrence of Ca-smectite is quite logical as abundant Ca was available (evidenced by calcretization) in the pore waters while Na was depleted (see Chapter IV). Other clays identified include illite, chlorite and kaolinite. No palygorskite or sepiolite was identified.

3.3 Diagenetic history of calcretized sands

The paragenetic sequence displayed by calcretized sands is:

1) Quartz - chert overgrowth
2) Hematite and authigenic clays ±
3) Syntaxial calcite overgrowth
4) Displacive growth of calcite
5) Passive calcite cement (PC)
6) Palisade and necmorphic spar development
7) Formation of calcite veins

Early quartz and chert overgrowth forming euhedral outlines was observed only on a few scattered grains and is volumetrically insignificant. It is believed that immediately after channel abandonment low pH and temperature conditions existed during which a little silica cementation as quartz and chert overgrowth occurred.

Generally hematite coats and authigenic clays are absent, however, when present they show very uneven distribution and are volumetrically insignificant. In a few samples near the base of lithofacies P, a little smectite/illite was seen to have developed. These clays are believed to have developed due to pore water reactions altering unstable grains such as feldspars and rock fragments. The appearence of clays in the vertical profiles perhaps marks the transition between lithofacies P and underlying uncalcretized sands.

Absence of hematite in calcretized sands is significant as it accounts for the decoloration of sediments towards the top of profiles. According to Walker (1967), sediments in hot dry climates are especially susceptible to red bed formation, because, they are normally in areas of low water table and

alkaline ground water. Under these conditions, the Eh and pH of the interstitial environment both above and below water table will favour formation and preservation of hematite. However, the absence of hematite coatings in calcretized sediments could be explained in two possible ways:

(a) Hematite was formed but subsequently replaced by calcite during calcretization. The fact that most of the detrital grains are either not or only slightly corroded negates this possibility. Also, bright fringes observed under cathodoluminescence (Fig. 3.15) and microspaces between grain surfaces and adjacent displacive calcite crystals observed under SEM (Fig. 3.23) suggests original mismatch between the two surfaces which would be difficult to explain if replacement of hematite by calcite is sought. In addition, the common occurrence of highly unstable but unaltered mafic rock fragments may also be difficult to explain if complete replacement of hematite by calcite is suggested.

(b) Hematite was never originally formed in these sediments. This possibility is here preferred as the critical factors i.e. Eh and pH controlling hematite formation would have been different in the top and bottom sediments of these profiles. The interstitial environment in the top sediments immediately following deposition might have been less alkaline and lay in the stability field of ferrous ions (Fig. 3.50). Hence, released Fe remained in solution and migrated with the interstitial water. On the other hand, alkalinity was high at the base causing iron precipitation initially as ferric hydrate, but ultimately formed hematite on ageing (Walker, 1967). Higher alkalinity at the base

is supported by the presence of smectite - smectite/illite fringes (Deer et al, 1962 and Millot, 1964). What caused this variation in alkalinity is not wholly understood but believed that it increased with time due to continuous evaporation and addition of alkali ions by intrastratal alteration of unstable rock fragments and minerals.

The third stage of diagenesis involved syntaxial growth of calcite on a few scattered carbonate grains (Fig. 3.21). It is believed to have occurred during early stages when evaporation had just begun and higher levels of saturation were not attained. This hetrogeneous nucleation can simply be considered as pure crystal growth as the seed is of the same mineral which acted as a template of similar atomic spacing, and hence, promoted the precipitation in optical continuity (Berner, 1980).

With continuous rapid evaporation influenced by hot sunlight, supersaturated conditions were soon generated, leading to crystallization and displacive growth of calcite. The displacive growth of calcite marks the major and fourth stage of diagenesis. It is responsible for expansion and floating of detrital grains and swelling and fracturing of host rock. The process of expansion is complex and shows variation in both micro and macroscopic scales. (See displacive calcite for details).

During fifth stage of diagenesis calcite precipitated passively (PC) in residual pores and microspaces around detrital grains (Figs. 3.9 and 3.15). This cement is believed to have formed from fluids with much lower levels of saturation. The saturation levels remained low, because, displacive calcite choked most of the pores and caused significant reduction in the

rate of evaporation.

By now the sediments were lithified and had been converted into a hard compact rock which on burial underwent the following changes.

Palisades of prismatic crystals around isolated detrital grains and a few randomly scattered patches of coarser calcite in micritic or microspar base were formed during the sixth stage of diagenesis and are considered to be neomorphic features formed during burial (see palisades for details).

Irregular cracks and sharp partings, sometimes showing strong parallelism and preferred orientation were developed during tectonic activity. These were subsequently filled with sparry centripitally grown calcite forming calcite veins.

3.4 Diagenetic history of uncalcretized sands

Although uncalcretized sands show some variations in their diagenetic events, in general they display the following paragenetic sequence:

1) Quartz and chert overgrowth
2) Iron oxide precipitation forming aureoles around grains and a few blebs
3) Authigenic clays forming rims
4) Authigenic feldspar, quartz and kaolinite formation
5) Carbonate (calcite) cementation
6) Compaction
7) Dissolution of carbonate cement and other unstable phases forming secondary porosity.

Early quartz and chert overgrowth formed euhedral outlines on some grains. Volumetrically it is insignificant but is more common than in overlying calcretized sediments. It is believed that silica cementation occurred under similar physico-chemical conditions as in calcretized sands during early diagenesis. The source of the silica is normally difficult to explain. Many workers, including Heald (1959), Thomson (1959) and Füchtbauer (1967) have invoked pressure solution as the principal source but the present petrographic evidence does not favour this. It is here believed that groundwaters contributed much of the silica although some might have been added through the downward percolating fluids as calcretization of overlying sediments caused slight corrosion of detrital grains increasing the silica content of pore fluids.

Hematite coatings give rise to the characteristic red colouration of the red beds. They are believed to have formed during early diagenesis by intrastratal alteration of iron bearing minerals, such as hornblende, biotite, olivine, augite and volcanic rock fragments. The Fe released from these unstable minerals was probably transported initially in solution as ferrous ions, but in the favourable Eh - pH conditions precipitated as ferric hydrate which upon ageing converted into hematite (Walker, 1967).

The third stage of diagenesis involved the formation of clay rims, dominantly smectite. Precise mode of formation and source for these clays is not known but they are believed to have formed from solutions produced by the post-depostional breakdown of

volcanic rock fragments and ferro-magnesian minerals. The presence of smectite fringes in these sediments is of considerable interest. Firstly it is a rare example of an occurrence in Lower Devonian times and suggests that these sediments were never buried deep enough to cause the alteration of smectite. Secondly, it questions the role of plant cover (suggested by Weaver, 1967 and later emphasised by Bjørlykke and Jørgensen, 1976) in their formation. According to Weaver (1967) smectite is either rare or absent in Lower Paleozoic sediments excluding bentonites. Hence, the presence of well developed smectite fringes (Figs. 3.35 and 3.36) in these sediments makes them a rarity and also suggests that the sediments were buried to a maximum depth of approximately 2500m (Dunoyer De Segonzac, 1970; Fig. 3.51).

Weaver (1967) examined the clay mineral content of Precambrian to Pliocene sediments and established that a major change in the makeup of the clay mineral suite occurred relatively abruptly in the Upper Mississippian. He observed that smectite is relatively insignificant before the Upper Mississippian but the post - Upper Mississippian sediments are dominated by smectite, mixed layer smectite-illite and kaolinite. Weaver (1967), suggested that the most likely controlling factor for this change is the extensive development of plant life. Recently, Bjørlykke and Jørgensen (1976) have emphasised the importance of a vegetation cover in smectite formation and thus questioned whether smectite could have formed in Lower Paleozoic times before the development of a plant cover.

The necessity of plant cover is here questioned and smectite fringes are believed to have formed from alteration of volcanic and basic igneous material during pedogenesis. It is more than likely that primitive organisms existed in these sediments and they may have been instrumental in the formation of the fringes. The possibility of existence of organisms in these sediments is based on the light stable isotope ($\delta^{13}C$ -4.72 to -6.93 ‰ and $\delta^{18}O$ -6.96 to -9.9 ‰ PDB - Chapter IV) values obtained from the associated calcite cement, although it could also be due to late diagenetic contamination. It is not known whether the smooth circular markings observed on grain surface (Fig. 3.52) could be organic signatures or not.

Products of the fourth stage of diagenesis show very patchy distribution and may even be absent. They include authigenic feldspar, quartz and kaolinite (Figs. 3.43, 3.46 and 3.45). Their random occurrence is believed to have been controlled by local variations in the composition of the pore fluids and their restricted circulation due to choking of pore throats by clay fringes. Hence, sometimes pores within the same and/or different samples show simple or multiple stages of cements. Pores with simple cement stratigraphy show complete occlusion of the residual pore (left after smectite growth) by carbonate cement (Fig. 3.53). Pores with multiple stages of cement show some variation in their sequence. A single sequence describing relative timings of development of feldspar, quartz and kaolinite could not be established as they were never found to occur together. It is at least clear that all these mineral species postdate smectite fringes and predate carbonate cement. The

mechanism for the growth of the authigenic minerals is believed to have been the hydrolysis of detrital silicates by alkaline intrastratal solutions; a process suggested earlier by Walker and Waugh (1973) and Walker (1976) for the development of authigenic mineral assemblages in continental red beds. It is believed that following the development of iron oxide and smectite fringes the pore waters were depleted in Fe, Mg, K,Al and Si ions. However, the depletion was not total because the subsequent phase resulted in the precipitation of feldspar, kaolinite and quartz in some places. After the precipitation of the above mentioned authigenic minerals, the pore waters would have been preferentially enriched in calcium and bicarbonate ions. This would have led to the eventual precipitation of the calcite cement occluding all the available pore spaces and sometimes corroding detrital grains. It is possible that the poor development or absence of clay rims in some places is due to their partial to complete replacement by calcite cement. It is also possible that calcite cement did not precipitate in some pores which were totally sealed off by clay rims.

The petrographic evidence (poikilitic texture) reveals that the calcite cement is phreatic spar (P) formed possibly as a result of slow regular crystallization from permanently saturated pores. The poikilitic texture and overall uniform luminescence without any zoning (Fig. 3.33) suggest slow and easy crystallization in a phreatic environment. This is consistent with Folk's (1974) ideas that vadose diagenesis results in more rapid precipitation (higher rate of CO2 loss, Land, 1970; - as observed in the zone of displacive calcite) or less easy

crystallization than in phreatic environment. In addition, the geochemical data including trace element shows similarity that would be expected of phreatic environments (see Chapter IV).

Compaction caused slight grain interpenetration, bending of micas (Fig. 3.26) and sometimes fracturing of grains (Fig. 3.35). Most of the grains show only indentation of their margins by means of plastic deformation (Fig. 3.28). Besides physical midifications, some of the smectite is believed to have altered into illite by combining with feldspars during burial. Chemically K-feldspar provides the necessary Al and K for the conversion of smectite to illite in the mixed layer clays. Excess silica formed quartz while Fe and Mg formed chlorite as per the following reaction (Bjørlykke, 1983).

Smectite + K feldspar = illite + chlorite + quartz

This would explain the formation of chlorite and associated quartz observed in some places (Fig. 3.42).

The last stage of diagenesis involved formation of secondary porosity by dissolution of calcite cement and other unstable grains. Generally the dissolution has been partial and patchy, but at places vuggy porosity has also developed due to extensive dissolution of calcite cement and unstable minerals. To understand the mechanism of formation of secondary porosity in these sediments, all possible known processes were assessed excluding leaching by CO2 from maturing kerogen. These include

(a) Leaching by meteoric water and

(b) Transformation of smectite and kaolinite to illite

Of these, the second process is here considered to be more likely or at least playedadominant role, because, the secondary

porosity is present mainly in the uncalcretized sediments while the calcretized sands (lithofacies P) show insignificant or no dissolution. Leaching by meteoric water would have caused more dissolution in calcretized sediments not only because they are rich in calcite but also as the circulation of dissolving fluids would be much restricted in uncalcretized sediments due to choking of pore throats by clay fringes. Besides the restriction of secondary porosity to uncalcretized sediments, partial and patchy dissolution and common occurrence of highly unstable mafic rock fragments would be difficult to explain if leaching by meteoric water is suggested. Hence, transformation of smectite and kaolinite during late diagenetic stage is believed to have been the dominant process if not exclusive. During transformation smectite and kaolinite capture cations and release protons (H^+) as per following reactions (Bjørylykke, 1983), causing acid products. These acid products later dissolve other minerals, particularly carbonate and feldspars to form secondary porosity (Bjørlykke, 1983).

$$\text{Smectite} + K^+ + Al^{3+} \rightarrow \text{illite} + \text{quartz} + H^+$$

$$\text{Kaolinite} + 2K^+ \rightarrow \text{illite} + 2H^+ + 3\ H_2O$$

Fig. 3.2. Photomicrograph showing floating of clastic grains in calcite groundmass. Note that grains are only slightly etched. Plane polarized light. Scale bar equals 200 μm.

Fig. 3.3. Photomicrograph showing highly expanded biotite to form a concertina like structure, owing to displacive calcite growth. Floating of clastic grains in calcite groundmass can also be seen. X nicols. Scale bar equals 200 μm.

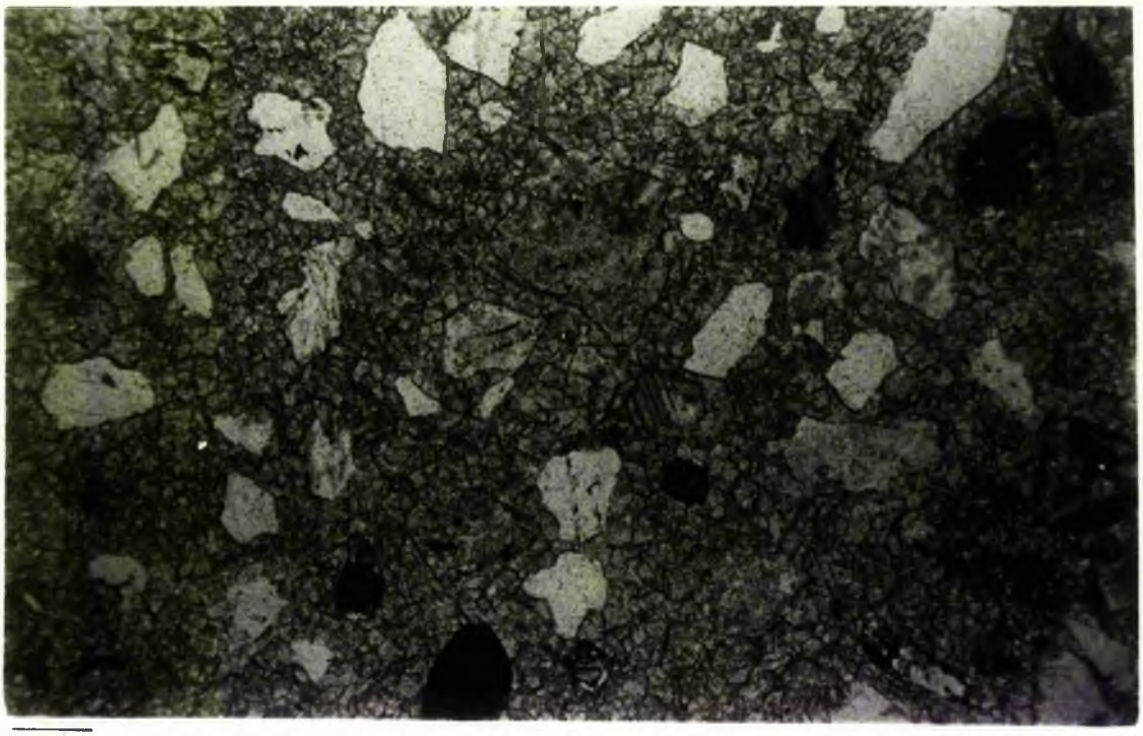

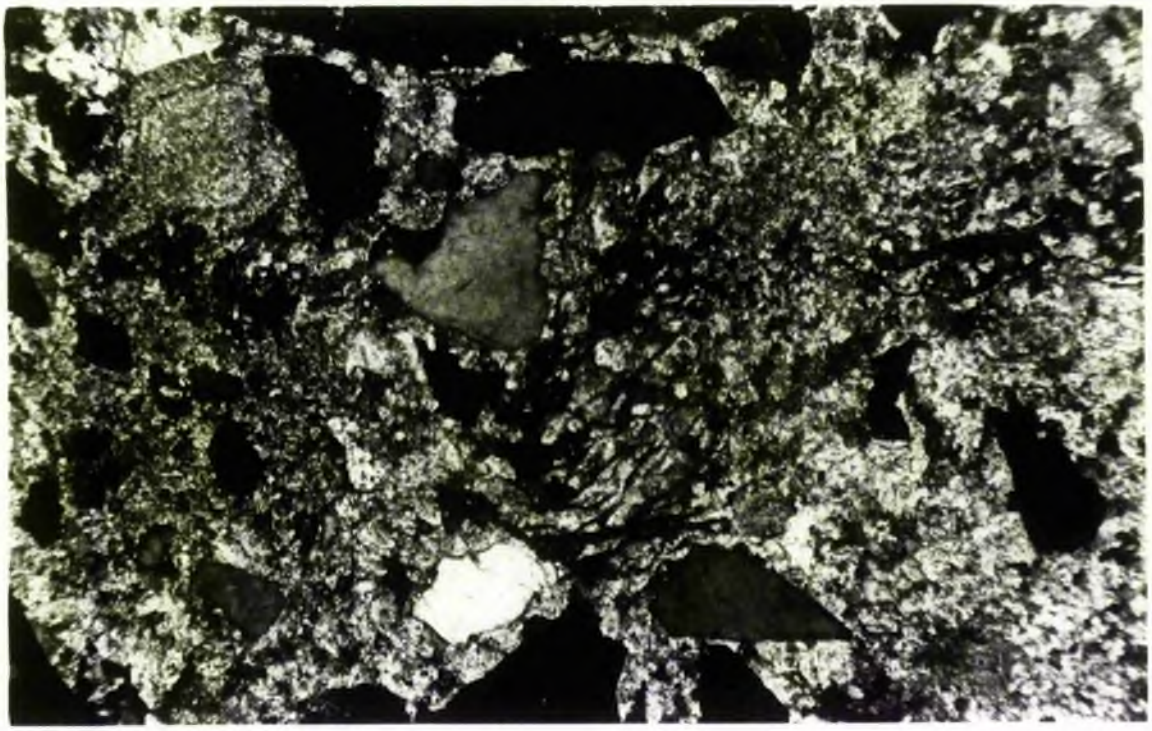

Fig. 3.4. Photomicrograph showing a biotite flake beginning to expand from the right side due to displacive growth of calcite. Plane polarized light. Scale bar equals 100 μm.

Fig. 3.5. Expanded quartzitic rock fragment. Note that fragments towards the top are comparatively less displaced and can easily be fitted together. X nicols. Scale bar equals 100 μm.

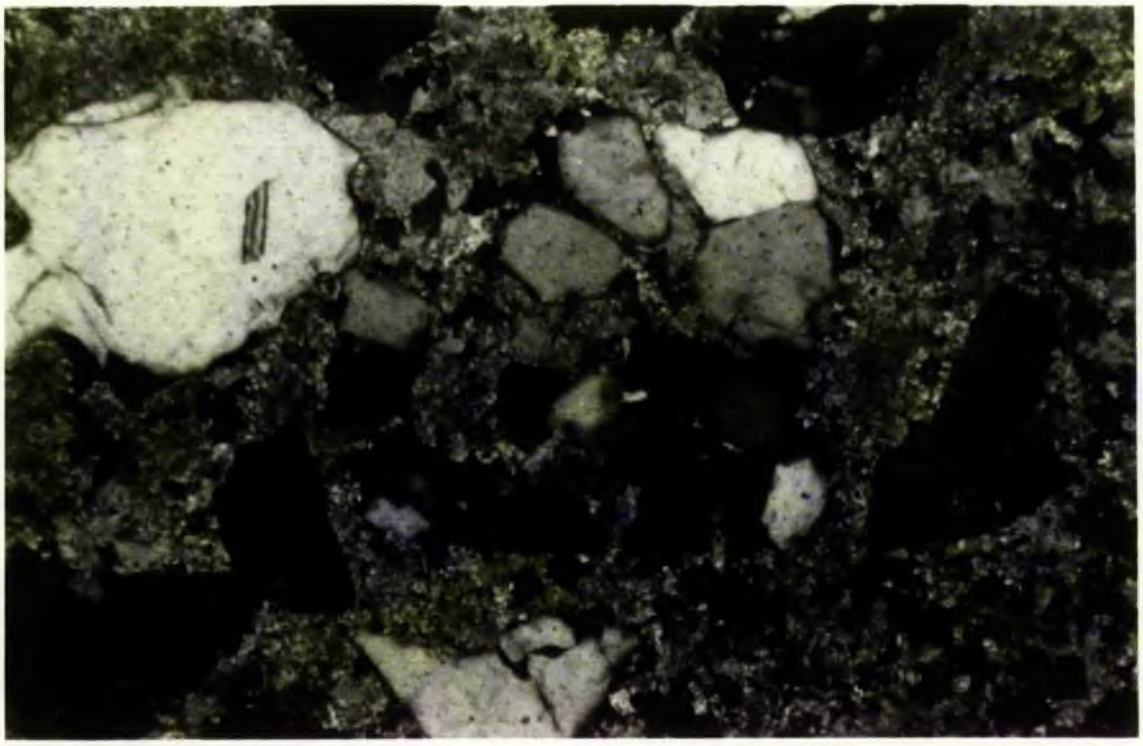

Fig. 3.6. Photomicrograph showing slightly expanded quartzitic rock fragment. Although other rock fragments have been highly expanded the photomicrograph shows one which is only slightly expanded; this has been intentionally chosen to demonstrate that the fragments may be fitted together. X nicols. Scale bar equals 100 μm.

Fig. 3.7. Plagioclase feldspar expanded along a fracture by displacive growth of calcite. X nicols. Scale bar equals 100 μm.

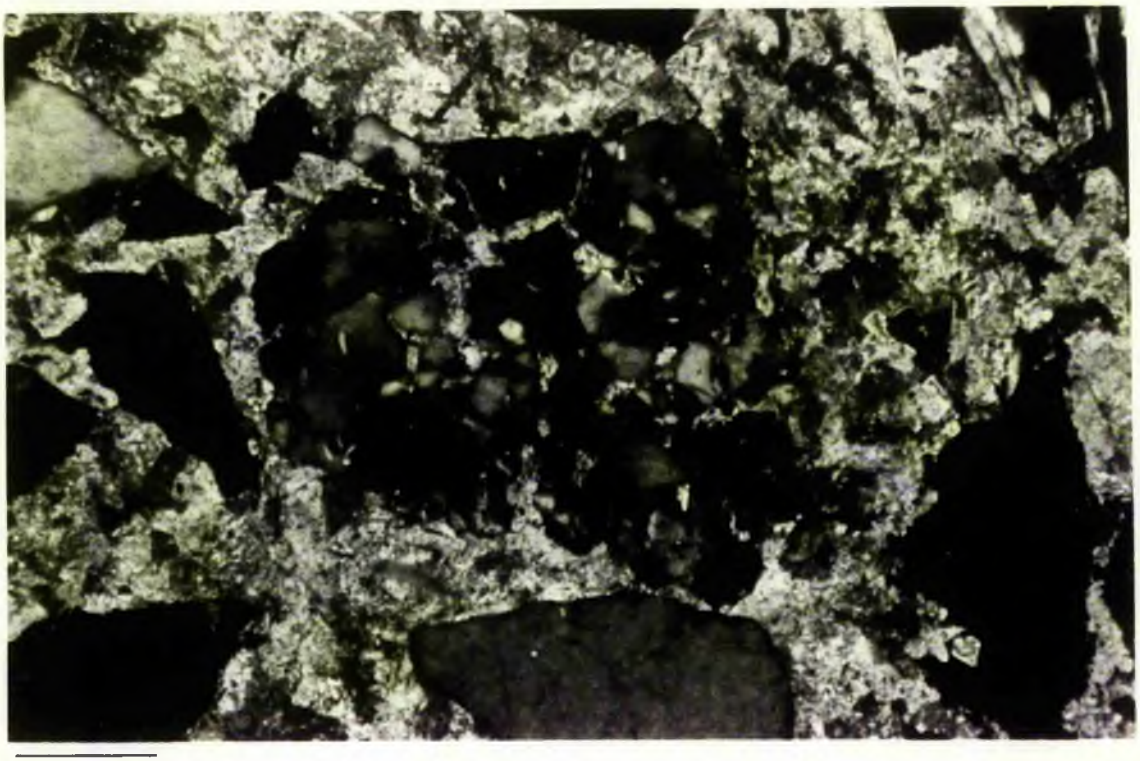

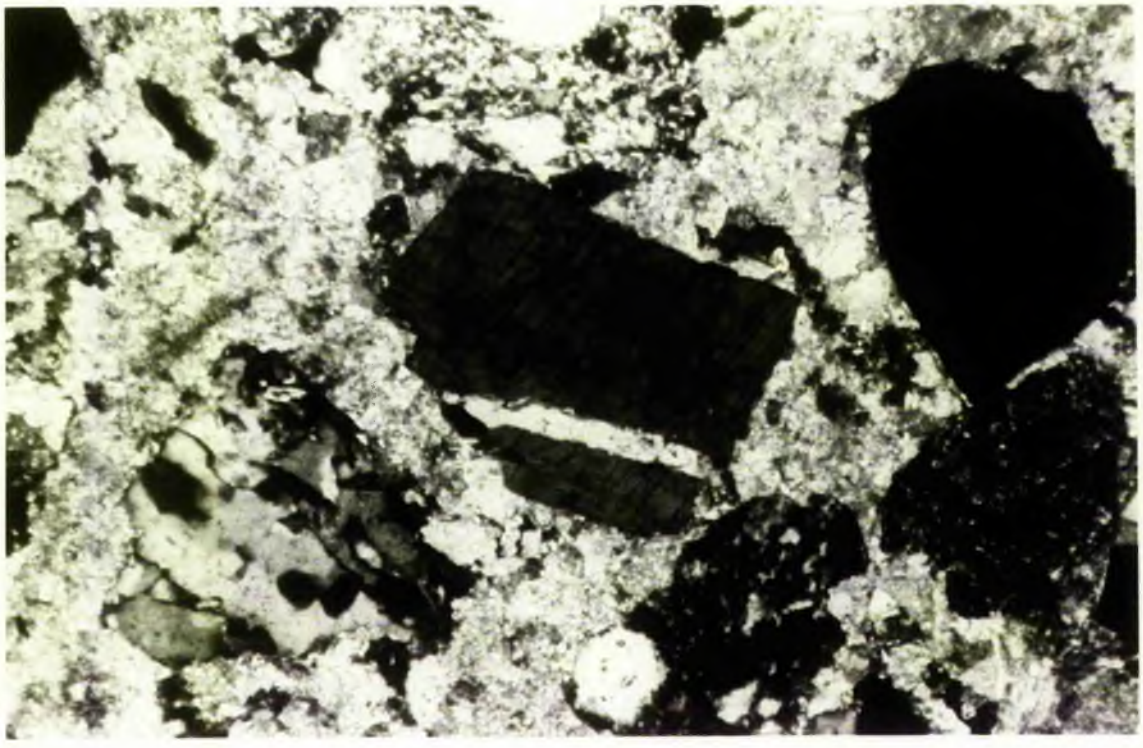

Fig. 3.8. Quartz grain with fragments separated due to displacive calcite growth. Note that the grain is only slightly etched and separated parts may be fitted together. X nicols. Scale bar equals 100 µm.

Fig. 3.9. Under cathodoluminescence displacive calcite reveals growth bands with morphologies that suggest it is not a passive pore filling cement but have grown in confined spaces (from supersaturated solutions) by displacing the constraining medium. Photomicrograph shows expansion of biotite by well developed simple and compound calcite crystals. Crystals in squares A, B and C have been sketched (see Fig. 3.16) to demonstrate the formation of a few simple and compound crystals. Brighter patches showing uniform luminescence (PC) represent passive calcite. Scale bar equals 50 µm.

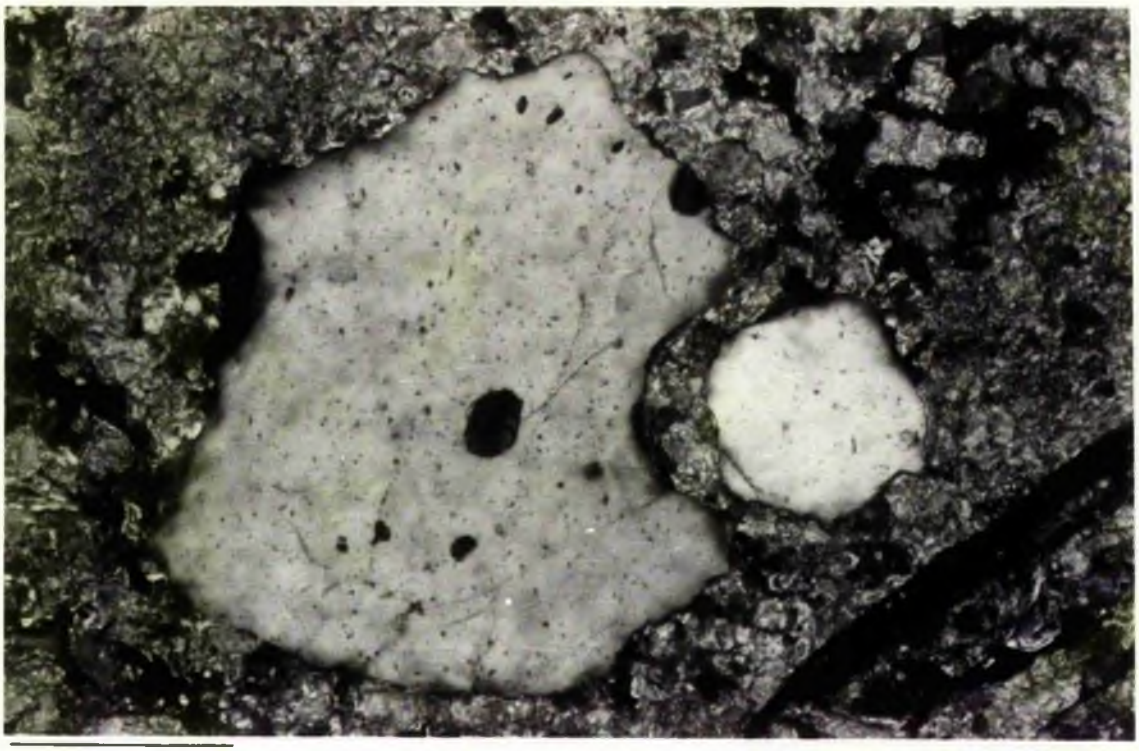

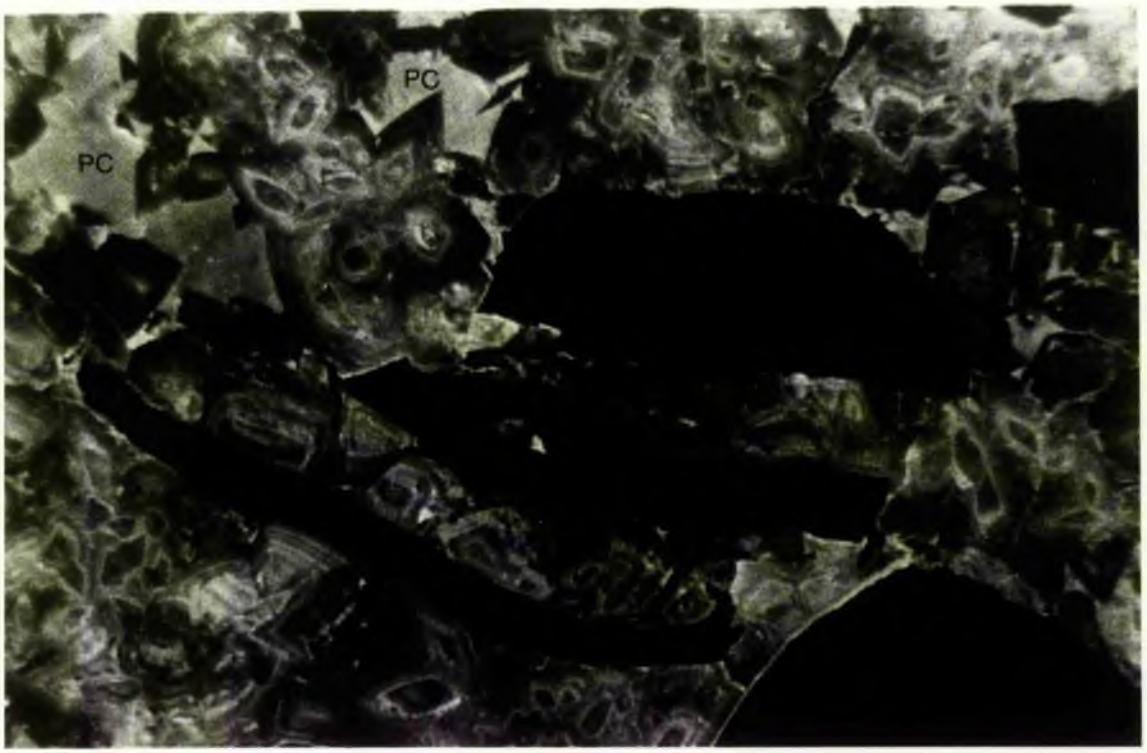
PC
PC

Figs. 3.10 and 3.11. Highly expanded biotite flakes under cathodoluminescence. Note variation in shape and size of displacive calcite crystals. Scale bar equals 50 μm.

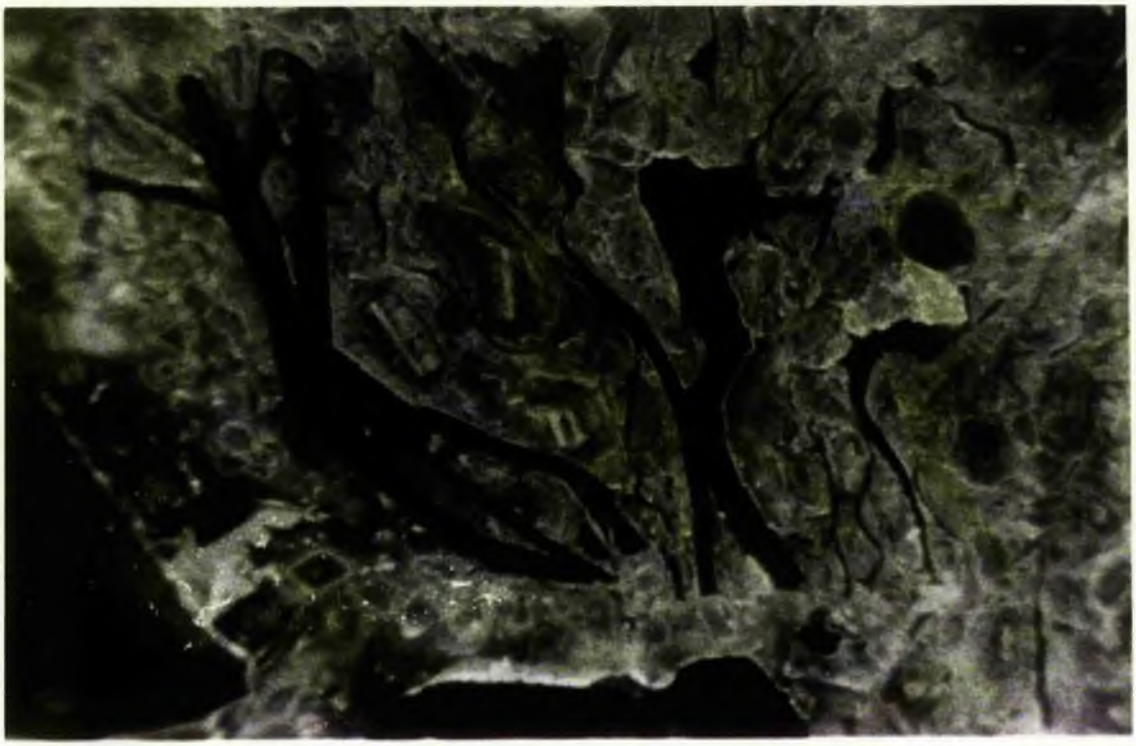

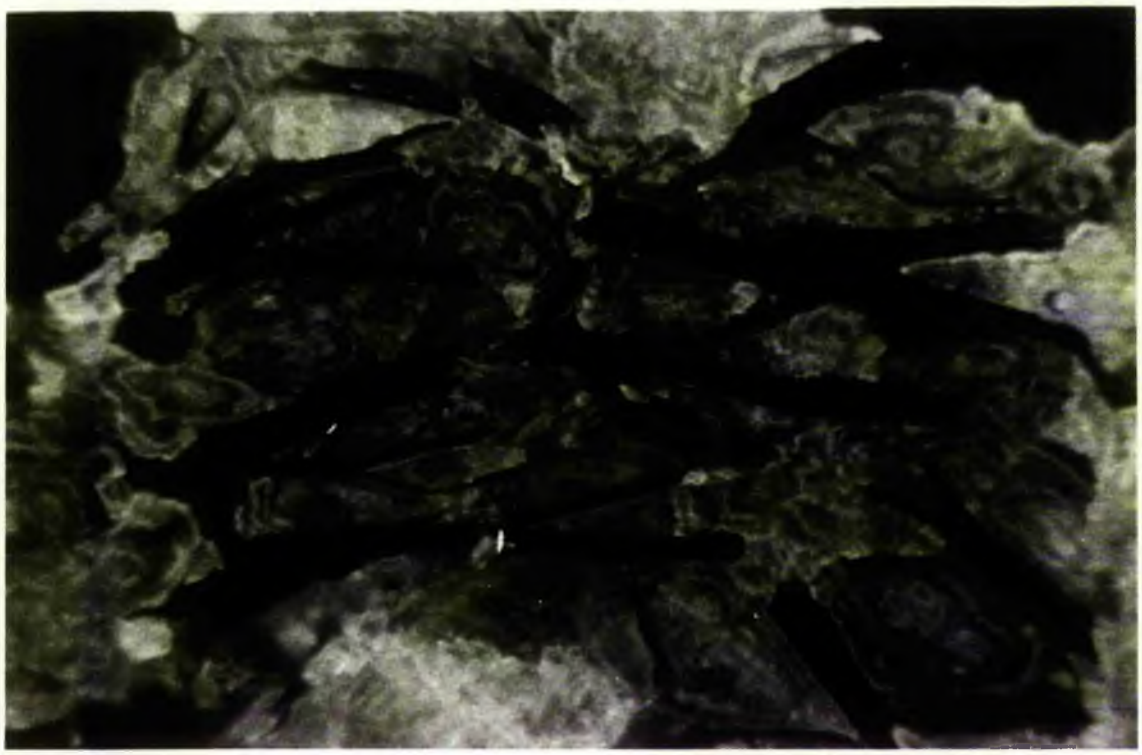

Figs. 3.12 and 3.13. Expanded biotite flakes under cathodoluminescence. Note variation in shape and size of the displacively grown calcite crystals. Biotite flake in Fig. 3.12 is slightly corroded at a few places but sharp outlines of biotite in Fig. 3.13 allows no possibility of replacement. Scale bar equals 50 μm.

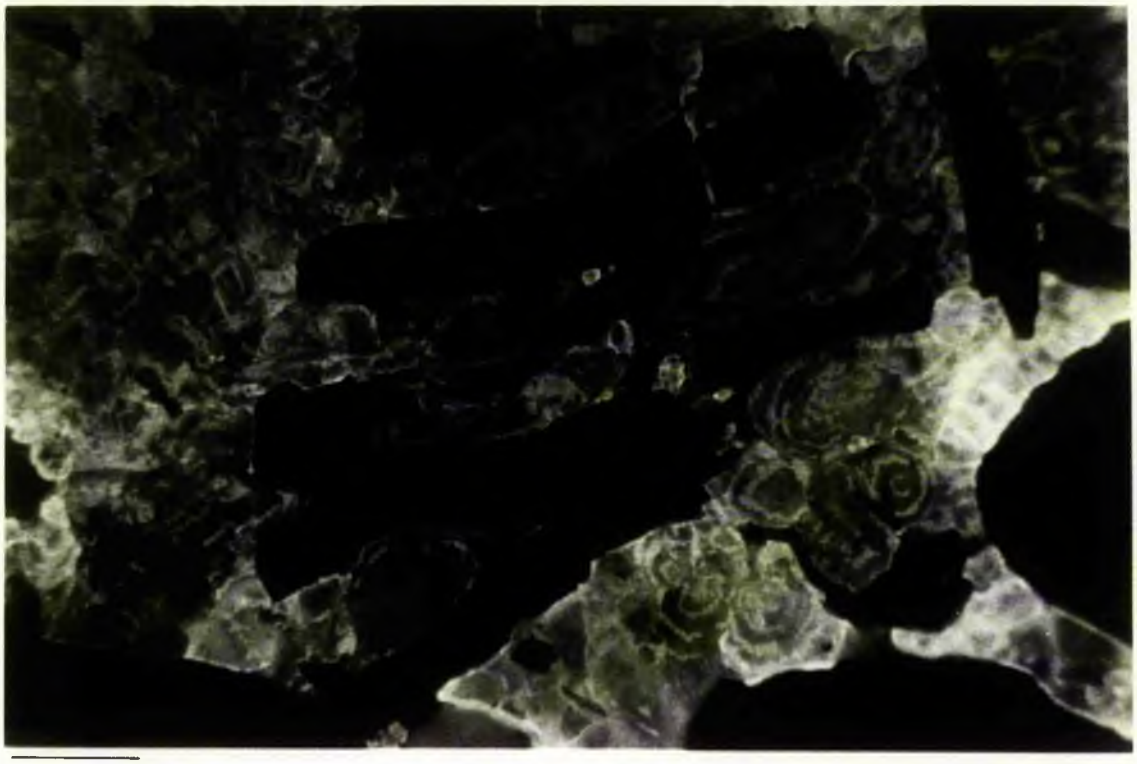

Fig. 3.14. Highly expanded biotite flake and dispersed clastic grains under cathodoluminescence. Note sharp outlines of biotite and clastic grains. Scale bar equals 100 µm.

Fig. 3.15. Photomicrograph shows grain dispersal by displacive calcite growth. Brightly luminescent fringe around clastic grain (centre) and bright patches (PC) represent passively grown sparry calcite cement in residual pores. Scale bar equals 50 µm.

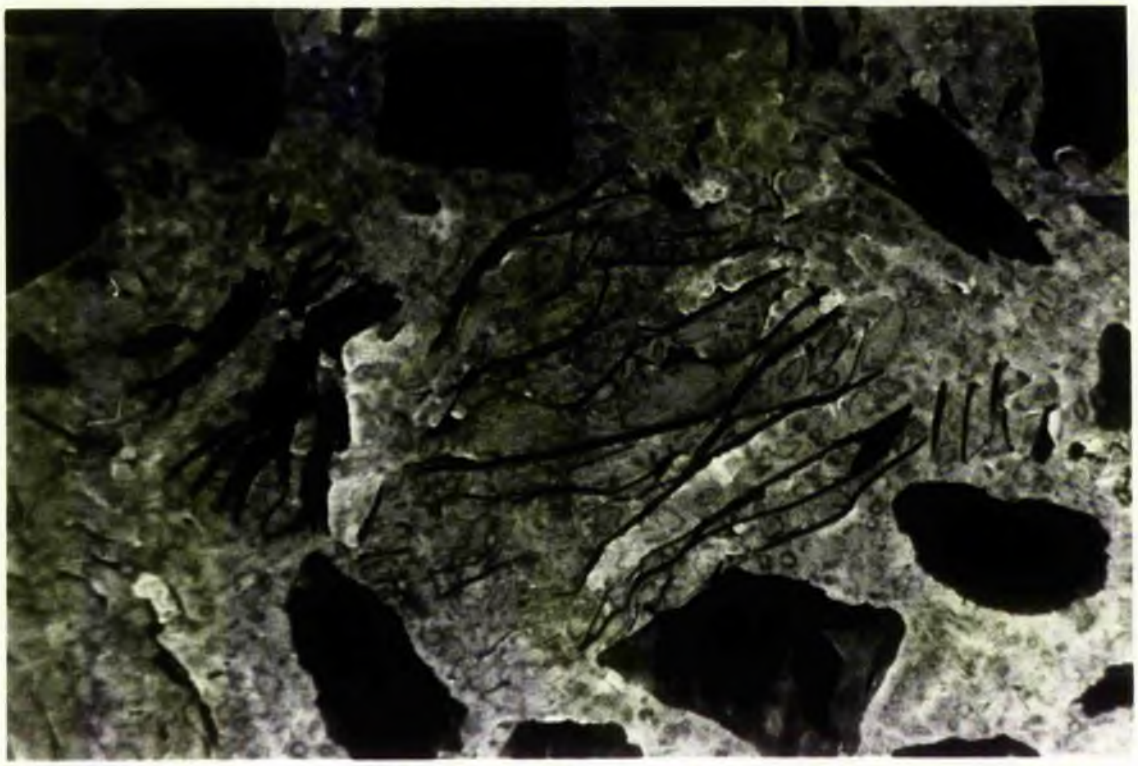

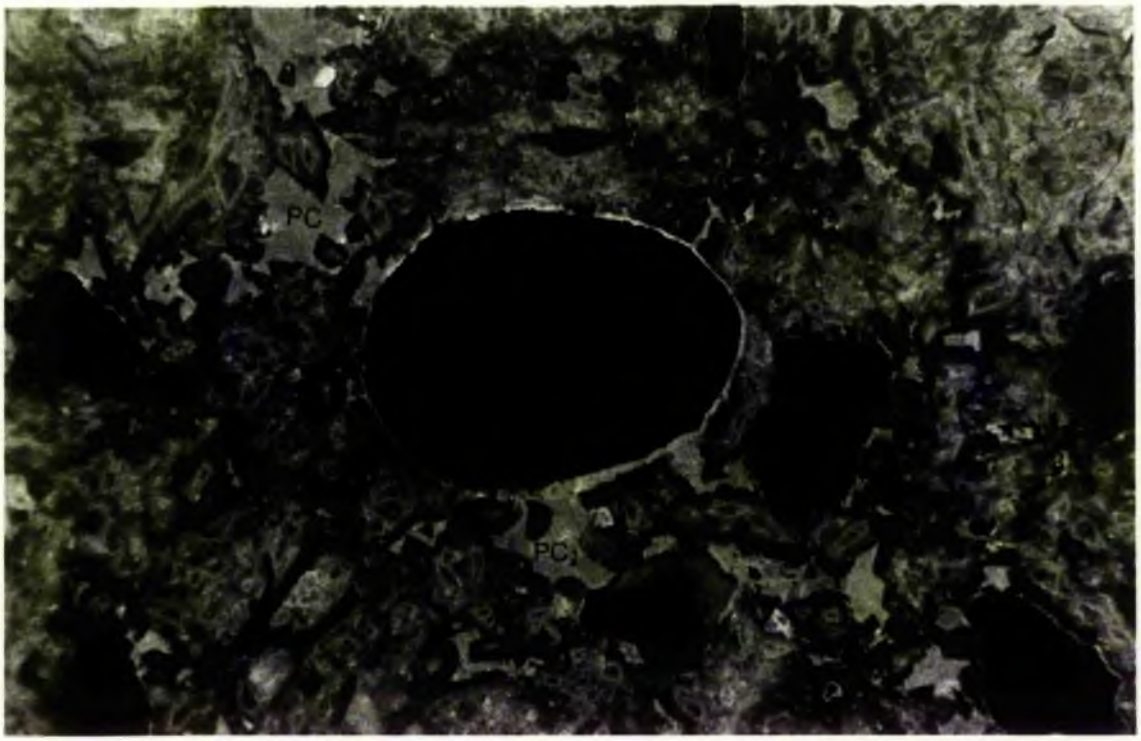
PC
PC

Fig. 3.16. Sketch showing successive stages of growth of a few simple and compound crystals as seen in Fig. 3.9. Crystal B in Fig. A shows more pronounced growth towards top (displacing biotite) and right. Its growth towards left is restricted by the forces exerted by simultaneously growing crystal A. Fig. B depicts various stages of growth of two crystals and demonstrate that during early stages both crystal A and B grew individually. With increase in size both approached so close to each other that they coalesced along line C.

Subsequently, both crystals grew together around each other pushing biotite and quartz grains apart. Fig. C depicts formation of a compound crystal by coalescing of several crystals.

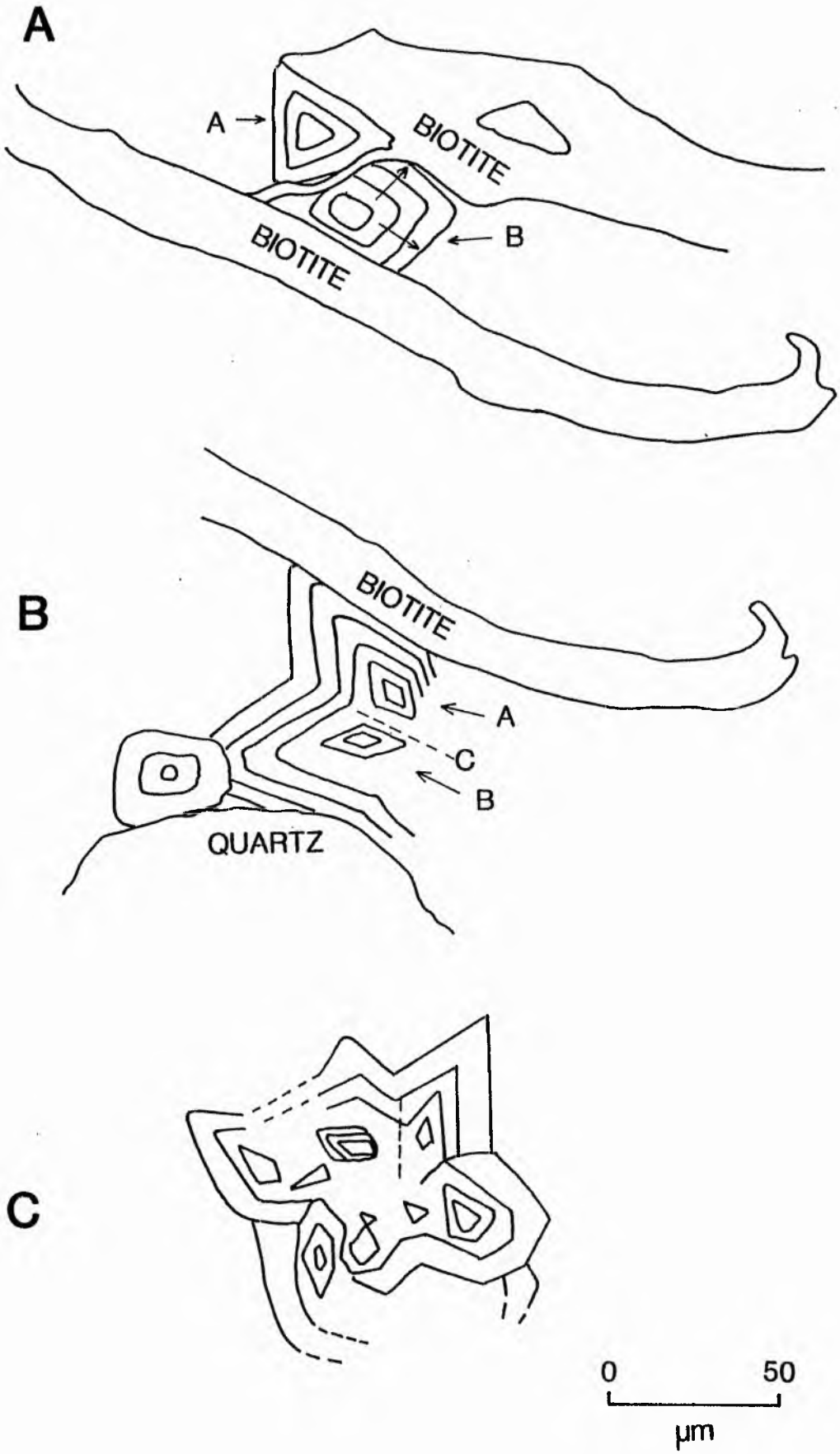
A
A
BIOTITE
B
BIOTITE
B
BIOTITE
A
C
B
QUARTZ
C
0
50
µm

Fig. 3.17. Sketch (A) shows a grain supported mixture of terrigenous grains in an unlithified sand body above the water table. Within this, during periods of channel abandonment, rapid surface evaporation influenced by hot sunlight generates supersaturated conditions. Subsequently, calcite nucleates and starts growing by its displacive force of crystallisation exerting an outward pressure causing expansion and dispersal of clastic grains (sketch (B)). Microspaces such as cleavage planes in detrital micas (B), between component grains of rock fragments (RF) and fractures in quartz (Q) grains offer an unusually favourable environment for nucleation. The displacive growth of calcite within these confined spaces subsequently expands these grains along the microspaces (sketch (B)). The margins of these separated fragments can be visually fitted back together. PC represents passively grown sparry calcite in residual pores (sketch (B)).

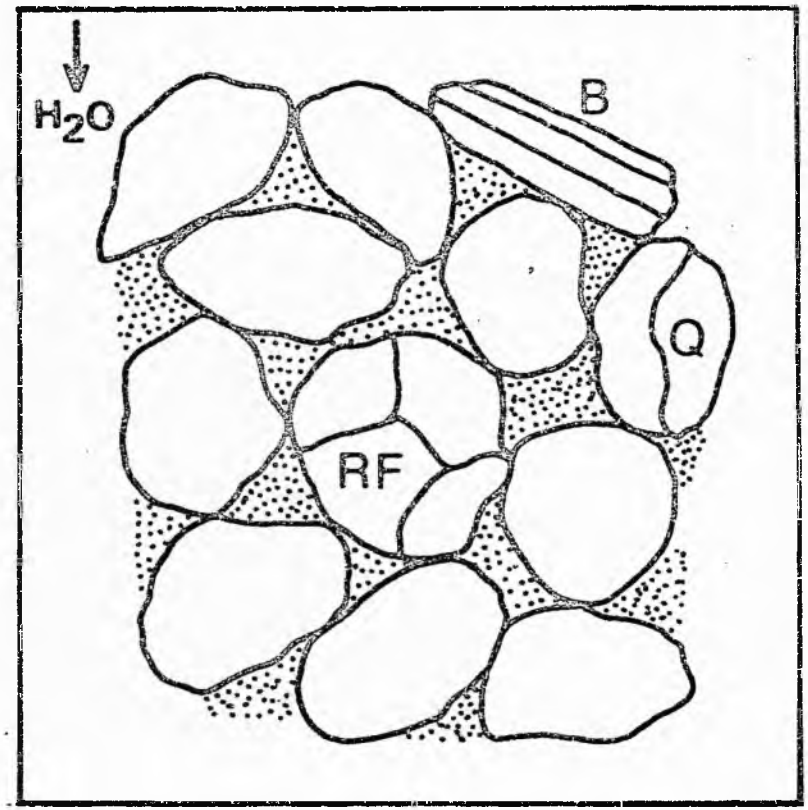

(A)

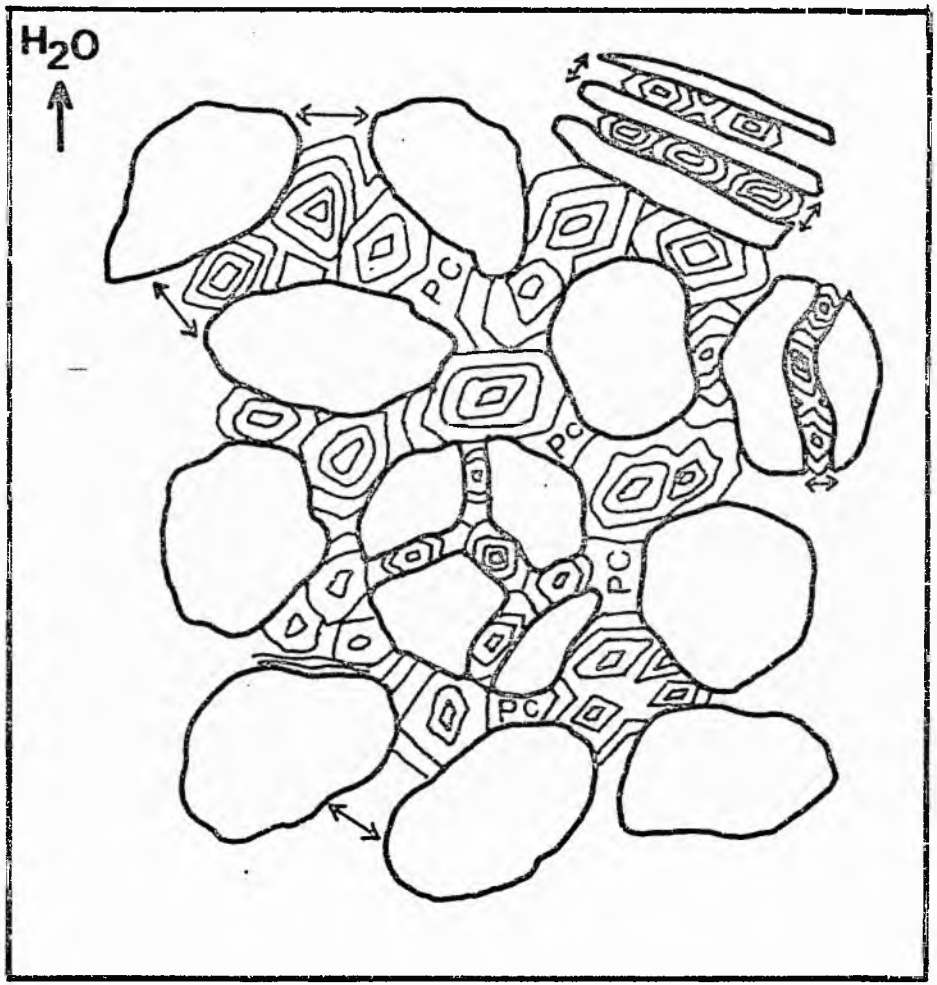

(B)

Figs. 3.18 and 3.19. Palisades of sparry prismatic crystals on isolated grains. The prismatic crystals are oriented perpendicular to the grain surface and usually tend to be of constant thickness. Note the palisade is better developed around basic igneous rock fragment (Fig. 3.18), whereas, around quartz grain it has developed only on a part of the grain surface (Fig. 3.19). X nicols. Scale bar equals 50 μm.

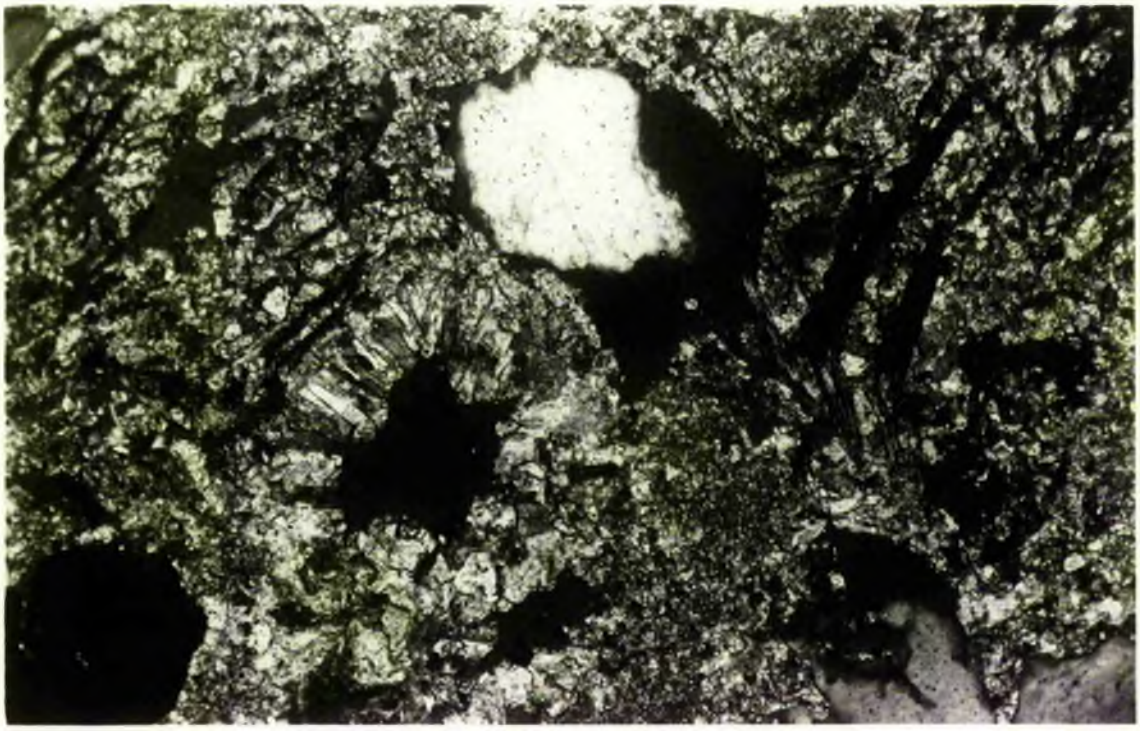

Fig. 3.20. Neomorphic spar with irregular interpenetrant grain boundaries in microsparry groundmass. X nicols. Scale bar equals 200 µm.

Fig. 3.21. Syntaxial overgrowth of calcite on a carbonate grain. Note that a part of the dark grain in the top left corner has been pushed apart by displacively grown calcite. The separated parts can easily be visually fitted back together. X nicol. Scale bar equals 100 µm.

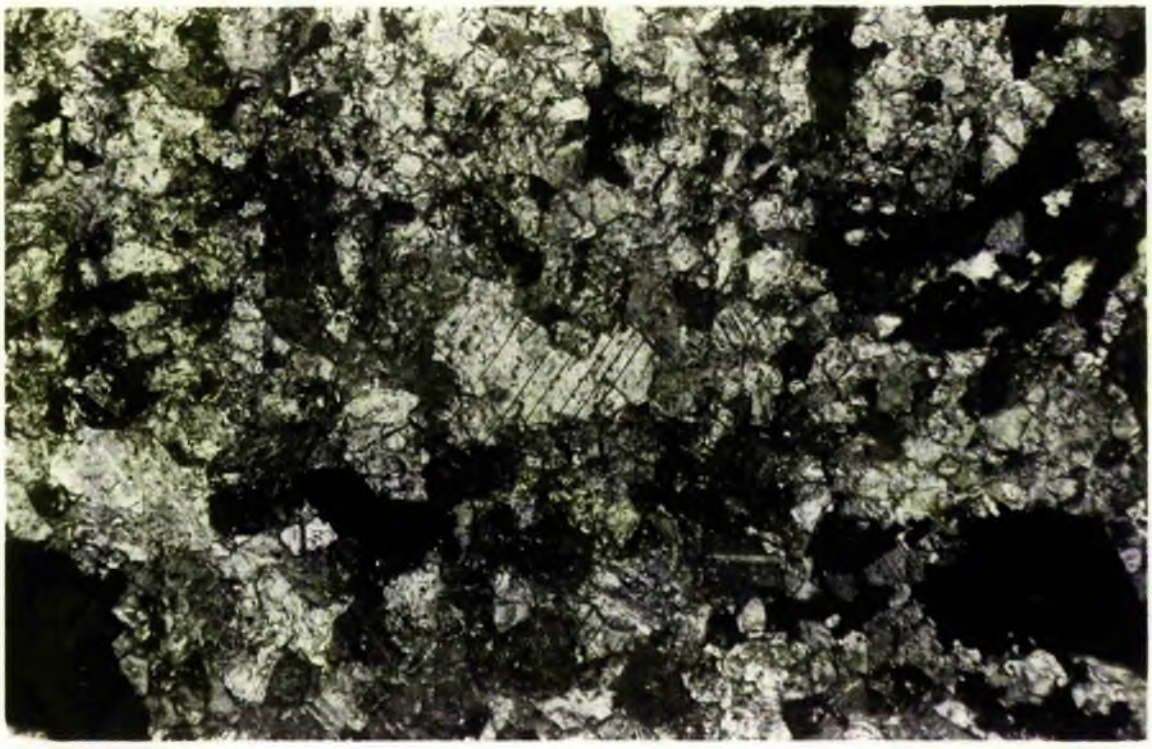

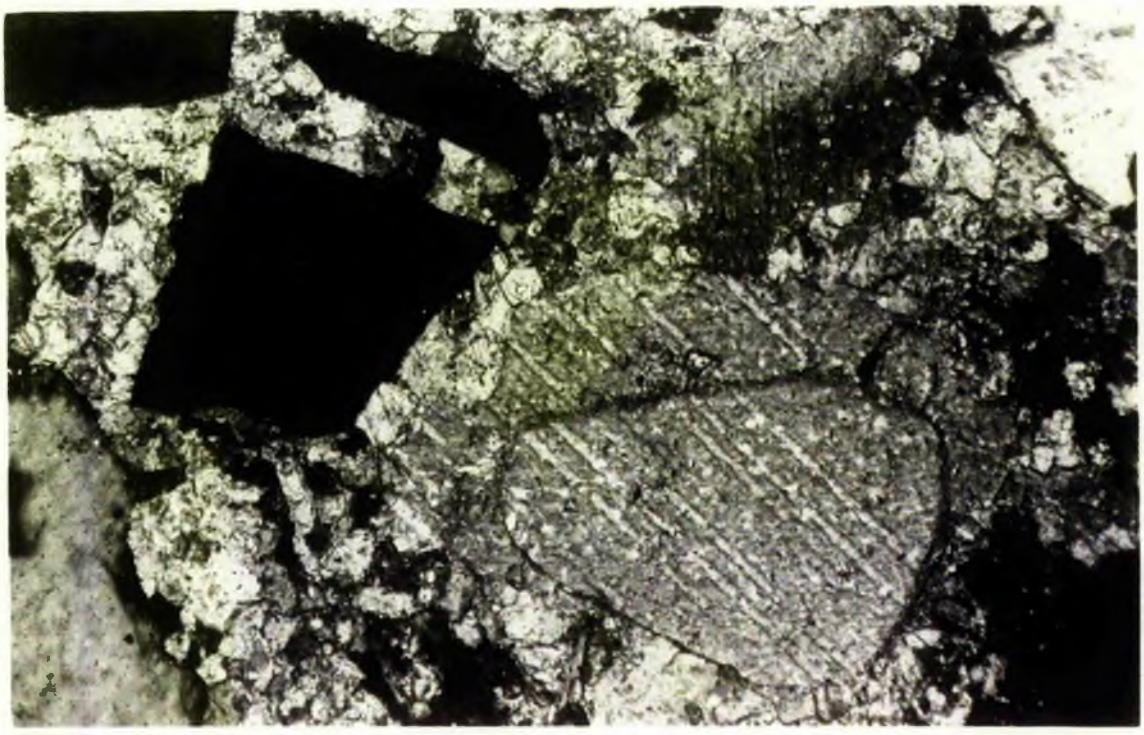

Figs. 3.22 and 3.23. SEM photographs showing sparry calcite crystals and micro-lamellar pores between crystals and along detrital grain surfaces. When these microspaces have been filled with passive calcite are believed to have formed bright fringes around grains observed under cathodoluminescence. Scale bar equals 40 μm.

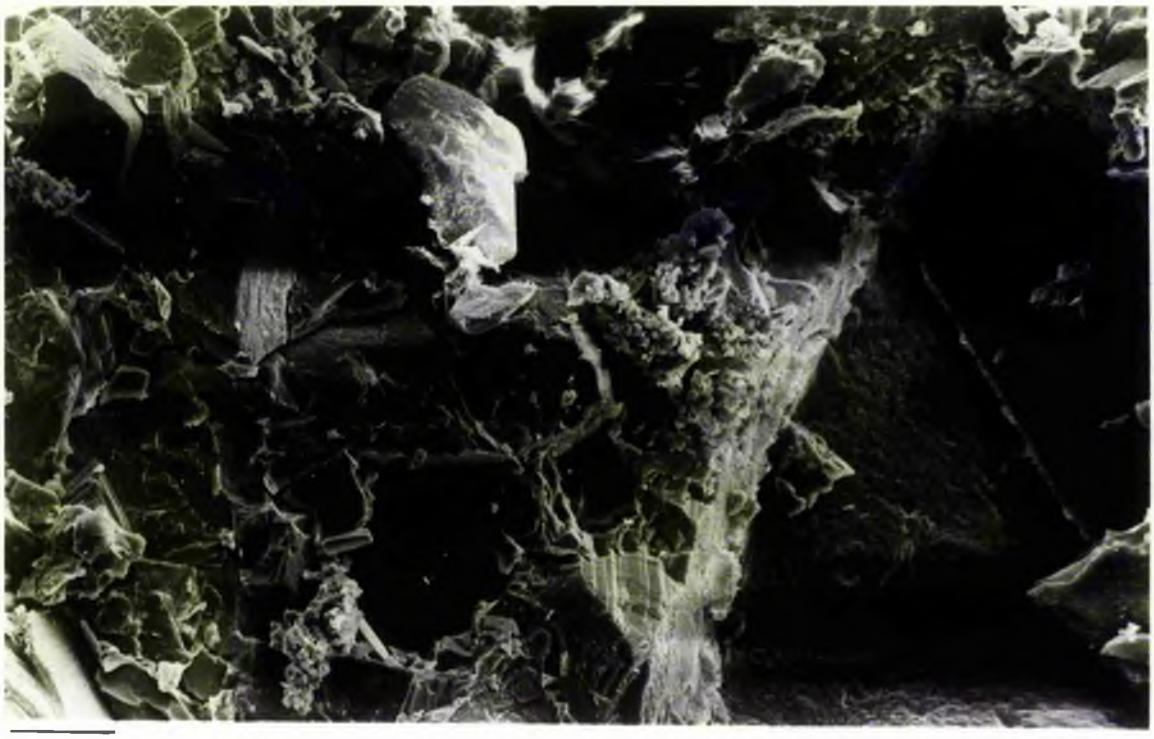

Fig. 3.24. SEM photograph showing irregular fractures within sparry calcite crystals. Scale bar equals 10 μm.

Fig. 3.25. SEM photograph showing illite flakes bridging across micro-lamellar pore seen on the right hand side of figure 3.22. Scale bar equals 10 μm.

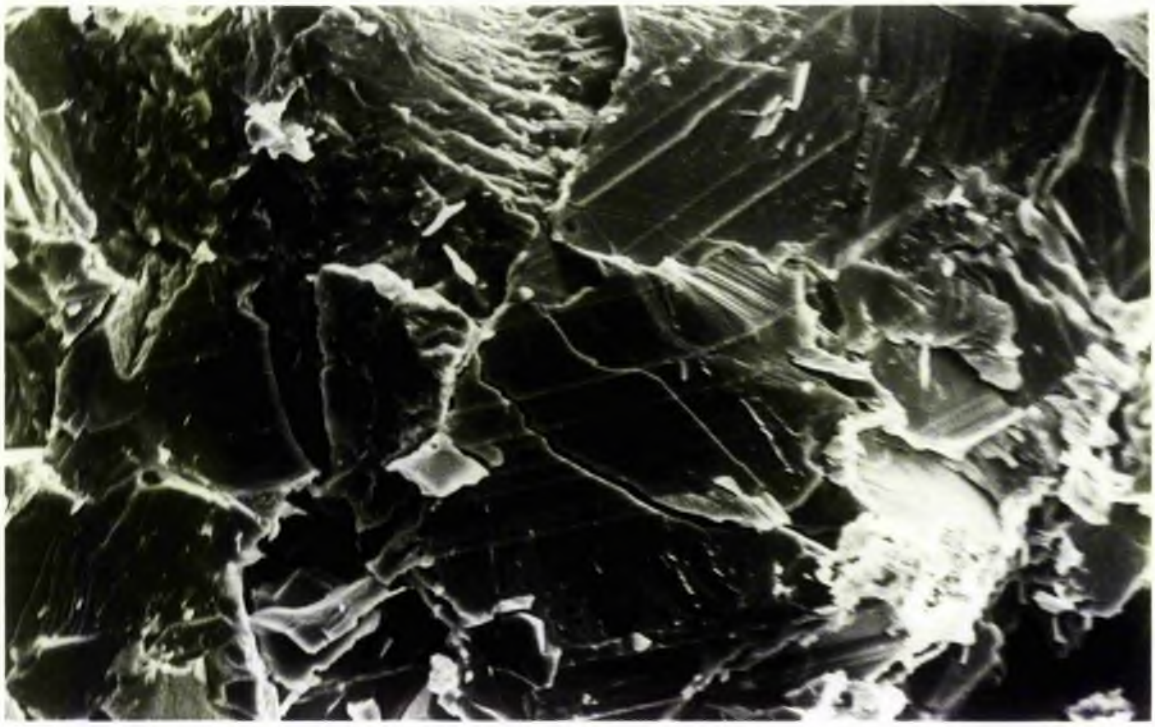

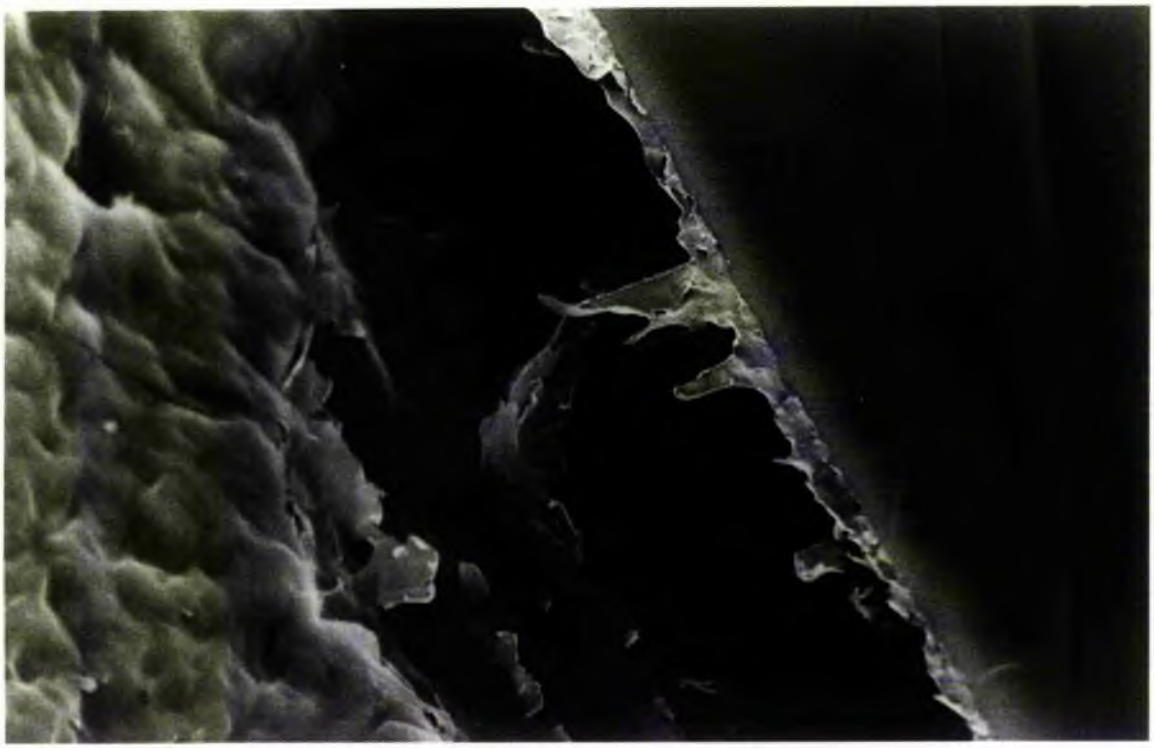

Fig. 3.26. Slightly compacted uncalcretized sands. Note bending of micas and grain interpenetration by means of plastic deformation. X nicols. Scale bar equals 200 µm.

Fig. 3.27. Quartz overgrowth forming euhedral outlines followed by hematite coats and clay (smectite) fringes development. Arrow shows hematite and smectite coating euhedral outline of quartz. Plane polarized light. Scale bar equals 100 µm.

Fig. 3.28. Photomicrograph showing hematite and clay (smectite) fringes. Note that hematite is absent at places of contact between grains and clay fringes are choking pore throats. Chert grain (bottom centre) shows indented margin due to plastic deformation and euhedral outlines suggesting overgrowth. Plane polarized light. Scale bar equals 100 μm.

Fig. 3.29. Vuggy porosity formed due to dissolution of carbonate cement and clay fringes. Note hematite coating on euhedral outlines of quartz grain. Plane polarized light. Scale bar equals 100 μm.

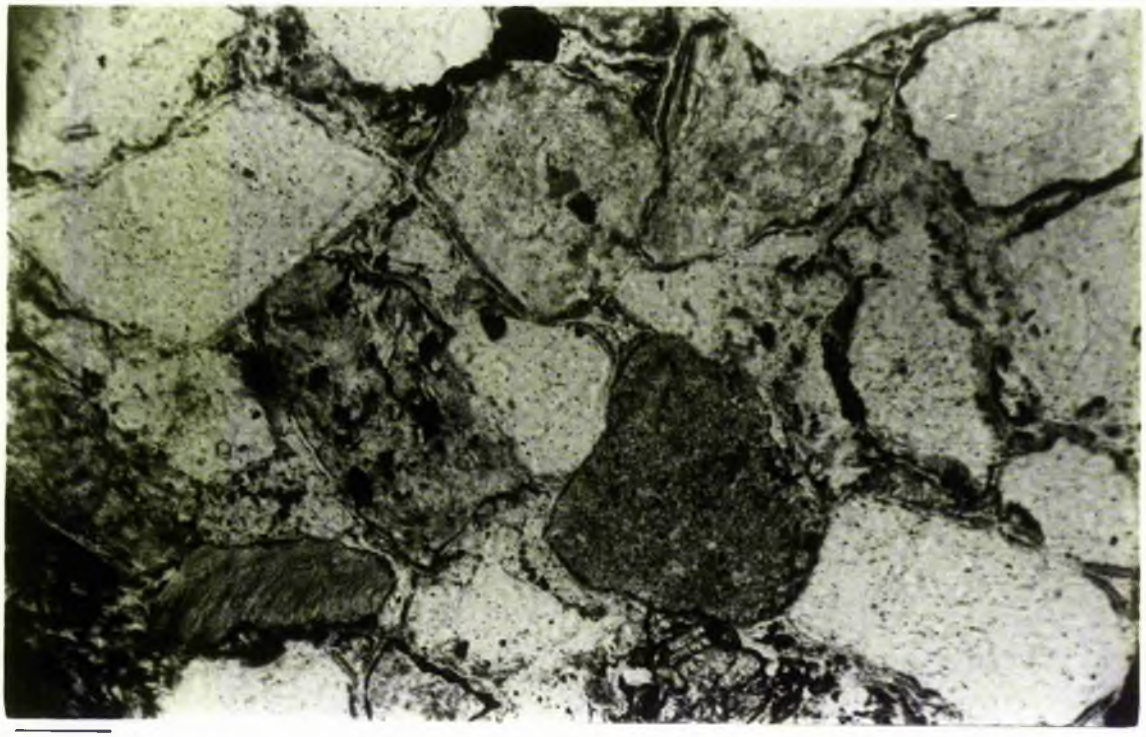

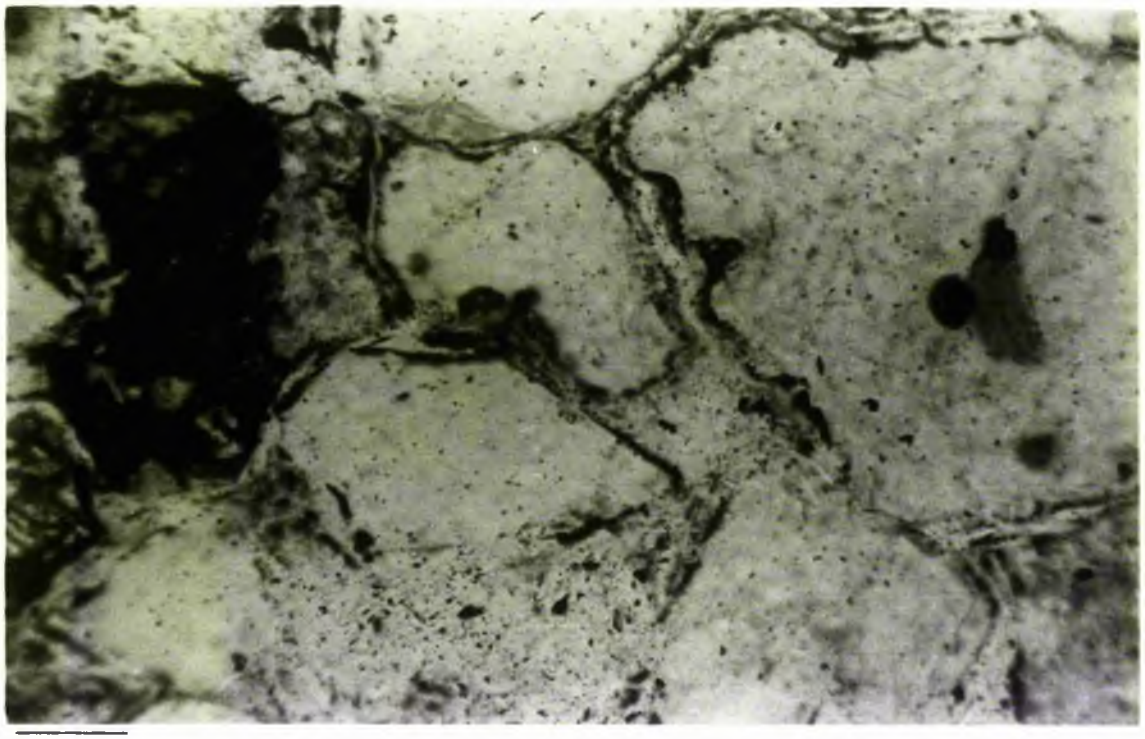

Fig. 3.30. Photomicrograph showing hematite coatings and blebs and clay fringes. Note that clay rims are enveloping hematite blebs (top centre). This suggests that clays grew subsequent to the formation of hematite. Plane polarized light. Scale bar equals 100 μm.

Fig. 3.31. Photomicrograph showing poikilitic calcite filling all the residual pores left after the formation of hematite and clays. Plane polarized light. Scale bar equals 100 μm.

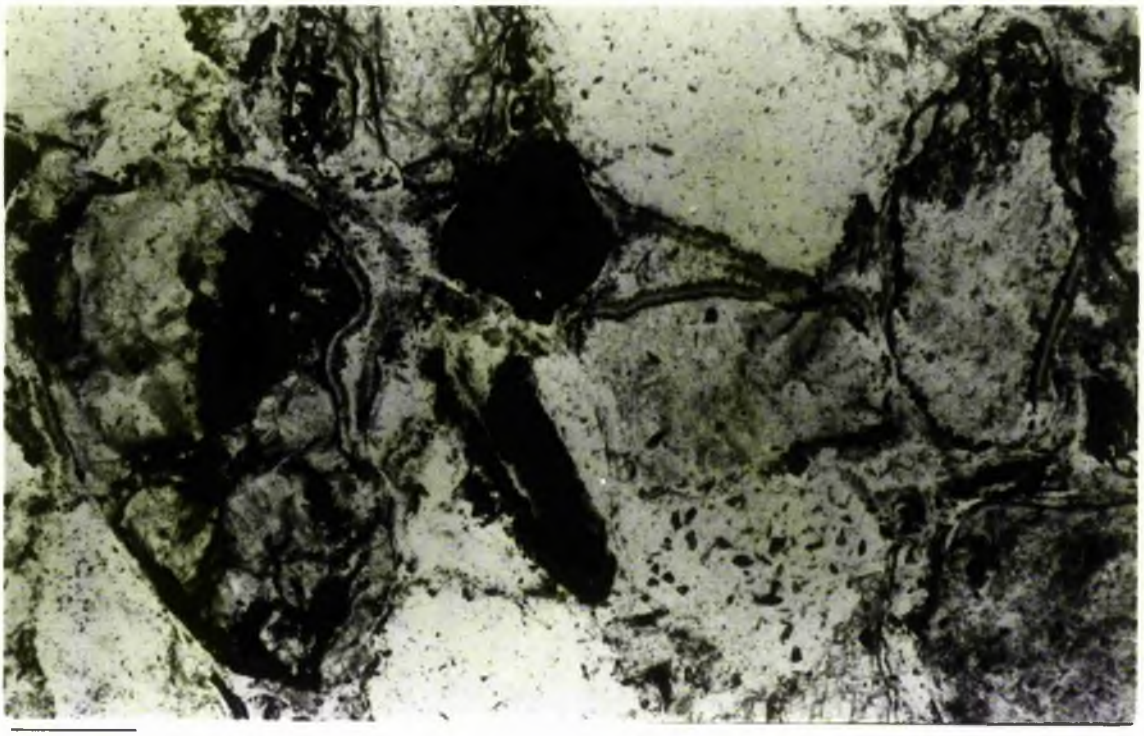

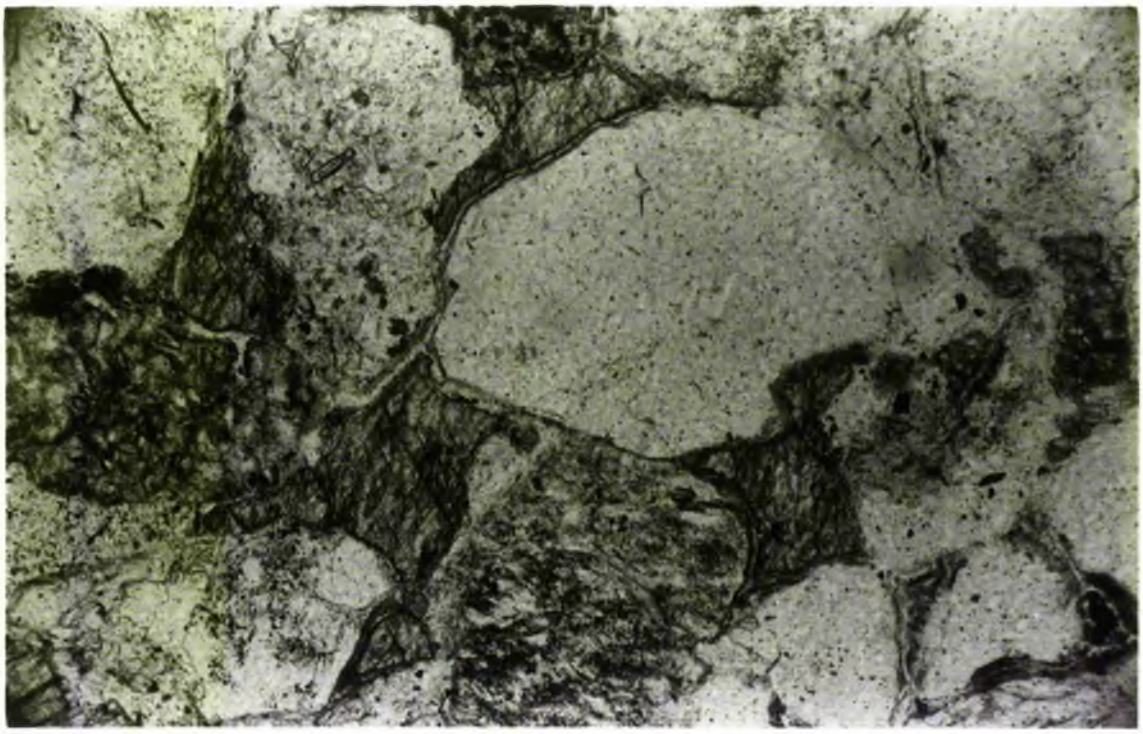

Fig. 3.32. Poikilitic calcite corroding detrital grains. Arrow shows a ghost of the grain. X nicols. Scale bar equals 200 µm.

Fig. 3.33. Poikilitic calcite showing bright and uniform luminescence. Scale bar equals 200 µm.

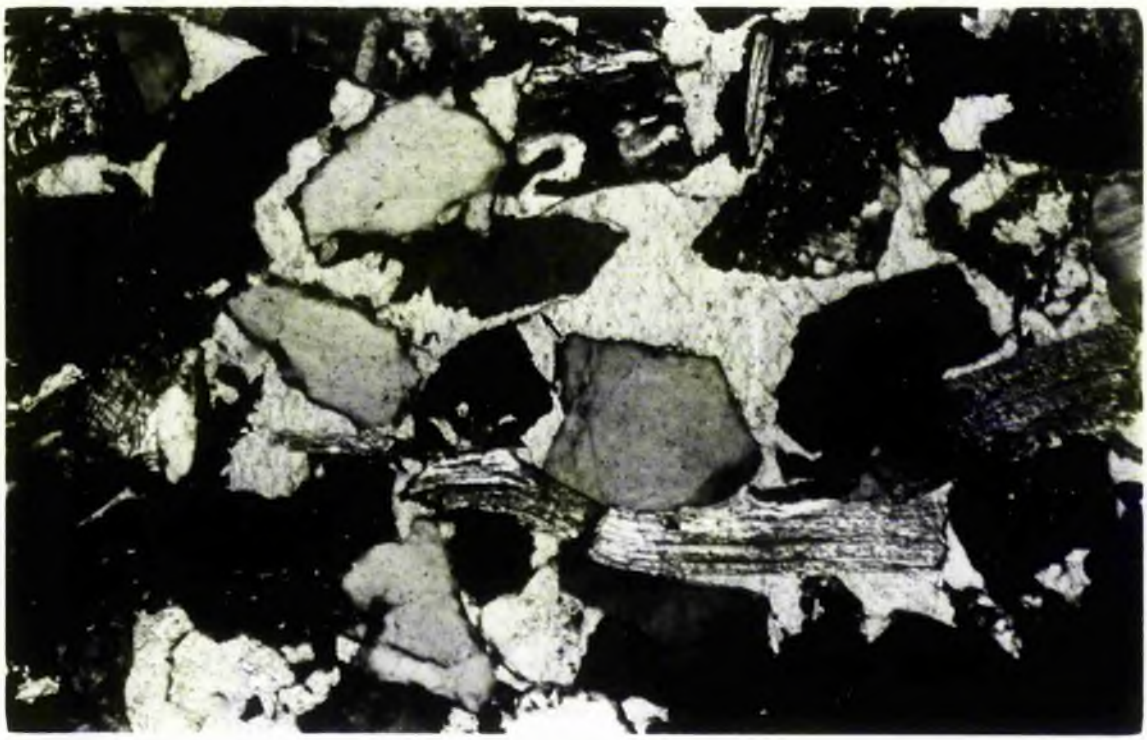

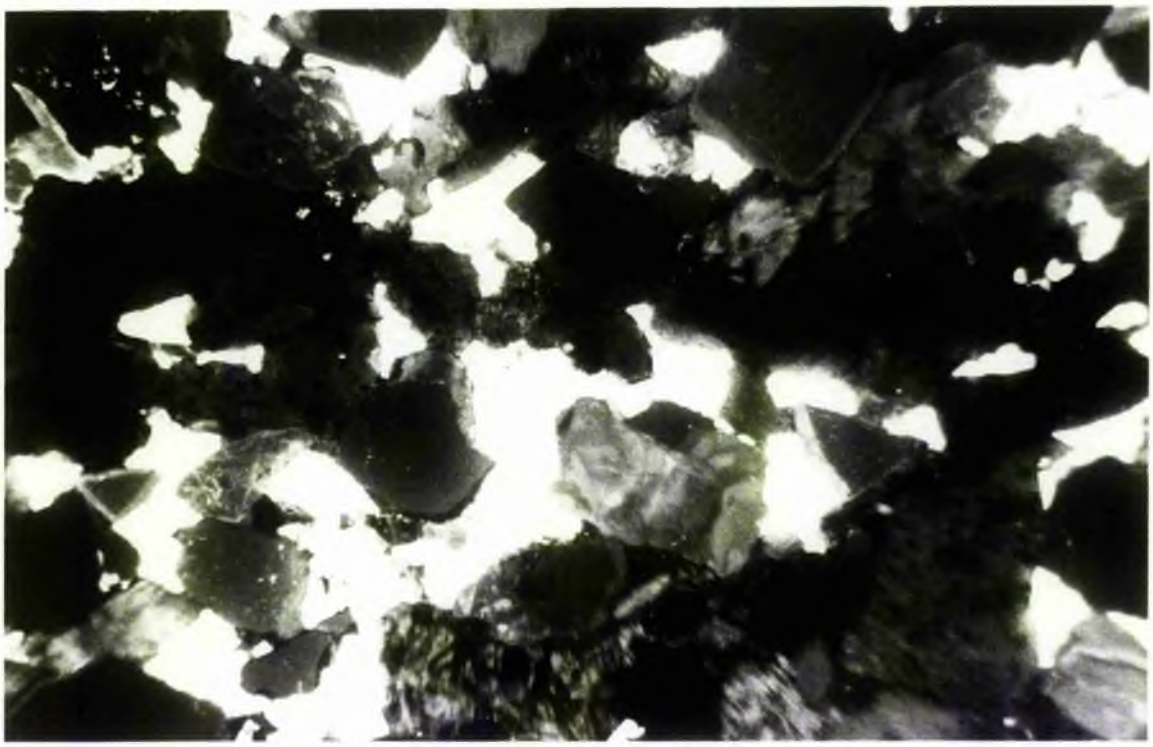

Fig. 3.34. Poikilitic calcite showing some variation in luminescence. Scale bar equals 100 μm.

Fig. 3.35. SEM photograph showing wavy plates of smectite growing on a grain surface. Scale bar equals 10 μm.

Note: Identification of authigenic clays is based on their morphology.

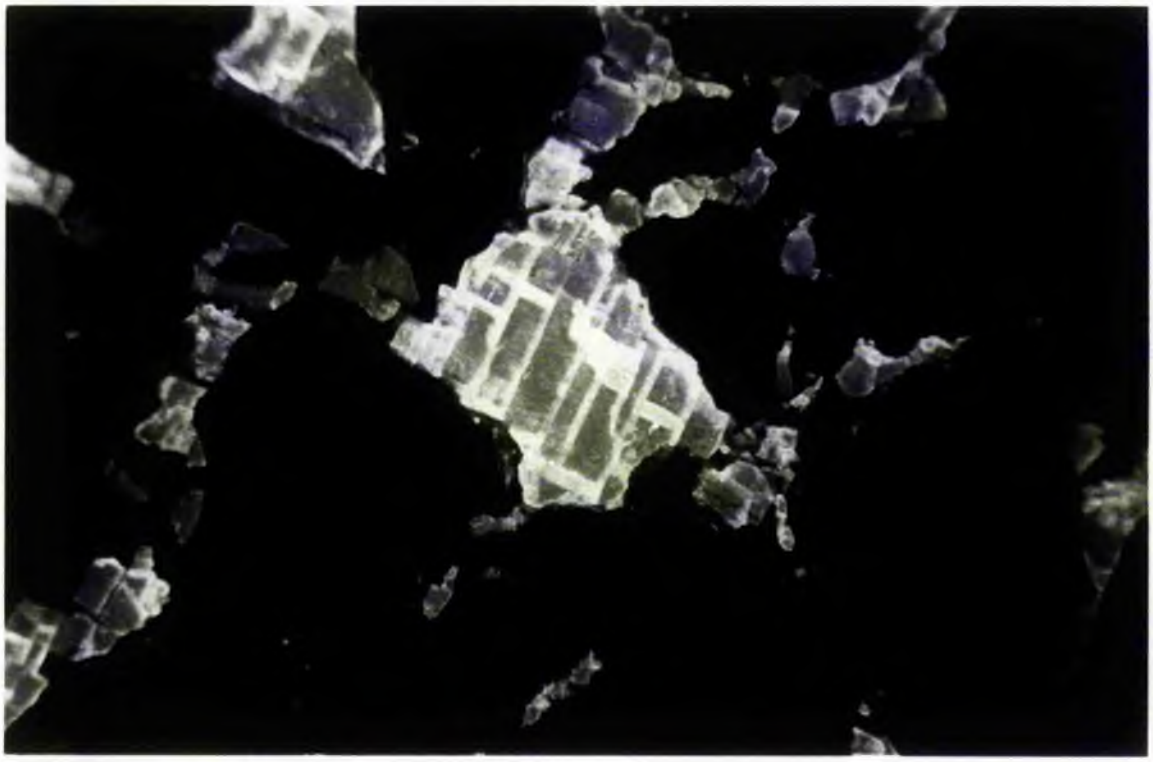

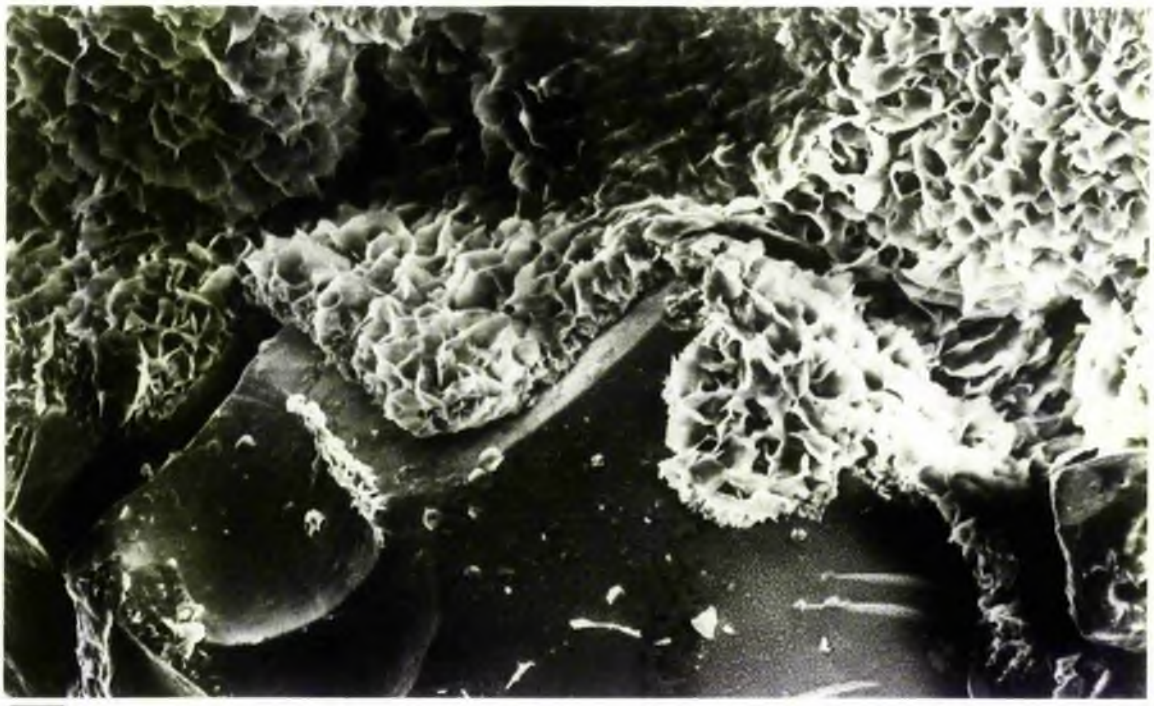

Fig. 3.36. SEM photograph showing clay fringe of uniform thickness (app. 10 μm) choking pore throat. Thread like terminations are perhaps of illite. Scale bar equals 20 μm.

Fig. 3.37. Authigenic smectite showing honeycomb texture formed by smooth fusing of highly crenulate adjacent crystals. SEM photograph. Scale bar equals 10 μm.

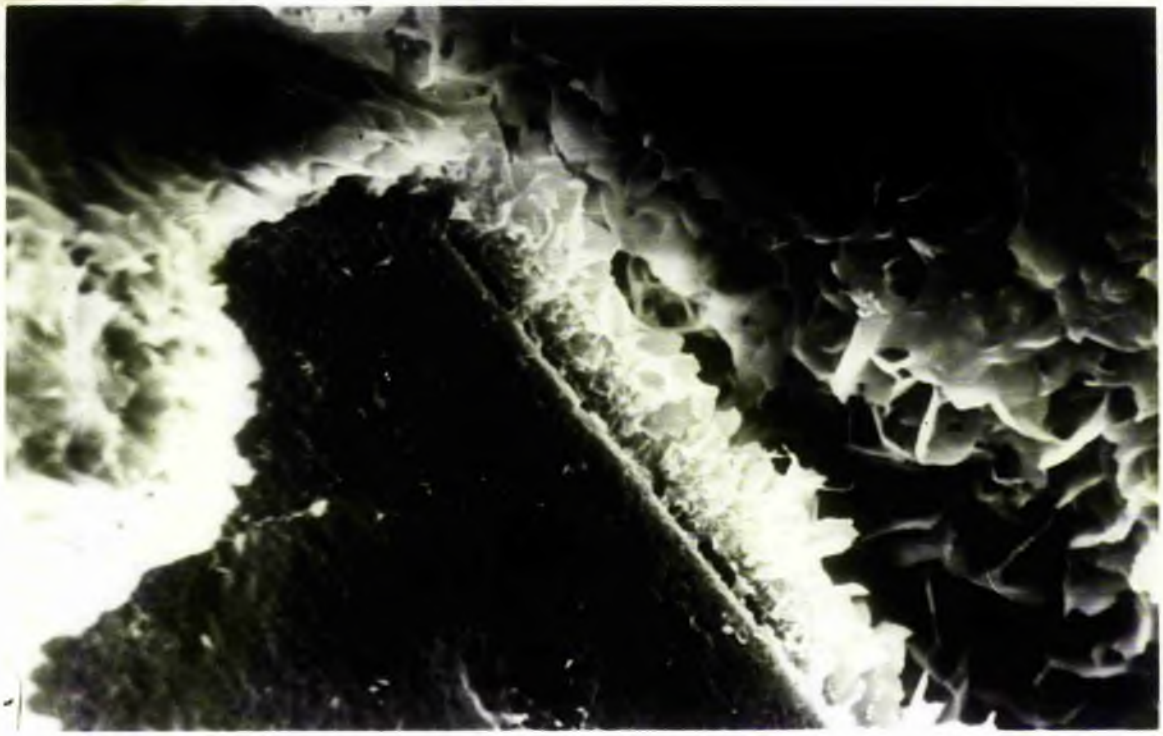

Fig. 3.38. SEM photograph showing authigenic smectite filling a pore. Note smectite is showing preferred orientation and increase in crystal size towards the centre of the pore forming coarser box-work texture in the centre. Scale bar equals 10 μm.

Fig. 3.39. SEM photograph showing smectite partially engulfed in quartz overgrown face. Scale bar equals 10 μm.

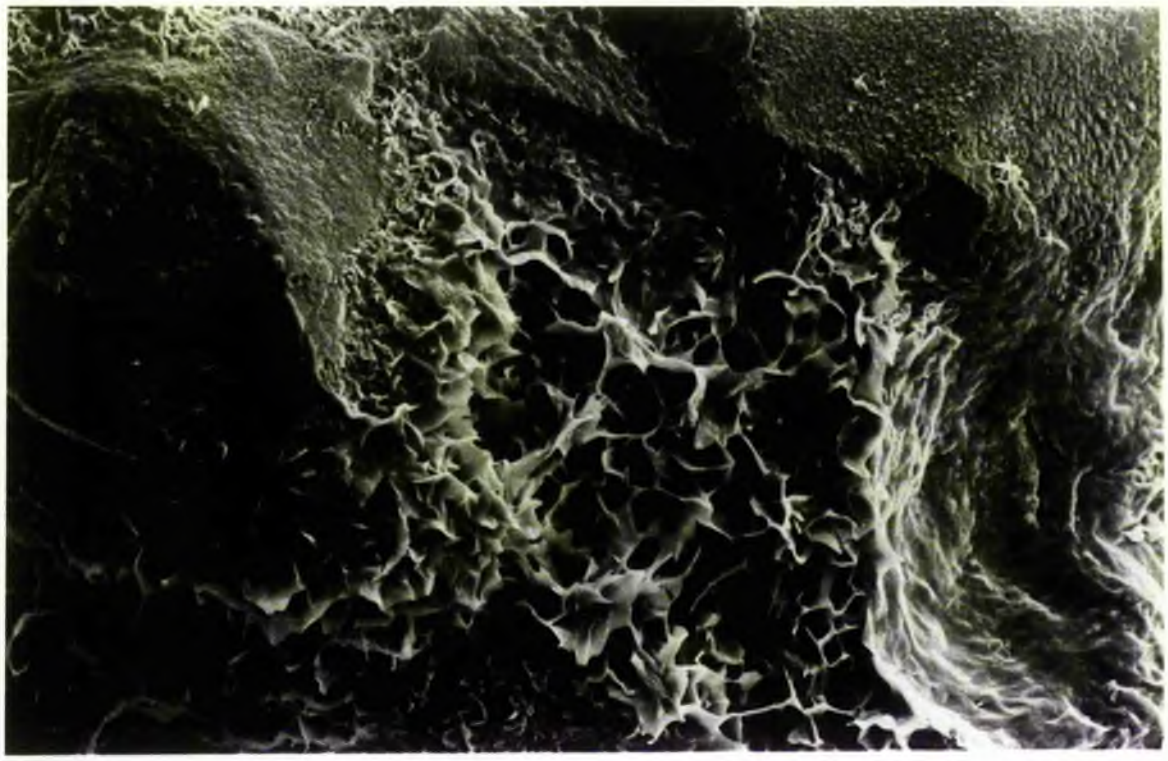

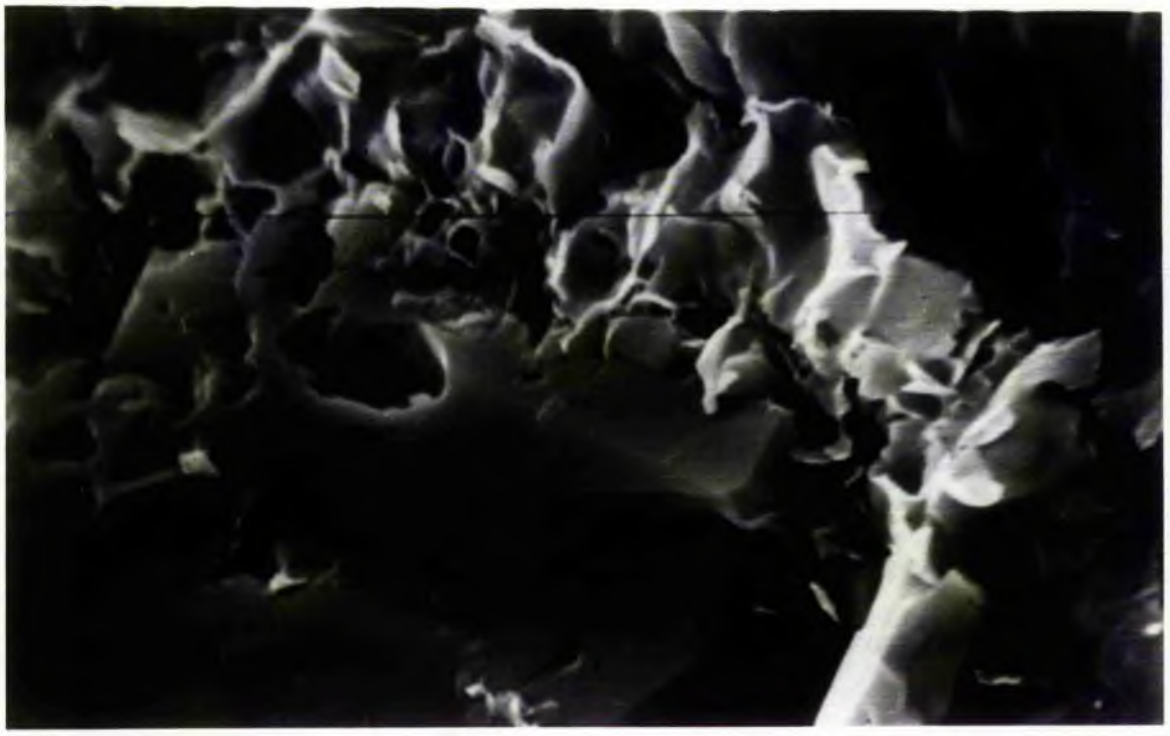

Fig. 3.40. SEM photograph showing authigenic clay rims (smectite and illite) choking pore throats. Note illite threads bridging across the pore (central area). An authigenic feldspar crystal that grew after clays can also be seen in the top left corner. Scale bar equals 10 μm.

Fig. 3.41. Authigenic illite with wispy terminations filling a pore. SEM photograph. Scale bar equals 10 μm.

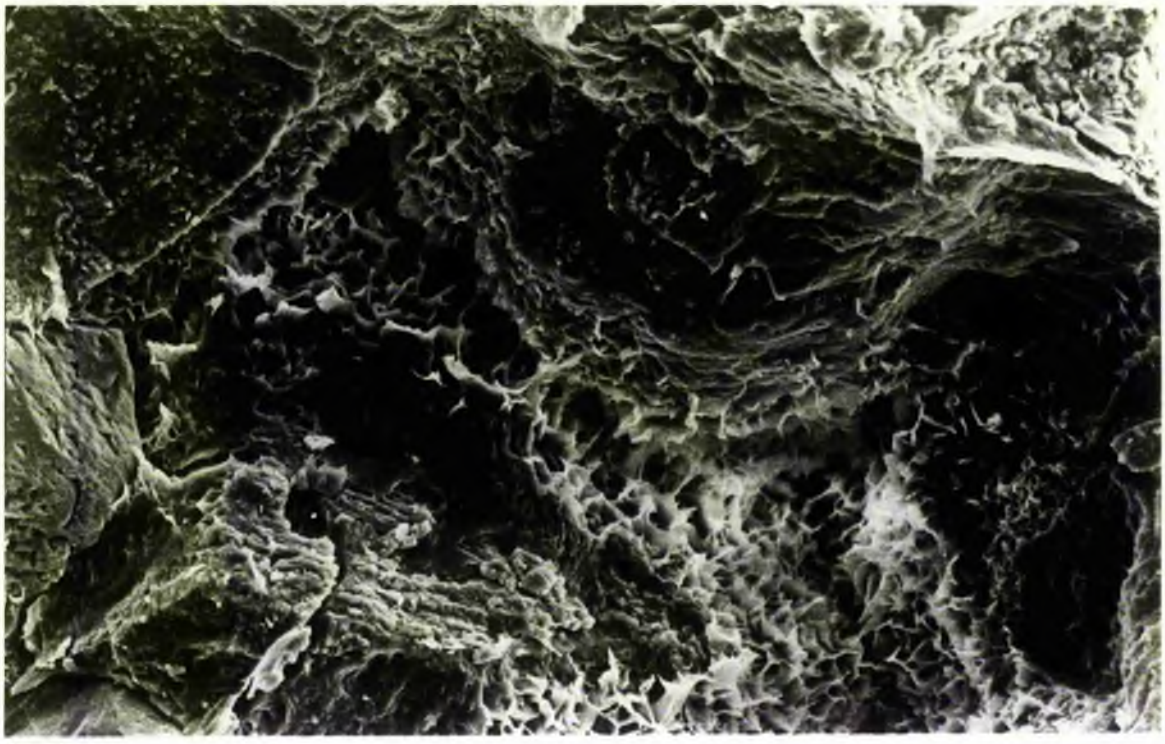

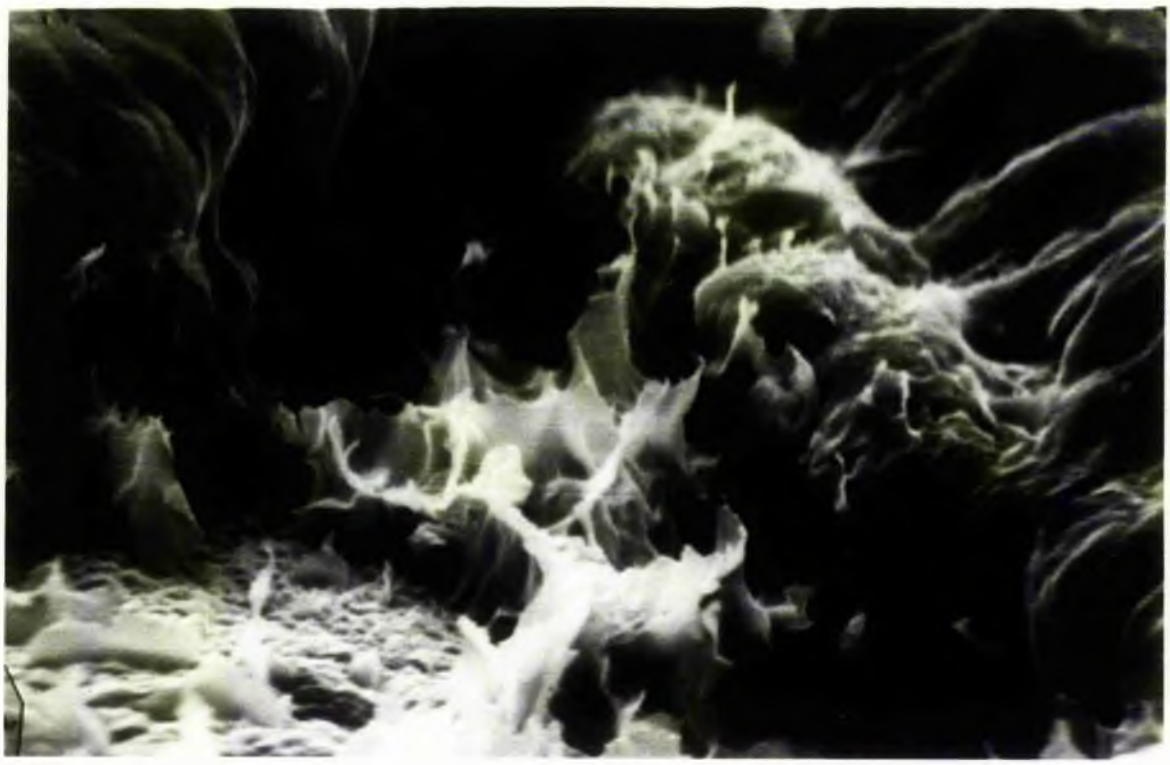

Fig. 3.42. SEM photograph showing rosette-like clusters of finely crystalline hematite/chlorite (central area). Authigenic crystal (centre) is perhaps of feldspar while thin clouds with wispy terminations are of illite. Scale bar equals 10 μm.

Fig. 3.43. Authigenic feldspar crystals (5 μm to 20 μm) resting on smectite flakes. SEM photograph. Scale bar equals 20 μm.

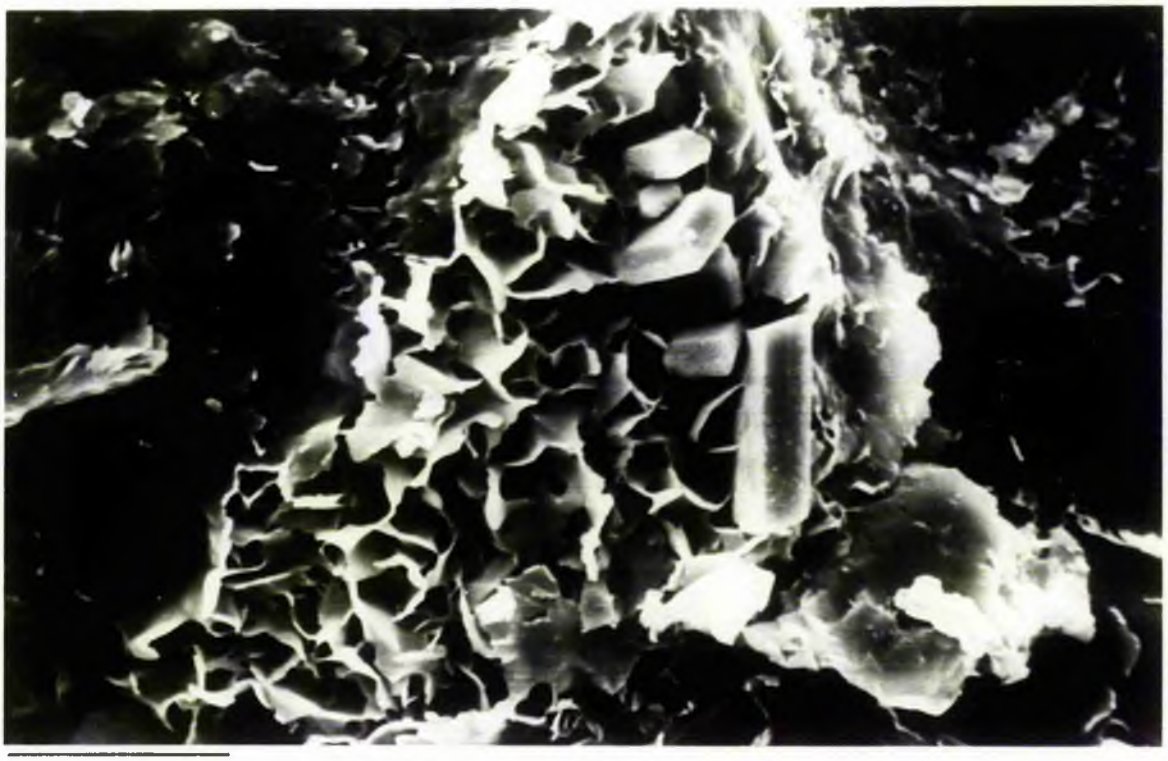

Fig. 3.44. SEM photograph showing authigenic quartz crystals occurring within the microspaces between smectite flakes. Note feldspar crystal is partially engulfing smectite flake (in circle) suggesting their simultaneous growth. Scale bar equals 10 μm.

Fig. 3.45. SEM photograph showing curved vermicular stack of kaolinite succeeding smectite. Scale bar equals 10 μm.

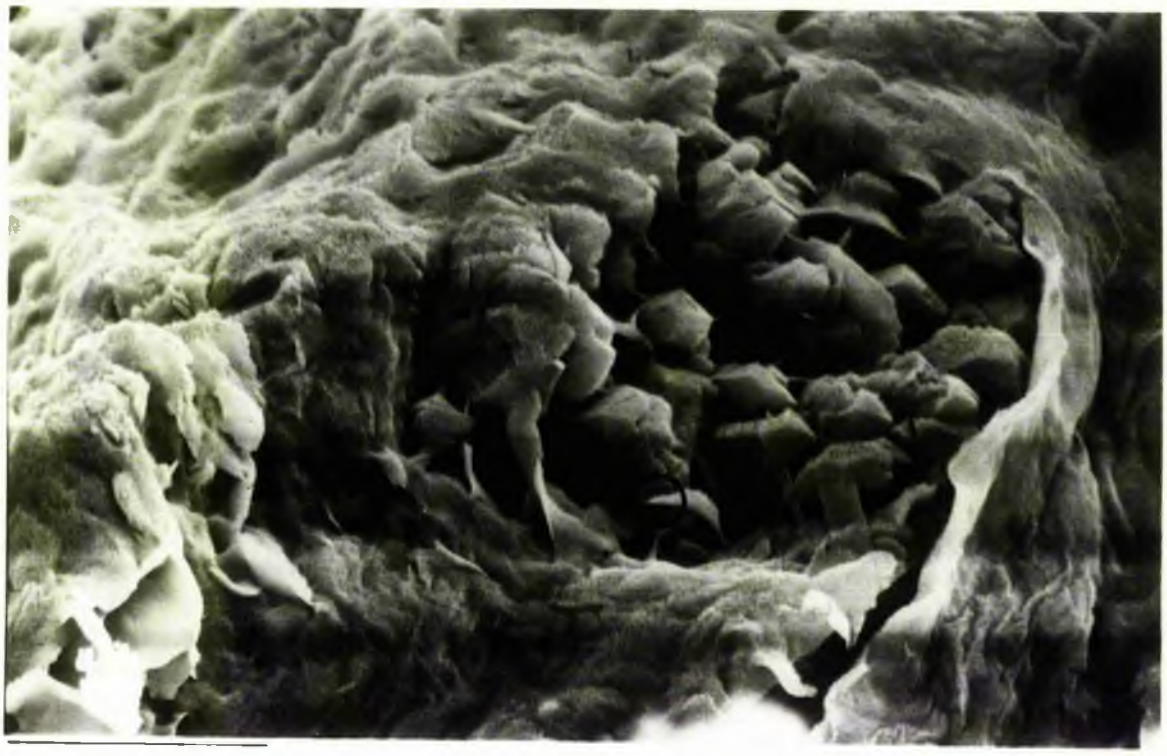

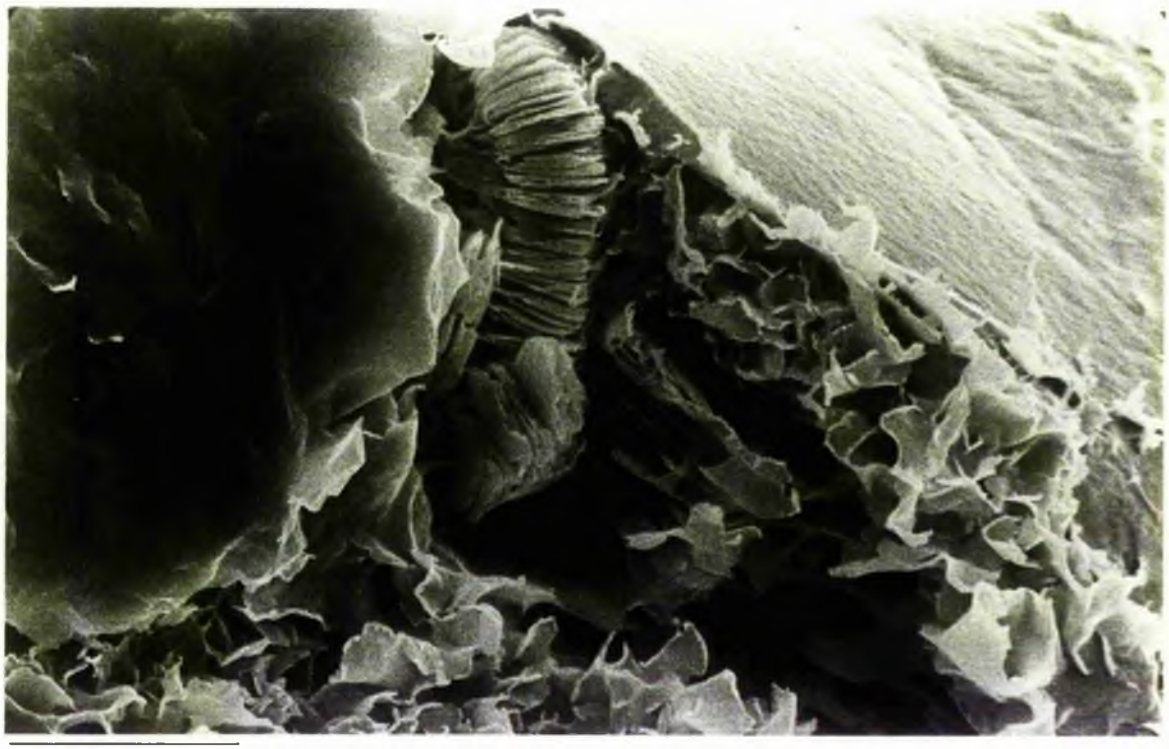

Fig. 3.46. SEM photograph showing authigenic quartz crystal resting on smectite flakes. Scale bar equals 10 µm.

Fig. 3.47. Detrital feldspar showing smooth V-shape pits on the surface. SEM photograph. Scale bar equals 10 µm.

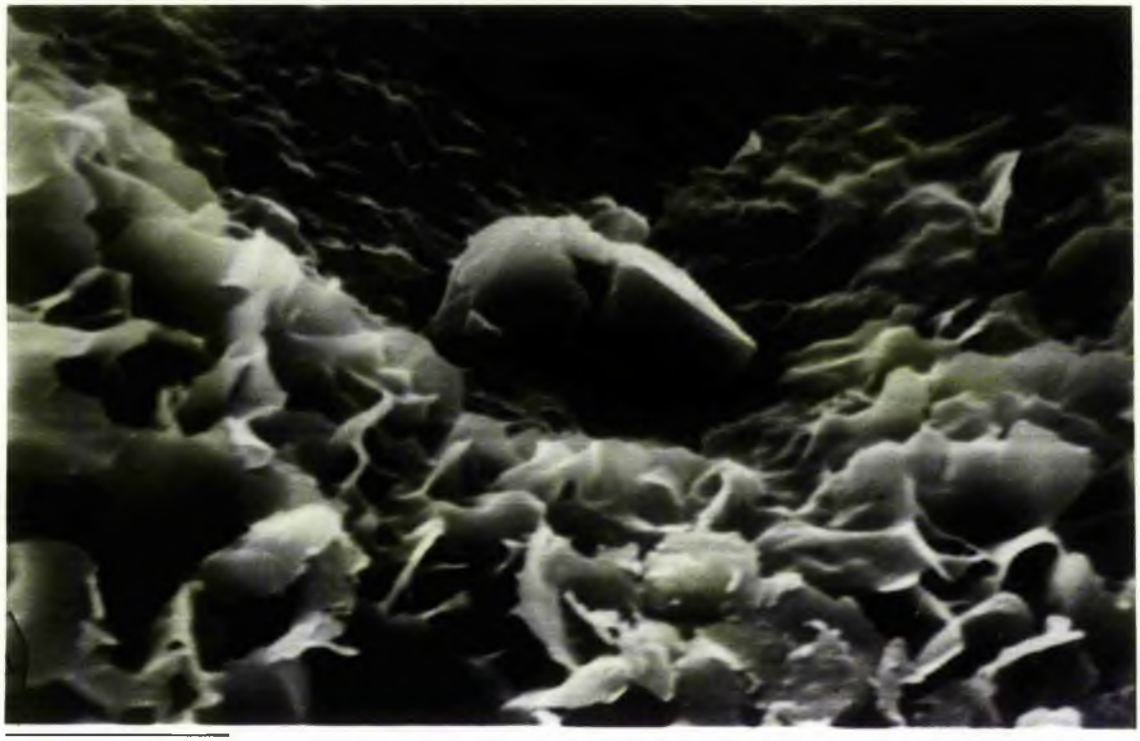

Fig. 3.48. SEM photograph showing alteration of detrital feldspar into clays and enlargement of pits during diagenesis. Scale bar equals 10 μm.

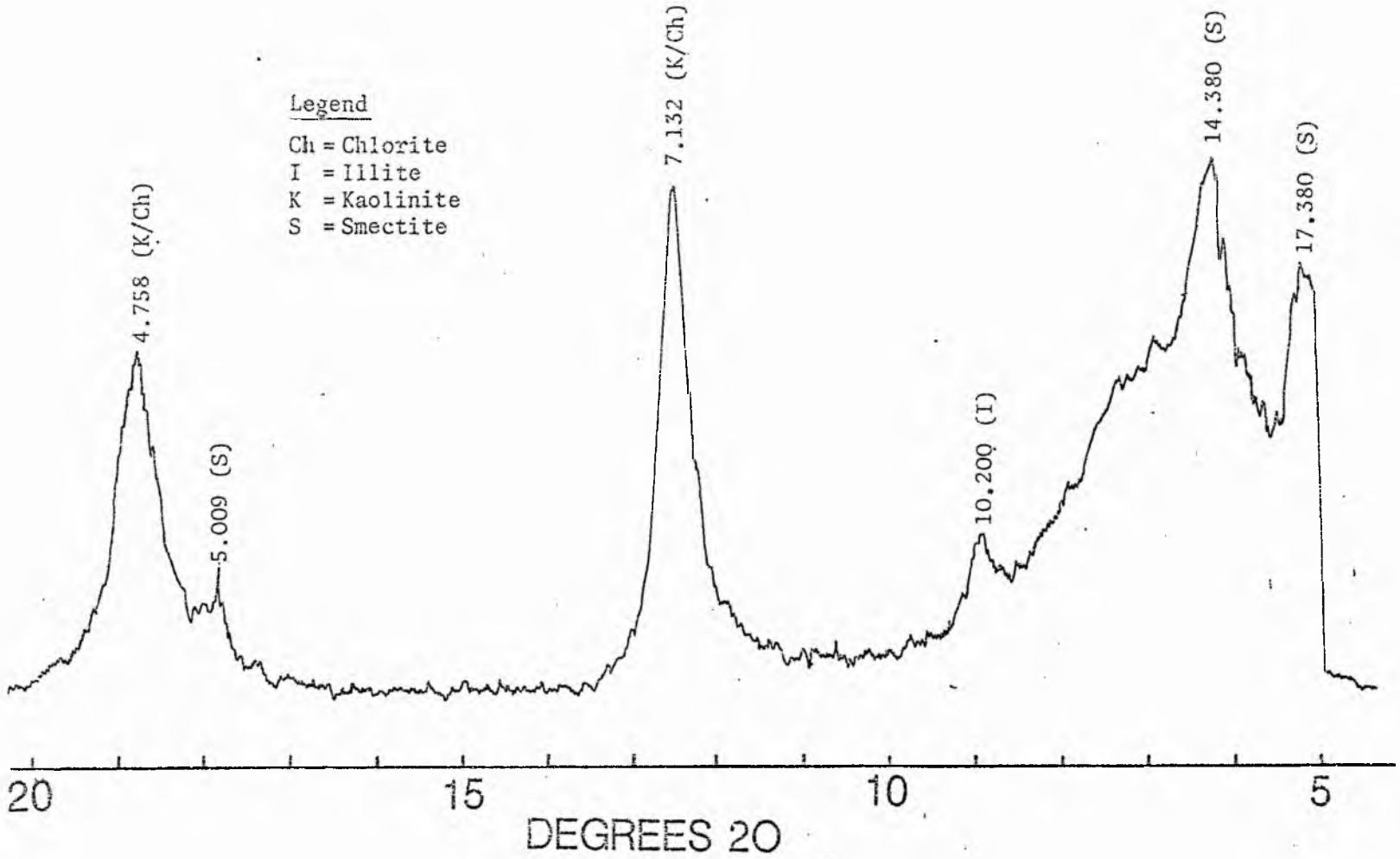

Fig. 3.49. X-Ray Diffraction pattern showing prominent reflections of smectite between 14 to 15 Å and a diffused tail down to 10 Å.

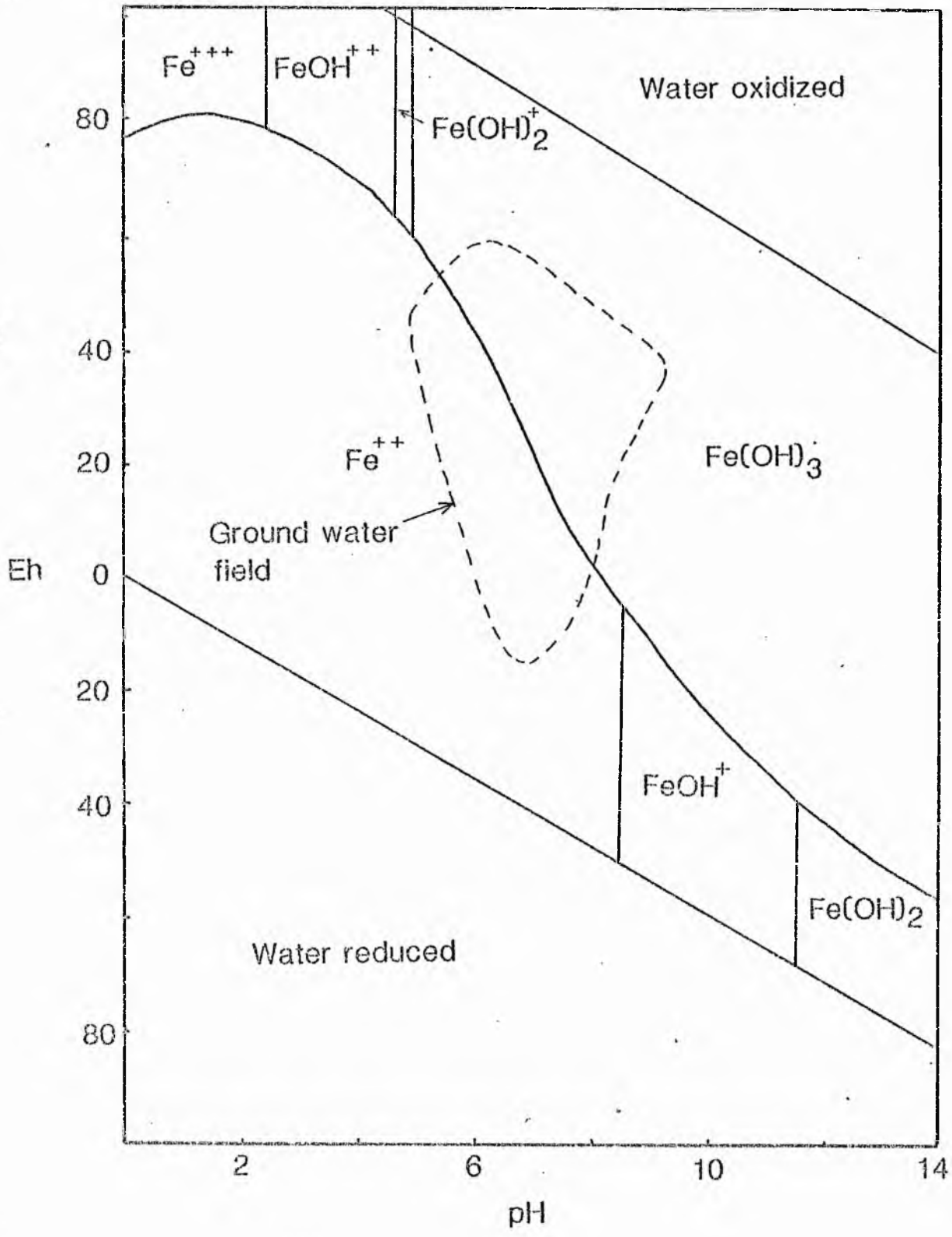

Fig. 3.50 Stability field diagram for aqueous ferric-ferrous system (after Walker, 1967).

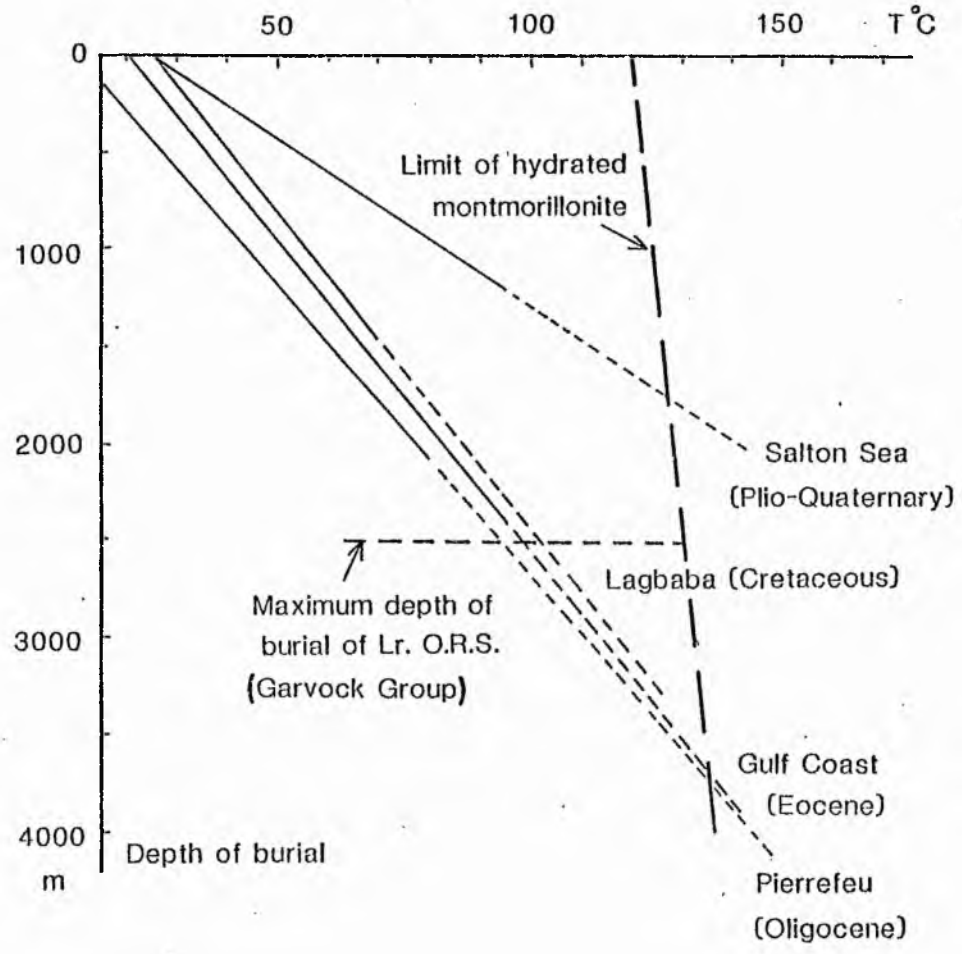

Fig. 3.51 The disappearance of smectite by burial. Dotted line: smectite are transformed into mixed layer illite-smectite (after Dunoyer De Segonzac, 1970).

Fig. 3.52. SEM photograph showing smooth circular markings on a grain surface. Could it be organic signatures? Scale bar equals 1 μm.

Fig. 3.53. SEM photograph showing simple cement stratigraphy. Note complete occlusion of the residual pore (left after smectite growth) by carbonate cement. Scale bar equals 10 μm.

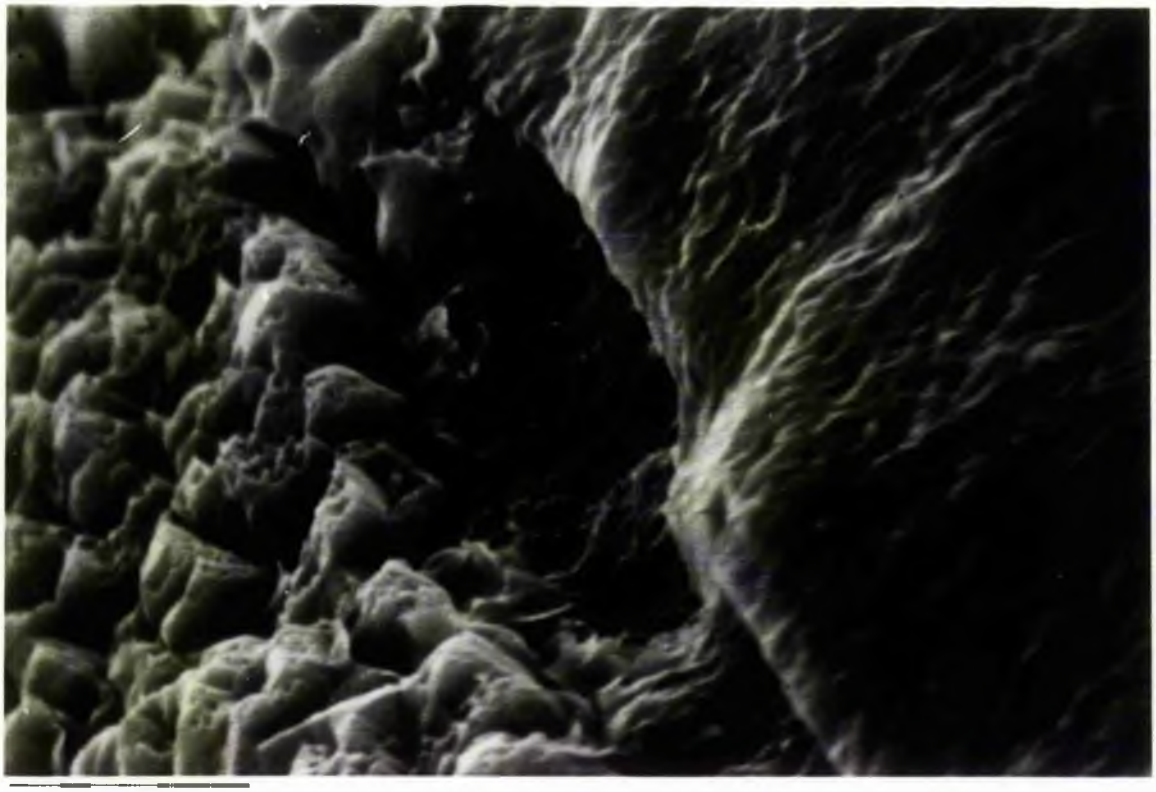

CHAPTER IV

GEOCHEMISTRY

Introduction

Samples from five selected profiles were subjected to electron-microprobe analyses for determining the major and trace element content of calcite. The elements analysed are plotted against each analysed profile. Instrumental techniques are listed in Appendix 4.1. In the following section the distribution of major and trace elements in specific profiles will be described and discussed, followed by consideration of the geochemistry of vadose and phreatic calcite.

4.1 Geochemistry of profiles

The amount of total calcite present in these profiles varies from 55% (near the top) to 8% (near the base, Figs. 4.1-4.5 and Table 4.1). It may show a gradual or an abrupt decrease downwards. Figs. 4.1 to 4.5 show that calcite content remains high (>35%) upto greater depths when lithofacies Sp and St (particularly Sp) are involved, whereas it tends to decrease rather rapidly in the case of lithofacies Sh. It is believed that comparatively easier circulation of pore fluids along the cross beds (due to higher permeability) than across flat beds is the major controlling factor for the depth of calcretization.

Element Variations

Major and trace elements analysed include Si, Ti, Al, Fe, Mg, Ca, Na, K, Mn and Sr. Elements other than Ca, Mg, Fe and Mn are generally very low and their variation is within the limits of analytical error, hence, they have not been plotted.

SiO_2 and TiO_2 are either absent or vary from .01% to 0.37% and 0.001 to 0.016% respectively. Although SiO_2 varies randomly within the profiles, it tends to be higher near the top (Table 4.1) and generally shows negative correlation with calcium. Al_2O_3 content ranges between 0.008 and 0.356% and like TiO_2 tends to show little variation within the profile, suggesting that these elements are fairly immobile. They show a generally negative correlation with calcium. Na and K are generally very low and vary from 55 to 227 ppm and 5 to 735 ppm respectively (Table 4.1). K shows a larger variation than Na and this is believed to be due to its limited substitution into calcite lattice (discussed later). Overall both Na and K show inverse relationships with CaO and their low values represent low salinity in pore fluids. Sr is normally absent but has been detected in a few samples from the base of the profiles. When detected, it varies randomly between 12 and 275 ppm (Table 4.1). It is difficult to interpret the Sr distribution but its common absence is believed to be due to the original deficiency in pore waters.

CaO

Although CaO content shows little variation, it tends to be maximum near the base (54.63 to 55.78%) and minimum in the middle (52.87 to 54.87%) of the profiles (Figs. 4.1 to

4.5 and Table 4.1). Near the top, it varies between 53.68 and 55.43%. Any increase or decrease in CaO values within the profile is accompanied by corresponding decrease or increase in the values of other elements (Figs. 4.1 to 4.5 and Table 4.1) excluding Mn. Generally, Mg and/or Fe account for the bulk of the change in the CaO values, hence, they also show a good negative correlation with CaO (Fig. 4.1 to 4.3 and 4.5). In Figs. 4.4 and 4.5 this relation is not very clear as the variation in CaO values is here partly accomodated by Si along with Mg and/or Fe (Table 4.1).

MgO

Unlike CaO, MgO content tends to be minimum near the base (0.05 to 0.46%) and maximum near the top (0.14 to 0.69%) of the profiles (Table 4.1 and Figs. 4.1 to 4.5). In the middle, it varies between 0.09 and 0.48%. MgO shows a negative correlation with CaO. The low MgO values are characteristic of most calcretes (See Reeve, 1976) and suggest precipitation from 'fresh' vadose waters wih low Mg/Ca ratios (Bricker, 1971 and Folk and Land, 1975).

Fe

Overall Fe shows large variation between 175 and 3606 ppm. It varies between 841 and 3189 ppm near the top of the profile while at the base it ranges between 175 and 3606 ppm (Table 4.1). Within the profiles Fe values are quite comparable near the top and the base but may be higher or lower in the middle (Figs. 4.1 to 4.5). Like Mg, Fe tends to show negative relation with CaO (Figs. 4.1 to 4.3). A few anomalously high values obtained from the base are

believed to be due to the influence of hematite present as grain coatings and blebs (See Chapter III). Overall high Fe content is believed to represent its original higher concentration in carbonate precipitating fluids.

Mn

Like Fe, Mn shows large variation within the profiles. It tends to be maximum near the base (1383 to 5497 ppm) and minimum in the middle (1146 to 2895 ppm). Near the top it varies between 1856 and 3756 ppm. Mn tends to show positive relation wih CaO. Overall higher values (average Mn content in carbonate rocks is 550 ppm - Wedepohl, 1978) of Mn suggest its original higher concentration in carbonate precipitating fluids. Because of its ionic size Mn^{2+} is known to fit well into the calcite.

The source of excess Mn and Fe is believed to be the unstable mafic minerals and rock fragments which during early diagenesis by intrastratal alteration released these elements.

4.2 Geochemistry of vadose (diplacive calcite - DC) and phreatic (P) calcite

Petrologically vadose (DC) and phreatic (P) calcite have been distinguished earlier in Chapter III and they occur near the top and base of the profiles respectively. Vadose calcite shows petrographic variations from well developed sparry crystals with simple or complicated morphologies to micritic, whilst phreatic calcite is always poikilitic upto a few millimetre in dimensions. This section gives an account of the geochemistry of these

calcites separately with the intention of establishing geochemical evidence to support the initial distinction between vadose and phreatic calcites made on the petroraphic and textural criteria.

Several calcite crystals filling adjacent pores were analysed using microprobe to see and compare the major and trace element variations between these calcites (Table 4.2). Elements analysed include Si, Ti, Al, Fe, Mg, Ca, Na, K, Mn and Sr. Of these only CaO, MgO, Fe and Mn have been compared and plotted as other elements are either very low or their variation is within the limits of analytical error. The average CaO, MgO, Fe and Mn values of DC and P calcites are given in Table 4.2 and complete analysis of individual crystals is given in Appendix 4.2. Samples examined come from the four selected profiles described earlier.

The standard deviation of CaO, MgO, Fe and Mn in DC is consistently higher than their respective values in P calcite in all the profiles (Table 4.2). Figs. 4.6 to 4.9 depicts more pronounced variation in DC than P calcite crystals in all the profiles. The large variations in the displacive calcite point to a vadose environment while the smaller variation in the poikilitic calcite are consistent with a phreatic formation (Pingitore, 1976).

4.3 Isotope Geochemisty

Stable isotope analyses were carried out on five samples (bulk) collected from profiles 1 and 3. Four of these samples were collected from the top and bottom of these profiles (to represent DC and P calcite zones) while

the fifth one was collected from the middle of the profile no. 3. The composition ranges of DC and P calcite are comparable and are $\delta^{13}C$ -4.72 to -6.93°/oo and $\delta^{18}O$ -6.96 to -9.9°/oo PDB (Table 4.3). The sample from the middle of the profile shows anomalous values, $\delta^{13}C$ -9.06 and $\delta^{18}O$ -13.38 (Table 4.3). The light $\delta^{13}C$ values may be the result of precipitation from pore waters affected by organically derived CO_2 and the light $\delta^{18}O$ values suggest meteoric waters (Pers. comm., Jim Marshall).

4.4 Discussion

The consistent higher degree of elemental variation between DC than P calcite crystals is significant and provides insight into the aqueous conditions. Considering the difference between the aqueous conditions in the vadose and phreatic environments, the transfer of ions by diffusion or physical motion of water would be expected to be much greater and rapid in the phreatic zone than in the vadose zone. Pingitore (1976) suggested that since all interconnected pores in the phreatic zone are in liquid and continuous ionic communication with one another, the water of the phreatic zone tends to be relatively homogeneous in chemical composition while such transfer potential exists on only a limited basis in the vadose zone. Hence the resultant phreatic calcites would be more homogeneous in chemical composition than the vadose calcites.

According to the above principle, the more pronounced variation of various elements between the displacive calcite (DC) crystals suggests a vadose environment while comparatively homogeneous nature of passive (P) calcite

indicates a phreatic environment. This supports the earlier made distinction on the basis of petrographic and textural criteria in Chapter III.

The cathodoluminescence of the DC and P calcite also suggests that the P calcite is chemically more homogeneous than the DC. Following the recent publications by Pierson (1981), Richter and Zinkernagel (1981), Frank et al, (1982), and Fairchild (1983), it is now believed that the cathodoluminescence of calcites is controlled by its chemistry, particularly Mn and Fe contents. Hence the overall uniform luminescence of P calcite (Fig. 3.33) shows that it is comparatively chemically homogeneous while the alternating darker and brighter zones in the DC crystals (Figs. 3.9 and 3.10) indicate rhythmic enrichment and/or depletion of Mn and/or Fe. The darker zones in displacive calcite crystals are perhaps richer in Fe and/or poorer in Mn than brighter zones, because, the absence of luminescence is believed to be due to high Fe and/or low Mn content (Fairchild, 1983). The rhythmic variation is here believed to be related to repeated wetting and drying periods causing dilution and concentration of ions.

Although overall phreatic calcite shows less elemental variation than vadose calcite, variation within phreatic calcite can sometimes be considerable. One of the possible factors responsible for this variation could be the clay fringes as they greatly restrict the mixing of pore waters by choking pore throats. On the contrary, chemical homogenety within vadose calcite can also occur. Pingitore (1976) suggested that this could be due to local wet spots near the vadose environment which would show chemistry

similar to the phreatic environment.

4.5 The Two Water System

Pingitore (1976) differentiated between the phreatic and vadose altered calcites in Barbados corals and explained the transformation mechanism by suggesting the two water system. He also stated that it remains to be seen whether this model can be applied under all conditions of climate and hydrologic settings but pointed that the principle of the two water system and its nature under vadose and phreatic conditions should be applicable to many aqueous diagenetic settings. A similar two water model is here believed to have operated during calcretization of these sediments. Field, petrological and geochemical evidences presented above and in earlier chapters suggest that following channel abandonment a low water table existed in unlithified sand bodies. Hence, phreatic conditions prevailed near the base of the profile while pores above the water table were intermittently filled with water or air (vadose environment). Several isolated pools also existed adjacent to the sand bodies and appears to have been the major source of carbonate clasts occurring in these sandstones.

In the vadose zone, water is spread to all hydrophilic surfaces by surface tension and by capillary attraction. This moisture absorption draws water into all available spaces including microspaces such as between cleavage planes in detrital micas and between component grains of rock fragments. Assereto and Kendall (1977) also indicated that moisture absorption draws water films of molecular

dimensions into all available spaces and this process alone is capable of generating swelling pressures of a few tens of atmospheres (Nepper-Christense, 1965, and Ravina and Zaslavsky, 1974). Subsequently during episodic high supersaturations (generated by rapid surface evaporation in dry times) in the vadose zone, calcite nucleates at multiple sites (perhaps favouring microspaces as less and less free energy is required; Berner, 1980) resulting in tiny crystals surrounded by a film of solution. Henniker (1949) presented a considerable amount of evidence of the existence of such solution films and according to Weyl (1959) "the solution can produce precipitation in the region of stress only if a film of solution separates the crystal from its constraint". The solution in these films is completely bound to crystal substrate and is immobile. Although the film is only a few molecules thick, it acts mechanically like a solid and is able to support shear stress and maintain a high diffusion rate (Hennicker, 1949). Rapid diffusion of ions through these films results in the displacive growth of these crystals by adding new crystal material. In so growing, the crystals exerts a stress against its constraint and causes expansion and dispersal of grains (see Chapter III). This phenomenon has been called the phenomenon of the force of crystallization and the pressure exerted by the growing crystal is transmitted through the film of the supersaturated solution (Weyl, 1959). The water in these films represents one type of water and is considered immobile. The second type of water (mobile) does pass through the interconnected modified pores in the vadose zone both during wet (under the force of

gravity) and dry (capillary rise) times. It is this water which maintains the supply of ions and hence the two waters intermittently come in contact in the vadose zone. Diffusion of ions takes place through the film as soon as sufficient supersaturation levels are attained (due to rapid evaporation) further displacive growth of crystals and pore occlusion results. The minimum level of supersaturation that is required to initiate the diffusion is not known. The process of crystal growth and pore occlusion continues till significant reduction in the rate of evaporation due to ever increasing pore occlusion occurs. This prevents generation of higher levels of supersaturation and hence the displacive growth stops. Ultimately, the residual pores are filled by passively grown sparry calcite (PC) (See Chapter III).

In the phreatic zone, comparatively homogeneous and very coarse crystals grew by the slow but continuous addition of ions (Fyfe, 1964).

4.6 Implications of the Two Water System

The significance of the two water model is that it neatly accounts for following problems:

1) the excessive (more than that can be accomodated in a normal sandstone as non-replacive cement) amount of carbonate in the zone of displacive calcite,

2) the problem of volume of fluid required to produce a lithified rock and

3) the preservation of sharp crystal edges.

The excessive amount of carbonate in the zone of displacive calcite is accounted for by the expansion and

dispersal of grains by displacive calcite. During the displacive growth of calcite, adequate supply of ions is maintained by the mobile water as it freely circulates between the interconnected pores until ultimately the pores are plugged.

Opinion differs as to the volume of fluid required to produce lithified rock. Kinsman (1969) and Bathurst (1975) favours a figure of 100,000 and 10,000 pore volumes respectively, while Berner (1980) has argued for at least 300,000 pore volumes to pass through a given volume of sand to enable the pore spaces to be completely filled with calcite. In the present sediments these figures would be reduced due to increased levels of supersaturation. However, movement of mobile water both during wet and dry periods is believed to have achieved similar figures (Pingitore, 1976).

It could be questioned that how the sharp crystal edges (see Chapter III, Figs 3.9 and 3.15) survived dissolution during the introduction of fresh solution (wet periods) which is initially undersaturated. It is here suggested that the immobile water which is bound strongly and completely to crystal substrate in the films prevented any dissolution while most of the water passed quickly through the larger interconnected pores in the vadose zone. According to Pingitore (1976) the films act as a temporary closed system.

4.7 Geochemistry of displacive calcite occurring within expanded biotite (EB) and between dispersed grains (BG)

In the vadose zone during dry periods, ratio of various

trace elements to calcium would build up in the thin films of immobile water until they come in contact with freshly introduced water (Pingitore, 1976). The degree of build-up would vary depending upon the chemical nature of the constraining grains (eg. it would be expected to be more pronounced within the expanding biotites than between more stable quartz grains). To test this hypothesis, microprobe analyses were carried out on the displacive calcite occurring within expanded biotite (EB) and between dispersed grains (BG). The trace element content of these two types of calcites (EB and BG) has been compared (Table 4.4 and Fig. 4.10). The data show that most of the elements including Si, Al, Fe, Mg, Na and K are enriched in the calcite occurring within expanded biotite while Mn tends to be more in the calcite occurring between grains. This confirms that Si, Al, Fe, Mg, Na and K to Ca ratios in thin films within expanding biotites build up probably until the introduction of fresh water during a wet period. All these enriched elements are believed to have entered the film by diffusion from the biotite and eventually go into calcite during the following phase of displacive growth when new crystal material is added. Ca is either replaced or diffuses out of the calcite to accomodate these elements, hence, is always found to be depleted in the calcite occurring within expanded biotites. Such enrichment of trace elements by preferential removal of calcium from the diagenetic site has been called "autoenrichment" by Pingitore (in press c.f. Watts, 1977).

The model presented above supports Pingitore's (1976) opinion that the principle of the two water system under

vadose and phreatic conditions is applicable to many aqueous diagenetic settings. It also explains the calcretization of Carnoustie sandstones by dominantly displacive calcite. It remains to be seen whether these sediments are unique or whether there are more examples of similar calcretes elsewhere, to which this model can be applied.

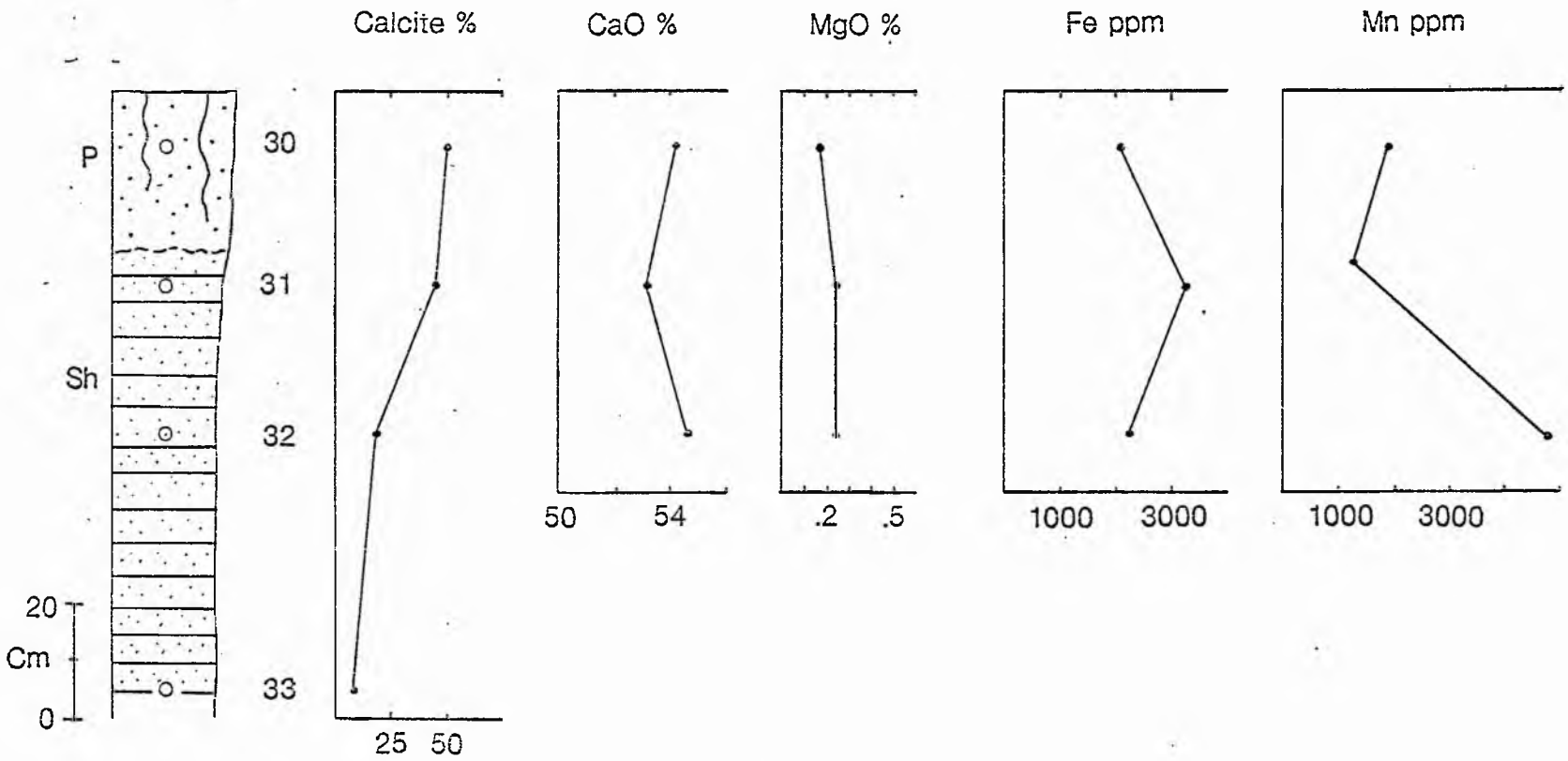

Fig. 4.1 Element variations (in calcites) within profile 1 (microprobe analyses).

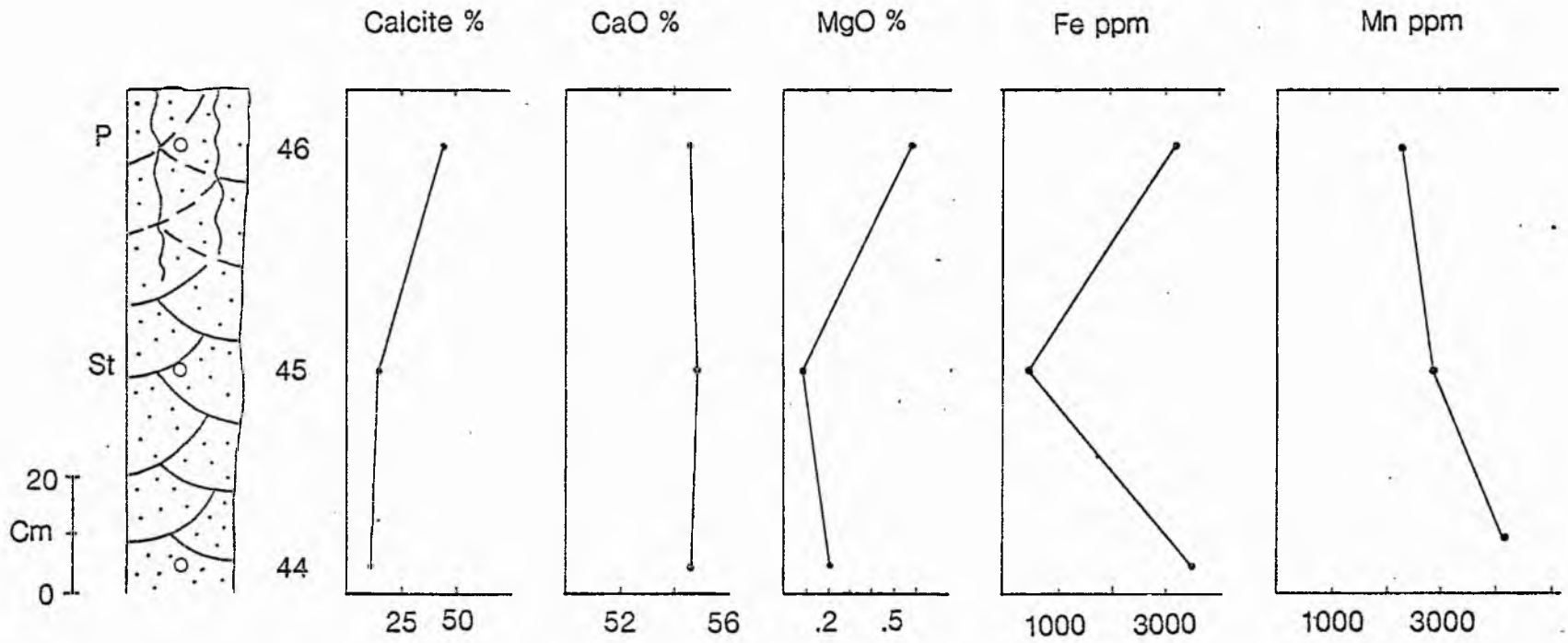

Fig. 4.2 Element variations (in calcites) within profile 2 (microprobe analyses).

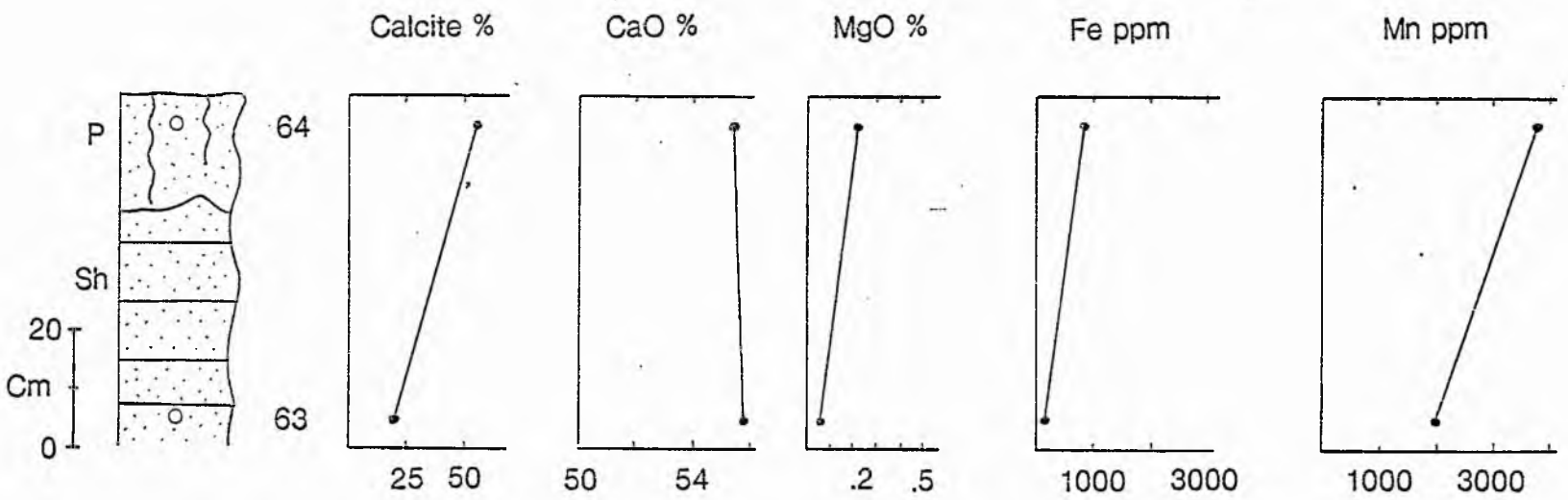

Fig. 4.3 Element variations (in calcites) within profile 3 (microprobe analyses).

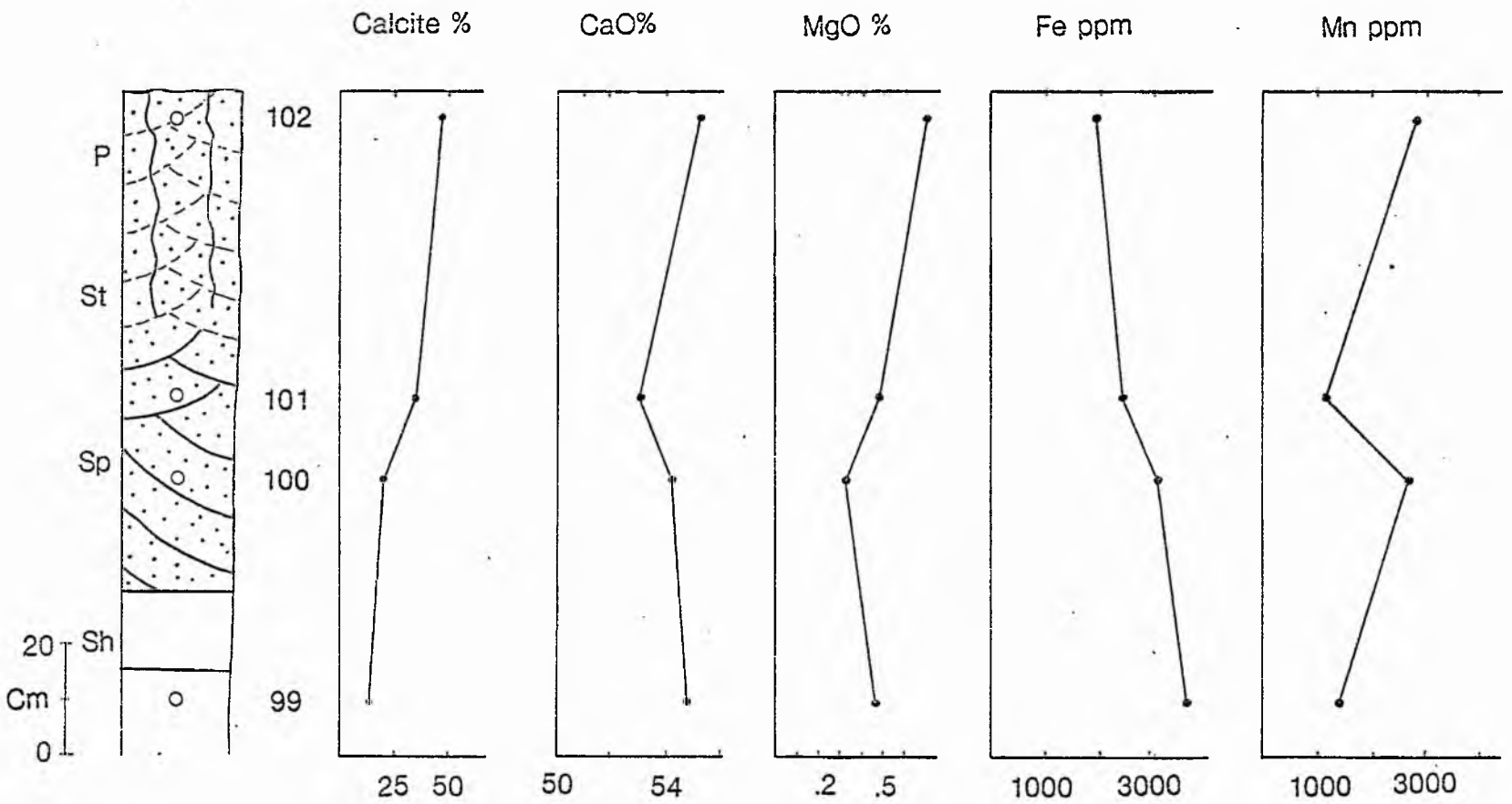

Fig. 4.4 Element variations (in calcites) within profile 4 (microprobe analyses).

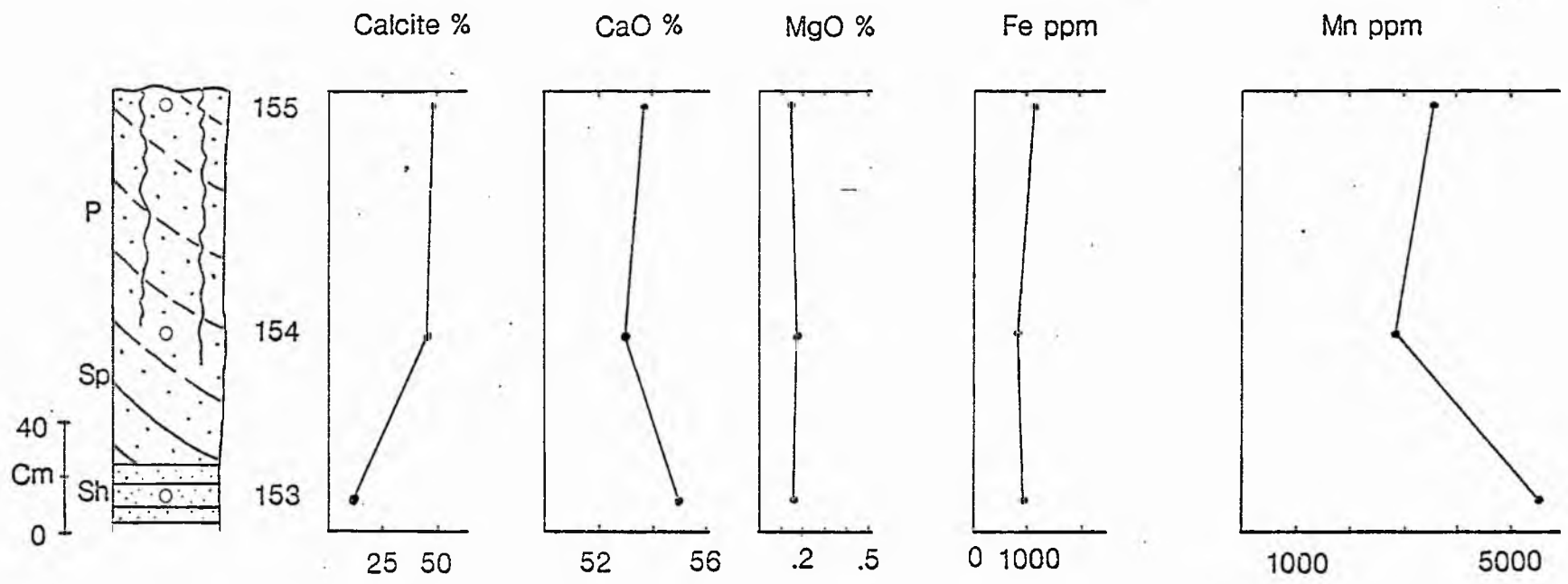

Fig. 4.5 Element variations (in calcites) within profile 5 (microprobe analyses)

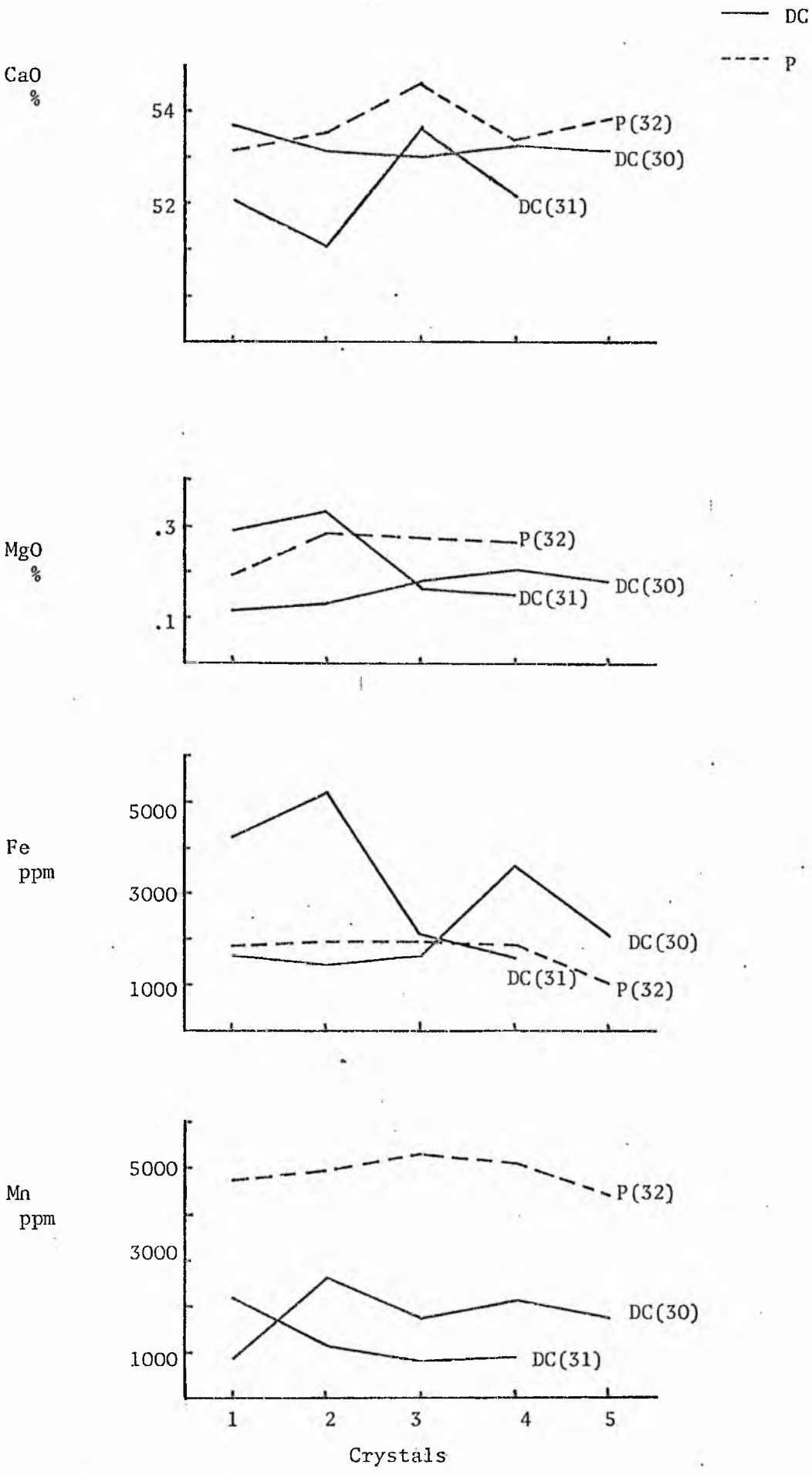

Fig. 4.6 Element variations in vadose (DC) and phreatic (P) calcite crystals (profile 1).

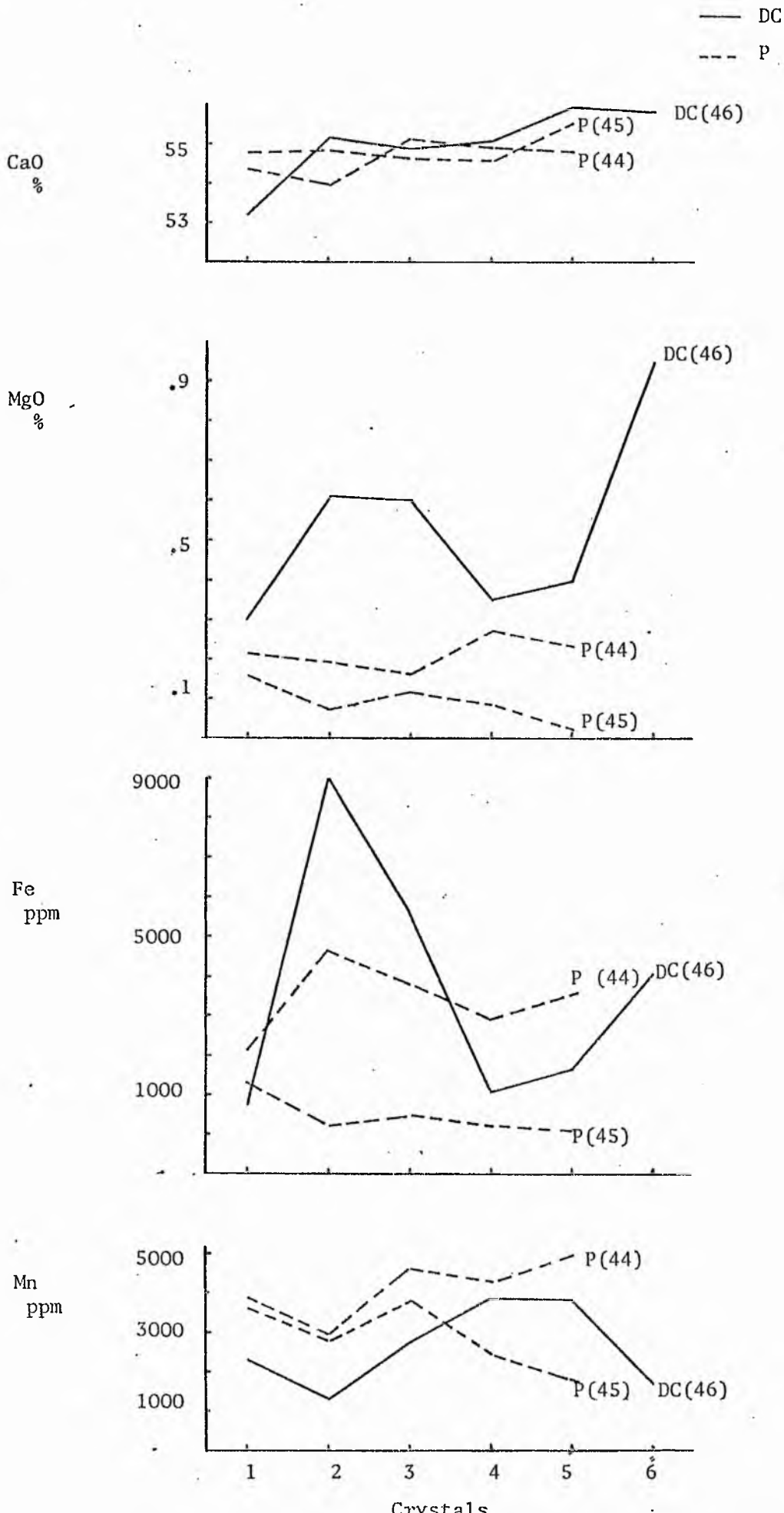

Fig. 4.7 Element variations in vadose (DC) and phreatic (P) calcite crystals (profile 2).

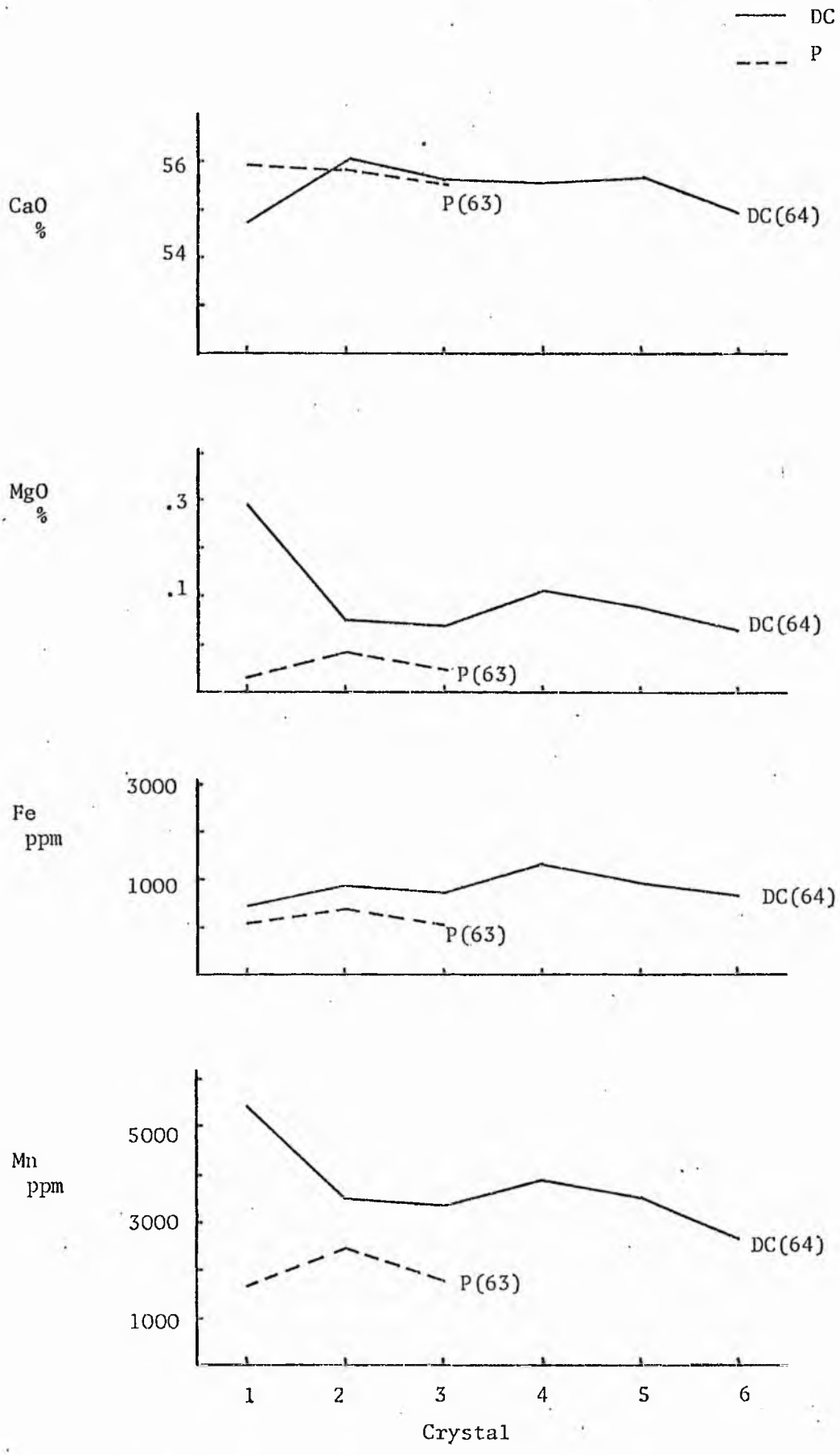

Fig. 4.8 Element variations in vadose (DC) and phreatic (P) calcite crystals (profile 3).

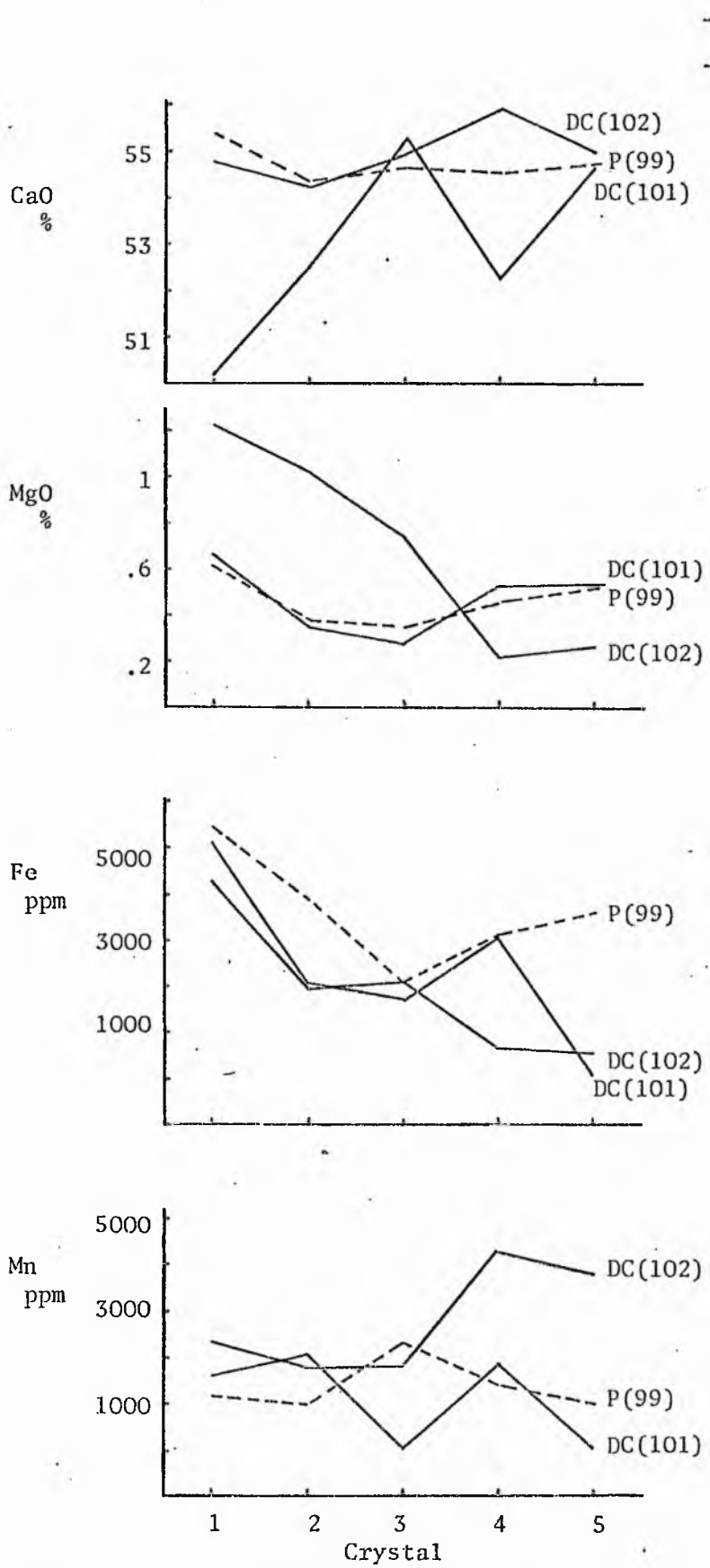

Fig. 4.9 Element variations in vadose (DC) and phreatic (P) calcite crystals (profile 4).

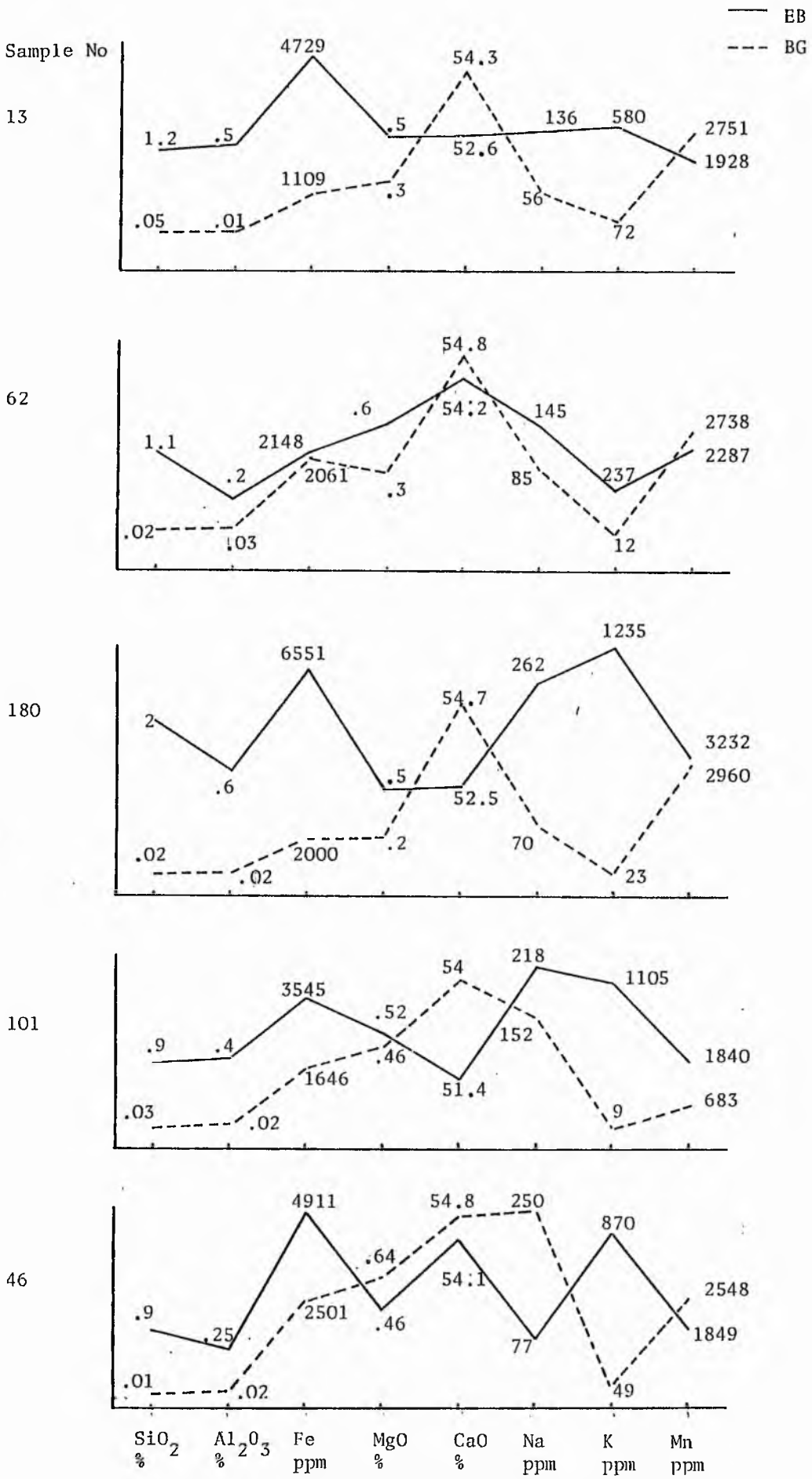

Fig. 4.10 Major and trace element variations in Displacive Calcite occurring within expanded biotite (EB) and between dispersed grains (BG).

Table 4.1 Mean values of major and trace elements in calcite from different profiles.

Sample No	Calcite %	n	SiO_2 %	TiO_2 %	Al_2O_3 %	Fe ppm	MgO %	CaO %	Na ppm	K ppm	Mn ppm	Sr ppm
30	50	5	0.053	0.016	0.040	2084	0.162	54.26	152	276	1856	ND
31	45	4	0.165	0.058	0.356	3272	0.236	53.21	207	735	1283	ND
32	18	6	0.187	0.0136	0.0175	2267	0.2405	54.64	155	48	4773	275
46	45	7	0.252	0.008	0.09	3189	0.5941	54.66	200	283	2348	ND
45	15	5	ND	ND	0.015	458	0.095	54.87	90	41	2895	51
44	12	5	.002	ND	.009	3425	0.212	54.63	68.2	98	4164	101
64	55	6	ND	0.008	0.008	841	0.205	55.43	63	22	3756	ND
63	20	3	0.011	ND	0.009	175	0.058	55.78	68	17	1994	ND
102	47	5	0.0187	0.004	0.021	1940	0.697	55.19	55	5	2828	ND
101	35	5	0.371	0.015	0.170	2405	0.4837	53.00	178	447	1146	ND
100	20	4	0.016	0.0031	0.0191	3054	0.3216	54.15	128	97	2689	ND
99	13	5	0.013	ND	0.025	3606	0.4632	54.76	82	22	1383	12
155	48	5	0.0113	0.001	0.018	1124	0.1457	53.68	70	110	3558	ND
154	45	4	0.205	ND	0.085	798	0.17	52.87	55	180	2858	ND
153	11	6	0.010	0.003	0.014	917	0.1513	54.96	64	72	5497	ND

n= Number of crystals analysed

Table 4.2 Elemental variation between Vadose (DC) and Phreatic (P) calcite

Element	Calcite type	Profile 1 n	Profile 1 Mean	Profile 1 SD	Profile 2 n	Profile 2 Mean	Profile 2 SD	Profile 3 n	Profile 3 Mean	Profile 3 SD	Profile 4 n	Profile 4 Mean	Profile 4 SD
CaO %	DC	9	53.79	0.88	6	54.99	0.99	6	55.39	0.43	10	53.99	1.76
	P	5	54.71	0.59	10	54.75	0.41	3	55.78	0.18	5	54.76	0.39
MgO %	DC	9	0.19	0.07	6	0.54	0.24	6	0.206	0.09	10	0.58	0.33
	P	5	0.23	0.05	10	0.15	0.07	3	0.06	0.02	5	0.46	0.10
Fe ppm	DC	9	2612	1389	6	3699	32 32	6	841	297	10	2166	1599
	P	5	1733	404	10	1941	1723	3	176	162	5	3606	1258
Mn ppm	DC	9	1600	674	6	2654	1054	6	3756	927	10	1987	1343
	P	5	4900	347	10	3529	1009	3	1994	423	5	1383	556

n = Number of crystals analysed

SD = Standard deviation

Table 4.3 $\delta^{13}C$ and $\delta^{18}O$ compositions of samples

Sample No	$\delta^{13}C$ (PDB)	$\delta^{18}O$ (PDB)
30	-6.725	-8.536
32	-4.723	-9.938
102	-6.937	-6.958
100	-9.063	-13.38
99	-6.335	-8.875

Table 4.4 Mean values of major and trace elements in displacive calcite occurring within expanded biotite (EB) and dispersed grains (BG).

Sample No	n	Description	SiO_2 %	TiO_2 %	Al_2O_3 %	Fe ppm	MgO %	CaO %	Na ppm	K ppm	Mn ppm
13	3	EB	1.156	0.025	0.4848	4729	0.5362	52.62	136	580	1928
13	3	BG	0.045	0.0015	0.013	1109	0.2827	54.31	56	72	2751
62	4	EB	1.08	0.0155	0.189	21 48	0.583	54.17	145	237	2287
62	2	BG	0.0243	0.007	0.025	2061	0.3278	54.75	85	12	2738
180	1	EB	2.018	0.027	0.57	6551	0.47	52.46	262	1235	3232
180	3	BG	0.015	0.002	0.02	1999	0.22	54.68	70	23	2960
101	2	EB	0.886	0.036	0.3941	3545	0.524	51.38	218	1105	1840
101	3	BG	0.0276	0.0008	0.021	1646	0.456	54.09	152	9	683
46	2	EB	0.86	0.021	0.2528	4911	0.4613	54.16	77	870	1849
46	5	BG	.0096	0.004	0.025	2501	0.647	54.87	249	49	2548

n= Number of crystals analysed

CHAPTER V

PEDOGENESIS

An intergrated petrological , mineralogical and geochemical approach has been applied to the study of diagenesis of Lower Old Red Sandstone of Carnoustie and a specific pedogenic model for their calcretization has been proposed.

5.1 The Pedogenic Model

Goudie (1973) recognized two subdivisions within the pedogenic model, the *per ascensum* and *per descensum*.

The *per ascensum* hypothesis states that undersaturated percolating waters penetrate to a certain depth, dissolve carbonate and other material and return to the surface by capillarity where deposition may take place through evaporation, CO_2 loss or both. The *per descensum* model involves leaching of carbonates and other material from the upper soil horizons and their deposition and accumulation at depth.

The field, petrological and geochemical evidences presented in earlier chapters all support the *per ascensum* model for calcretization of the Carnoustie sandstones. The calcretization of only the top (few centimetre to a few decimetre) sediments with displacively grown calcite in all the profiles suggests that during dry episodes water ascended by capillarity and spread to all hydrophilic surfaces. Subsequently on rapid evaporation

perhaps with some CO2 loss calcite precipitated from supersaturated solutions in the vadose environment as described earlier in Chapter IV.

Although the displacive growth of calcite in calcretes has been described earlier by a few workers including Allen (1974), Read (1974) and Watts (1978), a precise mechanism of the growth has not been proposed. The two water model suggested earlier in Chapter IV is an attempt to explain the mechanism of growth of displacive calcite crystals and to differentiate between vadose and phreatic calcite present in these sediments.

Although texturally the displacive calcite found in these sediments is unique, chemically being low Mg calcite (MgO content varies between 0.14 and 0.69%), it is similar to most worldwide calcrete calcites (Reeves, 1976). The common absence or low content of Na and K in the low Mg calcites of Carnoustie suggests precipitation from 'fresh' vadose waters with low Mg/Ca ratios (Folk and Land, 1975).

Recently, following Yaalon and Wieder (1976), Watts (1980) suggested that high Mg-calcite is the initial precipitate which then alters to a low Mg form. The magnesium released during such transformation contributes to the formation of palygorskite, sepiolite and dolomite, a common mineral association found in calcretes and other arid zone calcareous soils. Watts (1980) suggested the above model for the Quaternary pedogenic calcretes of the Kalahari and questioned if it can be applied universally. This is discussed below.

5.2 Absence of originally high Mg calcite in Carnoustie calcretes

The crystal morphologies (well developed simple rhombs) of displacive calcite observed in these sediments suggest that the calcite was originally low Mg-calcite, as the crystal morphologies of high Mg-calcite would be much different. Mg ions poison sideways growth of calcite crystals and result in fibrous crystals or elongate rhombs (Folk, 1974). No fibrous crystals were found in these sediments (Chapter III) and textural evidence for originally high Mg-calcite is also absent. In addition, absence of common associates such as palygorskite, sepiolite and dolomite is also significant in terms of calcretization model suggested by Watts (1980). Mg released during transformation should have converted smectite into palygorskite.

The petrographic (particularly cathodoluminescence) and geochemical evidences suggest that the process of calcretization in Lower Old Red Sandstone of Carnoustie is not consistent with the Quaternary calcretization model of Watts (1980). Textural evidence suggests that displacive calcite was originally low in Mg and its growth is believed to have occurred from pore waters with original extremely low Mg/Ca ratios. It is believed that the Mg/Ca ratio of the pore water was so low that even on rapid and forced crystallization only low Mg-calcite could form. Watts (1977) also examined Siluro-Devonian calcretes from Wales and stated that "they somewhat pose a problem as evidence for originally high Mg-calcites is generally absent (except for rare, possibly aragonitic or high Mg-calcite, early fibrous cements) and palygorskite is lacking". He attributed this discrepancy in his Quaternary model of calcretization to ground water influence.

Watts (1977) suggested that high ground water levels during loss of Mg from original high Mg-calcite would cause dilution of Mg inhibiting palygorskite formation, hence, only dolomite would precipitate. The absence of dolomite, palygorskite and high Mg-calcite in Lower Devonian calcretes of Carnoustie taken together questions the universal applicability of Watts (1980) Quaternary model of calcretization.

5.3 Absence of Palygorskite

The absence of palygorskite is considered significant in terms of calcretization model as it could mean that either the Quaternary calcretization model of Watt's (1980) is not universal or some other unknown factors are involved in this discrepancy. Assuming that the Quaternary model of Watt's (1980) is consistent through time and high Mg-calcite was precipitated (although crystal morphologies and textural evidence are against it), then there would seem no reason why palygorskite should not have formed. It might be argued that palygorskite was formed but subsequently altered to mixed-layer clays and smectite at fairly low temperature (Mumpton and Roy, 1958). If such transformation occurred, abundant dolomitization and authigenic silica cement would be expected. The absence of dolomite and much late silica cementation in these profiles, thus argues for the absence of palygorskite.

Finally, the original absence of high Mg-calcite, palygorskite and dolomite suggests that the Quaternary model of Watts (1980) cannot be applied to these sediments and hence its

universal applicability is questioned. It is here suggested that displacive calcite (low Mg) growth in these profiles occurred from rapidly evaporating pore waters with extremely low Mg/Ca ratios. Hence, the chemistry of pore waters and micro-environmental conditions within the pores are considered to be major significant factors controlling process of calcretization. Although, the dominance of palygorskite and sepiolite in many calcrete profiles is well explained by Quaternary calcretization model of Watts (1980), it seems that no one process applies to all calcretes and therefore further research on this major process in semi-arid, continental environments is essential.

5.4 Source of Ca

The source of Ca and carbonate ions is not known at present. Goudie (1973) and Reeves (1976) considered aeolian dust to be the major source of ions while Gardner (1972) and Stalder (1975) favoured rainwater (to a limited extent) and sheet floods respectively. A mixed source involving aeolian dust, rainwater, sheet floods, carbonate clasts, marls and volcanic fragments is here thought to have contributed the required ions.

5.5 Significance of calcretization

Calcretes are commonly thought to be restricted to arid and semi-arid environments but Harrison (1977) stated that they may form even in sub-humid climates. Goudie (1973) pointed that

caution "needs to be exercised in the use of calcretes as a paleoclimatic indicator, for climate is but one of the factors in its developments". However, calcretization of Lower Old Red Sandstone of Carnoustie with displacively grown calcite must have occurred in warm and semi-arid climate. Another significant feature that calcretes reperesent is periods of geomorphological stability. The formation of mature and comparatively thin calcretes on channel switching in Carnoustie sandstone is thought to represent rather short geological periods (4 - 20,000 years, by comparison with profiles described by Robbin and Stipp, 1979; Hay and Reeder, 1978 and Gile et al, 1966) of stability. The precise cause of channel switching is not known, however, if it was due to tectonic activity, the repeated formation of calcretes suggest that stable periods prevailed subsequent to channel switching. Hence, the tectonic activity must have been less subdued towards the top of the Lower Old Red Sandstone as compared to the early Lower Old Red Sandstone during which volcanism was still active as suggested by earlier workers (Mykura, 1983).

SECTION - II

CHAPTER VI

LITHOLOGIES AND ENVIRONMENT OF DEPOSITION OF VIKING, CARDIUM AND BELLY RIVER FORMATIONS

This section is based on studies carried out under the auspices of Shawa Geoconsultants Ltd. of Calgary, Canada, during a project on "The Geology of the Belly River, Cardium and Viking Reservoirs of Southcentral Alberta". Identification and description of lithologies, sedimentation and environmental reconstructions were primarily carried out by E.K.Walton and M.S.Shawa while the present author worked on the petrology and diagenesis of the sediments. The interpretation of sedimentation and environment of deposition is based on data collected from stratigraphic synthesis and the geometry of sand bodies, cutting and core description and gamma ray curves which generally mimic the vertical distribution of grain size. A total of 77 wells, comprising 33 from the Viking Formation, 21 from the Cardium Formation, 3 including both the Cardium and the Viking, and 20 from the Belly River Formation were examined. The areal distribution of the wells and cuttings is variable amongst the formations (Figs. 6.1 to 6.3).

6.1 Sedimentation and Lithologies of Viking Formation

The Viking Formation is a sandy unit of variable coarseness and thickness (120 to 150 m) within the shales of the Lower Colorado Group. From central Alberta towards the east and

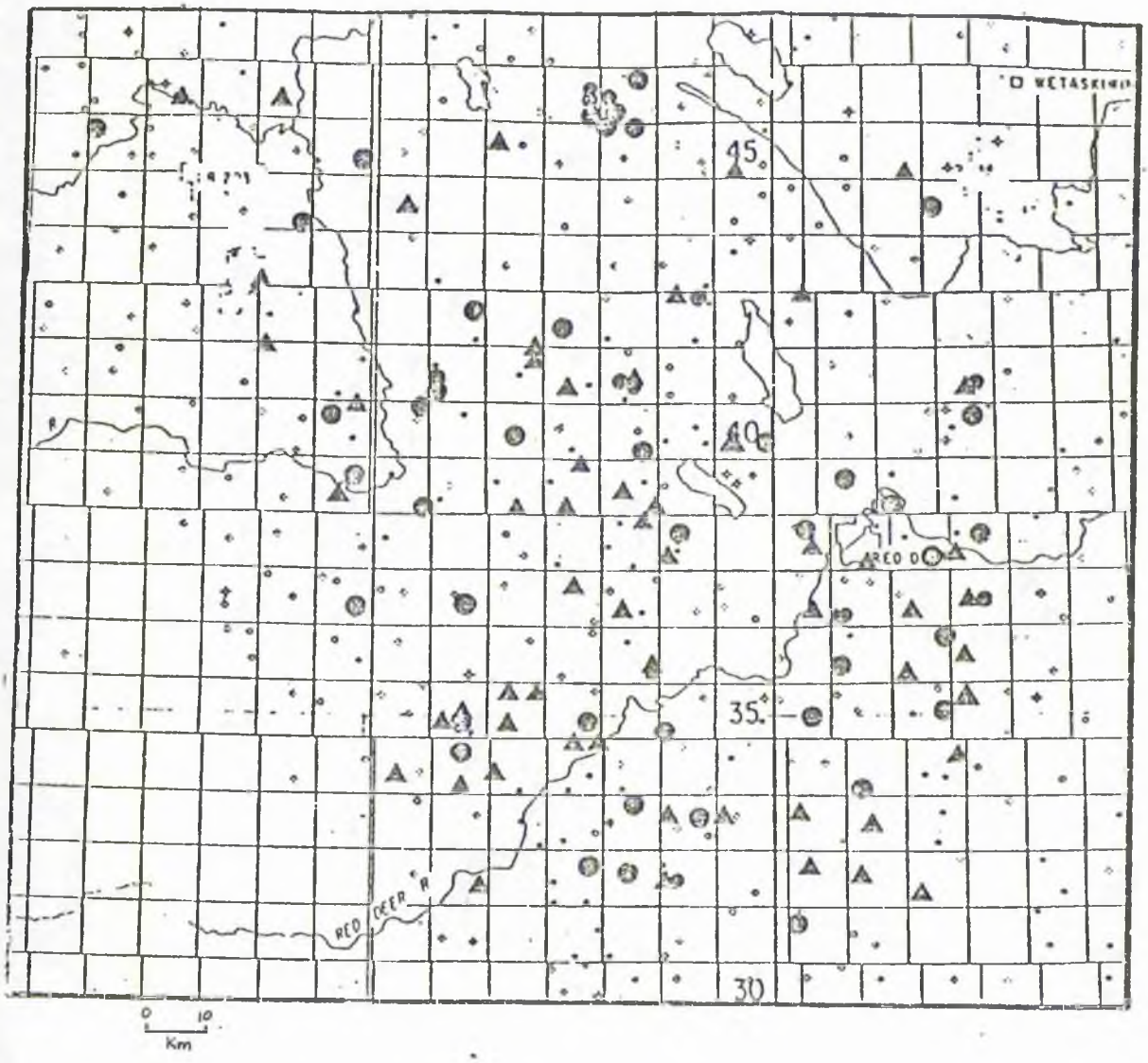

Fig. 6.1 Distribution of Cores (circles) and cuttings (triangles) analyzed from the Viking Formation.

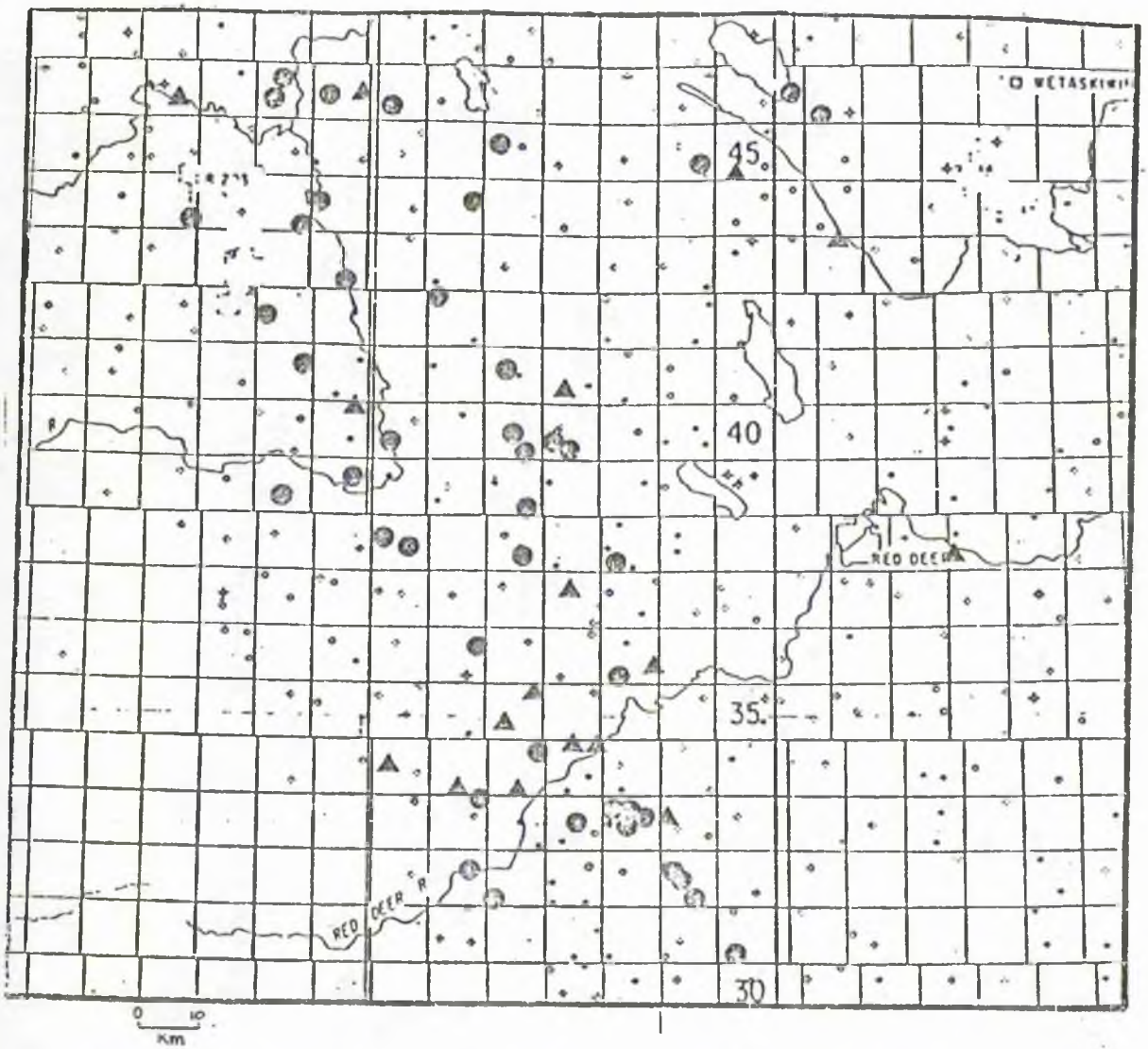

Fig. 6.2 Distribution of cores (circles) and cuttings (triangles) analyzed from the Cardium Formation.

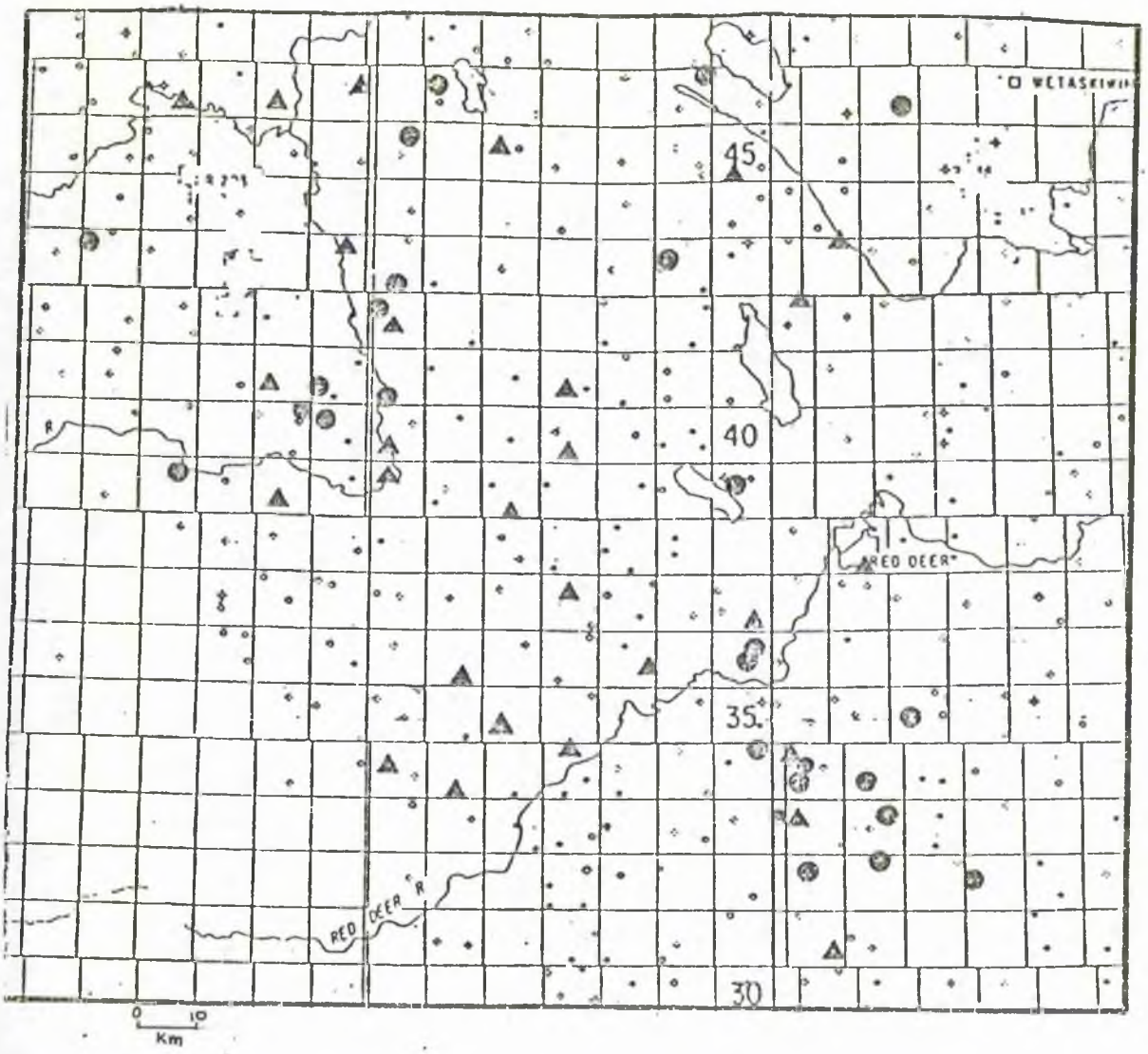

Fig. 6.3 Distribution of cores (circles) and cuttings (triangles) analyzed from the Belly River Group.

northeast the Viking becomes progressively finer grained and more shaly until it disappears as a sandstone unit into the marine shales of the Ashville Formation in Manitoba. Two separate genetic sandstone units were recognized for the Viking Formation. They are designated in descending order 'A' and 'B'. A third genetic unit, which is very thin, poorly developed and has a limited areal distribution was also recognized. This latter unit is present just above unit 'A' and referred to here as "Upper unit". Fig. 6.4 shows type log of the Viking Formation.

Both units 'A' and 'B' show dominant coarsening upward distribution of grain size and in some places uniform vertical distribution. Most of the sandstone between the two units is rich in silty matrix and generally bioturbated. Even the sandstones of the two units contain a high content of silt matrix and bioturbation. The degree of bioturbation and the silty matrix content of both units 'A' and 'B' when present, seem to be less than in the rest of the Viking sediments. The two units can always be identified on both gamma-ray and SP curves.

Unit 'A' could consist of two coarsening upward cycles or at some places one coarsening upward cycle overlain by a blocky cycle. At times this blocky cycle is replaced by a thin interval of clean sandstone. Occasionally, however, Unit 'A' exhibits a fining upward cycle overlain by a thin interval of clean sandstone. The vertical distribution of Unit 'B' is in general very similar to that of Unit 'A'.

Various lithologies that comprise Viking Formation consists predominantly of sandstone, siltstone, shale with lesser amounts of conglomerate, bentonite and occasional coal. The conglomerate

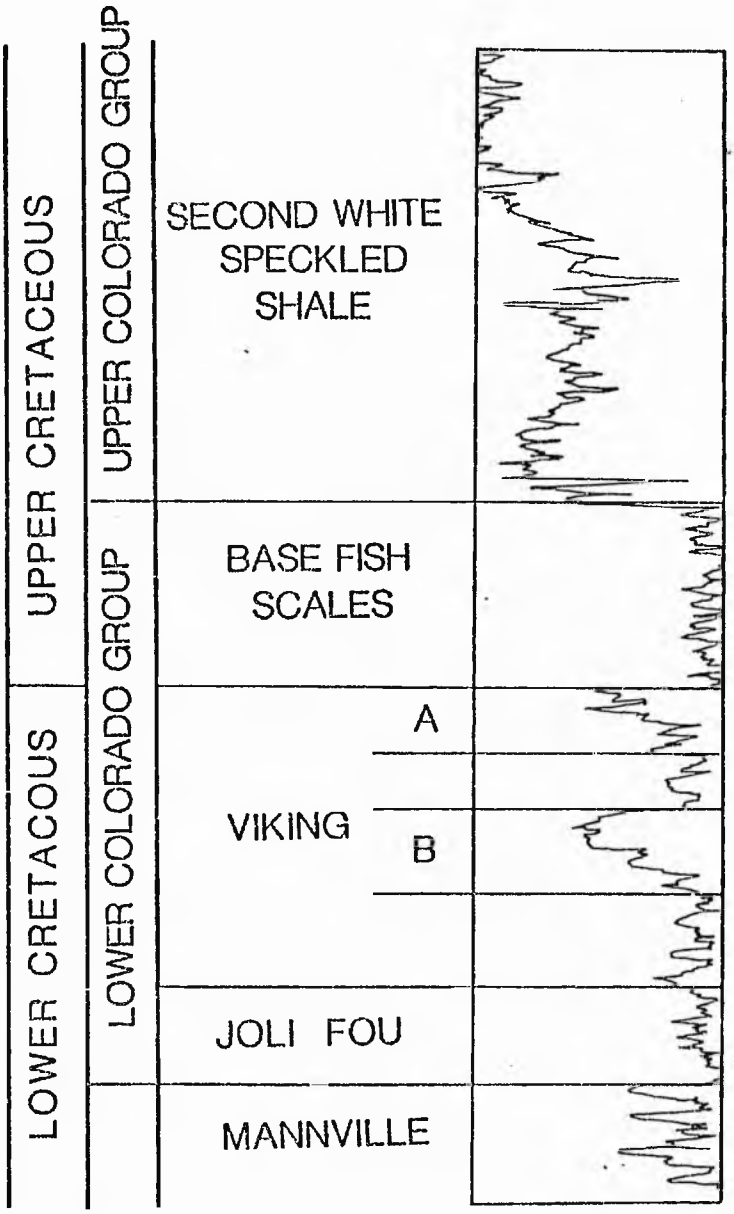

Fig. 6.4 Type gamma-ray log for the Viking Formation (eastern part) showing the stratigraphic position of the A and B units.

is usually found in thin beds on or near the top of Units 'A' and 'B' and sometimes within the 'Upper Unit'. Bentonite and coal seams are found within the Viking Formation at various levels. The sandstone, however, is the dominant lithology in the Viking Formation. In general, the mineralogical composition of the above mentioned three units of Viking Fm. is identical.

Four main lithologies that makeup the Viking and the Cardium Formations are described below. The sedimentary signatures of the Viking and Cardium Formations are sufficiently similar to warrant their being taken together.

a. Shale - medium to dark and sometimes very dark grey, often silty and sometimes wih siltstone and sandstone stringers. In the Cardium Fm. horizons with scattered pebbles are recorded. Plant fragments and fish remains occur. In the two formations the plant fragments are restricted to wells in the south-west. Fish remains are reported from the Viking along with plant fragments in the Viking, south and west. Siderite nodules are fairly common throughout the region and occasionally a siderite band occurs. Pyrite is recorded but is less common than siderite; it is found in Viking shales in the south-east but in Cardium in the north as well as the south. Bioturbation is common.

b. Siltstone, Very fine (VF)-grained and Fine (F)-grained Sandstone.

These lithologies commonly occur together and tend to grade into one another. Colours are light grey or grey sometimes with a salt and pepper appearance. Sorting is good and the commonest lamination is microcross-lamination associated with ripples and

lenticular or wavy bedding. Unit thickness varies from very thin laminated horizons to thickly bedded sandstones. Medium-scale cross-lamination also occurs as does horizontal lamination but primary structures are disturbed by very widespread and sometimes intense bioturbation. Shale drapes are recorded from two wells. Mica is a common constituent; glauconite is widely reported as an important constituent in the core descriptions but this is not confirmed by thin-section examination which suggests that glauconite although fairly widespread is a very minor constituent. Pyrite is present but scarce and less common than siderite nodules which, according to Krause (1983) may reach 10 cm thick.

Trace fossils reported from the Cardium Fm. (Krause. 1983; Wright and Walker, 1981) include Zoophycus, Rhizocorallium, Chondrites, Skolithos Neonereites, Scalarituba, Planolites and Palaeophycus.

c. Coarser Sandstones. A less common lithology is made up of medium-grained to very coarse-grained sandstones. These have a pepper and salt appearance due to black chert grains in a buff-coloured blackground. Some are well sorted but most only moderately or poorly sorted. Structures vary, with horizontal, micro- and medium-scale cross-lamination less disturbed by bioturbation than in lithology B; as in B, micro-cross-lamination is most common.

d. Conglomerates. The coarsest rocks are pebble and granule conglomerates whose appearance is dominated by black and white chert clasts which often form the dominant constituents. Quartz as well as sideritic pebbles also occur. Sorting is usually poor

even though individual bands may be only a less than one inch thick. The thickest conglomerate recorded in the present area is 10 ft. (south-central area).

6.2 Environment of deposition of Viking Formation

The sediments of Viking Fm. were deposited in a multi-environment setting ranging from near shore marine to lagoonal. The presence of fish remains, shell fragments and glauconite supports a marine origin for most of the Viking and the presence of coal seams suggest a lagoonal or coastal environment. Two main pulses of sand deposition took place during Viking time. One pulse was responsible for the deposition of Unit 'B' sediments and the other was responsible for the deposition of Unit 'A' sediments. A third minor pulse deposited 'Upper Unit' sediments. The bulk of the Viking sediments were deposited on a shallow near-shore marine shelf characterized by a low energy environment as suggested by the high degree of bioturbation throughout most of the formation. The presence of ripples and trough cross beds on a small scale also lends support to the interpretation of a low energy setting for most of the Viking Formation (Shawa, 1984). Longshore currents reworked and redistributed the sediments of both Units 'A' and 'B' to form off-shore bars that were parallel to the shore and kept migrating seaward. The lower part of these off-shore bars was deposited under fair weather conditions characterized by the presence of ripples, trough cross-beds on a small scale and a high degree of bioturbation. The upper part was deposited above wave base level

during storms or when the bathymetry of the shelf decreased. The presence of pebbles, lack of bioturbation and the low content of silt and clay matrix support this conclusion. The occasional presence of shale stringers and coal seams near or above both units suggests lagoonal conditions associated with coastal environments (Shawa, 1984).

6.3 Sedimentation and Lithologies of the Cardium Formation

The Cardium is the main sandstone unit within the Colorado Group and varies in thickness from 25 m to 125 m (Stott, 1963). Like Viking, two separate genetic sandstone units were recognized for the Cardium Fm. They are designated in descending order 'A' and 'B' and shown in Figure 6.5. Genetic unit 'A' is widespread in the study area unlike unit 'B' which has a limited areal distribution. The thickness of unit 'A' is highly irregular. In general, this unit shows slight coarsening upward in grain size and consists of one sedimentary cycle. Occasionally, unit 'A' consists of two sedimentary cycles that show a somewhat coarsening upward distribution of grain size. Also, in many wells, this unit exhibits a uniform distribution of grain size that can be observed on gamma ray curves by its blocky character. Unit 'B' also shows coarsening upward or blocky cycles but is much thinner than unit 'A'. In many places the sandstone of unit 'A' is bioturbated and contains a high proportion of silt matrix. According to Shawa (1984), the reservoir facies of unit 'A' is restricted to the western half of the study area and is distributed as elongated and relatively narrow bodies that trend generally in a

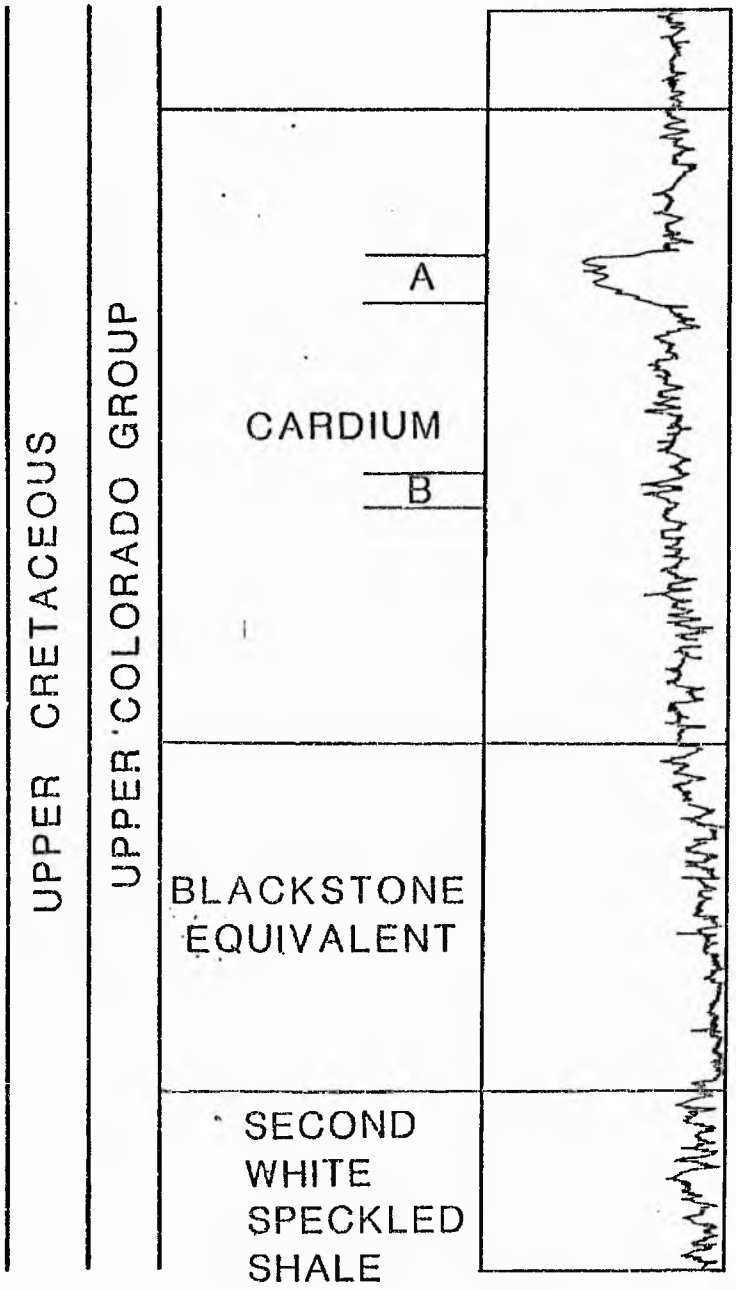

Fig. 6.5 Type gamma-ray log for the Cardium Formation (central area) showing the stratigraphic position of the A and B units.

northwest-southeast direction. The average thickness of the reservoir facies is 5 m although in places it attains thickness slightly over 15 m. In general the reservoir facies is defined as an almost clean sandstone which is segregated from the other sandstone which may be bioturbated or contain a large volume of fine matrix. It is detected on both gamma-ray and SP curves where both are deflected well to the left of the shale line.

Unit 'B' is restricted to the western part of the study area and has much less areal extent than unit 'A'. Its vertical distribution of grain size is very similar to that of unit 'A'. The reservoir facies of unit 'B' form elongated narrow bodies and have an average thickness of slightly over 2.5 m. They also have a preferred northwest-southeast trends.

Various lithologies that comprise Cardium Formation are similar to that observed in Viking Formation and include shale, siltstone, sandstone, lesser amounts of conglomerate and occasional coal. The sandstone is restrictsd mainly to units 'A' and 'B' with an occasional occurrence on top of the formation. Siltstone is present throughout while the conglomerate, when present, is usually found on top of both 'A' and 'B' units as well as at the top of the formation. The Cardium sequence below unit 'B' is represented by silt and shale facies that are bioturbated at several levels. These facies were followed by the deposition of unit 'B' which consists of two facies; one bioturbated silt and sand facies, rich in silt and clay matrix, the other located on top of the first is the reservoir facies which consists of sandstone and conglomerate. The sequence on top of unit 'B' represents a silt and shale facies which is

bioturbated at several intervals. Overlying this facies is unit 'A', which like unit 'B', consists of two facies; 1) a silt and sand facies heavily bioturbated and 2) overlain by the reservoir facies that consists of sandstone and conglomerate. Unit 'A' is overlain by a silt and shale facies which is also bioturbated at several intervals. The final facies is one located at the top of the Cardium. This thin facies consists of sand and silt or conglomerate.

Detailed description of individual lithology has been given earlier along with Viking Formation lithologies (see 6.1).

6.4 Environment of deposition of the Cardium Formation

The Cardium Formation represents deposition in a near-shore and marine shelf that received sediments in two main pulses, one during the deposition of unit 'B' and the other during the deposition of unit 'A'. The coarsening upward sequences seen in units 'A' and 'B' represent progressive shallowing in water depth during the deposition of both 'A' and 'B'. As the bathymetry of the shelf decreased coarser sediments were deposited over finer ones. At the end of unit 'A' and 'B' deposition high energy currents reworked and redeposited clean sand in elongated bodies over the shelf. These currents were flowing from the northwest (Shawa, 1984). Although Shawa (1984), agrees that the geometry of the sandbodies closely resembles off-shore bar deposits, on the basis of internal structure and composition he argues against it.

Recently on the basis of petrographic and SEM analyses, and

core descriptions, Walton and Saigal (1984) observed similarites between the Cardium and the Viking lithologies including their sedimentary structures. On the basis of these similarites Walton and Saigal (1984) classifed the Viking and the Cardium Formations together and ascribed them a common environment of deposition. Their interpretation differs somewhat from those stated earlier especially for the Cardium Formation. The following is an account of their interpretation.

"The widespread and often intensive bioturbation together with the genera identified by other workers suggest a marine environment. This, on the basis of forms like Skolithas might be very shallow indeed, although Wright and Walker (1981) argue for an inner to middle-shelf situation on the basis of foraminiferal assemblages in the Cardium Formation. On the other hand, Tizzard and Lerbekmo (1975), take Viking assemblages to indicate different parts of a barrier shoreface. The occurrence of glauconite, although scarcer than previously thought and often detrital, suppports a marine environment while the common plant fragments might be taken as lagoonal or the effect of an approaching shoreline in the south.

While a marine environment is favoured by the fossil evidence the precise locus of deposition is in doubt and one curious feature is the lack of macro-bodyfossils. When compared with modern environments, the lack of shell-lags is surprising. Inorganic structures and textures are consistent with a marine-shelf environment which was characterized for the most part by low energy. There is a general absence of beach structures. No emergent features are recorded with perhaps the

one exception of rootlets in the Cardium Formation (western part).

The above criteria point to the accumulation of sands as offshore bars rather than barriers. The predominance of V.F. or F. sandstones suggests deposition on bar flanks in offshore situations. The extent of the sands suggest a migratory system rather than isolated single bars resting in place. Elongation of the bar system is difficult to establish on the present data although there is a suggestion in the thickness data of a northwest-southeast elongation. This would be parallel to a northwest-southeast shoreline but a trend parallel with the overall basin margin cannot be assumed. The Campanian, Duffy Mountain Sandstone of Northwest Colorado, for example, is elongated northeast-southwest (Boyle and Scott, 1982).

A full bar sequence with the crest preserved is represented by wells with sands coarsening up into medium and coarse-grains. The complete sequence was not often preserved during bar migration eastwards. Most of the time, like migrating ripples, only the lower portion of the structure was preserved. Occasionally, through some change in supply or energy conditions, the bar crest was preserved.

The formation of the conglomerates has been the cause of some debate (Wright and Walker, 1981, and references therein) and current opinion, following Walker and others, tends to favour a model involving accumulation of the finer-grained sediments under fairweather conditions below wavebase and the coarser-grained under the influence of storms. Transportation of conglomeratic clasts was effected, on this model, by storm-generated mass

flows, and the coarser sands exhibit hummocky cross-stratification, a structure ascribed specifically to high energy storm conditions (Hamblin and Walker, 1979).

The model comprises two systems: fairweather and storm, impinging on one another at random.

The presence of conglomerates in very fine sandstones, and even shales, may well represent two disparate environmental conditions, but the preferred position of the conglomerates suggests that a model involving random intersection of two unrelated sets of conditions is untenable. The two systems are not independent; sandstone prescribes the occurrence of conglomerate.

Moreover, density currents have been invoked as a major mechanism for the transportation of the coarse-grained debris in Cardium conglomerates (Wright and Walker, 1981) and in the Cretaceous Lower Gates Member in British Columbia (Leckie and Walker, 1982). This mechanism may have operated in certain locations but the Cardium and Viking conglomerates would have been deposited from bottom-hugging currents only if the sand-covered areas were lower in level than neighbouring muddy floors. This seems a most unlikely situation for the area under discussion.

In many respects, as has been recognized before, (eg. Tizzard and Lerbekmo, 1975) the coarsening upward sequence sometimes culminating in a conglomerate bears comparision with the barrier model of Brenner and Davies (1973). As those two workers pointed out conglomeratic bands develop as one of channel lag, storm swell or storm lag. Modern deposits are largely made

up of shells, whereas the Viking and Cardium conglomerates are largely quartz and chert with some siderite. The last could have been incorporated into the conglomerates in a similar way to the shells in a lag deposit. It seems unlikely, however, that the quartz and chert clasts could have been concentrated by storms from a dispersed condition in the fine-grained sands or shales. They may have been transported with sand by wave-driven currents as coarser patches in the higher energy conditions of the bar crests and distributed into the fine sands and occasionally into the muds as deposits formed as storm-lags or by storm-swells."

6.5 Sedimentation and lithologies of the Belly River Formation

In the study area, the thickness of the Belly River Group varies from about 240 m along the eastern margin to slightly more than 335 m along the western margin. Three separate sandstone genetic units were recognized for the Belly River Formation. They are designated in descending order as 'A', 'B' and 'C' and shown in Figure 6.6. The three genetic units are present in the lower part of the Belly River within a sequence of sandstone, siltstone, shale, coal and bentonite. The sequence is overlain by a widespread shale unit recognizable over most of the study area but less easily identifiable towards the western margin where it grades into sandstone beds. Genetic units 'C' and 'B' are separated by a shale or a shale and coal interval that ranges from a few metres to about 20 m. Unit 'A' is situated 60 m from 'C' and directly overlain by the widespread shale unit. Unit 'C' has the highest lateral continuity followed by 'B' which has a

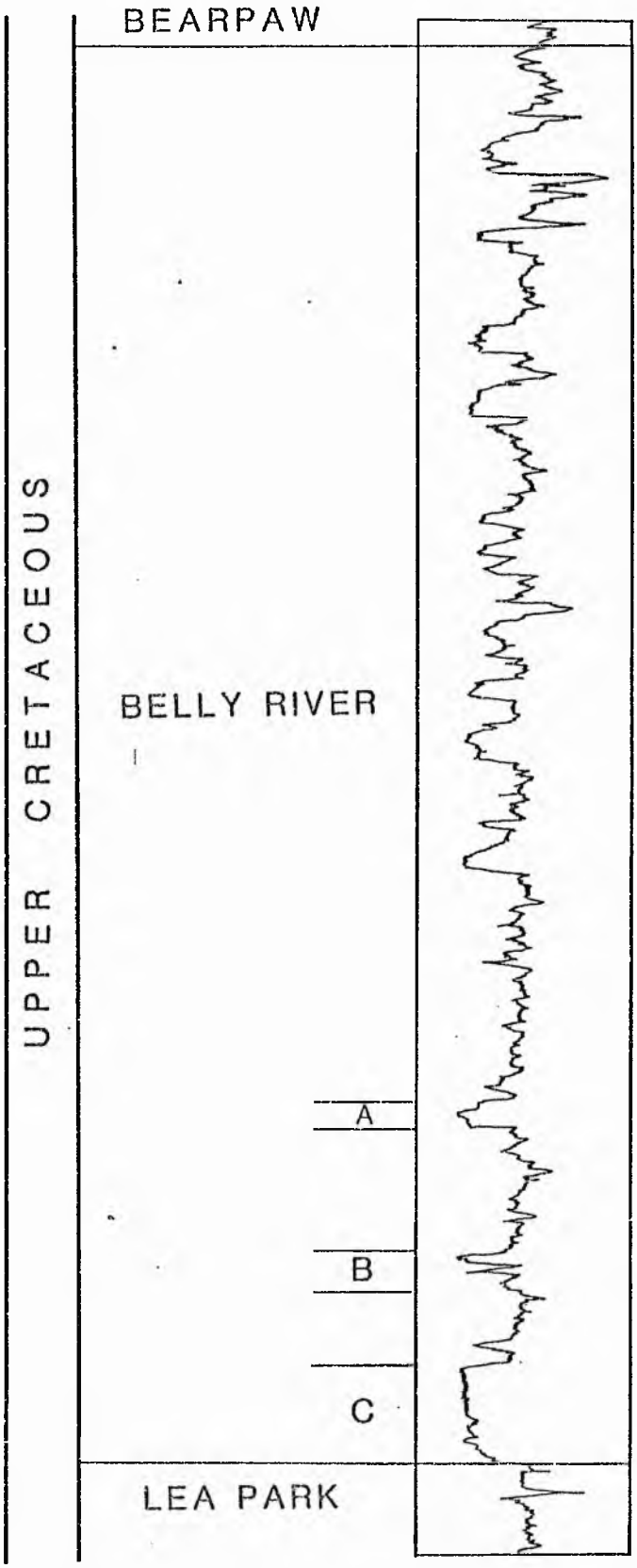

Fig. 6.6 Type gamma-ray log for the Belly River Group (northern part) showing the stratigraphic position of the A, B and C units.

high lateral continuity in the eastern limit of the study area.

Unit 'C' shows a coarsening upward in grain size (CU). Occasionally, however, it fines upward (FU) and in a few places a uniform distribution can be seen. In general, unit 'B' shows a fining upward sequence except in the eastern part of the area where it generally shows coarsening upward. In a few places, however, unit 'B' shows a coarsening upward followed by a fining upward sequence. Unit 'A' shows in most parts a fining upward sequence, however, in some places it also shows uniform distribution.

On the basis of core descriptions Walton and Saigal (1984) stated that overall sequences are rather more varied in the Belly River sandstones than in previous formations. Asymmetrical CU and FU units occur sometimes in multi-storey sequences as well as symmetrical CUFU units.

The CU units occur in the South and are reminiscent of the Viking sandstones. The similarity is striking in the south-east where conglomerates occur at the top of two CU units.

In the south-central area the sandstones are mixed, with one FU, one CU and one CUFU.

In the north the wells have sandstones, which tend to be made up of single or multi-storey FU units. These sandstones contain much the thickest in this study, a multi-storey 90 ft. bed with a thin conglomerate at the base, a 70 ft. unit above, which shows a slight coarsening upwards, and two thin F units above.

Various lithologies that comprise the Belly River Formation are similar to those in the two older formations. Sandstone,

siltstone and shale are present in all the three genetic units while bentonite and coal are occasionally present in units 'C' and 'B' respectively. The description of these lithologies based on core examination is given below.

a) Shale is grey to green, medium or dark grey and usually silty. Plant fragments are common and coal streaks occur. Siderite occurs as thin bands as well as nodules.

b) Siltstone, V.F. and F.-grained sandstones. These are green to grey, well sorted with micro- and medium scale cross-lamination and some shale drapes. Bioturbation occurs less frequently in Belly River sandstones and is more common in the south.

c) Coarser sandstones. Coarser-grained sandstones may have a salt and pepper appearance and generally have a higher feldspar content than in the Viking and Cardium Fms. In the northeasterly wells the coarser sandstones tend to be more common than in the two earlier formations. Sorting tends to be moderate.

d) Conglomerates tend to be thin and poorly sorted; they occur in only three of the wells (two in the northwest and one in the southeast) although pebbly horizons are found in two others (southeast).

e) Coal is found as beds up to 1 ft. in one well (northeast) and as streaks in a few others.

6.6 Environment of deposition of the Belly River Formation

The Belly River Formation represents deposition in a multi-environment setting ranging from near shore marine to

fluvial and associated environments. Both the predominantly shaly Lea Park and Bearpaw Formations lying under and over the Belly River Formation respectively were deposited in a marine environment, while the Belly River represents a regressive phase as a result of either renewed uplift in the Cordillera or a climate change that promoted its erosion, or both (Shawa, 1984). According to Shawa (1984), the unit 'C' represents deltaic sediments that prograded the shore-line eastward while the interval above this unit represents a pre-dominantly fluvial environment that contains many coal beds throughout. Overall the Belly River sediments are believed to have been deposited in a moderately subsiding basin in which the rate of its sediment deposition, or shore-line progradation slightly exceeded the rate of basin subsidence (Shawa, 1984). The particular arrangement of facies in this type of basin produces from initiation to maturity, a moderately thick deposit that attains a thickness of anywhere from 300 to 900 m (Weimer, 1961). The lower part is deposited under marine conditions and so is the basinward part of a regressive sedimentary wedge. The internal part of the wedge is made up of fluvial sediments and its upper part is deposited under marine conditions. The marine facies that envelope the fluvial facies, increases in thickness basinward. Figure 6.7 is a model of a moderately subsiding basin that deposited the Belly River sedimentary wedge (Shawa *et al.*, 1984). This model shows the approximate position of the Belly River genetic units 'B' and 'C'. The unit 'A' could be somewhere in the middle part of the fluvial facies.

On the basis of petrographic and SEM analysis and core

descriptions, Walton and Saigal (1984) gave an alternative interpretation for the environmental model of the Belly River Formation:

"Sequences from the southern wells resemble those of the Viking Fm. and might therefore have had a similar origin as marine bar or bars. The middle and northern sequences present a contrast in the scarcity of bioturbation, the frequency of medium-grained sandstones, the occurrence of FU units and the richness in carbonaceous materials including coals or coaly streaks.

Two interpretations of the palaeogeographic situation might be pursued. The first envisages a lagoonal sequence prograding over a barrier sand; the second sees the northerly sequences as non-marine, delta-plain in origin.

The succession in the west is instructive in having elements of both northerly and southerly sequences. A lower 'Viking-type' CU unit is bioturbated VF and F sands passes up into silty coaly shales with plant fragments and no bioturbation. These are followed by a sharp-based M-grained sand which fines abruptly at the top, like other Belly River sands.

On the first model, marine conditions are represented by the lowest, bioturbated shales, a migrating barrier by the lower sand, and the lagoonal deposits by the coaly shales. The upper sandstone might be interpreted as prograding intertidal sands or inter-tidal creek deposits.

On the second model the lower sequence would be taken to be pro-delta mouth-bar deposits leading to top-delta shales with the sharp based sandstone as either minor channel sands or as splay sands introduced by periodic flooding."

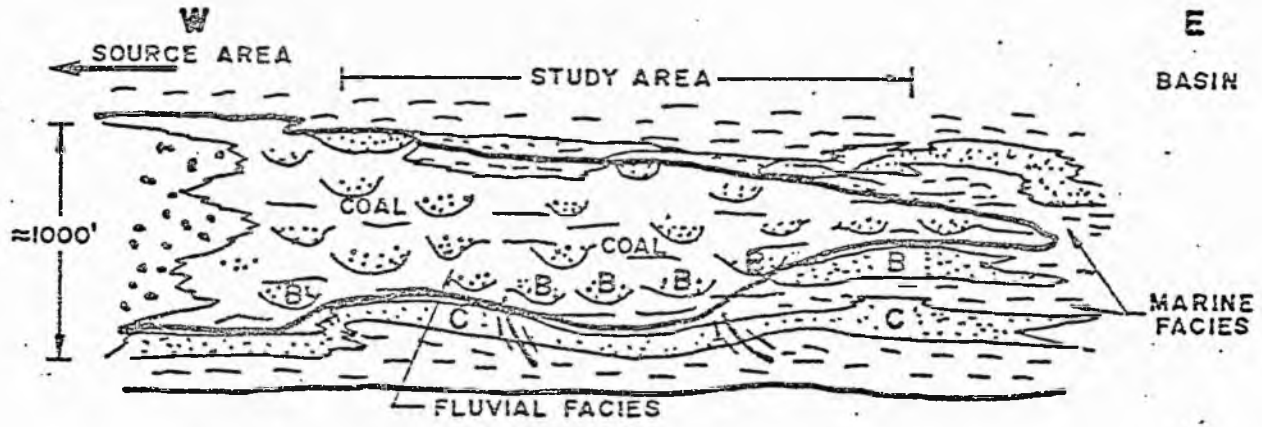

Fig. 6.7 A depositional model for the Belly River Group of the study area. Deposition took place in a moderately subsiding basin where progradation of the shoreline slightly exceeded rate of subsidence. (Based on Weimer 1961; from Shawa et al., 1984).

CHAPTER VII

Petrology and diagenesis of the Viking, Cardium and Belly River Formations

Introduction

Specimens from conventional cores were removed for thin section and SEM analyses to establish the diagenetic history of the sediments. A total of 289 samples, comprising 115 from the Viking, 73 from the Cardium and 101 from the Belly River Formation were examined under SEM. Out of these 155 thin sections, comprising 68 from the Viking, 46 from the Cardium and 41 from the Belly River Formation were prepared for analysis under the optical microscrope. Sample numbers 1 to 115 come from the Viking Fm., 116 to 188 from the Cardium Fm. and 189 to 289 from the Belly River Fm. The precise location of each sample is given in Appendix 7.1.

This chapter gives an account of the petrology and diagenetic histories of the Viking, Cardium and Belly River Formations separately. It is aimed to assess various textural, compositional and diagenetic differences and similarites between the sediments of these formations. Samples analysed come from the sandy genetic units (e.g. unit 'A', 'B' and 'C' described earlier in chapter VI) but for the purpose of present study each formation is treated as a whole rather than in individual units.

7.1 Petrology of the Viking Formation

Mean grain size varies from silt to pebble conglomerate. Very fine or fine sandstone form the bulk of the samples and come from all over the area. The sediments are poorly to well sorted. In general, finer samples are better sorted and more densely packed than coarser. Nearly 46% of the samples show triple junctions (Fig. 7.1) due to abundant early silica overgrowth and nearly 27% samples show sutured contacts due to pressure solution. Samples with abundant carbonate cement normally show modification in original packing by replacement of detrital grains by carbonate.

Porosity varies from zero to 21% (as measured visible). Nearly 67% of the samples examined under optical microscope show porosity between 0 and 5% and only 10.5% show between 15 and 20%. Finer-grained samples show mainly microporosity and a few isolated reduced pores (Fig. 7.2). These are either straight-edged due commonly to some silica overgrowth or irregular due to some cement dissolution. Microporosity observed in the samples is of lamellar, within particle (WP) and between particle and cement (BPC) type. Between particle (BP) porosity occurring as straight-edged reduced pores is more common in medium-grained samples, whereas vuggy porosity formed by dissolution of carbonate cement and/or some unstable grains has developed in coarser samples (Fig. 7.3).

The major constituents are quartz and chert (Fig. 7.4 and Appendix 7.2). Feldspars, rock fragments, micas and opaques represent minor components. Cement and matrix show large variations in amount. Authigenic clays include kaolinite,

illite, smectite and chlorite.

Quartz and chert are dominant and taken together vary in amount from 46% to 97% with averages of 41.2% and 37.2% respectively (Appendix 7.2). Quartz is dominant in the finer-grained samples whereas chert always predominates in conglomeratic samples. The feldspar content of plagioclase and orthoclase varies from 0 to 9% with an average of 2.1%. Plagioclase is more common than orthoclase in most of the samples. The feldspars often show alteration into clays or partial dissolution forming WP porosity as irregular pits and elongated tiny pores along cleavage planes. The rock fragment content varies from 0 to 8% with an average of 4%. They are normally volcanic or quartzitic in composition and more abundant in coarser and conglomeratic samples. The mica content varies from 0 to 6% with an average of 0.9%. It is normally more abundant in the finer-grained samples. Mostly the micas are bend around grains due to compaction and sometimes they show alteration into clays. Opaques occur mainly as ferruginous or as organic material filling residual pores, fractures and irregular voids. Total opaque content varies from 0 to 15% with an average of 2.8%. Some samples show abundant development of pyrite cubes. Glauconite occurs only in traces as detrital grains. The matrix is normally argillaceous or a ferruginous clayey mixture. The average matrix content is 3.1% although it varies from 0 to nearly 20%.

Cement content varies from 0 to 31% with an average of 5%. Different types of cements identified are (i) quartz, (ii) chert, (iii) ankerite/ferroan-calcite, (iv) siderite, (v) dolomite and

(vi) clays. Quartz and chert occur firstly in optical continuity with the host grains (referred to as overgrowth, Fig. 7.1) and secondly not in optical continuity (this is referred to as cement, (Fig. 7.5). Overall quartz overgrowths and cement are much more abundant than chert, particularly, in the Viking Formation. Triple-junctions formed by syntaxial quartz overgrowths are most frequent in the fine-grained samples of this formation. Ankerite normally occurs as late diagenetic cement filling residual pores and fractures. Normally it shows patchy distribution corroding and replacing detrital grains (Fig. 7.6). The subsequent dissolution of the carbonate cement has led to the formation of vuggy porosity (Fig. 7.3). SEM examination reveals that authigenic clay minerals have developed diagenetically in nearly 75% of the samples. Clay minerals identified include kaolinite, illite, smectite and chlorite. Kaolinite normally occurs as well developed books (Fig. 7.7). Illite forms thin clouds and wispy threads bridging across the pores (Fig. 7.8) Smectite occurs as wavy plates and often shows honeycomb texture. Chlorite occurs as individual sharp blades and commonly surrounds authigenic quartz crystals (Fig. 7.9). Overall the Viking Formation is richest in illite and chlorite and authigenic clays are better developed in coarser samples.

7.2 Diagenetic history of the Viking Formation

Mineralogical and textural relationships observed in samples from the Viking Formation show frequent variations in the diagenetic patterns within small areas (even between adjacent

wells). The coarser samples commonly show more variation in the diagenetic products than the finer samples. A generalized diagenetic sequence displayed by the majority (nearly 80%) of Viking samples is: -

1) quartz/chert overgrowths

2) growth of diagenetic clays

3) compaction

4) late diagenetic carbonate (ankerite) cement in residual pores and scattered development of dolomite rhombs replacing detrital grains

5) dissolution of carbonate cement and unstable grains forming secondary porosity.

Early quartz or chert overgrowth took place in nearly all the samples but there is some variation in its development. In some samples it is slight and has only resulted in straight grain boundaries whereas in others (particularly finer samples) where it is extensive has led to the formation of triple-junctions with prism faces and dust rims (Fig. 7.1). The syntaxial quartz overgrowth has caused partial to considerable loss of reducible primary porosity (chemical compaction; Fig. 7.2).

The second stage of diagenesis involved the growth of clay minerals, such as kaolinite, chlorite, illite and smectite. These species vary frequently (even between adjacent wells) and show complex distributions. Samples from the northern part of the present area show dominant growth of chlorite. Illite and smectite are next to chlorite in abundance whereas kaolinite is least common. In contrast, samples from the south show abundant kaolinite growth (Fig. 7.10). Illite and smectite are also

common but chlorite is rare. These clays are believed to have developed at the expense of feldspars, volcanic rock fragments and micas. Changes in pore fluid chemistry caused feldspars, etc. to become unstable in the diagenetic environment and to alter to one of the clay minerals depending upon their composition. Feldspars altered to kaolinite, illite or smectite depending upon local variations in the Na and K concentration in the pore fluid and feldspar composition (Tillman and Almon, 1979). Smectite might have also formed by the decomposition of rock fragments containing ferro-magnesium minerals. Some of the illite probably also formed as a result of alteration of kaolinite and smectite. Authigenic feldspar has also developed in a few samples (Fig. 7.11). It is believed that the potassium, aluminium, and silicon ions required for the formation of feldspar were supplied by detritial feldspar, rock fragments, clay minerals and interstitial water. Since the solubilities of feldspars are very low (eg. for K-feldspar 3×10^{-7} mole/litre, and for Na-feldspar 6×10^{-7} mole/litre in pore water; Berner, 1978) saturation is reached easily with a small amount of dissolution (Bjørlykke, 1983). Subsequently, under favourable interstitial environment the liberated ions precipitated as authigenic feldspar. Authigenic pyrite as framboids and cubes was also observed in a few samples from the central part of the area, formed during early diagenesis. Conglomeratic samples show some variations in their early cement stratigraphy. For example a few conglomerate samples from the south-east show complete pore occlusion by organic matter subsequent to the formation of kaolinite books (Fig. 7.12), while samples from the south-west

show extensive siderite cementation replacing and corroding detrital grains (Fig. 7.13). The formation of siderite cement in the south-west area is taken to suggest existence of non-marine conditions (Füchtbauer, 1983).

Besides the chemical compaction, mechanical compaction has further reduced the primary porosity in most of the samples. Penetration of sharp edges formed by early silica overgrowth into surrounding grains (Fig. 7.14), concavo-convex contacts, sutured contacts, squeezing of clay matrix and fracturing of grains are common features found in most of the samples. On increased burial, the clay mineral assemblage was also modified by alteration of unstable clays into more stable ones. Some of the smectite and kaolinite may have been altered to illite and chlorite. Chemically K-feldspars and/or pore solutions provided the necessary Al and K for the conversion of kaolinite and smectite to illite. Excess silica released formed quartz whereas iron and magnesium lost by smectite in the reaction formed chlorite (Hoffman and Hower, 1979). This probably explains the common association of chlorite blades and authigenic quartz crystals (Fig. 7.9) and perhaps suggests that there was quartz cementation simultaneous or even later than clays.

The fourth stage of diagenesis involved the precipitation of carbonate cement (ankerite) in residual pores and fractures and random development of dolomite rhombs replacing detrital grains. In general, carbonate cement is more abundant in coarser sediments than finer samples. This probably is because of greater availability of larger pore spaces in coarser samples, permitting the better circulation of the pore solutions needed

for large scale chemical cementation. The late diagenetic origin of ankerite and particularly dolomite perhaps suggests that these minerals have developed from pore waters at higher temperature (60-100° C) and with low Mg/Ca ratios (Bjørlykke, 1983).

The last and fifth stage of diagenesis involved the formation of secondary porosity by dissolution of carbonate cement and other unstable grains. Most of this porosity may have been generated during mature, meso-diagenesis due to the leaching effect of CO2 derived from maturing kerogen, a process explained by Schmidt and McDonald (1979). Vuggy porosity in particular must have involved dissolution of unstable rock fragments and/or feldspars along with carbonate cement (Fig. 7.3). As secondary porosity formation is mainly a function of chemical dissolution, controlled by several factors such as circulation of pore fluids, presence of unstable grains and cement etc., it normally varies largely within and between samples. Generally it is patchy unless there has been extensive dissolution. Overall, secondary porosity is higher in coarser samples and sometimes is as high as 20%.

7.3 Conclusion

Of the diagenetic stages described above, extensive quartz overgrowths, growth of diagenetic clays, compaction and late diagenetic carbonates are responsible for the destruction of primary porosity in the majority of the Viking samples (particularly finer grained). Silica precipitation as quartz overgrowths might have occurred due to mixing of fresh waters

with marine pore waters (Bjørlykke, 1983). The variation in other authigenic mineral species between samples is believed to have been controlled by local variations in original composition and pore fluid circulation, the understanding of which will require a much closer sampling than available in the present study. Formation of kaolinite in samples from the south-east of the area during early diagenesis suggests relatively acid conditions which may have existed locally and have been produced by flushing of sandstone with fresh water (Hancock, 1978). The presence of siderite cement in some samples from the south-west area is an evidence favouring non-marine conditions (Füchtbauer, 1983). The formation of silica overgrowths, kaolinite and siderite re-inforce one another as they suggest existence of non-marine pores solutions during early diagenesis.

7.4 Petrology of the Cardium Formation

The grain size of samples compared closely with that of samples from the Viking Fm. and vary from silt to pebble conglomerate. Almost half of the samples in thin section show poor sorting with moderately well-sorted and well-sorted samples constituting some 15%. This probably reflects the sampling rather than indicating the overall situation as seen in cores which is of a predominance of good sorting. In general sorting improves with decrease in grain size. Like the Viking, the finer and better sorted samples are more densely packed than the coarser and poorly sorted ones. In contrast to the Viking, very few samples (9%) show triple junctions formed by abundant early

silica overgrowth (Fig. 7.15). Sutured contacts are also less frequent (22%).

Porosity varies from zero to 23%. Nearly 89% of the samples examined under optical microscope show porosity between 0 and 5% and only 7% show between 20 and 25%. Like the Viking Fm. finer-grained samples mainly show microporosity and a few isolated reduced pores. Different types of microporosities observed include lamellar, BPC and WP. Vuggy porosity formed by dissolution of carbonate cement and/or some unstable grains is dominant in the coarser sediments. Moldic porosity formed by dissolution of carbonate cement has also developed in some samples. The majority of smaples (94%) examined under optical microscope and SEM show poor permeability.

Like the Viking Fm., quartz and chert are dominant but their average content taken together is less than found in the Viking Fm. (Fig 7.4 and Appendix 7.3). They vary in amount from 5% to 90%, with averages of 41.1% and 29.5% respectively. Chert is higher in conglomeratic samples. In a few samples the total quartz and chert content is as low as 9%. This is due to excessive replacement by carbonate cement forming a floating texture. Overall feldspar (plagioclase + orthoclase) content is minimum in this formation and varies from 0 to 2%, except for two samples which contain 6%. The rock fragment content varies from 0 to 7% with an average of 1.8%. Compositionally these are similar to the Viking and are normally volcanic or quartzitic. Mica content varies from 0 to 3% wih an average of 1.2%. It is more abundant in fine grained samples and normally bent around grains due to compaction. Opaques include ferruginous and

organic material and vary from 0 to 8% with an average of 3%. Some samples show abundant development of pyrite cubes. SEM examination reveals that a few of the samples contain framboidal pyrite (Fig. 7.16). Glauconite is minimum in the Cardium Fm. and occurs only in traces as detrital grains. Compositionally the matrix is normally argillaceous or a ferruginous clayey mixture (average 7.3%) as observed in the Viking Fm. Normally it is more abundant in silty or very fine grained samples and has been squeezed into pores on compaction.

Cement content varies from 5% to 35% with an average of 11.5%. A few samples show an exceptionally high cement content (84%) forming floating texture due to excessive replacement of detritals. Different types of cements observed include i) quartz, ii) chert, iii) ankerite/ferroan-calcite, iv) siderite, v) dolomite and vi) clays. As mentioned in Viking Fm. quartz and chert cements occur as syntaxial overgrowths or pore fillings without any optical continuity with the host grains. Triple junctions formed by abundant quartz overgrowth are common in very fine-grained samples but are less abundant than seen in the Viking Fm. A noteworthy cement of the Cardium Fm. is the spherulitic or colloform siderite (in samples from the western part of the area). It varies from 11% to 35% depending upon late diagenetic dissolution. Commonly samples with abundant siderite cement show corrosion of detrital grains. Like Viking, ankerite occurs as late diagenetic cement in residual reduced pore and fracture fillings corroding adjoining grains. Dolomicrite to dolosparite replacing detrital grains occurs in a few samples. Normally dolomite occurs as scattered late diagenetic rhombs

replacing other grains.

SEM examination reveals that authigenic clay minerals have developed diagenetically in nearly 66% of the samples. Clay minerals identified include illite, smectite, kaolinite and chlorite. Illite is most abundant and more widely distributed than other clays. Thin clouds with wispy thread-like terminations of illite (Fig. 7.17) are most abundant in samples from the extreme south and extreme north. A few samples from the central part of the area also show frequent development of illite. Smectite is abundantly developed in a few samples from the western part of the area. Overall smectite is sparsely distributed in samples throughout the area. Kaolinite and chlorite are least abundant and samples containing traces of kaolinite and chlorite are widely scattered. Like Viking, commonly authigenic clays are better developed in coarse-grained samples than the finer ones.

7.5 Diagenetic history of the Cardium Formation

Mineralogical and textural relationships within the Cardium Formation show differences in the sequence of diagenetic events. Like the Viking Formation, the finer samples (silt-fine-grained sandstones) show rather less variation than the coarser ones. A generalized diagenetic sequence displayed by the Cardium samples from the western part is: -

1) quartz overgrowth
2) growth of diagenetic clays
3) siderite cementation

4) compaction

5) scattered dolomite rhombs replacing detrital grains

6) dissolution of carbonate cement and other unstable phases forming secondary porosity.

Syntaxial quartz overgrowth can be seen in almost all the samples, but it shows large variation in the extent of its development. Triple-junctions are only developed in a few fine grained samples. Normally quartz overgrowth is difficult to assess as most of the grains have been corroded by carbonate cement. Overall quartz overgrowth is less abundant than seen in the Viking Formation.

The second stage of diagenesis involved the growth of diagenetic clays. These clays show large variation in their abundance and mineral species over the entire area controlled presumably by the environment of deposition, sandstone composition and pore fluid circulation. Overall illite and smectite are most common but chlorite has also been found to be abundant in some samples from the south-east part of the area. Commonly chlorite occurs as pore linings and occasionally forms knots (Fig. 7.18). These chlorite pore linings are similar to the Frontier Formation of Spearhead Ranch Field and taken to suggest marine environment (Tillman and Almon, 1979). Elsewhere chlorite needles are commonly associated with authigenic quartz crystals as observed in the Viking Formation. Abundant kaolinite books growing on quartz prism faces have also been observed in a few samples from the south. The formation of these clays is believed to be similar to those in the Viking Formation.

The third stage of diagenesis in majority of samples from

the western part of the area involved extensive siderite cementation replacing and corroding detrital grains (Fig. 7.20). The floating texture suggests that cementation took place during early diagenesis before significant burial. Most of these samples show spherulitic siderite cement (Fig. 7.21) but a few samples show well develloped colloform growth (Fig. 7.22). The formation of siderite cement suggests existence of non-marine conditions in the western part of the area (Füchtbauer, 1983). In the south-east where chlorite pore linings indicate marine conditions, the third diagenetic stage involved chert cementation. It is believed that conditions were favourable for silica precipitation but chlorite pore linings probably inhibited the development of large syntaxial quartz overgrowths as thick clay rims resulted in the inability of quartz to seed on the grain surface and led instead to chert cementation. Some pores are filled with ankerite cement (Fig. 7.23). The ankerite cement is found randomly in residual pores and/or fractures in samples over the entire area and believed to have developed during late diagenesis as seen in the Viking Formation. A few chert conglomerate samples from the north-west show dominant pyrite cement indicating marine conditions (Figs. 7.24 and 7.25).

Compaction further reduced the primary porosity by squeezing the clay matrix and causing some grain interpenetration. Some recrystallization of siderite around grain boundaries forming coarser fringes probably also took place due to compaction. After compaction, during deeper burial scattered dolomite rhombs developed replacing detrital grains (Fig. 7.26). The late

diagenetic formation of ankerite and dolomite is similar to that observed in the Viking Formation and believed to have occurred in a similar way.

The dissolution of carbonate cement and other unstable phases during the last stage of diagenesis formed secondary porosity. Overall the secondary porosity shows patchy distribution as in the Viking Formation. It seems that the CO2 - rich solutions responsible for generation of secondary porosity did not dissolve siderite but leached ankerite (sometimes forming moldic porosity, Fig. 7.21) and chlorite pore linings (Fig. 7.23).

7.6 Conclusion

Quartz overgrowth and the formation of ankerite, dolomite and secondary porosity are similar but less well developed than in the Viking Formation. A significant feature restricted to samples from the western part of the area is the abundance of siderite cement which is taken to be due to the effect of non-marine waters, while samples from the south-east show well developed chlorite pore linings suggesting the effect of marine conditions.

7.7 Petrology of the Belly River Formation

The majority of samples (app. 70%) are fine to medium grained and differ from the previous two formations in the lack of conglomerates and very fine-grained sandstone. Overall the

Belly River samples show poorer sorting (poor-moderate) and are less well packed than the Viking and the Cardium Fms. In contrast to the Viking Fm., triple junctions formed by abundant early silica overgrowth were seen only in a few samples while the majority of samples show modification in original packing due to replacement of grains by carbonate cement and its subsequent dissolution.

Porosity varies from zero to 28% wih almost 75% of the samples in thin section showing less than 10%. Different types of porosities identified include vuggy, BP, WP, BPC and lamellar. Vuggy porosity is more abundant in this formation as compared to the Viking and the Cardium Fms. It is mostly formed by carbonate cement dissolution and is normally patchy. Overall the Belly River Fm. is more porous and permeable than the Viking and the Cardium Fms.

Major and minor constituents are the same as observed in the Viking and the Cardium Fms. but it shows clearly an increase in the abundance of chemically unstable phases such as feldspars, rock fragments and carbonate cement while quartz and chert content are less (Fig. 7.4 and Appendix 7.4). Quartz and chert taken together vary in amount from 50% to 76% with an average of 27% and 35.8% respectively. Feldspar content of plagioclase and orthoclase varies from 3% to 10% with an average of 6%. Like other formations, plagioclase dominates over orthoclase and they show alteration or partial dissolution forming WP porosity. Compositionally the rock fragments are similar to those found in the Viking and the Cardium Formations and vary in content from 2% to 9% with an average of 6%. Mica content varies from 0 to 3%

with an average of 2.1%. Opaques occur mainly as ferruginous material (average 3.3%) filling irregular fractures and scattered reduced pores. Unlike the other two formations, no pyrite cubes or matrix were observed in the Belly River Formation. Glauconite is present in a majority (76%) of samples but always in traces.

Different types of cements identified are i) quartz, ii) chert, iii) ferroan-calcite/ankerite and iv) clays. Quartz and chert occur as syntaxial overgrowths and cements. Cements are more commonly seen in samples with well developed chlorite rims. It is believed that chlorite fringes inhibited the syntaxial quartz overgrowths and as a result silica precipitated to form cement. Carbonate cement is clearly more abundant in the Belly River Formation than the Viking and the Cardium Formations and this in turn has led to the formation of vuggy porosity. It varies from 5% to 41% (with an average of 13%) depending upon the extent of late diagenetic dissolution.

SEM examination reveals that authigenic clay minerals are most abundant in Belly River Formation. Nearly 90% of the samples show the development of clays. The Belly River Formation is richest in kaolinite and chlorite. Chlorite pore linings (Figs. 7.27 to 7.29) are particularly well developed in the south-eastern part of the area. Chlorite is also found to be abundantly developed in north-west part of the area. Kaolinite is most abundant in the northern part of the area . In contrast to Viking and Cardium, kaolinite in the Belly River Formation might have developed during or subsequent to dissolution as discussed later in diagenetic history. Illite and smectite are least common but a few samples do show their abundant growth.

Samples with traces of illite and smectite are randomly scattered over the entire area. Like Viking and Cardium, coarser samples show better development of authigenic clays.

7.8 Diagenetic History of the Belly River Formation

Mineralogical and textural relationships in samples from the Belly River Formation show a rather more uniform series of diagenetic events than the Viking and the Cardium Formations. The sequences displayed by Belly River samples have been divided into the following two types:

Type I

The majority of samples (nearly 70%) from all over the area fall in this category, where the paragenetic sequence is

1) Quartz and chert overgrowths
2) Growth of authigenic clays
3) Chert and quartz cement
4) Slight compaction
5) Late diagenetic carbonate cement in residual reduced pores
6) Dissolution of cements and unstable grains forming secondary porosity.

Early quartz or chert overgrowth took place in most of the samples forming straight grain boundaries. Overall these overgrowths are less well developed than seen in the Viking and the Cardium Formations. The syntaxial quartz overgrowth has caused only partial loss of reducible primary porosity. The second stage of diagenesis involved abundant growth of clay minerals. Of these, chlorite is the most striking as it commonly

occurs as pore linings forming fringes around grains and knots. The very best development of these fringes, constituting up to 16% of the total cement to be seen in samples from the south-east (Figs. 7.27 to 7.29). These fringes are very similar to the chlorite pore-linings observed in the Frontier Formation of Spearhead Ranch Field by Tillman and Almon (1979). In some samples tiny authigenic quartz crystals developed simultaneously with chlorite knots as they partially engulf chlorite blades (Fig. 7.30) while in others the quartz crystals are absent (Fig. 7.31).

The EDX analysis (Fig. 7.32) shows that these chlorites are Fe-rich. Hence, they are believed to have formed in low temperature environments during early diagenesis as suggested by Grim (1968). Other authigenic clays formed in some samples include kaolinite, smectite and illite (Figs. 7.33 and 7.34). Of these kaolinite is most abundant whereas smectite and illite are rarely seen. These clays are believed to have developed at the expense of feldspars and other silicates.

The third stage of diagenesis involved chert and quartz cementation in the residual pores (Fig. 7.35). A few pores with chlorite fringes are filled with carbonate cement which is believed to have formed during late diagenesis (Fig. 7.36). At this stage most of the pore spaces were occluded by the above mentioned cements and the sediments were subjected to differential compaction. Commonly the compaction is slight and has formed concavo-convex grain contacts by means of plastic deformation and fracturing of grains (Fig. 7.37). Many samples do not show any compaction.

The fifth stage of diagenesis involved the precipitation of carbonate in the residual reduced pores. Samples show large variation (traces to 10%) in the total carbonate cement. It is difficult to assess the total carbonate cement content that had initially precipitated because most of the samples have suffered late dissolution. The secondary porosity formed by dissolution during the last stage of diagenesis varies largely as it was controlled by such factors as circulation of fluids, presence of unstable grains and cement. Generally it is patchy unless there has been extensive dissolution. In some samples, even chlorite fringes have partly been removed during dissolution forming vuggy porosity. As suggest by Bjørlykke (1983), in a situation similar to this where carbonates and feldspars were dissolved, leaching may have been due to i) CO_2 from maturing kerogen and/or ii) by meteoric water. The common occurrence of unaltered rock fragments perhaps may be difficult to explain if the sediments had been subjected mainly to intensive leaching by meteoric water.

Type II

The paragenetic sequence of this type is

1) Quartz overgrowth
2) Growth of diagenetic clays
3) Carbonate cementation
4) Slight compaction
5) Dissolution forming secondary porosity
6) Kaolinite formation

Samples showing above mentioned paragenetic sequence are concentrated in the extreme north part of the study area. Early quartz overgrowth is overall rare and has formed euhedral grain boundaries causing partial reduction in the primary porosity (Fig. 7.38). Some samples do show development of abundant tiny quartz crystals in patches (Fig. 7.39). Early diagenetic authigenic clays are overall rare and may be totally absent at times. Chlorite and smectite are the common clays when present (Figs. 7.40 and 7.41). It is possible that early diagenetic clays were replaced by carbonate cement as they are found to be common in samples where the carbonate is less (<5%). Samples with rare or no clays usually show 20-33% replacive carbonate cement formed after early quartz overgrowth (Fig. 7.38). It is difficult to assess the total carbonate cement content that had initially precipitated because these samples have suffered late diagenetic dissolution. The loosely packed grains suggest that abundant carbonate cementation took place during the early stages, occluding most of the pore spaces. Normally the contact between the overgrown quartz prism faces and the carbonate cement is sharp (Fig. 7.38) but sometimes it does show a certain degree of mismatch forming BPC porosity (Fig. 7.42). Compaction caused bending of micas, fracturing of carbonate cement and slight grain interpenetration forming concavo-convex contacts by means of plastic deformation.

Dissolution of carbonate cement and other unstable grains took place during the late diagenesis forming secondary porosity. Interestingly, the samples with high secondary porosity also have abundant authigenic kaolinite. The kaolinite books are randomly

scattered all over along with some carbonate (matrix) and appears to be precariously perched either on the carbonate cement or grain surfaces (Fig. 7.43). This textural relationship is markedly different from that commonly shown by early diagenetic kaolinite which usually grows on overgrown prismatic quartz faces and may even be partially engulfed (Fig. 7.10). Hence, the textural relationship and association with carbonate matrix suggests that the kaolinite formed subsequent to dissolution of unstable grains and carbonate cement. The carbonate matrix shows rounded edges (Fig. 7.44) and is believed to have formed by disintigration of cement during dissolution.

Recently, Curtis (1983) explained theoretically simultaneous carbonate dissolution and kaolinite precipitation using thermochemical data of Hemingway et al (1978) and Robie et al (1978). He established the contours of the solubility of kaolinite as a function of dissolved aluminium and pH for different silicon levels (Fig. 7.45). Kaolinite solubility increases rapidly to high and low pH while the silica minerals show no such increased solubility in acid solutions. According to Curtis (1983), aluminium activity is of the order 10^{-2} M at pH 3 and gradually decreases to 10^{-8} M at pH 6 (Fig. 7.45). However, within this range calcite dissolves and cause kaolinite precipitation by increasing pH of the pore fluids. This process explains why late diagenetic kaolinite is more abundant in samples wih high secondary porosity as described above. Similar observations of pore filling kaolinite following porosity enhancement during burial diagenesis have also been made by several earlier workers including Loucks et al (1977), Lindquist

(1977) and Flournoy and Ferrell (1980).

7.9 Conclusion

The most striking feature observed in the Belly River Formation is the early diagenetic development of chlorite pore linings, particularly in the south-eastern part of the area. These are very similar to chlorite pore linings observed by Tillman and Almon (1979) in the reworked bar facies within the Frontier Formation of Spearhead Ranch Field. The chemical composition and textural relationships of the chlorite suggests low temperature, early diagenetic origin in marine environment. Amongst other diagenetic stages, only the first stage of quartz overgrowth shows some similarity with the Viking and the Cardium Formations. Abundant chert and quartz cementation found characteristically in this Formation is probably due to the early diagenetic clays (particularly chlorite), inhibiting syntaxial quartz overgrowth. Other contrasted features of the Belly River Formation are the absence of late diagenetic dolomite and, locally, the formation of kaolinite during or subsequent to late diagenetic dissolution, particularly in the northern part of the area.

The sparseness of smectite in the Viking, the Cardium and the Belly River Formations over the entire area suggests that the sediments have undergone a marked burial. Commmon association of chlorite blades and authigenic quartz crystals is considered to be the result of smectite transformation during burial. This suggests that these sediments were buried to a maximum depth between 2500 to 3700 m (Dunoyer De Segonzac, 1970).

Fig. 7.1. Early quartz overgrowth (showing prism faces and dust rim) forming triple-junction caused complete loss of reducible primary porosity (chemical compaction). X nicols. Scale bar equals 200 μm.
(Vik. Fm.; 2789 m)

Fig. 7.2. SEM photograph showing isolated straight edged reduced pores due to silica overgrowth. Scale bar equals 100 μm.
(Vik. Fm.; 1777 m)

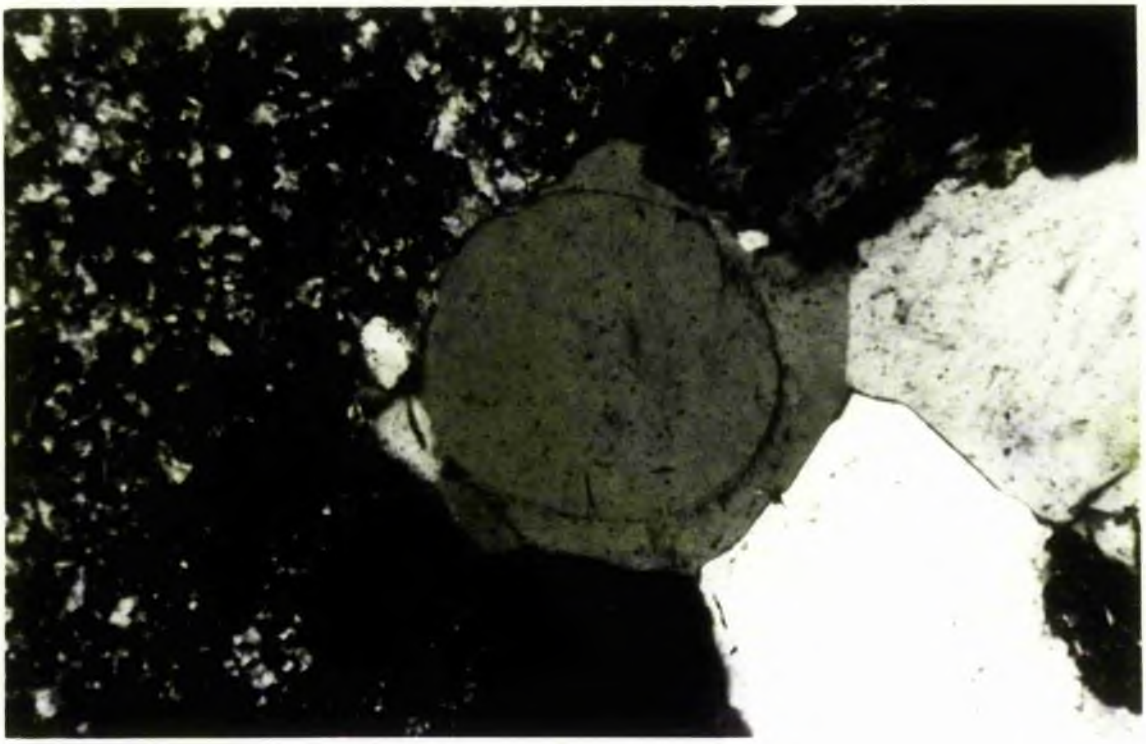

Fig. 7.3. Photomicrograph showing vuggy porosity (central bluish area) formed by dissolution of carbonate cement and/or some unstable grains. Note some residual carbonate cement is still present (dark blue). Plane polarized light. Scale bar equals 200 μm.

(Vik. Fm.; 1672.8 m)

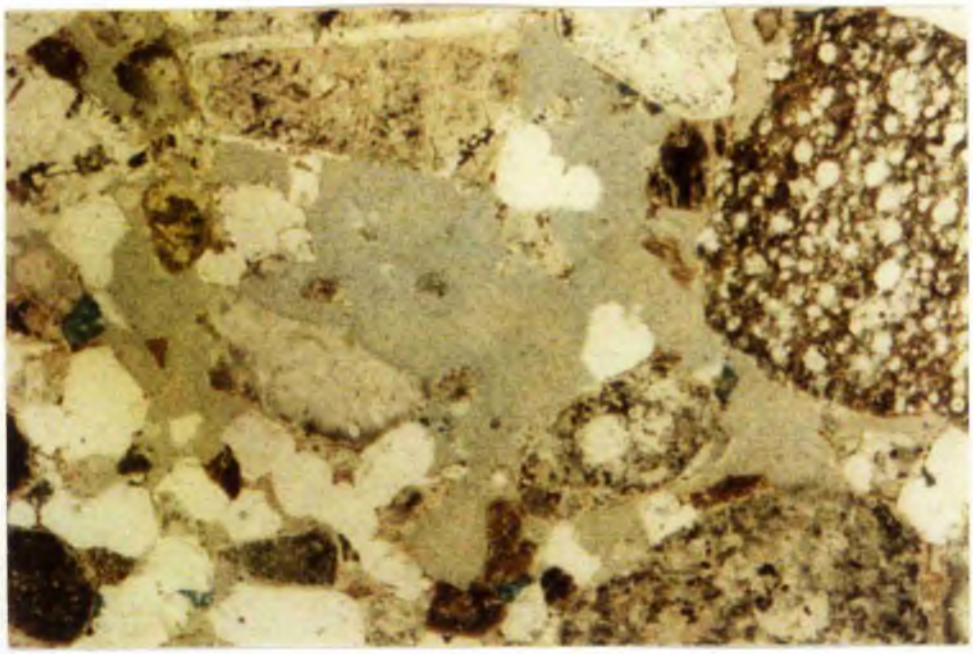

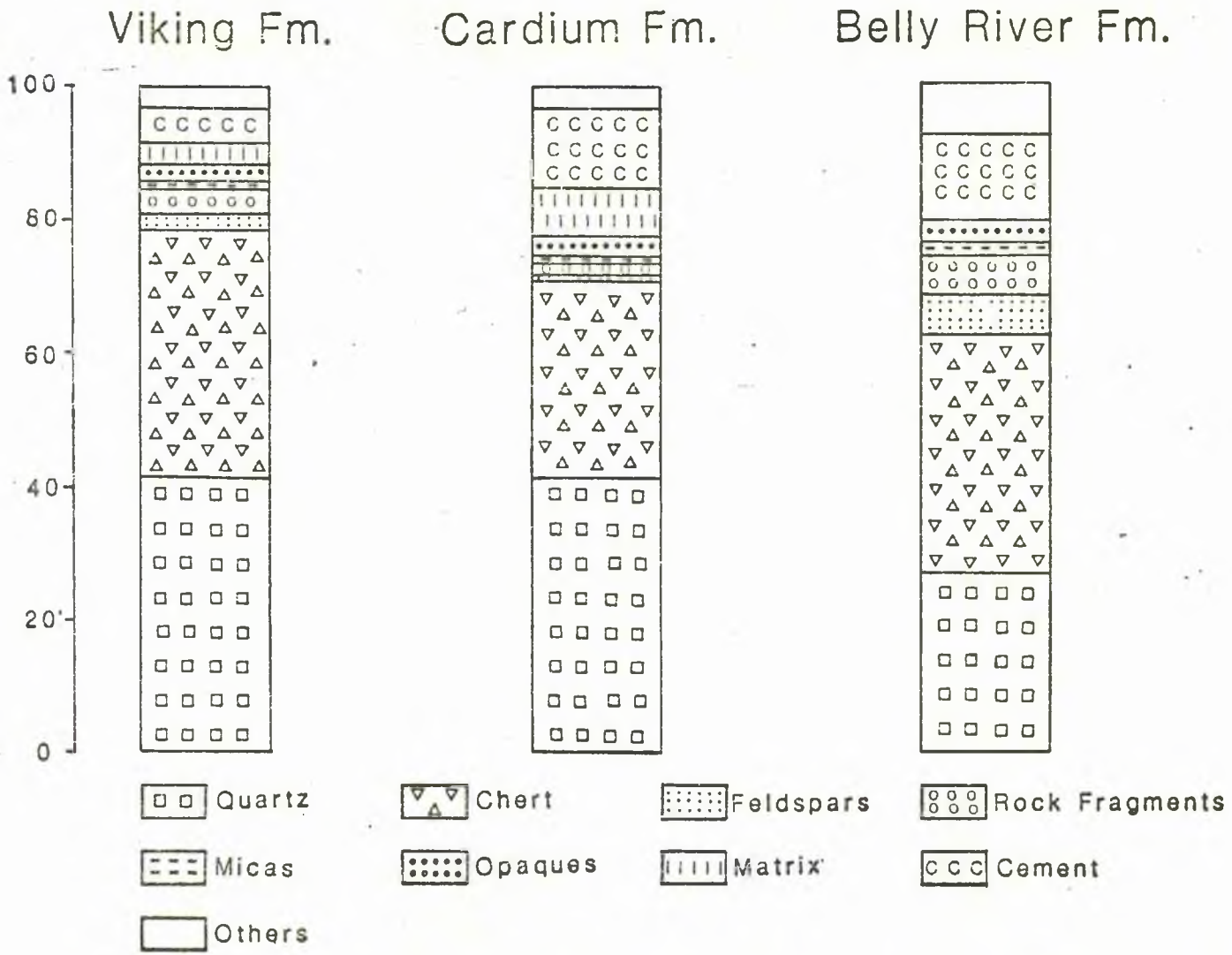

Fig. 7.4 Average mineralogical composition of the Viking, Cardium and Belly River Formations, based on thin section estimates.

Note:- Others mainly include porosity and authigenic clays.

Fig. 7.5. Authigenic quartz crystals growing in a pore with considerable intercrystalline microporosity. SEM photograph. Scale bar equals 20 μm.
(Vik. Fm.; 1570.4 m)

Fig. 7.6. Carbonate cement corroding and replacing detrital grains. A few grains show early quartz or chert overgrowths forming straight grain boundaries. X nicols. Scale bar equals 200 μm.
(Vik. Fm.; 1974.7 m)

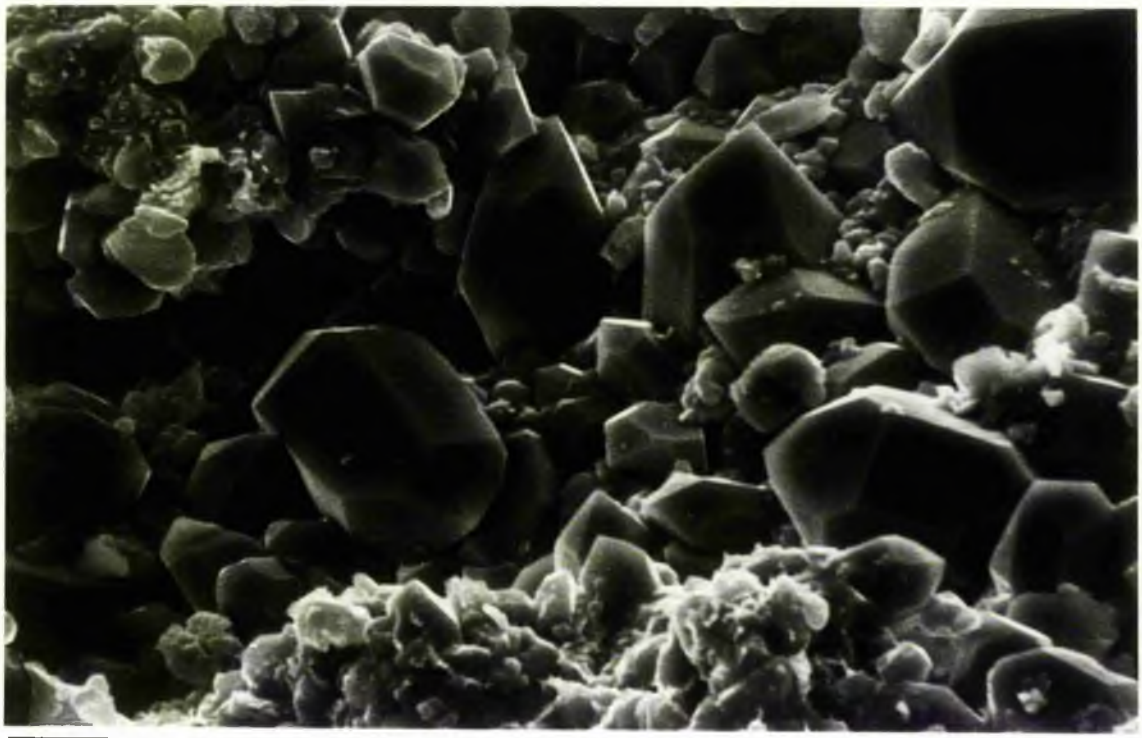

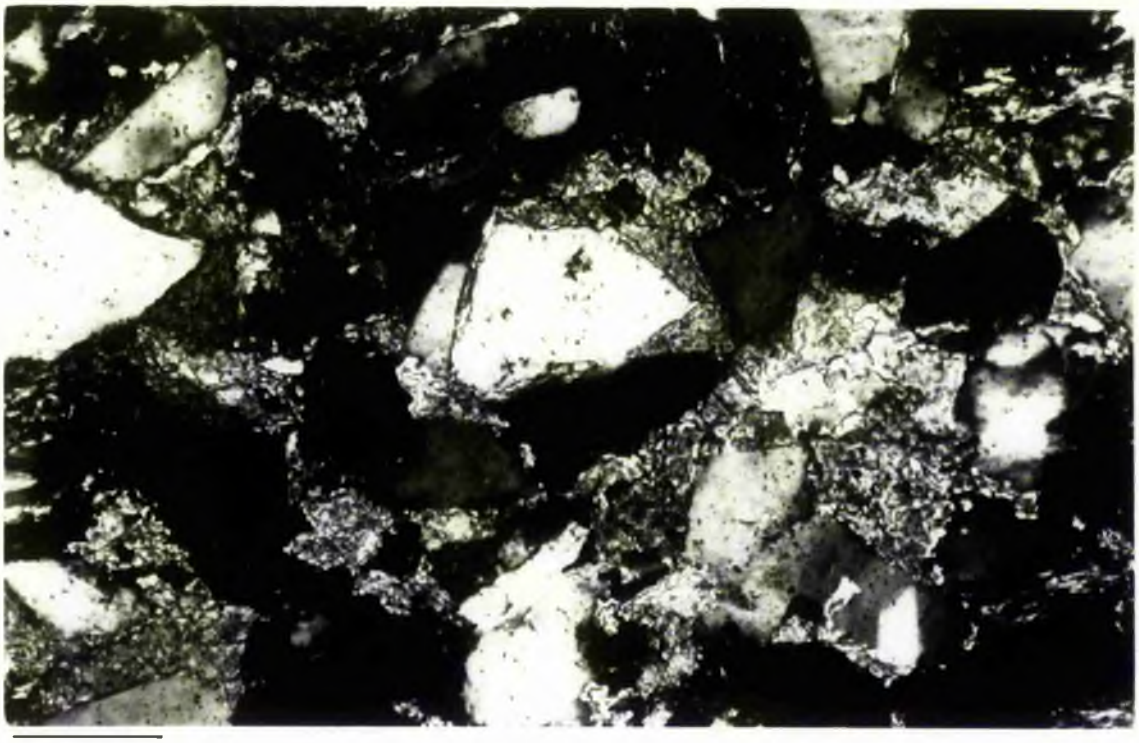

Fig. 7.7. Vermicular stacks of kaolinite with considerable micro-porosity. SEM photograph. Scale bar equals 20 μm.
(Vik. Fm.; 2010.7 m)

Fig. 7.8. SEM photograph showing authigenic illite cement consisting of sheets with wispy termination associated with authigenic quartz crystals. Scale bar equals 20 μm.
(Vik. Fm.; 2715.m)

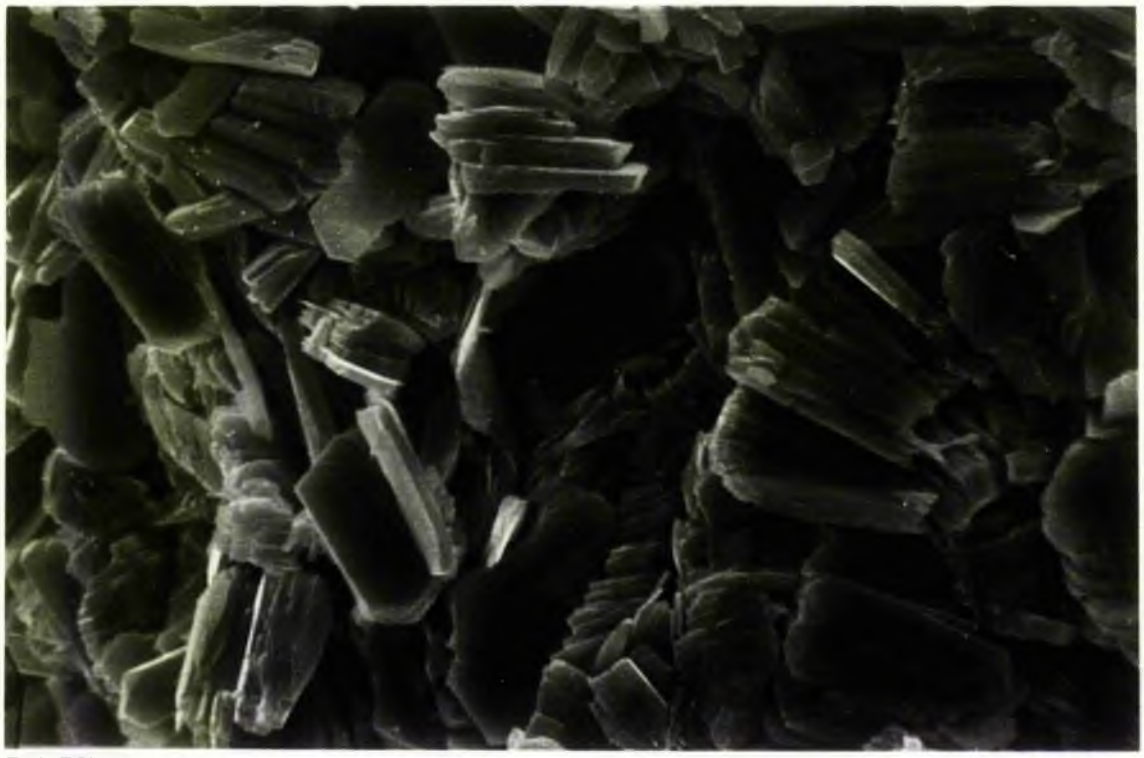

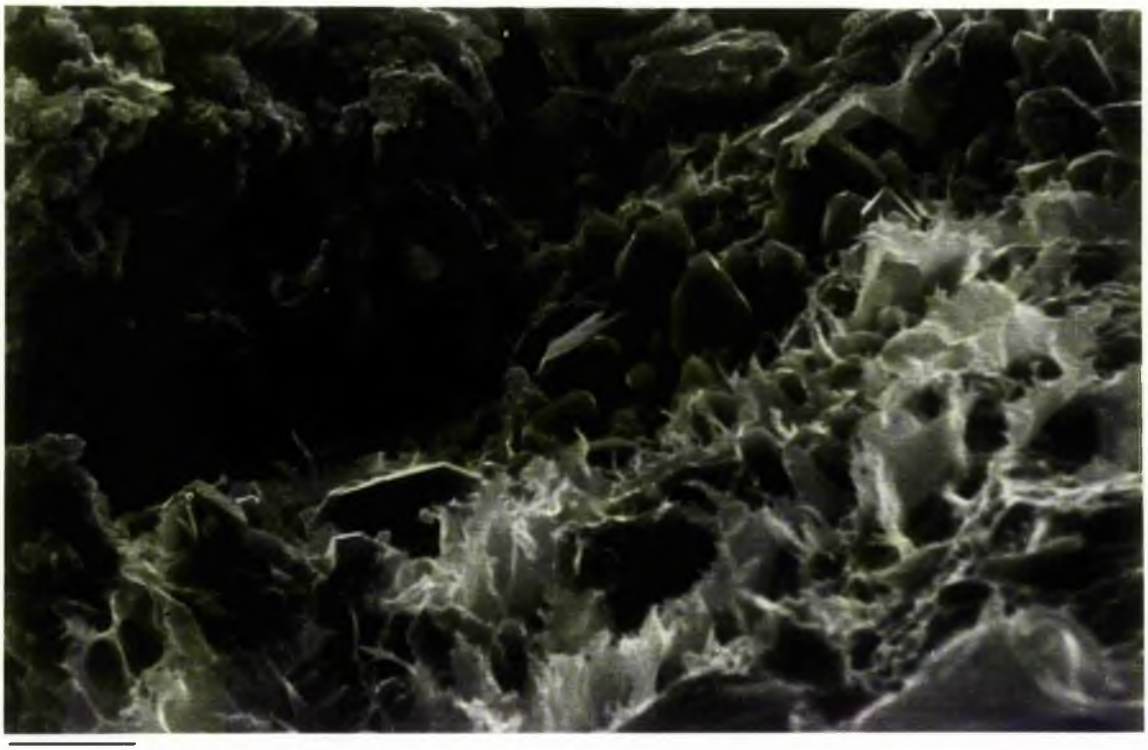

Fig. 7.9. SEM photograph showing scattered individual idiomorphic crystals of chlorite associated with larger authigenic quartz crystals. Scale bar equals 10 μm.
(Vik. Fm.; 2010.7 m)

Fig. 7.10. Quartz overgrowth cementation forming interlocking crystals followed by abundant growth of kaolinite as stacks of pseudo-hexagonal plates. Note kaolinite plates are partially engulfed in quartz overgrown faces. SEM photograph. Scale bar equals 20 μm.
(Vik. Fm.; 1672.2 m)

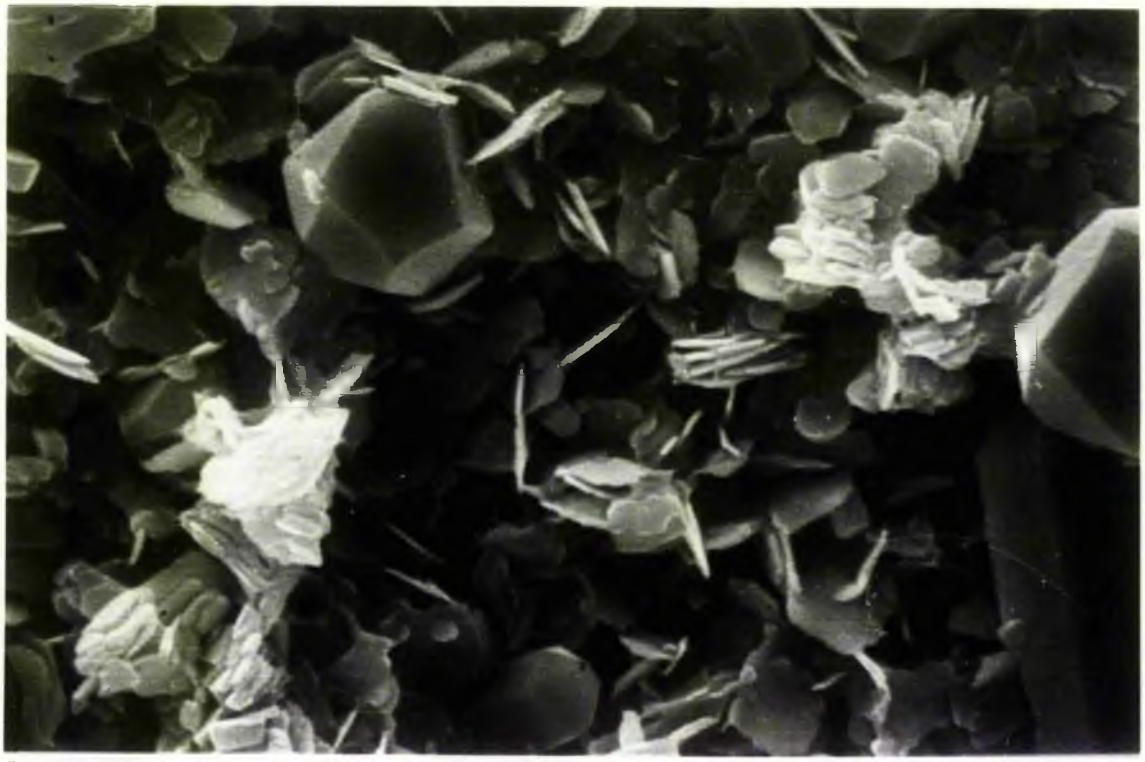

Fig. 7.11. Authigenic feldspar crystal altering into smectite (lower left). Micro-pores within the crystal forms W.P. porosity. SEM photograph. Scale bar equals 20 μm.
(Vik. Fm.; 2175.7 m)

Fig. 7.12. Photomicrograph showing abundant kaolinite books with opaque cement filling a pore. Opaque cement is composed mainly of organic matter but disseminated pyrite and hematite are also present. Plane polarized light. Scale bar equals 200 μm.
(Vik. Fm.; 1742.9 m)

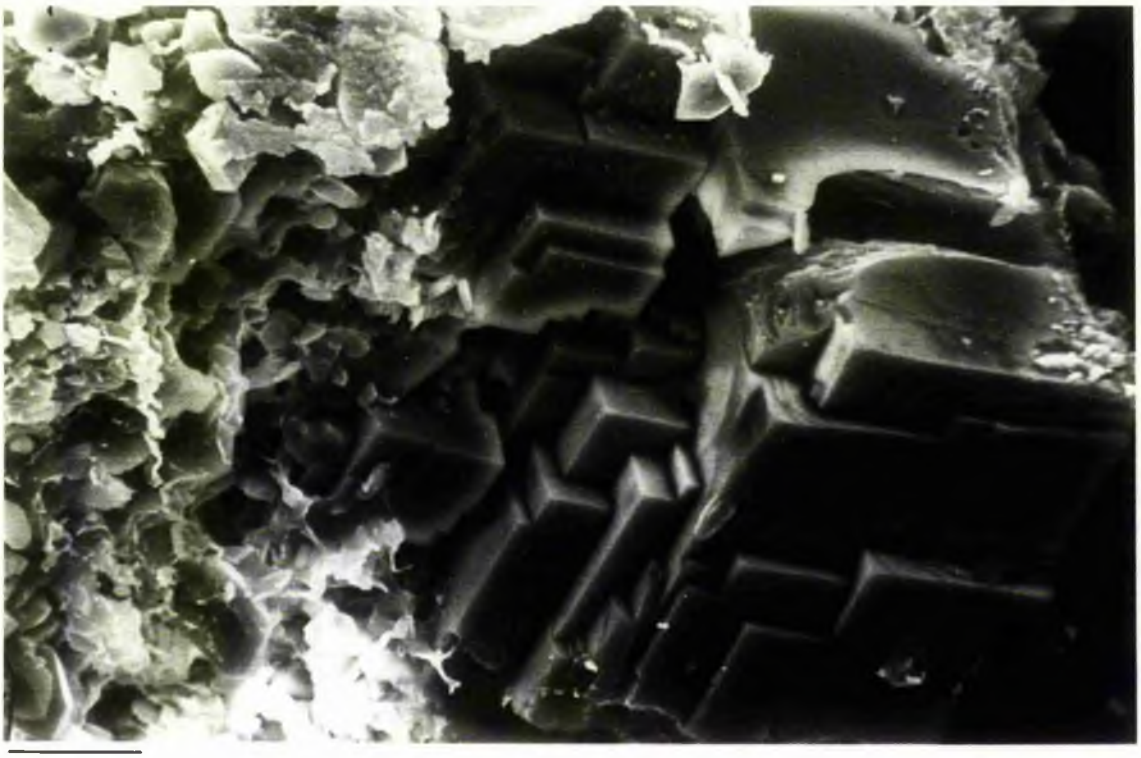

Fig. 7.13. Photomicrograph showing well rounded chert grain surrounded by spherulitic siderite cement showing pseudo-uniaxial figure. Abundant early siderite cementation has caused complete loss of reducible primary porosity. X nicols. Scale bar equals 400 μm.
(Vik. Fm.; 2390 m)

Fig. 7.14. Sharp edges of quartz formed by early silica overgrowth are penetrating a chert grain by means of plastic deformation causing significant reduction in the primary porosity. X nicols. Scale bar equals 200 μm.
(Vik. Fm.; 2244.3 m)

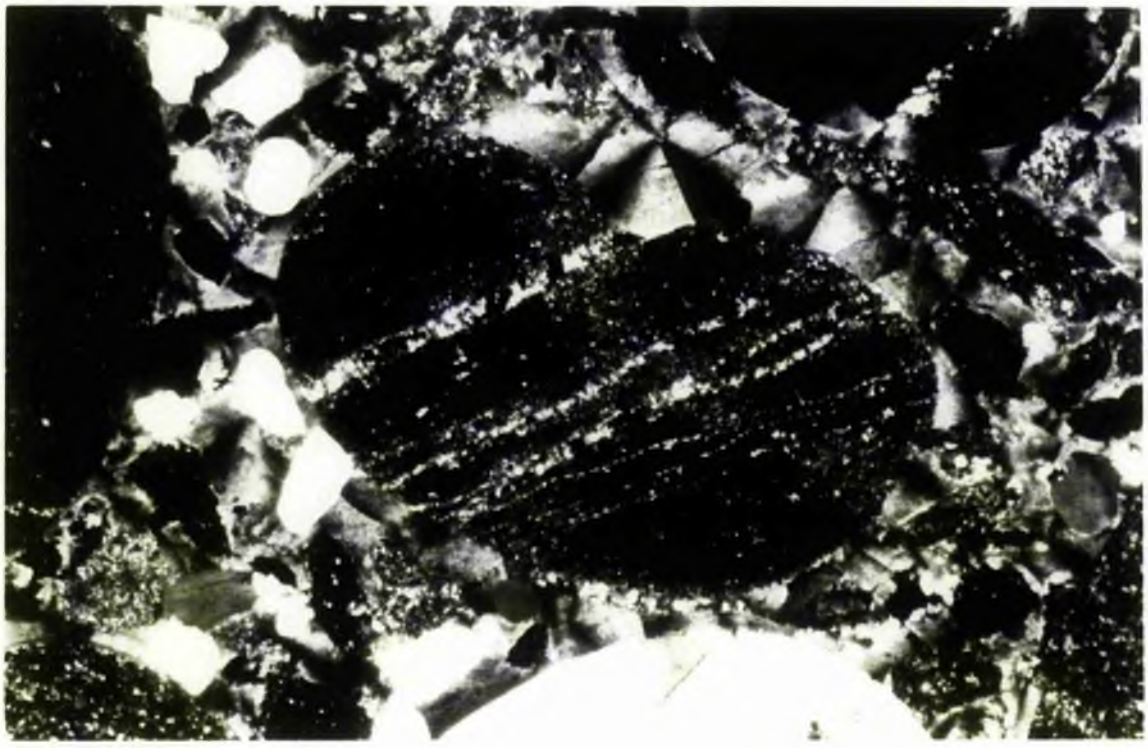

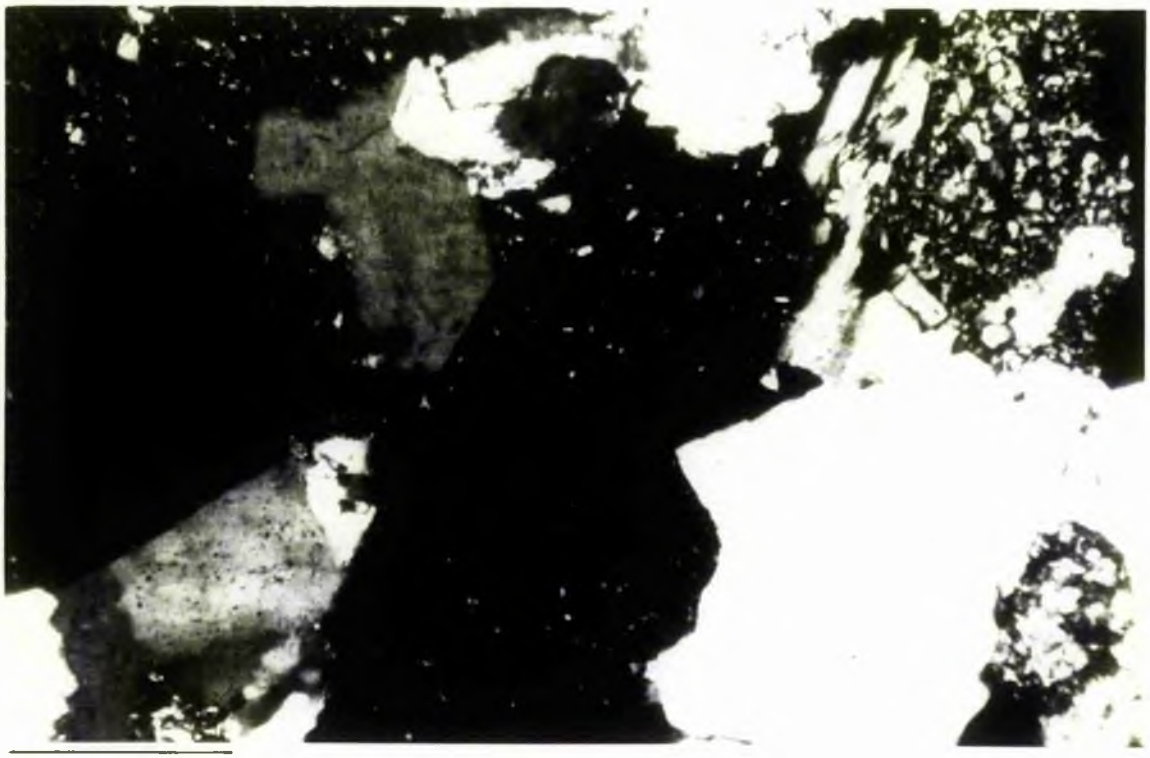

Fig. 7.15. Photomicrograph showing complete loss of reducible primary porosity by abundant syntaxial quartz overgrowth (chemical compaction). X nicols. Scale bar equals 200 μm.
(Card. Fm.; 2420.4 m)

Fig. 7.16. SEM photograph showing framboidal pyrite and abundant authigenic quartz crystals filling a pore. Scale bar equals 10 μm.
(Card. Fm.; 2135 m)

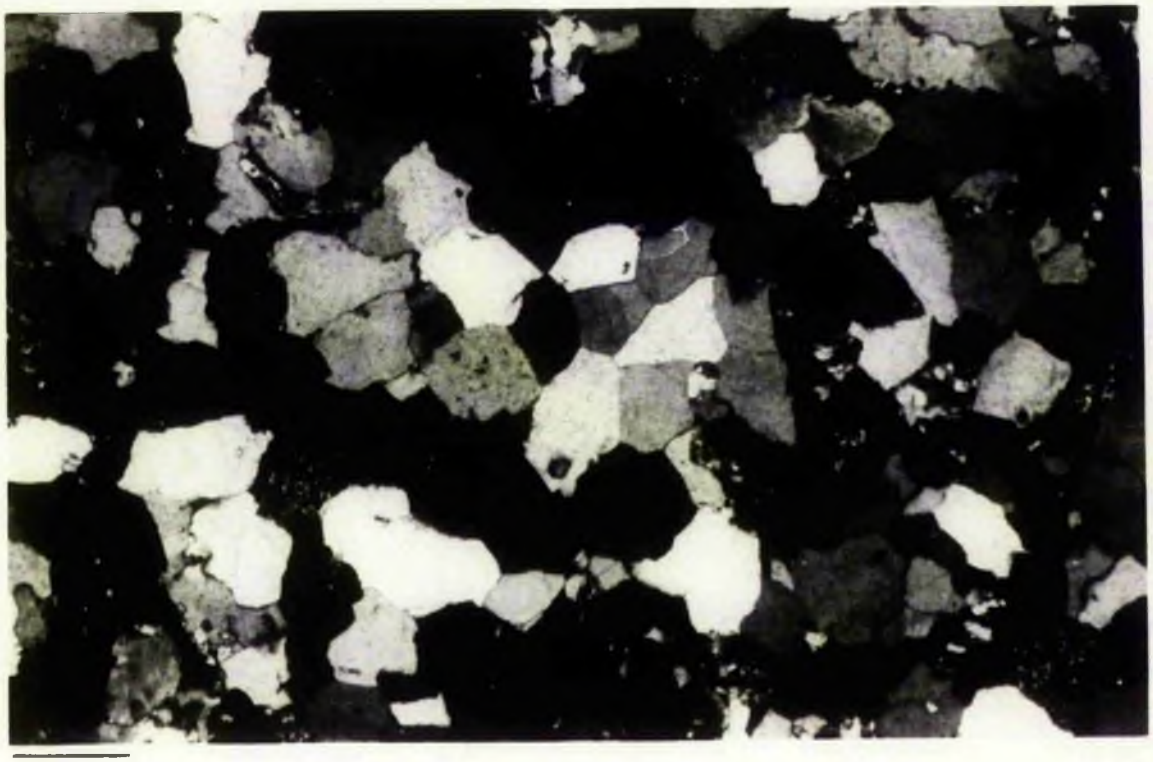

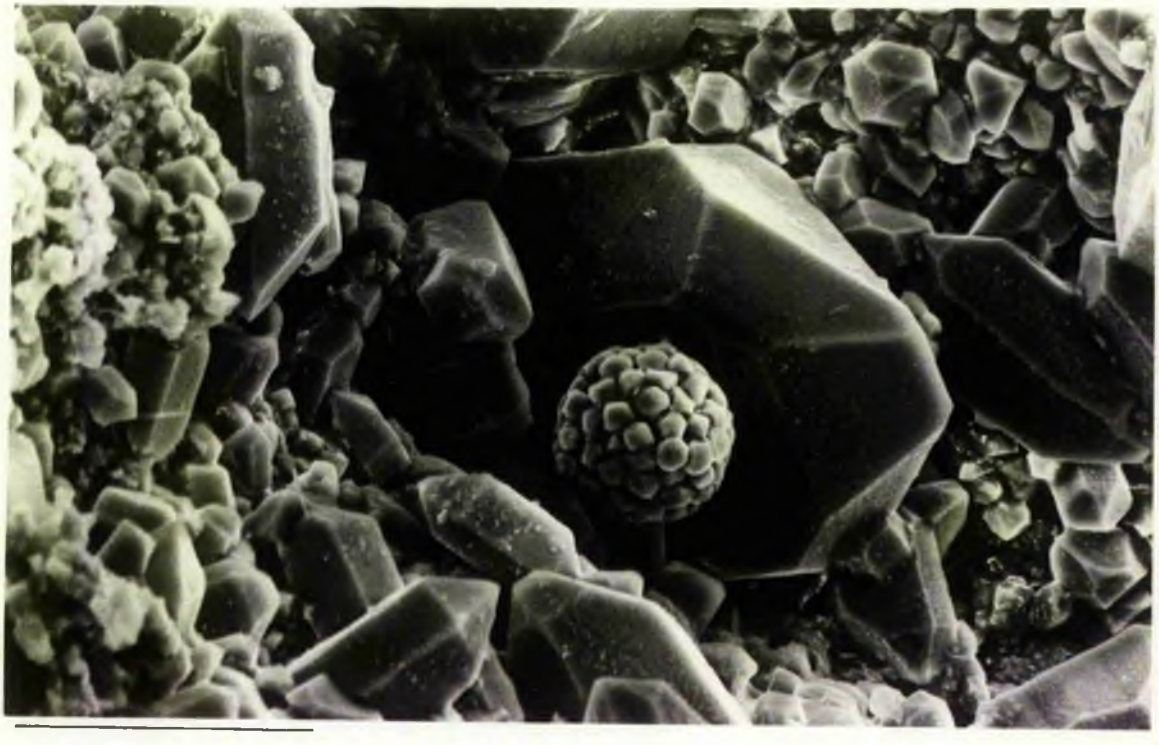

Fig. 7.17. SEM photograph showing authigenic illite with wispy thread-like terminations growing in a pore. Scale bar equals 10 μm.
(Card. Fm.; 2496.9 m)

Fig. 7.18. Dense well developed chlorite grain-coating as individual needle-like crystals and knots. Quartz grain surface to which chlorite is attached oriented parallel to plate. SEM photograph. Scale bar equals 10 μm.
(Card. Fm.; 2132.5 m)

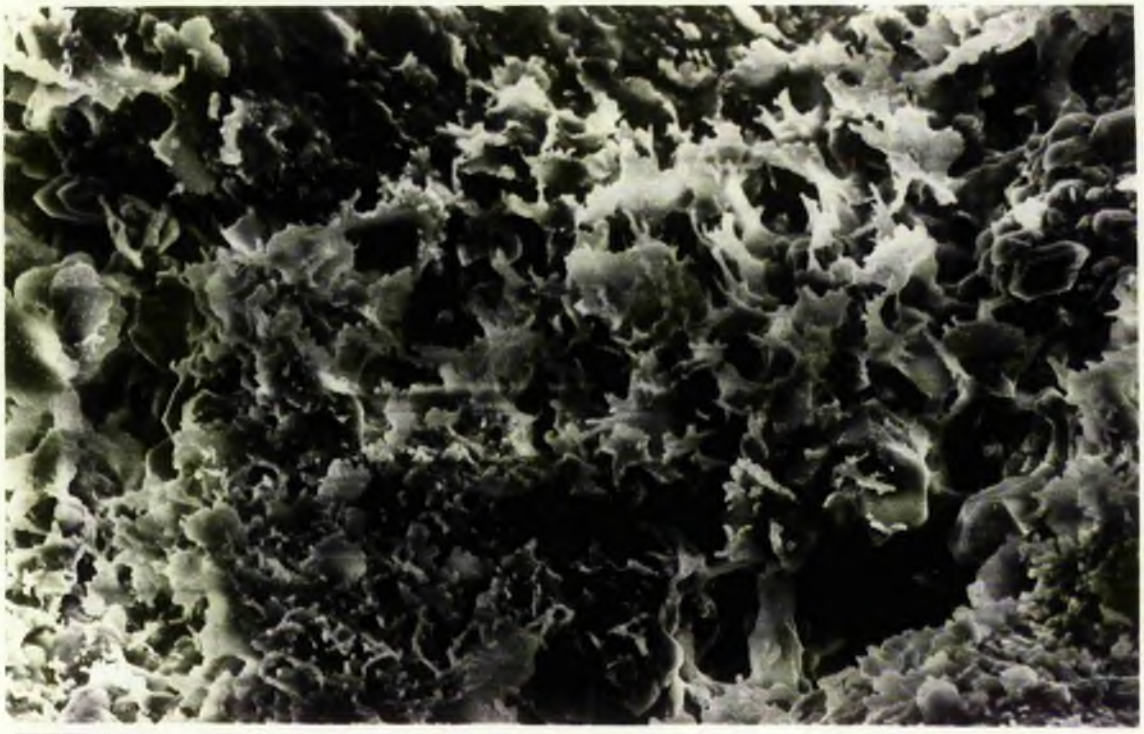

Fig. 7.19. SEM photograph showing silica cementation forming interlocking quartz crystals followed by chlorite growth as individual platy crystals. Note that chlorite crystals are sometimes partially engulfed in quartz (central area). Scale bar equals 10 μm.

(Card. Fm.; 1602·4 m)

Fig. 7.20. Photomicrograph showing chert grain being replaced by siderite cement. Residual chert is present in the central left dark area. Arrow shows ghost of former chert grain. Pseudo-uniaxial figure of siderite can be seen in the lower left area. X nicols. Scale bar equals 500 μm.
(Card. Fm.; 1929.5 m)

Fig. 7.21. Photomicrograph showing chert grains cemented by spherulitic siderite. The centre of the picture (dark area) shows moldic porosity formed by dissolution of ankerite/ferroan calcite. Arrow shows residual ankerite/ferroan-calcite. X nicols. Scale bar equals 500 μm.
(Card. Fm.; 1929.5 m)

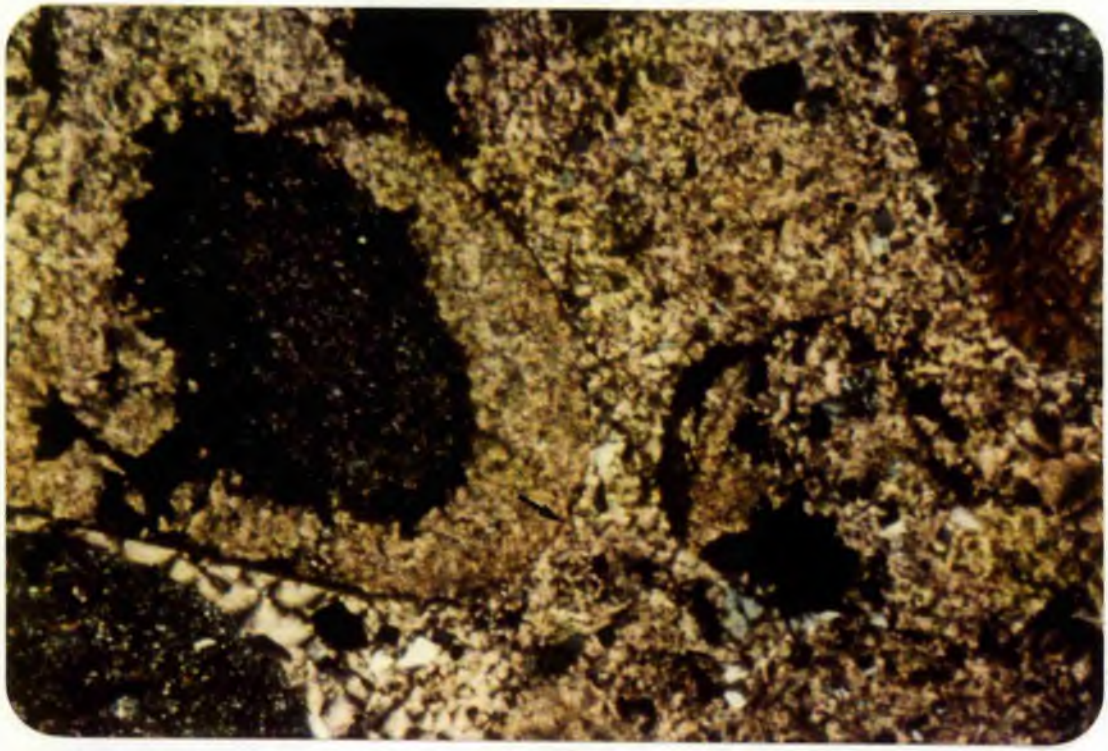

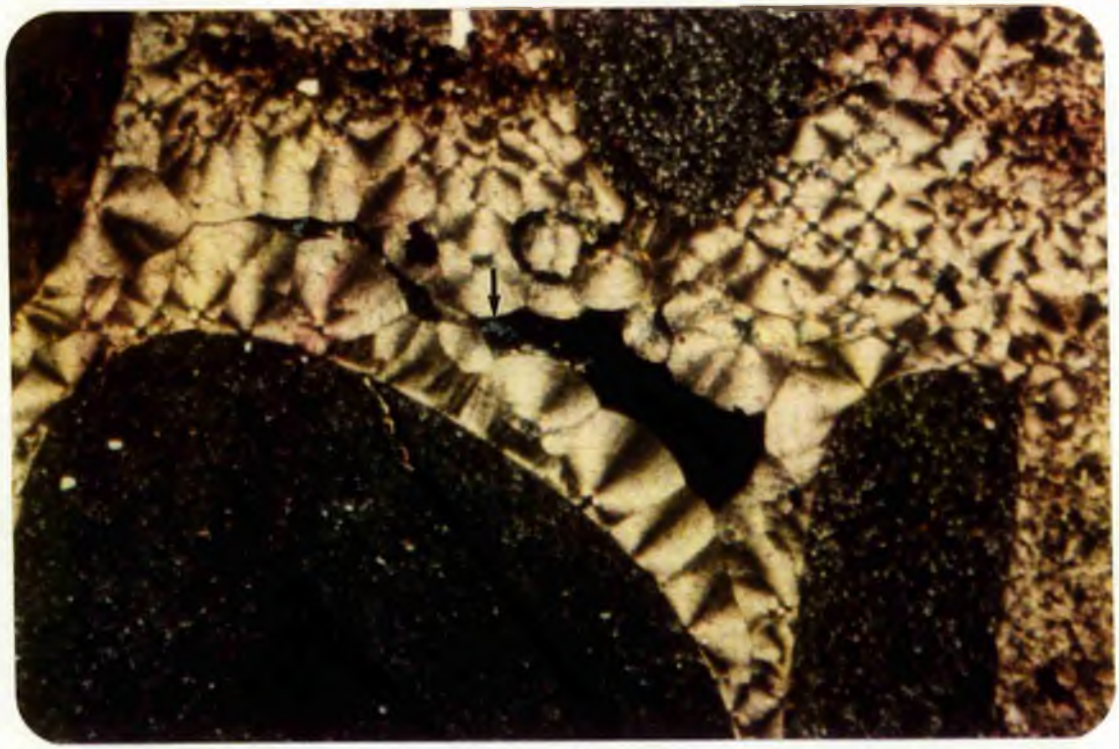

Fig. 7.22. Siderite cement showing colloform textural growth and subsequent fracturing. Blue rims around the grains and a patch (in the centre, lower left and right) are of ferroan-calcite/ankerite. X nicols. Scale bar equals 250 μm.

(Card. Fm.; 1781·5 m)

Fig. 7.23. Photomicrograph shows vuggy porosity (blue areas) formed by extensive dissolution of carbonate cement and/or unstable grains. Authigenic chlorite (shown by an arrow) forms fringes around grains and has also been removed along with carbonate from some places. Plane polarized light. Scale bar equals 200 μm.

(Card. Fm.; 1207 m)

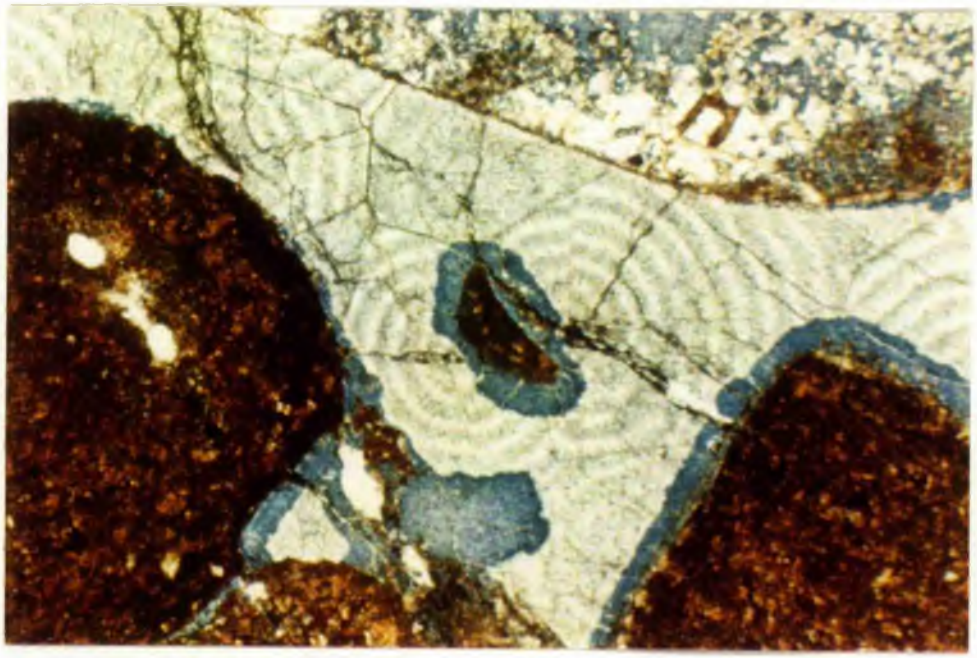

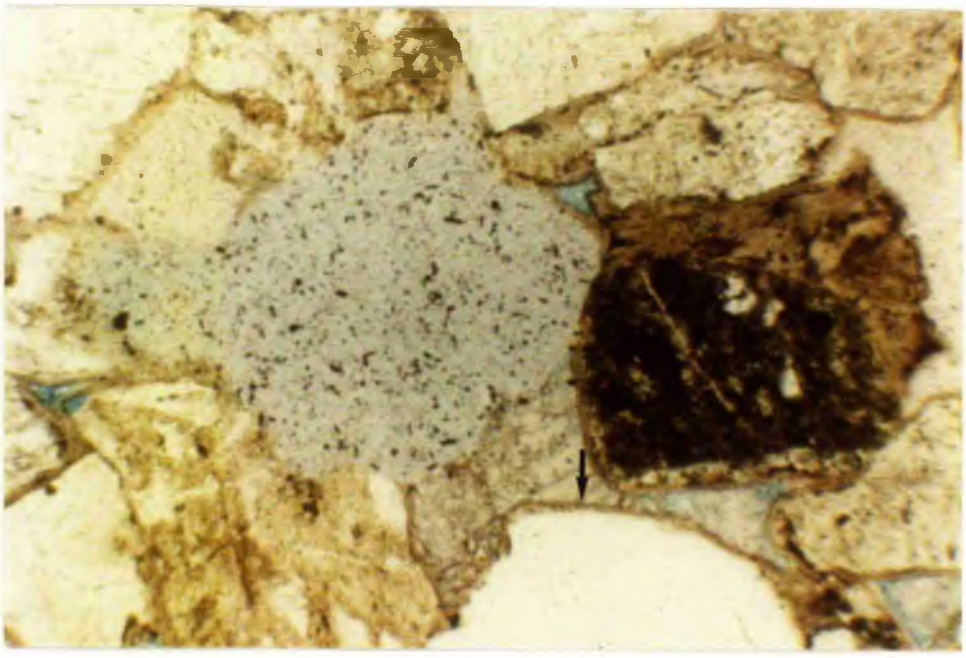

Fig. 7.24. Photomicrograph showing abundant pyrite cement dispersed all around grains. Plane polarized light. Scale bar equals 100 μm.
(Card. Fm.; 1630.4 m)

Fig. 7.25. SEM photograph showing pyrite cement (seen in Fig. 7.24) as individual cubes dispersed around grains. Scale bar equals 10 μm.
(Card. Fm.; 1630.4 m)

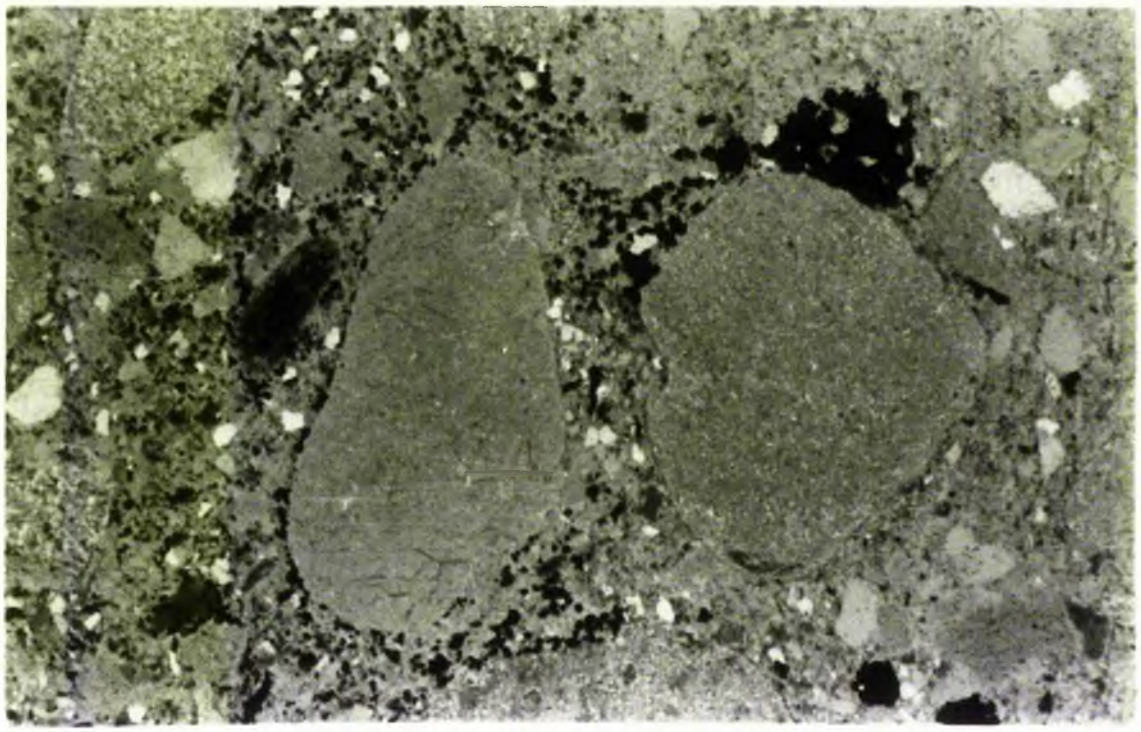

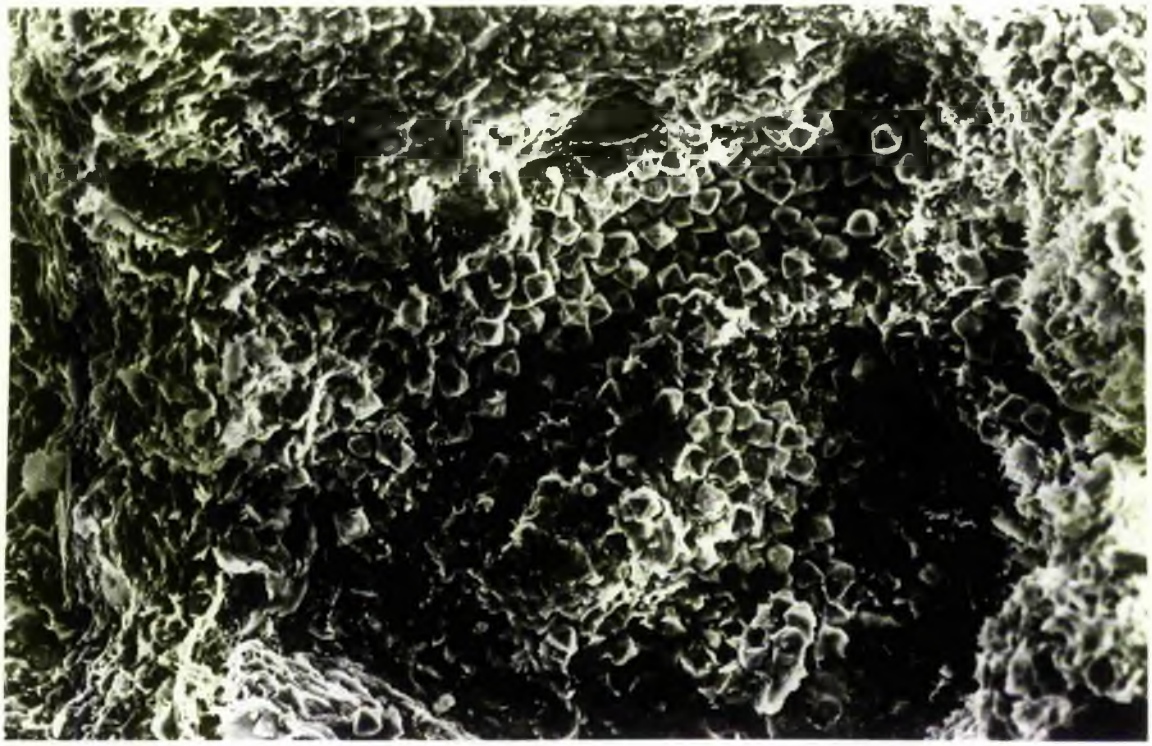

Fig. 7.26. SEM photograph showing clusters of authigenic dolomite rhombs which are believed to have formed during late diagensis. Scale bar equals 10 μm.
(Card. Fm. ; 1861.2 m)

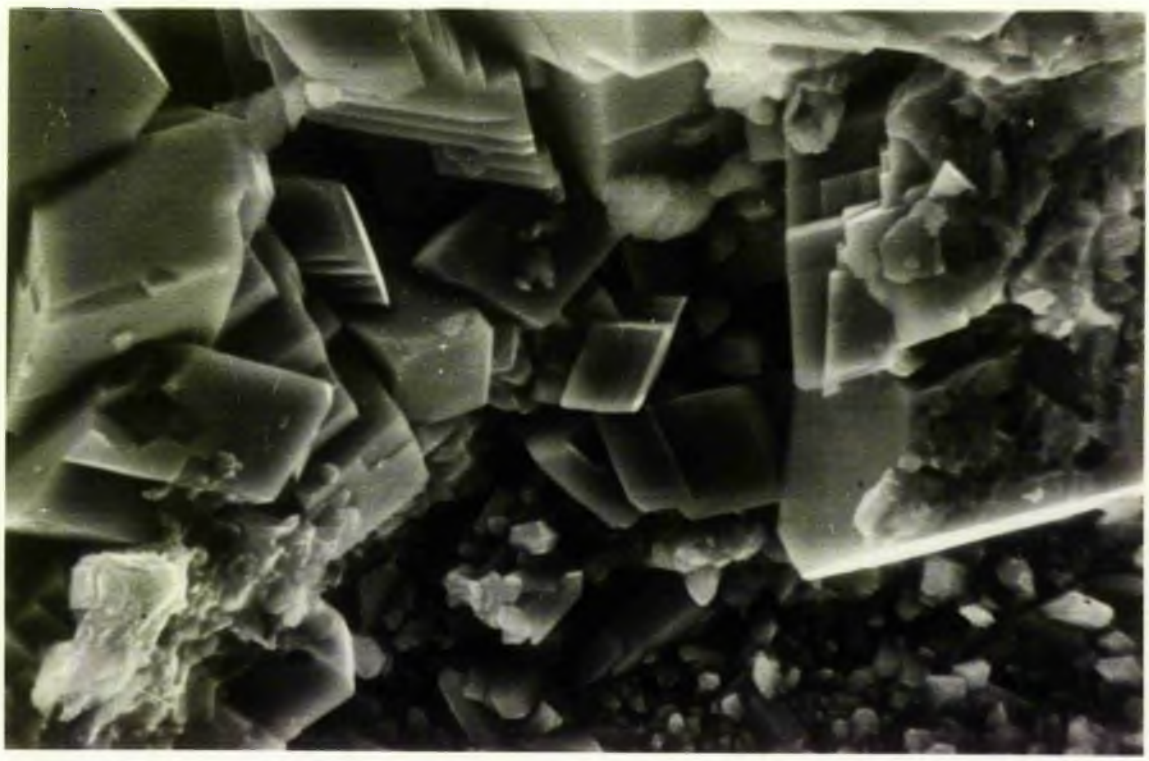

Fig. 7.27. Silica overgrowth followed by abundant chlorite growth perpendicular to the grain surfaces forming fringes around grains. Chert cement (c) filling the residual reduced pores. Arrow shows dust line. Plane polarized light. Scale bar equals 100 μm.
(B.R.Fm.; 1175 m)

Fig. 7.28. Chlorite growing perpendicular to grain surfaces forming fringes followed by chert cementation in the residual pores (shown by arrow). Note that birefringence colours of chlorite are slighty exaggerated. X nicols. Scale bar equals 100 μm.
(B.R.Fm.; 1169.4 m)

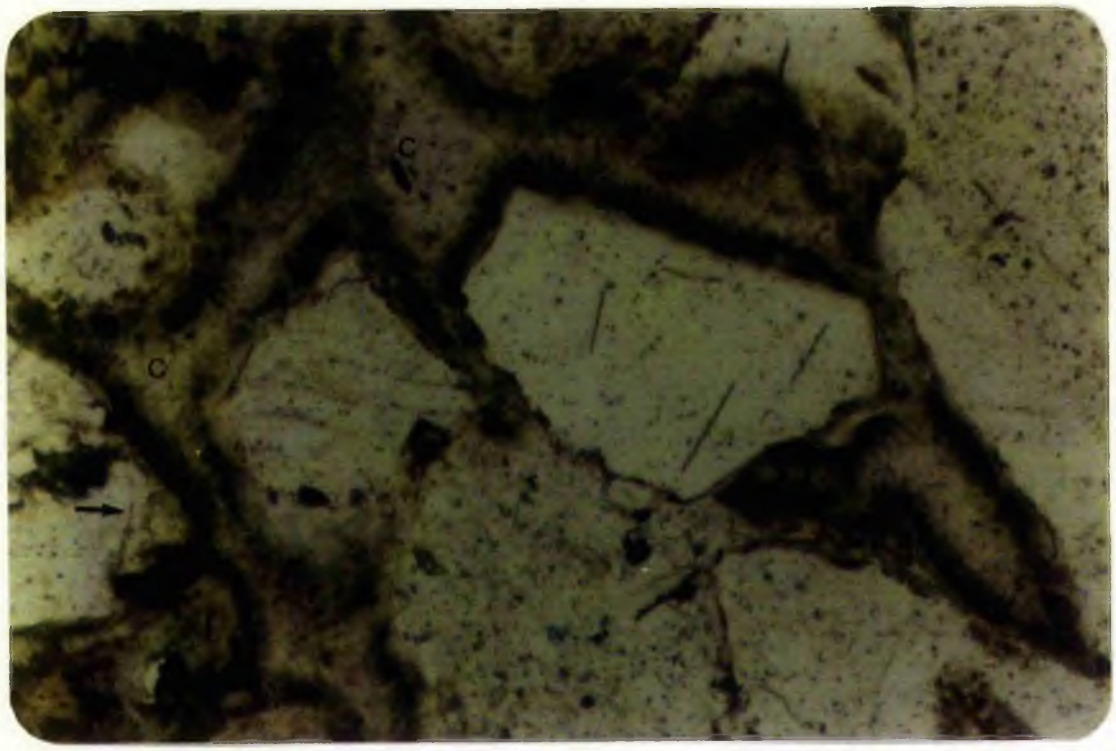
C
C

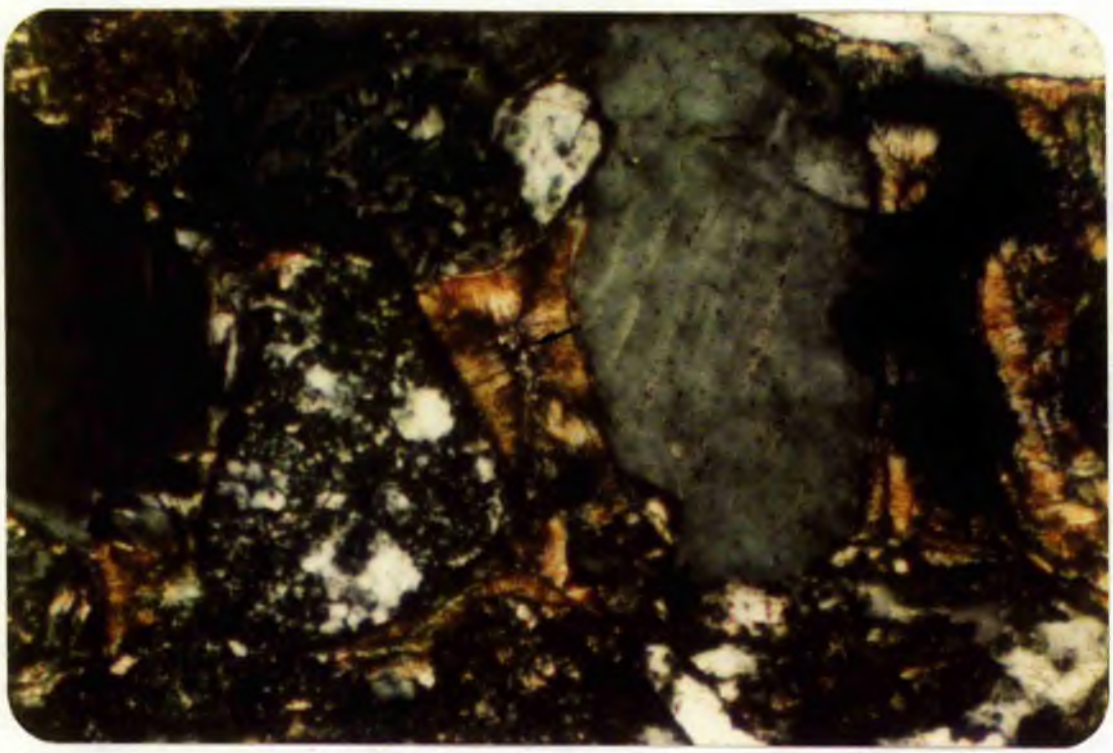

Fig. 7.29. SEM photograph showing chlorite growing perpendicular to the grain surface and choking pore throat. Scale bar equals 20 μm. (B.R. Fm.; 1175 m)

Fig. 7.30. Abundant growth of chlorite blades forming knots and clusters on the grain surface associated with growth of small doubly terminated authigenic quartz crystals. Chlorite blades are sometimes partially engulfed in quartz (shown by arrow). SEM photograph. Scale bar equals 10 μm. (B.R. Fm.; 1115.8 m)

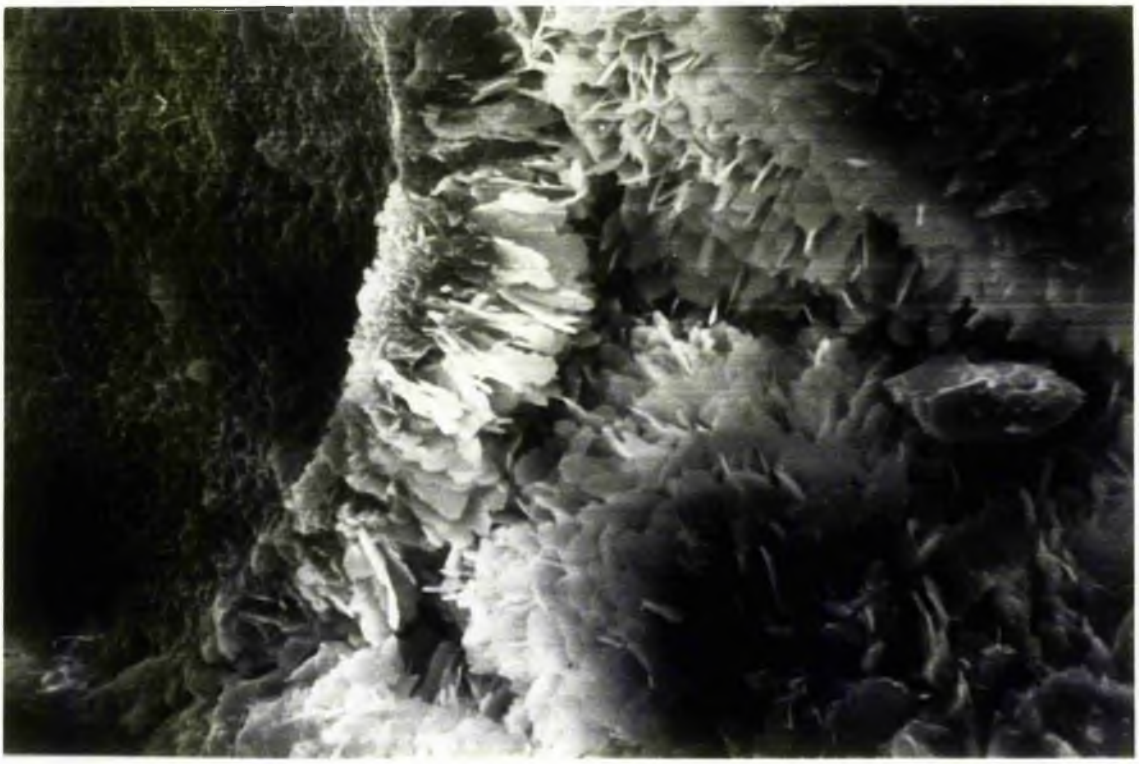

Fig. 7.31. SEM photograph showing abundant authigenic chlorite blades forming knots growing on overgrown quartz faces. Note chlorite knots are partially engulfed in overgrown face (shown by arrow). Scale bar equals 10 μm.
(B.R. Fm.; 1115.8 m)

Fig. 7.33. Kaolinite plates (right side) and thin illite clouds with wispy thread like termination (left side) filling a pore. SEM photograph. Scale bar equals 10 μm.
(B.R. Fm.; 1344.5 m)

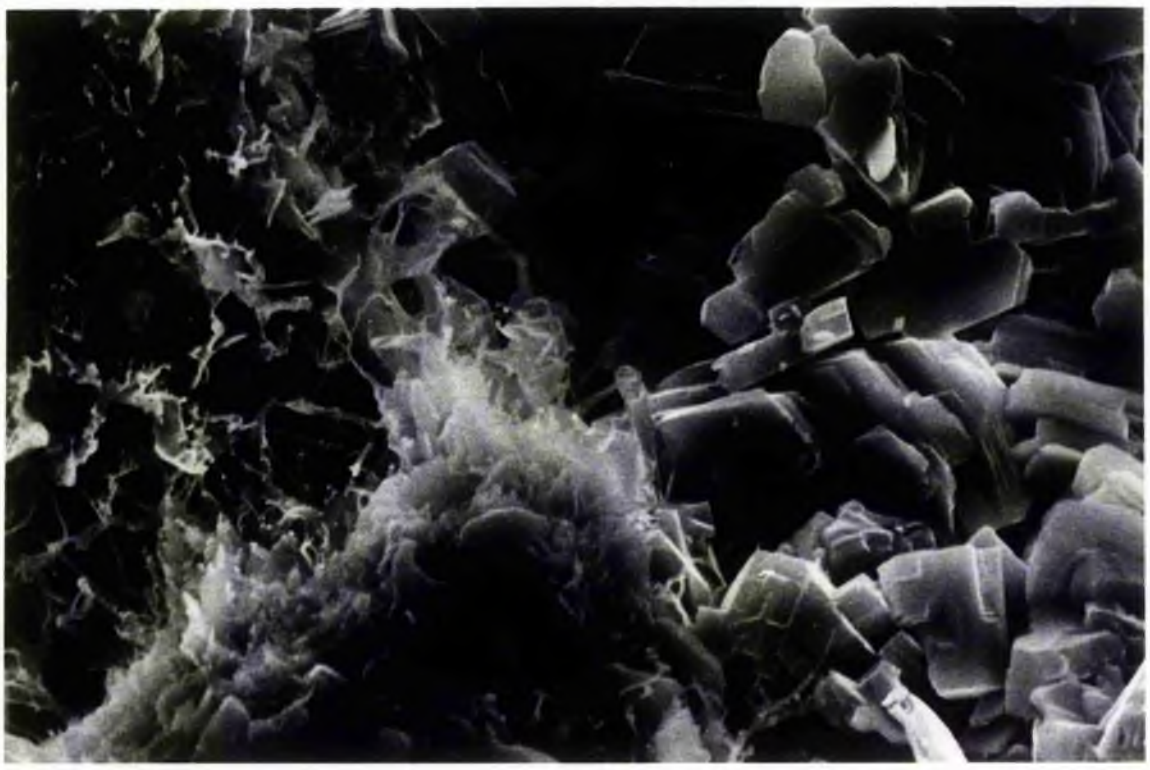

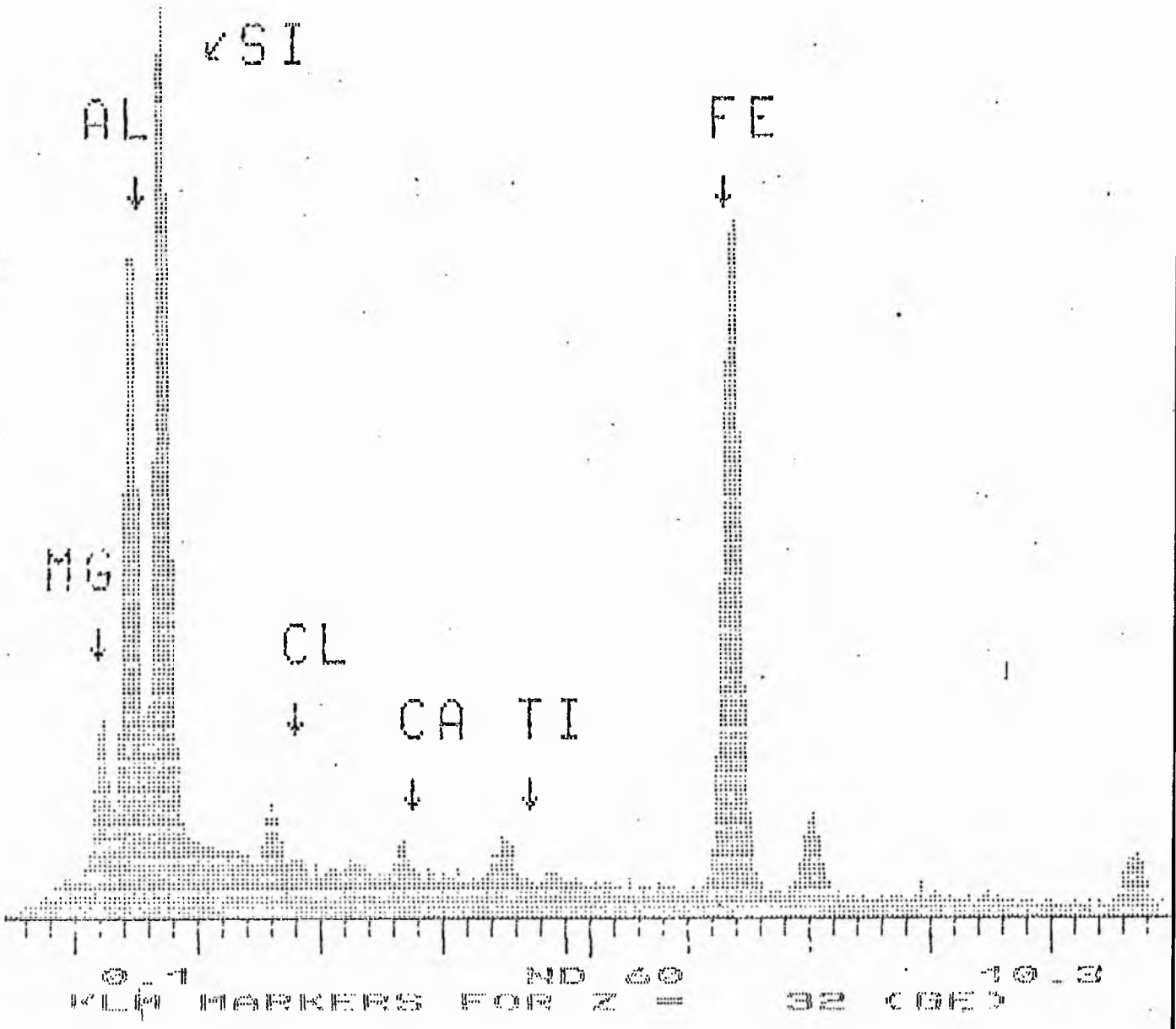

Fig. 7.32 EDX Spectrum of authigenic chlorite forming fringes around grains.

Fig. 7.34. SEM photograph showing highly crenulated smectite flakes forming box-work texture. Scale bar equals 10 μm.
(B.R. Fm.; 1169.4 m)

Fig. 7.35. Well rounded chert grain cemented by chert cement (c). Margins of the grains are outlined by authigenic chlorite forming fringes. X nicols. Scale bar equals 100 μm.
(B.R. Fm.; 1249 m)

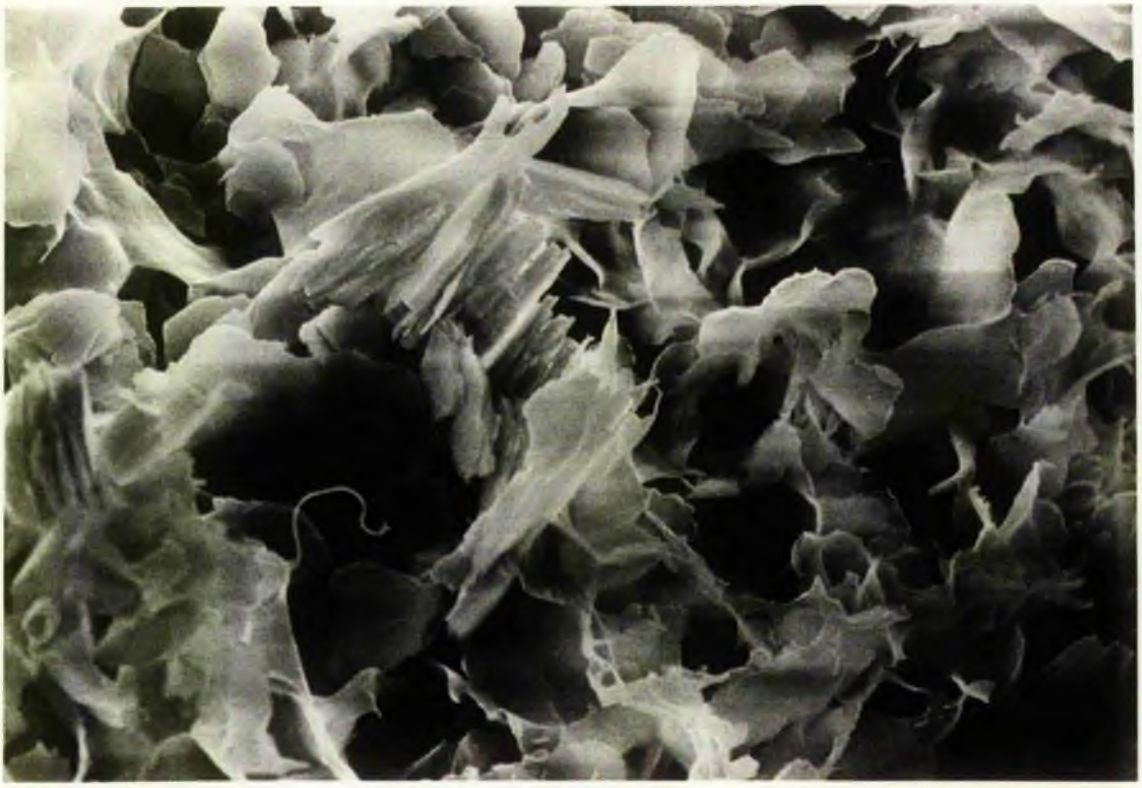

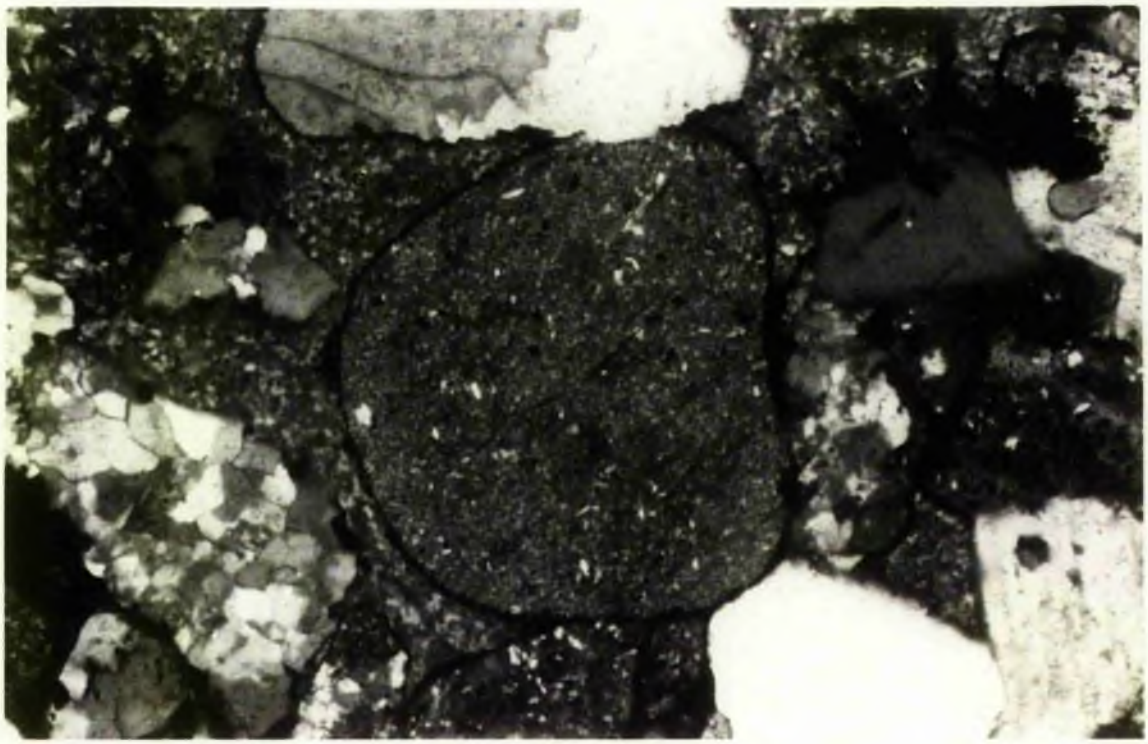

Fig. 7.36. Early quartz overgrowth followed by abundant perpendicular growth of chlorite forming pore linings (shown by arrow) and carbonate cementation (pinkish blue area in the centre) in the residual reduced pores. Blue areas represent secondary porosity (SP) formed by partial dissolution of carbonate cement. Plane polarized light. Scale bar equals 100 μm.
(B.R. Fm.; 1249 m)

Fig. 7.37. Photomicrograph showing W.P. fractured porosity in a chert grain. Large blue areas represent vuggy porosity. Plane polarized light. Scale bar equals 200 μm.
(B.R. Fm.; 1200.6 m)

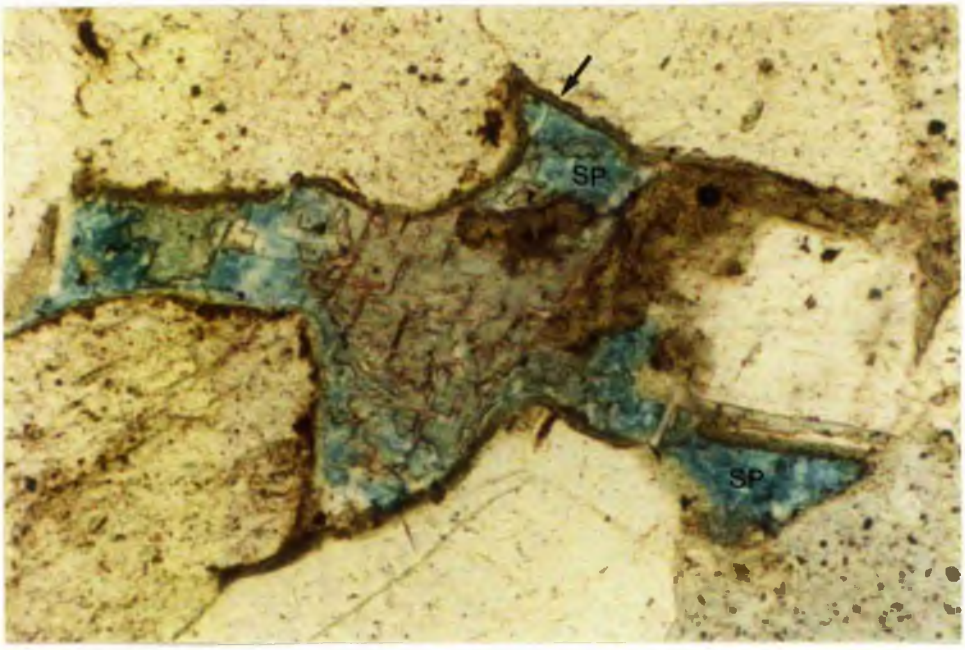
SP
SP

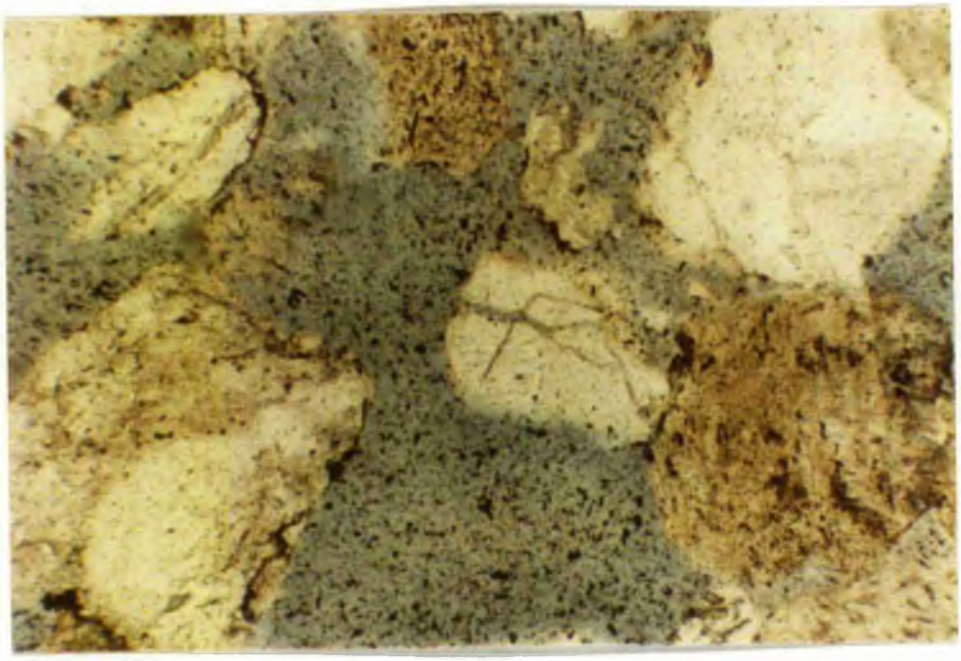

Fig. 7.38. Abundant early quartz overgrowth forming prism faces followed by carbonate cementation occluding all the residual pores. Note corrosion of quartz grains by carbonate cement (ferroan calcite/ankerite). X nicols. Scale bar equals 100 μm.

(B.R. Fm.; 1238.5 m)

Fig. 7.39. An early stage of quartz overgrowth showing numerous tiny crystals all growing parallel to one another (right) on a grain surface. On the left side are scattered chlorite plates associated with authigenic quartz crystals. SEM photograph. Scale bar equals 10 μm.

(B.R. Fm.; 1492.3 m)

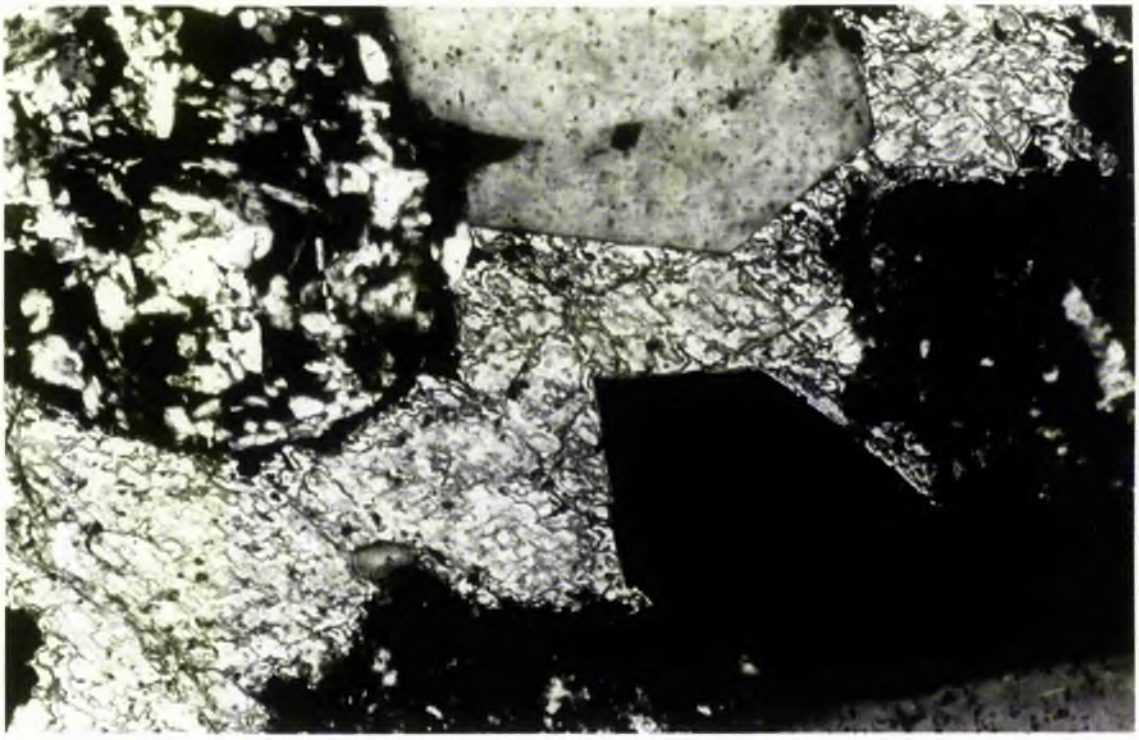

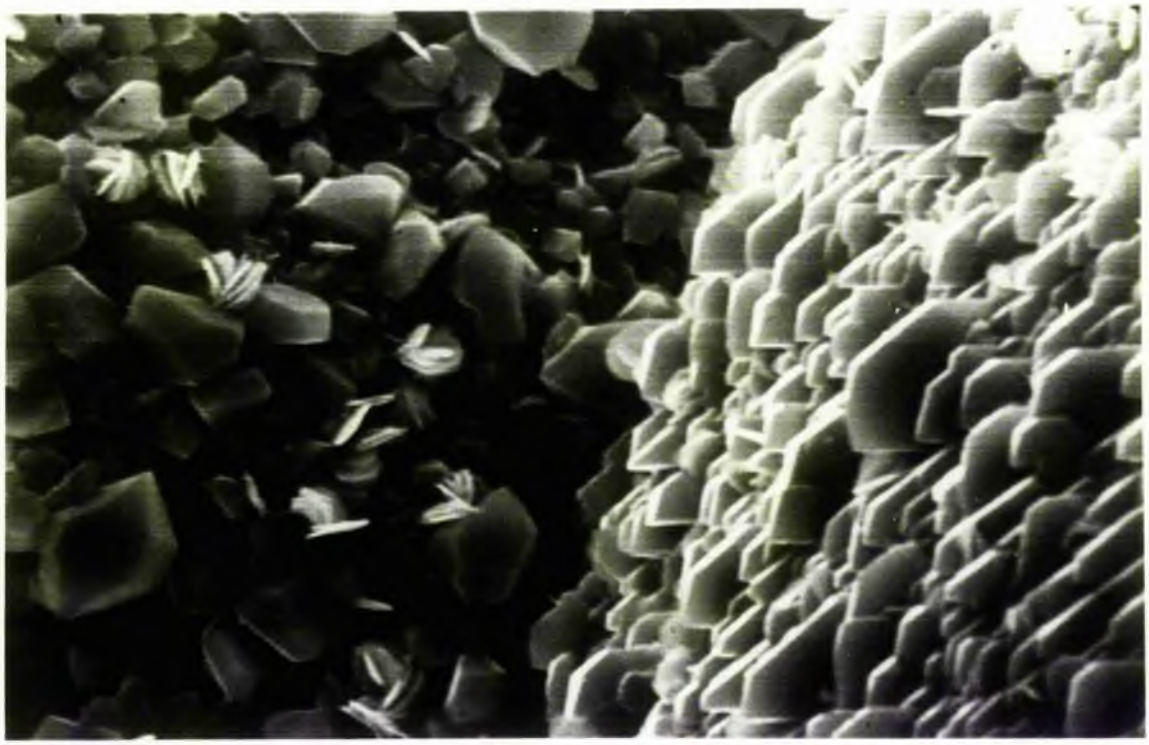

Fig. 7.40. SEM photograph showing quartz overgrowth forming interlocking crystals followed by chlorite (middle and upper left) and smectite (lower left) formation in a pore. Scale bar equals 20 μm.
(B.R. Fm.; 1496·3 m)

Fig. 7.41. SEM photograph showing wavy plates of smectite forming honeycomb texture associated with authigenic quartz crystals. Scale bar equals 10 μm.
(B.R. Fm.; 1492·3 m)

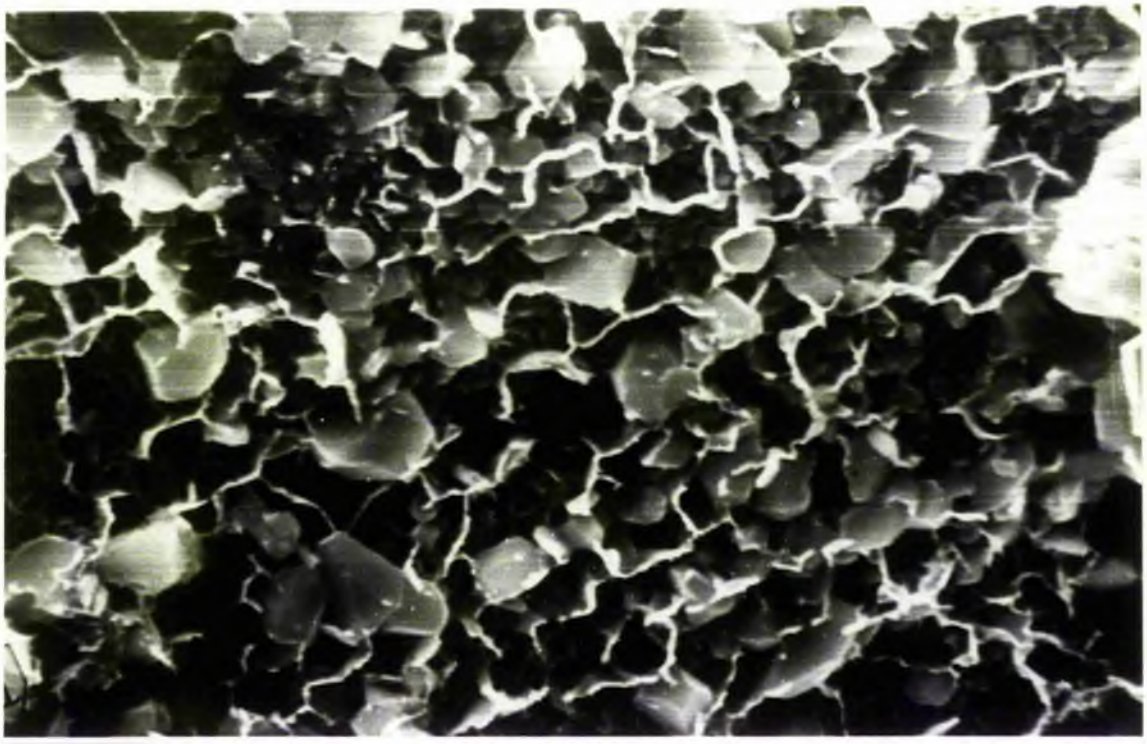

Fig. 7.42. SEM photograph showing microporosity (B.P.C., shown by arrow) between quartz grain surface (with numerous tiny crystals) and carbonate cement. Scale bar equals 40 μm.
(B.R. Fm.; 1238.5 m)

Fig. 7.43. SEM photograph showing abundant kaolinite books and carbonate matrix precariously perched on grain surface (right). Scale bar equals 10 μm.
(B.R. Fm.; 1238.5 m)

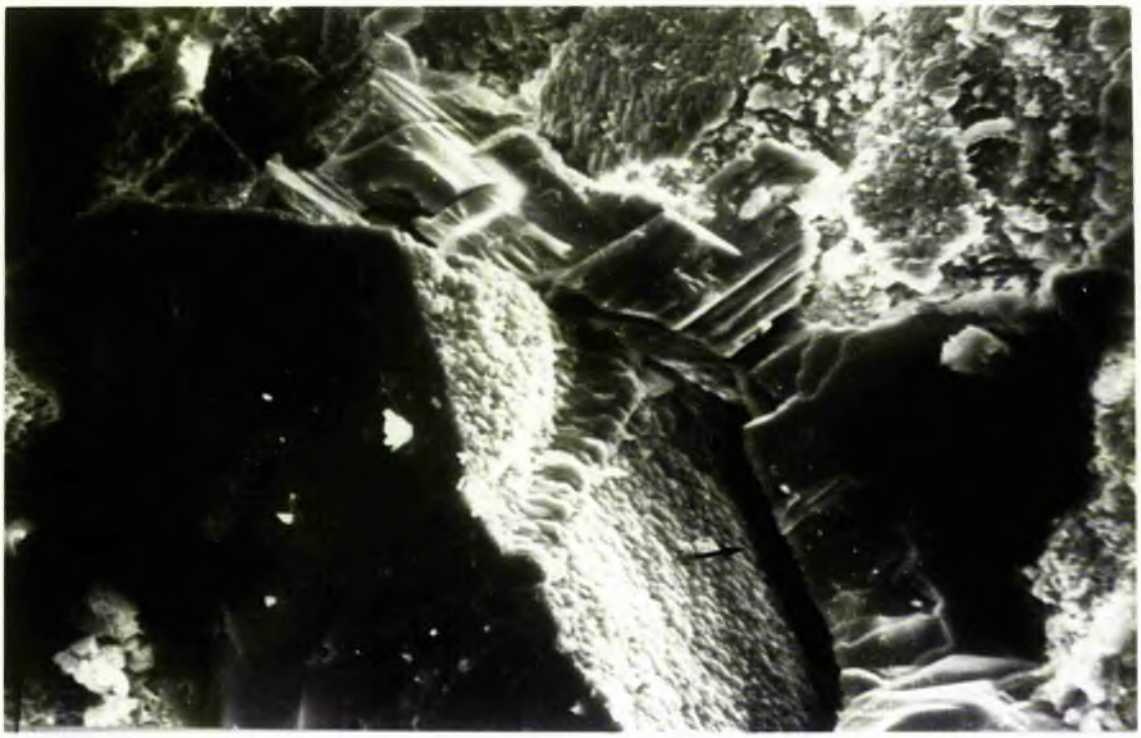

Fig. 7.44. Kaolinite books associated with carbonate matrix in a pore. Note carbonate matrix shows rounded edges and is believed to have formed by disintegration of carbonate cement during dissolution. SEM photograph. Scale bar equals 10 μm.

(B.R. Fm.; 1238.5 m)

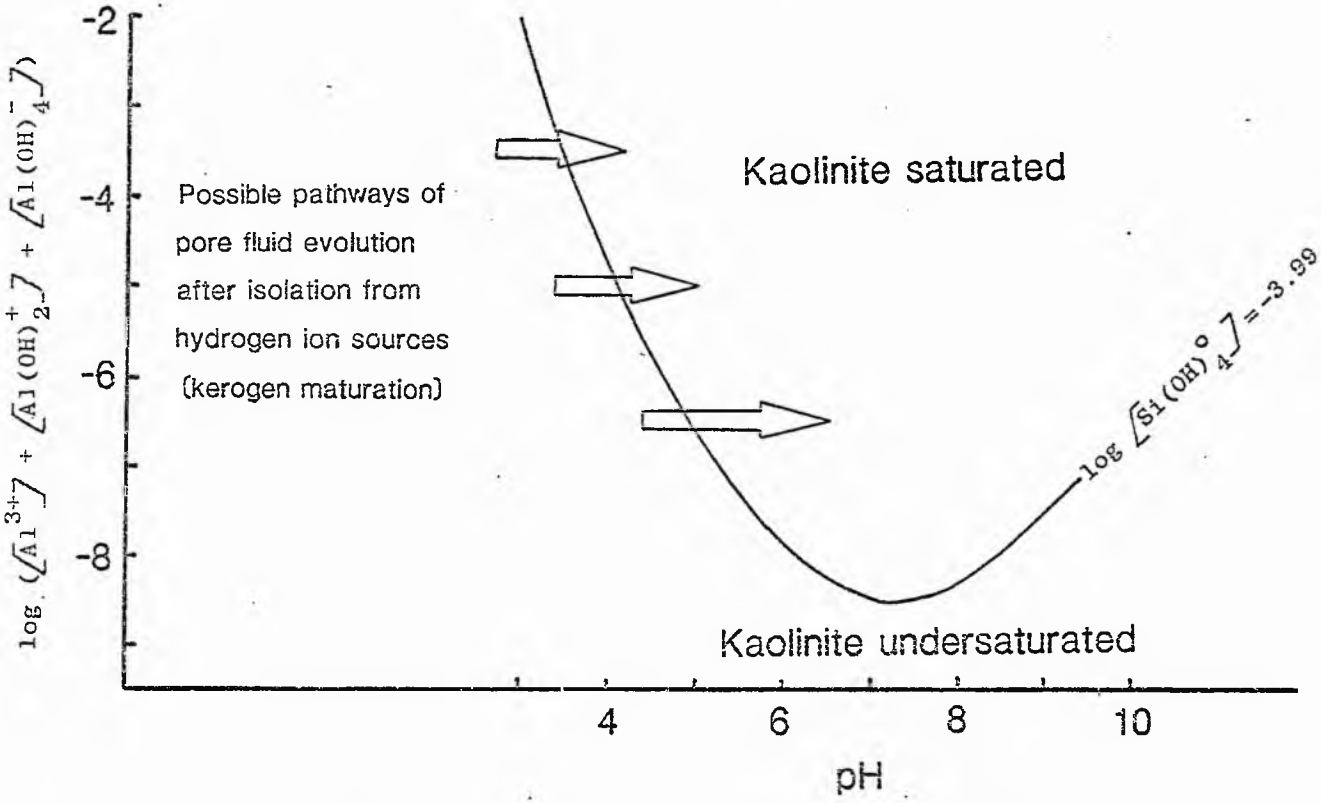

Fig. 7.45 Stability of kaolinite relative to dissolved species of silicon and aluminum as a function of pH (Curtis, 1983).

CHAPTER VIII

SUMMARY AND CONCLUSIONS

The findings of the present sedimentological, petrological and geochemical studies have been applied to analyse the process of calcretization and to understand the influence of environment of deposition on sandstone diagenesis.

The most important finding of this study is the calcretization of Lr. Old Red Sandstone by displacively grown calcite. Although displacive calcite has been described earlier by a few workers, a precise mechanism of the growth has not been proposed. The two-water model based on petrological and geochemical criteria suggested in Chapter IV is an attempt to explain the mechanism of growth of displacive calcite crystals and has been applied for the first time to sediments formed in continental environments. It also supports the differentiation made between vadose and phreatic calcite on petrological grounds and neatly accounts for the (a) excessive amount of carbonate, (b) the problem of the volume of fluid required to produce a lithified rock and (c) preservation of sharp crystal edges. Hence, the present studies emphasise Pingitore's (1976) opinion that the principle of the two-water system under vadose and phreatic conditions is applicable to many aqueous diagenetic settings. It remains to be seen whether the Carnoustie sediments are unique or whether there are more examples of similar calcretes elsewhere to which this model can be applied. However, the occurrence of displacive calcite in these sediments is strong evidence to support the view that the area lay near the equator

and experienced a dry hot climate.

Although the full significance of displacive growth of calcite has not been widely recognized, Watts (1978) emphasised that displacive calcite is neither a cement nor a neomorphic product. The present studies support Watt's (1978) opinion and in view of the specialized set of conditions required for the displacive growth of calcite, such as supersaturated and near surface conditions, it is here suggested that a separate class of "Displacive Calcite" should be recognized.

On the basis of the field, petrological and geochemical evidence gathered during the present studies, the per ascensum model of Goudi (1973) has been proposed for calcretization of the Carnoustie sandstone. Crystal morphologies observed under cathodoluminescence and microprobe data suggests that the displacive calcite was originally low Mg-calcite and grew from rapidly evaporating fresh pore waters with extremely low Mg/Ca ratios. The growth of originally low Mg-calcite and absence of palygorskite, sepiolite and dolomite in the Carnoustie calcretes is considered significant as it questions the universal applicability of Watt's (1980) Quaternary model of calcretization. It has been emphasised that no one process applies to all calcretes and the chemistry of pore waters and micro-environmental conditions within the pores are major significant factors controlling process of calcretization.

The finding of smectite fringes in the uncalcretized sediments towards the base of profiles is also of considerable significance. Firstly it is a rare example of an occurrence in the Lr. Devonian times and is expected to be of great interest

to geophysicists who are trying to plot cross-sections across the Midland Valley. It suggests that these sediments could not have been buried more than to a depth of approximately 2500 m. Secondly, it questions the role of plant cover suggested by Weaver (1967) and later emphasised by Bjørlykke and Jørgensen (1976) in their (smectite) formation. The smectite fringes are believed to have formed from alteration of volcanic and basic igneous material.

To understand the pre-burial controls on sandstone diagenesis, comparisons between the Lr. Old Red Sandstone and the Viking, Cardium and Belly River Formations have been drawn. Although all the controls on diagenesis are not yet fully known, it is well established that the two major factors that accomplish all the complex chemical reactions during diagenesis are:

(1) detrital mineralogy and

(2) aqueous solutions migrating through the pore system of sandstones.

Of these, the detrital mineralogy is controlled not only by provenance and tectonic setting but also by mineralogical partitioning within the depositional environment. Although it is very difficult to reconstruct the original sand compostion, the present compositional variations (Chapter III and VII) show that the Lr. Old Red Sandstone and the Belly River sands were comparatively rich in chemically unstable feldspars (6 to 7%; present content) and rock fragments (6 to 10%; present content) while the Cardium and the Viking Formations had lesser amount of these unstable phases (2 to 4%; present content). These compositional variations account for the more abundant authigenic

clays found in the Lr. Old Red Sandstone and the Belly River Formation than in the Viking and the Cardium Formations. It is difficult to comment on how much difference in the content of feldspars, rock fragments or other detrital constituents is necessary to cause significant difference in the diagenetic products, because, according to Hancock (1978) "only a few percent are necessary to provide ample material for diagenesis".

Pore fluids are considered to be the dynamic agent redistributing material matter by dissolution and precipitation. To understand the influence of pore fluids on diagenetic modification, the pore fluids are divided into two types;

(a) pre-burial early diagenetic pore fluids and

(b) pore fluids generated during burial and late diagenesis.

The second type of pore fluids pose more serious problems as at present it is very difficult to reconstruct, (I) where the pore fluids came from; (II) what were their initial chemical composition before entering the pores; (III) how the chemical composition evolved during movement through the pore network and (IV) what their flow paths were through the basin. Because of these complex and unresolved problems our understanding of prediction and influence of late diagenetic pore fluids is limited. Hence, no attempt is made to interpret or relate the late stage diagenetic products with depositional environment. Also, the late stage pore fluids need not necessarily have any relation to the environment of deposition.

However, the waters which accomplish significant modifications during pre-burial diagenesis and have close links with the depositional environment are better understood and

discussed below using a few examples from the Lr. Old Red Sandstone and the Viking, Cardium and Belly River Formations.

In general, the Viking, Cardium and Belly River sediments show large variations in their pre-burial early diagenetic histories within small areas (even between adjoining wells) while the Lr. Old Red Sandstone show a monotonous paragenetic sequence over the entire area. This large and frequent variation in the diagenetic products in the Cretaceous sediments is believed to be due to more varied environment of deposition, causing frequent mixing of fresh, brackish and marine waters while the consistency in the paragenetic sequence of Lr. Old Red Sandstone is governed by the fact that they were all deposited in fresh waters(Figs. 8·1 & 8·2).

The diagenesis of Lr. Old Red Sandstone is dominated by pre-burial early diagenetic events including calcretization, formation of hematite coatings and formation of smectite fringes. All these require a hot dry climate and alkaline waters, a set of conditions typical of continental sediments. In contrast to the Cretaceous sediments, very little happened during late diagenesis in Lr. Old Red Sandstone. Only palisades of prismatic crystals around isolated detrital grains and few randomly scattered patches of coarse calcite were formed neomorphically in the calcretized zone while in the uncalcretized sediments secondary porosity by partial and patchy dissolution of calcite cement was formed. Calcite veins were also formed during late stages.

Quartz overgrowths forming triple junctions and causing nearly complete destruction of primary porosity is the most dominant pre-burial diagenetic event in the Viking and some of the Cardium sediments. This significant overgrowth is believed

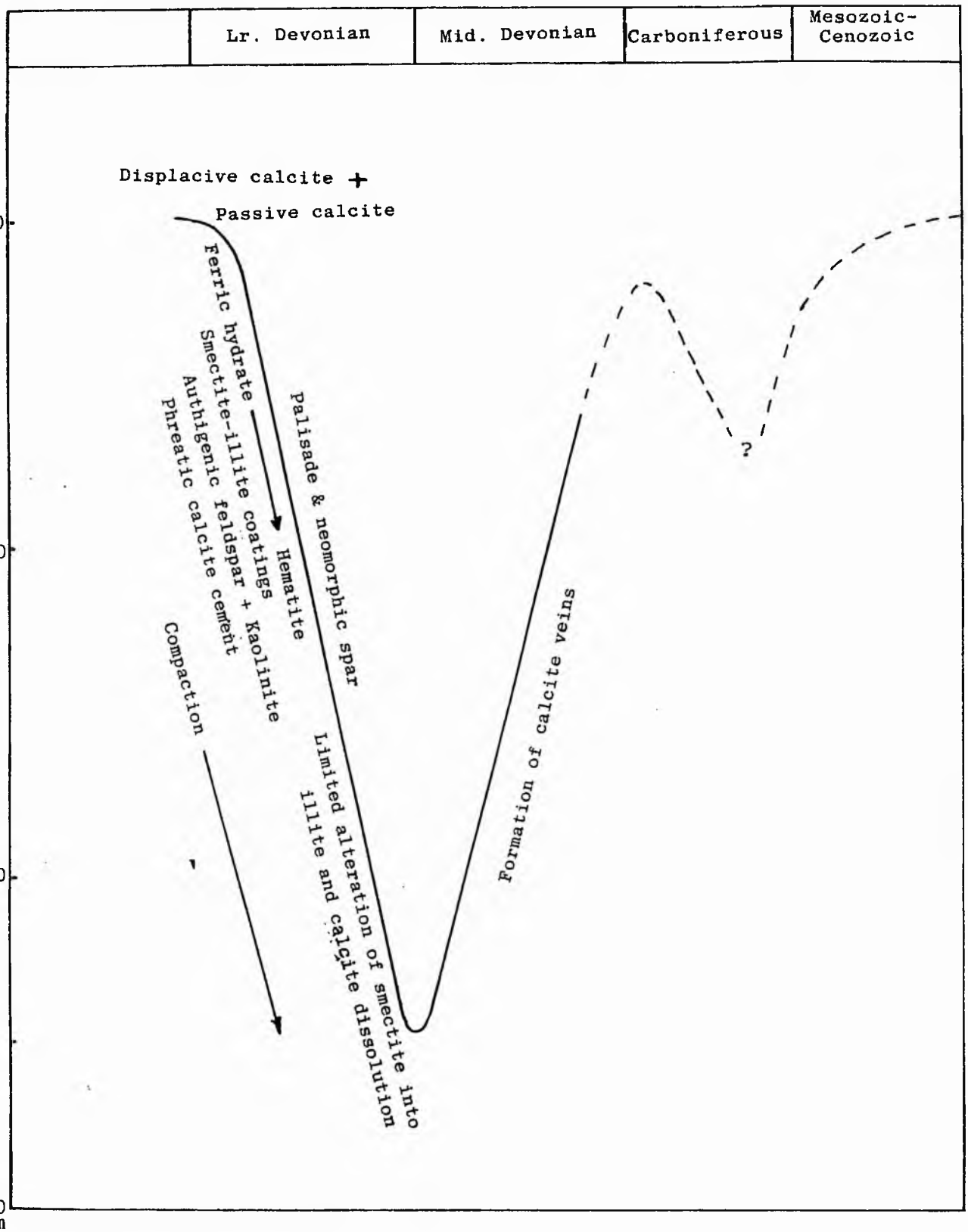

Fig 8.1 Burial history of the Lr Old Red Sandstone

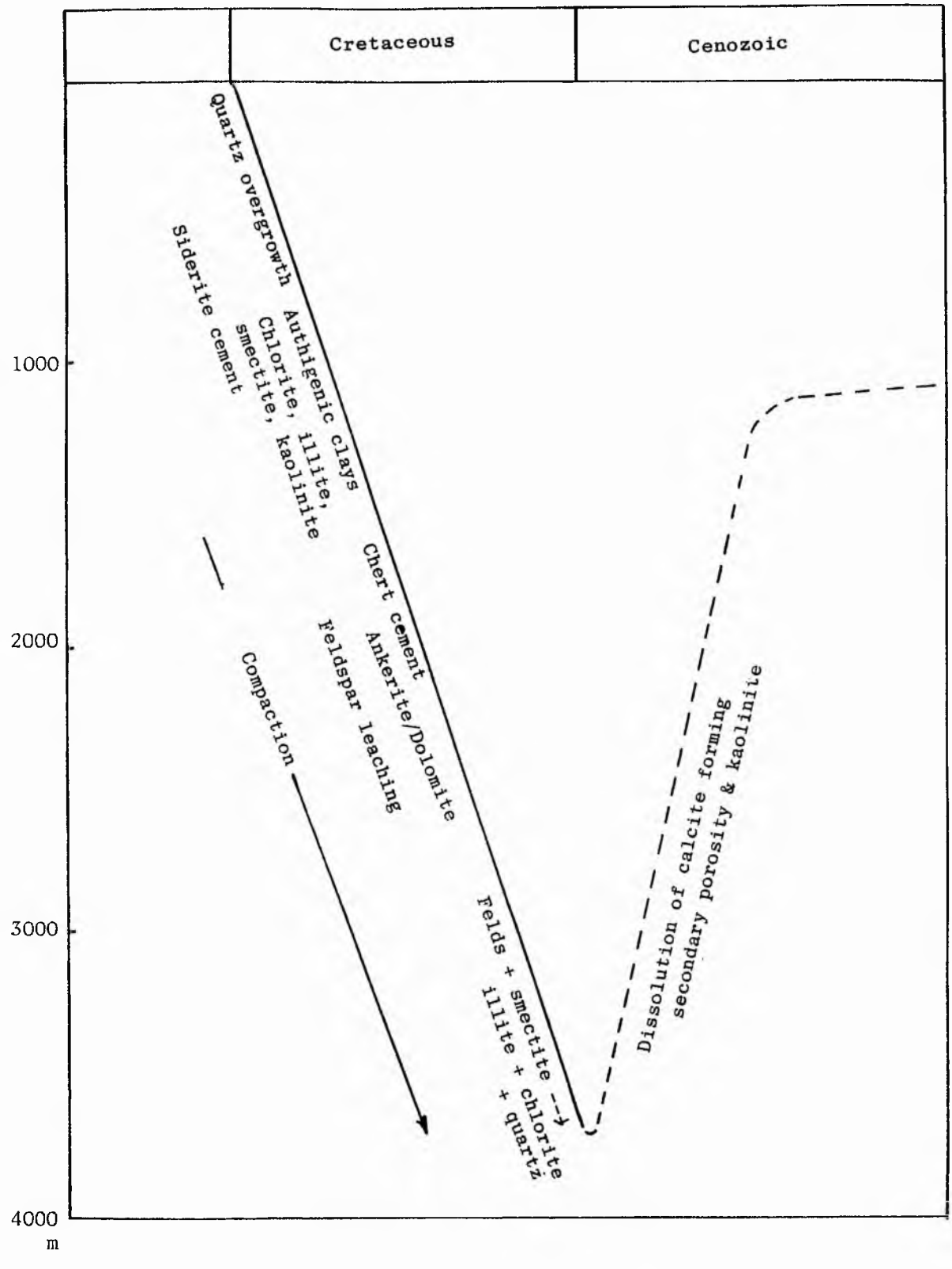

Fig 8.2 Burial history of the Cretaceous sediments

to be due to mixing of fresh waters with marine pore waters. Bjørlykke (1983) suggested that when fresh waters containing up to 13 ppm silica (Blatt, 1979) mixes with marine pore waters, it precipitates silica, because, quartz is not very soluble in marine waters (only 6 ppm SiO2, at 25° C; Siever et al 1965) and the values are further reduced in shallow nearshore waters to about 1 ppm SiO2 (Blatt, 1979) because of precipitation by diatoms. Hence the pre-burial early diagenetic silica cementation in the Viking and the Cardium Formations reflect conditions of the depositional environment.

Authigenic clays are also formed during early diagenesis and particular mineral species provide insight into early diagenetic environment. For example, dominance of smectite in the Lower Old Red Sandstone over the entire area suggests that similar chemical conditions (alkaline) prevailed over the entire area during early diagenesis. In contrast, authigenic clays found commonly in the Cretaceous sediments include kaolinite, chlorite, illite and smectite. These species vary frequently (even between adjoining wells) and show complex distributions controlled presumably by local variations in original sand composition, pore fluid circulation and composition dependent on textural and structural variations and environment of deposition; the understanding of which will require a much closer sampling than available in the present study. Formation of kaolinite books in some Viking and Cardium samples during early diagenesis suggest relatively acid conditions which may have existed locally and have been produced by flushing of sandstone with fresh water. Well developed chlorite fringes observed in some Cardium samples (from the

south-east) suggest their deposition in marine environment (Tillman and Almon, 1979).

Pyrite has also formed during early diagenesis in the Viking and Cardium Formations. It is believed to have formed by reactions between iron bearing minerals and H2S produced from sulphate in the sea water by sulphate reducing bacteria.

The late diagenetic events include ankerite/ferroan-calcite and scattered dolomite rhomb formation and dissolution of unstable phases forming secondary porosity.

The early diagenetic events in the Belly River Formation were dominated by formation of iron rich chlorite pore linings in the south-eastern part of the area and abundant carbonate cementation occluding most of the pores in the northern part of the area. The chlorite pore linings are believed to have formed in marine environments and inhibited the syntaxial quartz overgrowth as thick clay rims resulted in the inability of quartz to seed on grain surfaces (Tillman and Almon, 1979). Hence, the residual pores were subsequently filled with silica or carbonate cement. The late diagenetic events in the south-eastern part of the area involved slight and patchy formation of secondary porosity while in the northern part extensive development of secondary porosity by carbonate dissolution and simultaneous kaolinite formation was observed. The identification of late stage kaolinite is considered significant as it is precariously perched on grain surfaces and in the pores. Its presence promotes formation damage as it could be easily lifted to block pore throats during Formation treatment.

The distributions of chlorite fringes and pyrite (eastern

part) and siderite (western part) in the Viking, the Cardium and the Belly River Formations are compatible with the expected variations in the pore-fluid chemistry deduced from the depositional environments from east (marine) to west (non-marine to marginal marine) within the area of study. Siderite and pyrite are the products of bacterial metabolism (Curtis et al 1972; Berner, 1970) formed in reducing conditions caused by organic matter oxidation (Gluyas, 1985). Pyrite formed in the eastern part by reduction of sulphate which was readily available in sea water while siderite precipitated in the western part where sulphide activity was low in the non-marine pore sections.

The above drawn comparisons between the Lr. Old Red Sandstone, the Viking, the Cardium and the Belly River Formations particularly highlight the varations in the pre-burial early diagenetic processes and products according to their environment of deposition. Hence, it is here concluded that the pre-burial early diagenetic processes and products in clastic sediments are very much controlled by their environment of deposition which subsequently could influence the course of late stage diagenesis as well.

REFERENCES

Allen, J.R.L., 1968. Current ripples. Amsterdam: North-Holland Pub. Co., 433 p.

Allen, J.R.L., 1974. Sedimentology of the ORS (Silurian Devonian) in the Clee Hills Area, Shropshire, England. Sedim. Geol. V. 12, 73-167.

Armstrong, M. and Patterson, I.B., 1970. The Lower Old Red Sandstone of the Strathmore region. Inst. Geol. Sci. Great Britain. Report 70/12. 24 p.

Assereto, R.L.A.M., and Kendall, C.G. St. C., 1977. Nature, origin and classification of peritidal tepee structures and related breccias: Sedimentology, V. 24, p. 153-210.

Bathurst, R.G.C., 1958. Diagenetic fabric in some British Dinantian limestones. Liverpool Manchester Geol. J., V. 2, p. 11-36.

Bathurst, R.G.C., 1971. Two generations of cement: In Carbonate cements, John Hopkins. Univ., Stud. Geol. No. 19, p. 296.

Bathurst, R.G.C., 1975. Carbonate sediments and their diagenesis. Elsevier, Amsterdam, 658 p.

Becker, G.F. and Day, A.L., 1916. Note on the linear force of growing crystals. Jour. Geol. V. 24, p. 313-333.

Berner, R.A., 1970. Sedimentary pyrite formation. Am. Jour. Sci. V. 268, p. 1-23.

Berner, R.A., 1978. Rate controls of mineral dissolution under Earth surface conditions. Am. Jour. Sci., V. 278, p. 1235-52.

Berner, R.A., 1980. Early diagenesis: a theoretical approcah. Princeton Univ. Press, Princeton, N.J., 241 p.

Bjørlykke, K., 1983. Diagenetic reactions in sandstones. In: Sediment diagenesis Eds. A. Parker and B.W. Sellwood. NATO ASI Series, p. 169-214.

Bjørlykke, K. and Jørgensen, P., 1976. Comments on the paper: Chlorite and illite in some Lower Palaeozoic mudstones of Mid-Wales, Clay Minerals, V. 11, p. 165-167.

Blatt, H., 1979. Diagenetic processes in sandstones. SEPM Special Publication, V. 2, p. 141-157.

Bluck, B.J., 1971. Sedimentation in the meandering river Endrick. Scott. J. Geol. V. 7 p. 93-138.

Bluck, B.J., 1974. Structure and directional properties of some valley sandur deposits in southern Iceland, Sedimentology, V. 21, p. 533-54.

Bluck, B.J., 1976. Sedimentation in some non-sinuous Scottish Rivers, Trans. R. Soc. Edinburgh. 69, p. 425-56.

Bluck, B.J., 1979. Structure of coarse grained stream alluvium, Trans. R. Soc. Edinburgh. 70, p. 181-221.

Boothroyd, J.C., and Ashley, G.M., 1975. Processes, bar morphology and sedimentary structue on braided outwash fans, northeastern Gulf of Alaska: in A.V. Jopling and B.C. McDonald, eds., Glaciofluvial and glaciolacustrine sedimentation, Soc. Econ. Paleont. Mineral. Spec. Publ. 23, p. 193-222.

Boyle, J.M. and Scott, A.J., 1982. Model for the migrating shelf-bar sandstones in Upper Mancos Shale (Campanian), northwestern Colorado: Amer. Assoc. Petroleum Geologists, Bull. 66. p. 491-508.

Brenner, R.L. and Davis, D.K., 1973. Storm-generated coquinoid sandstone: genesis of high-energy marine sediments from the Upper Jurassic of Wyoming and Montana. Bull. Geol. Soc. Amer., V. 84, p. 1685-1698.

Bricker, O.P. (ed.), 1971. Carbonate cements. The John Hopkins Press, Baltimore and London, 360 p.

Cant, D.J., 1978. Development of a facies model for sandy braided river sedimentation: comparison of the South Saskatchewan river and the Battery Point Formation, in Fluvial Sedimentology, A.D. Miall (ed.). Canadian Soc. Pet. Geol. p. 627-639.

Church, M. and Gilbert, R., 1975. Proglacial fluvial and lacustrine environments: in A.V. Jopling and B.C. McDonald, eds., Glaciofluvial and glaciolaustrine sedimentation, Soc. Econ. Paleont. Miner. Spec. Pub. 23, p. 22-100.

Collinson, J.D., 1978. Vertical sequence and sand body shape in fluvial sequences. In: Fluvial Sedimentology (Ed. by A.D. Miall) Mem. Can. Soc. Petrol. Geol. 5, p. 577-586.

Curtis, C.D., 1983. Link between aluminium mobility and destruction of secondary porosity, Bull. Am. Ass. Petrol. Geol. V. 67, p. 380-384.

Curtis, C.D., Petrowski, C. and Oertel, C., 1972. Stable carbon isotope ratios within carbonate concrections: a clue to time and place of formation, Nature, V. 235, p. 98-100.

Deer, W.A., Howie, R.A. and Zussman. J., 1962. Rock forming minerals, V. 3. Sheet silicates, Longman, London, 270 p.

Duncyer De Segonzac, G. 1970. The transformation of clay minerals during diagenesis and low grade metamorphism. A Review Sedimentology V. 15, p. 281-346.

Engelund, F., and Fredsoe, J., 1974. Transition from dunes to plane bed in alluvial channels, Lyngby, Tech. Univ. Denmark, Inst. Hydrodynamics Hydraulic Engineering Series Paper 4. (General review of application of stability theory to bed forms, plus a specific example).

Fairchild, I.J., 1983. Chemical controls of cathodoluminescence of natural dolomites and calcites: new data and reviews, Sedimentology, V 30, p. 579-583.

Flournoy, L.A., and Ferrell, Jr. R.E., 1980. Geopressure and diagenetic modifications of porosity in the Lirette faile area, Terrebonne Parish, Louisiana: Gulf Coast Assoc. Geol. Socs. Trans., V. 30, p. 341-345.

Folk, R.L., 1974. The natural history of crystalline calcium carbonate: effect of magnesium content and salinity, Jour. Sed. Petr., V. 44, p. 40-53.

Folk, R.L., and Land, L.S., 1975. Mg/Ca ratio and salinity; two controls over crystallization of dolomite, Bull. Am. Ass. Petrol. Geol., V. 59, p. 60-68.

Frank, J.R., Carpenter, A.B. and Oglesby, T.W., 1982. Cathodoluminescence and composition of calcite cement in the Taum Sauk Limestone (Upper Cambrian), South-east Missouri, Jour. Sed. Petrol. V. 52, p. 631-638.

Füchtbauer, H., 1967. Influence of different types of diagenesis on sandstone porosity, Proc. 7th World Petrol. Cong. Mexico, V. 2, p. 353-369.

Füchtbauer, H., 1983. Facies controls on sandstone diagenesis, in: Sediment diagenesis, eds. Parker, A. and Sellwood, B.W. NATO, ASI, Series, p. 269-288.

Fyfe, W.S., 1964. The geochemistry of solids. McGraw-Hill Co., New York, 199 p.

Gardener, L.R., 1972. Origin of the Mormon Mesa Caliche, Clark County, Nevada. Geol. Soc. of Amer. Bull., V. 83, p. 143-156.

Gile, L.H., Peterson, F.F., and Grossman, R.B., 1966. Morphological and genetic sequences of carbonate accumulation in desert soils. Soil Sci. V. 101, p. 347-360.

Gluyas, J.G., 1985. Reduction and prediction of sandstone reservoir potential, Jurassic, North Sea, Phil. Trans. Roy. Soc. Britain (in press).

Goldman, M.I., 1952. Deformation, metamorphism and mineralization in gypsum-anhydrite cap rock, Sulphur Salt Dome, Louisiana. Geol. Soc. Am. Mem., 50, p. 1-169.

Goudie, A.A., 1973. Duricrusts in tropical and subtropical landscapes. Clarendon Press, Oxford, 174 p.

Grim, R.E., 1968. Clay mineralogy, 2nd ed., McGraw-Hill, New York.

Hay, R.L., and Reeder, R.J., 1978. Calcretes of Olduvia Gorge and the Ndolanya Beds of northern Tanzania, Sedimentology, V. 25, p. 649-673.

Hamblin, A.P., and Walker, R.G. 1979. Storm-dominated shallow-marine deposits: The Fernie-Kootenay (Jurassic) transition, southern Rocky Mountains, Can. Jour. Earth Sci. V. 16, p. 1673-1690.

Hancock, N.J., 1978. Possible causes of Rotliegendes sandstone diagenesis in northern W. Germany, Jour. geol. Soc. Lond., V. 135, p. 35-40.

Harms, J.C., Southand, J., Spearing, D.R., and Walker, R.G., 1975. Depositional environments as interpreted from primary sedimentary structures and stratification sequences, Lecture notes, Soc. Econ. Paleont. Mineral. Short course 2, Dallas, 161 p.

Harrison, R.S., 1977. Caliche profiles: indicators of near-surface

subaerial diagenesis, Barbados, West Indies, Bull. Can. Petrol. Geol., V. 25, p. 123-173.

Hatch, F.H., Rastall, R.H. and Black, M., 1938. The petrology of the sedimentary rocks, Allen and Unwin, London, 383 p.

Heald, M.T., 1959. Significance of stylolites in permeable sandstones, Jour. Sed. Petrol. V. 29, p. 251-253.

Hein, F.J. and Walker, R.G. 1977. Bar evolution and development of stratificatin in the gravelly, braided, Kicking Horse River, British Columbia, Can. J. Earth Sci. V. 14, p. 562-570.

Hemingway, B.S, R.A., Robie, and Kittrick, J.A., 1978. Revised values for the Gibbs free energy of formation of [$Al(OH)_{4}^{-}{}_{aq}$], diaspore, boehmite and bayerite at 298.15°K and 1 bar, the thermodynamic properties of kaolinite to 800° °K and 1 bar and the heats of solution of several gibbsite samples, Geochim. et Cosmochim. Acta, V. 42, p. 1533-1543.

Henniker, J.C., 1949. Depth of the surface zone of a liquid, Revs. Modern Phys., V. 21, p. 322-342.

Hoffman, J. and Hower, J., 1979. Clay mineral assemblages as low grade metamorphic geothermometers: Applications to the thrust faulted disturbed belt of Montana, U.S.A. In: Aspects of diagenesis, Eds. P.A. Scholle and P.R. Sihluger, SEPM Sp. Publ. no. 26, p. 55-79.

Jacka, A.D., 1974. Differential cementation of a Pleistocene carbonate fanglomerate, Guadalupe Mountains, Jour. Sed. Petrol, V. 44, p. 85-92.

Jopling, A.V., 1965. Hydraulic factors controlling the shape of laminae in laboratory deltas; Jour. Sed. Petrol., V. 35, p. 777-791.

Kahle, C.F., 1977. Origin of subarial Holocene calcareous crusts: role of algae, fungi and sparmicritization, sedimentology, V. 24, p. 413-435.

Kinsman, D.J.J., 1969. Interpretation of Sr^{2+} concentrations in carbonate minerals and rocks, Jour. Sed. Petrol., V. 39, p. 486-508.

Krause, F.F., 1983. Sedimentology of a Tempestite: episodic deposition in the Cardium Formation, Pembina Oilfield area, West central Alberta: In Sedimentology of Selected Mesozoic clastic sequences. Eds. McLean, J.R. and Reinson, G.E., Can. Soc. Petrol. Geol., p. 43-66.

Land, L.S., 1970. Phreatic versus meteoric diagenesis in limestone: evidence from a fossil water table, Sedimentology, V. 14, p. 175-185.

Leckie, D.A., and Walker, R.G., 1982. Storm-and-tide dominated Shorelines in Cretacoues Moosebar-Lower Gates Interval-outcrop equivalents of Deep Basin Gas Trap in Western Canada, Am. Assoc. Petrol. Geol.-Can. Inst. Min. Petrol. Soc. Calgary, Alberta, p. B1-B34.

Lindquist, S.J., 1977. Secondary porosity development and subsequent reduction overpressured Frio Formation sandstone (Oligocene), South Texas, Gulf Coast Assoc. Geol. Soc. Trans. V. 27, p. 99-107.

Loucks, R.G., Bebout, D.G., and Galloway, W.E., 1977. Relationship of

porosity formation and preservation to sandstone consolidation history-Gulf Coast Lower Tertiary Frio Formation, Gulf Coast Assoc. Geol. Soc. Trans., V. 27, p. 109-120.

McDonald, D.A. and Surdam, R.C., (Eds.) 1984. Clastic diagenesis, AAPG Memoir 37, 434 p.

Miall, A.D., 1970. Devonian alluvial fans, Prince of Wales Island, Arctic Canada, Jour. Sed. Petrol., V. 40, p. 556-571.

Miall, A.D., 1977. A review of the braided river depositional environment, Earth Sci. Rev., 13, p 1-62.

Miall, A.D., 1978. Lithofacies types and vertical profile models in braided river deposits: a summary. In Fluvial Sedimentology. Ed. by A.D. Miall Can. Soc. of Petrol. Geol. 5, p. 597-604.

Millot, G., 1964. Geologie des Argiles, Masson et Cie, Paris.

Mumpton, F.A., and Roy, R., 1958. New data on sepiolite and attapulgite clays, Clay Mineral, Fifth Nat. Conf. Natt. Acad. Sci., Natt. Counc. Publ. 566, p. 136-143.

Mykura, W., 1983. Old Red Sandstone, in: Geology of Scotland, ed. G.Y. Craig, p. 205-252.

Nelper-Christensen, P., 1965. Shrinkage and swelling of rocks due to moisture movement, Meded Dansk. geol. Foren., V. 15, p. 548-555.

Ori, G.G., 1982. Braided to meandering channel patterns in humid

region alluvial fan deposits, Remo River, Po Plain, nothern Italy, Sedimentary Geology, V. 31, p. 231-248.

Orme, G.R., and Brown, W.W.M., 1963. Diagenetic fabrics in the Avonian Limestone of Derbyshire and north Wales, Proc. Yorks. Geol. Soc., V. 34, p. 51-66.

Parker, A. and Sellwood, B.W., (eds.) 1983. Sediment diagenesis, NATO-ASI Series, D. Reidel Publishing Company, Dordrecht, Boston and Lancaster, 427 p.

Pierson, B.J., 1981. The control of cathodoluminescence in dolomite by iron and manganese, Sedimentology, V. 28, p. 601-620.

Pingitore, N.E. Jr., 1976. Vadose and phreatic diagenesis: processes products and their recognition in corals, Jour. Sed. Petrol., V. 46, p. 985-1006.

Plet-Lajoux, C., Monnier, G., and Pedro. G., 1971. Etude experimentale sur la genese et la mise en place des encroutements gypseux: Academie des Sciences comptes Rendus, V. 272, p. 3017-3020.

Ravina, I. and Zaslavsky, D., 1974. The electrical double layer as a possible factor in desert layer, Israel Jour. Chem. V. 10, p. 707-714.

Read, J.F., 1974. Calcrete deposits and Quaternary sediments Edel Province, Shark Bay. In: Evolution and diagenesis of Quaternary Carbonate Sequence, Shark Bay Western Australia. Ed. B.W. Logan et al, Amer. Asoc. Petrol. Geol. Mem. 22. p. 250-282.

Reeves, C.C. Jr., 1976. Caliche: Origin, classification, morphology and uses, Estacado Books, Texas, 233 p.

Ricci Lucchi, F., Colella, A., Ori, G.G. and Oglian, R., 1981. Pliocene fan deltas of the Intra-Apenninic Basin, Bologna. In: Excursion guide book, ed. F. Ricci Lucchi, IAS 2nd European Regional Meeting, Bologna, p. 80-138.

Richter, D.K., and Zinkernagel, U., 1981. Zur Anwendung der Kathodolumineszenz in der Karbonatpetrographie, Geol. Rdsch, V. 70, p. 1276-1302.

Robbin, D.M., and Stipp, J.J., 1979. Depositional rate of laminated soilstone crusts, Florida Keys, Jour. Sed. Petrol., V. 49, p. 175-180.

Robie, R.A., Hemingway, B.S., and Fisher, J.R., 1978. Thermodynamic properties of minerals and related substances at 298.5^{o}K and 1 bar (10^{5} Pascals) pressure and at higher temperatures, U.S. Geol. Survey Bull. 1452, 456 p.

Rust, B.R., 1972. Structure and process in a braided river. Sedimentology, V. 18, p. 221-245.

Rust, B.R., 1978. Depositional model for braided alluvium, in: Fluvial Sedimentology, ed. A.D. Miall, Cand. Soc. Petrol. Geol., p. 605-625.

Schmidt, V. and McDonald, D.A., 1979. The role of secondary porosity in the course of sandstone diagenesis, in: Aspects of diagenesis, eds. P.A. Scholle and P.R. Schluger, SEPM Spec. Pub. No. 26, p. 175-207.

Scholle, P.A. and Schluger, P.A. (Eds.), 1979. Aspects of diagenesis,

SEPM Speol. Publ. No. 26, 443 p.

Shawa, M.S., 1984. In: The geology of the Belly River, Cardium and Viking reservoirs of southcentral Alberta, M.S. Shawa, E.K Walton, St Gerard, G.C. Saigal and M.A. Riaz, report submitted to Shawa Geoconsultants Ltd. in March, 1984, 135 p.

Shawa, M.S., Walton, E.K., Gerrard, S.L., Saigal, G.C., and Riaz, M.A., 1984. The geology of the Belly River, Cardium and Viking reservoirs of southcentral Alberta, report submitted to Shawa Geoconsultants Ltd. in March, 1984, 135 p.

Siever, R., Beck, K.C., and Berner, R.A., 1965. Composition of interstitial waters of modern sediments, Jour. Geol., V. 73, p. 39-73.

Smith, N.D., 1972. Some sedimentological aspects of planar cross-stratification in a sandy braided river, Jour. Sed. Petrol., V. 42, p. 624-634.

Stalder, P.J., 1975. Cementation of Pliocene-Quaternary fluviatile clastic deposits in and along the Oman Mountains, Geologie Mijnb., V. 54, p. 148-156.

Steel, R.J., and Thompson, D.B., 1983. Structures and texture in Triassic braided stream conglomerates 'Bunter Pebble Beds' in the Sherwood Sandstone Group, north Staffordsire, England, Sedimentology, V. 30, p. 341-367.

Stott, D.F., 1963. The Cretaceous Alberta Group and equivalent

rocks, Rocky Mountain foothills, Alberta: G.S.C. Memoir 317.

Taber, S., 1916. The growth of crystal under extreme pressure, Amer. Jour. Sci., V. 41, p. 532-556.

Thirlwall, M.F., 1981. Implications for Caledonain plate tectonic models of chemical data from volcanic rocks of the British Old Red Sandstone, Jour. geol. Soc. London, V. 138, p. 123-138.

Thirlwall, M.F., 1983. Discussion on implications for Caledonian plate tectonic models of chemical data from volcanic rocks of the British Old Red Sandstone, Jour. geol. Soc. London, V. 140, p. 315-318.

Thomson, A., 1959. Pressure solution and porosity. In: Ireland, H.A. (ed.). Silica in sediments, Spec. Publ. Soc. Econ. Palaeon. Miner., Tulsa, V. 7, p. 55-79.

Thorez, J. 1976. The practical identification of clay minerals, G. Lelotte, Dison, Belgique.

Tillman, R.W., and Almon, W.R., 1979. Diagenesis of Frontier Formation offshore bar sandstones, Spearhead Ranch Field, Wyoming, In: Aspects of diagenesis, Eds. P.A. Scholle and P.R. Schluger, SEPM Spec. Publ. No. 26., p. 337-378.

Tizzard, M.B., and Lerbekmo, J.F., 1975. Depositional history of the Viking Formation, Suffield Area, Alberta, Canada, Bull. Can. Petrol. Geol., V. 23, p. 715-752.

rocks, Rocky Mountain foothills, Alberta: G.S.C. Memoir 317.

Taber, S., 1916. The growth of crystal under extreme pressure, Amer. Jour. Sci., V. 41, p. 532-556.

Thirlwall, M.F., 1981. Implications for Caledonain plate tectonic models of chemical data from volcanic rocks of the British Old Red Sandstone, Jour. geol. Soc. London, V. 138, p. 123-138.

Thirlwall, M.F., 1983. Discussion on implications for Caledonian plate tectonic models of chemical data from volcanic rocks of the British Old Red Sandstone, Jour. geol. Soc. London, V. 140, p. 315-318.

Thomson, A., 1959. Pressure solution and porosity. In: Ireland, H.A. (ed.). Silica in sediments, Spec. Publ. Soc. Econ. Palaeon. Miner., Tulsa, V. 7, p. 55-79.

Thorez, J. 1976. The practical identification of clay minerals, G. Lelotte, Dison, Belgique.

Tillman, R.W., and Almon, W.R., 1979. Diagenesis of Frontier Formation offshore bar sandstones, Spearhead Ranch Field, Wyoming, In: Aspects of diagenesis, Eds. P.A. Scholle and P.R. Schluger, SEPM Spec. Publ. No. 26., p. 337-378.

Tizzard, M.B., and Lerbekmo, J.F., 1975. Depositional history of the Viking Formation, Suffield Area, Alberta, Canada, Bull. Can. Petrol. Geol., V. 23, p. 715-752.

Walker, T.R., 1967. Formation of red beds in modern and ancient deserts, Bull. Geol. Soc. Am., V. 78, p. 353-368.

Walker, T.R., 1976. Diagenetic origin of continental red beds, In: Falke, H. (ed.). The continental Permian in central, west and south Europe, NATO Advanced Study Inst., Ser. C. Math & Phys., Sci., Reidel Dordrecht, Holland, p. 240-282.

Walker, T.R. and Waugh, B., 1973. Intrastratal alteration of silicate minerals in late Tertiary fluvial arkose, Baja California, Mexico. Geol. Soc. Am. Abs. with Prog. 7, p. 853-854.

Walton, E.K. and Saigal, G.C., 1984. In: The geology of the Belly River, Cardium and Viking reservoir of southcentral Alberta, M.S. Shawa, E.K. Walton, S.L. Gerrard, G.C. Saigal and M.A. Riaz, report submitted to Shawa Geoconsultants Ltd., in March, 1984.

Wardlaw, N.C., 1962. Aspects of diagenesis in some Irish Carboniferous limestones, Jour. Sed. Petrol., V. 32, p. 776-780.

Watts, N.L., 1977. A comparative study of some Quaternary, Permo-Triassic and Siluro-Devonian calcretes, Unpublished Ph.D. Thesis, University of Reading.

Watts, N.L., 1978. Displacive Calcite: Evidence from recent and ancient calcretes, Geology, V. 6, p. 699-703.

Watts, N.L., 1980. Quaternary pedogenic calcretes from the Kalahari (Southern Africa): mineralogy, genesis and diagenesis, Sedimentolgy, V. 27, p. 661-686.

Weaver, C.E., 1967. Potassium, illite and the ocean, Geochimica et Cosmochimica Acta, V. 31, p. 2181-2196.

Wedepohl, K.H., 1978. Handbook of geochemistry, Springer-Verlag, Berlin, Heidelberg, New York, V II/3.

Weimer, R., 1961. Uppermost Cretaceous rocks in central and southern Wyoming and northwestern Colorado: In symposium on late Cretaceous rocks, Wyoming and adjacent areas. Wyoming Geol. Assoc., 16th Annual Cnf., Casper Wyoming, Petroleum Inf., p. 17-28.

Westoll, T.S., 1977. Northern Britain, In: House et al, A correlation of Devonian rocks of the British Isles, Geol. Soc. Lond. Spec. report no. 7.

Weyl, P.K., 1959. Pressure solution and the force of crystallization, a phenomenological theory, Jour. Geophys. Res. V. 64, p. 2001-2025.

Williams, P.F. and Rust, B.R., 1969. The sedimentology of a braided river, Jour. Sed. Petrol., V. 39, p. 649-679.

Wright, M.E. and Walker, R.G., 1981. Cardium Formation (U. Cretaceous) at Seebe, Alberta, Can. Jour. Earth Sci. V. 18, p. 795-809.

Yaalon, D.H. and Wieder, M., 1976. Pedogenic palygorskite in some aridbrown (calciorthid) soils in Israel, Clay Miner., V. 11, p. 73-80.

Appendix 2.1

Palaeocurrent data

Lithofacies	S N	Reading in ozimuth	S N	Reading in ozimuth	S N	Reading in ozimuth	S N	Reading in ozimuth
P	1	145	7	205	13	200	19	182
	2	184	8	165	14	205	20	235
	3	205	9	175	15	210	21	208
	4	207	10	182	16	210	22	208
	5	210	11	200	17	220		
	6	202	12	195	18	195		
Sp	1	184	17	205	33	242	49	245
	2	205	18	210	34	190	50	230
	3	207	19	210	35	210	51	228
	4	210	20	190	36	200	52	210
	5	202	21	190	37	220	53	250
	6	195	22	220	38	185	54	230
	7	190	23	170	39	185	55	240
	8	185	24	190	40	192	56	230
	9	175	25	195	41	185	57	210
	10	198	26	215	42	175	58	202
	11	205	27	180	43	185	59	206
	12	165	28	190	44	185	60	208
	13	175	29	210	45	168	6	208
	14	180	30	165	46	235		
	15	182	31	180	47	210		
	16	195	32	202	48	240		
St	1	146	8	160	15	210	22	200
	2	150	9	175	16	190	23	198
	3	160	10	175	17	170	24	195
	4	145	11	170	18	150	25	200
	5	235	12	175	19	200		
	6	195	13	178	20	210		
	7	195	14	210	21	175		

NB Each reading is an average of three readings.

Appendix 3.1 Average mineralogical composition of the calcretized sands (Vol %)

Sample No	1	3	30	31	46	62	64	152	154	155	173	181	Average
Quartz	27	26	25	32	19	27	25	26	23	29	26	24	25.7
Chert	3	5	3	3	7	5	3	9	5	4	4	5	4.6
Plagioclase	2	3	3	2	2	2	2	2	1	1	1	2	1.9
Orthoclase	4	3	3	2	4	3	4	4	3	3	3	3	3.2
Rock Fragments	8	9	5	5	5	10	4	6	6	14	15	6	8
Micas	4	5	9	8	5	6	3	3	4	3	8	10	5.6
Calcite	52	50	52	48	53	53	57	50	50	45	52	48	50.8

Appendix 3.2 Average mineralogical compositi

Sample	1C	3C	14	15	16	32
Quartz	49	45	57	64	45	53
Chert	5	7	4	3	10	5
Plagioclase	2	6	4	3	4	2
Orthoclase	5	4	3	3	3	4
Rock Fragments	14	8	9	6	9	7
Micas	6	5	7	4	4	6
Auth. clays	4	5	3	2	5	3
Calcite Cement	9	20	10	8	18	18
Secondary Porosity	6	-	3	7	3	3

on of the uncalcretized sands (Vol %)

65	100	153	178	Average
51	51	54	55	52.4
7	5	7	5	5.8
3	1	3	4	3.2
5	5	2	3	3.7
7	10	9	8	8.7
5	5	4	3	4.9
4	5	4	5	4.0
17	16	8	5	12.9
1	3	9	12	4.4

Appendix 3.3 Procedure and Instrumental conditions of X.R.D.

All samples were treated with ethylene glycol for one hour and oriented mounts scanned on the Philips PW1540 diffractometer with the following settings:

Source: Cu K (α): normal focus: N; filter

Chart speed = 1200 mm/h

Angular goniometer speed = 1^{o}/min

Scan = 3 to 20^{o} 20

Range (C.P.S) = 4×10^{2}

Time constant = 2S: Z = 3

36 KV, 18 mA

Appendix 4.1 Electron Probe Microanalysis

All analyses were performed at the Grant Institute of Geology, University of Edinburgh, using the energy dispersive electron microprobe. Epoxy resin mounted polished thin sections were used for the study. Spot analyses of calcite occurring within expanded biotites and between dispersed grains were performed with spot size varying from 1 to 10 microns.

Calibration was monitored by a cobalt standard; accuracy was estimated by analysing a jadeite standard prior to the commencement of each session. Precision is 1% at 50% concentration level, 2% at 10% concentration level and 10% at 2% concentration level.

Appendix 4.2 Major and trace element content of Vadose (displacive - DC) and Phreatic (P) calcite crystals analysed using electron microprobe.

Sample No	crystals analysed	Type	SiO_2 %	TiO_2 %	Al_2O_3 %	Fe ppm	MgO%	CaO%	Na ppm	K ppm	Mn ppm	Sr ppm
30	1	DC	.03	.005	.035	1639	.115	54.70	85	347	898	ND
30	2	DC	.05	.013	.025	1467	.131	54.16	111	117	2691	ND
30	3	DC	.045	.007	.029	1648	.179	54.07	217	ND	178	ND
30	4	DC	.096	.031	.061	3654	.205	54.27	85	544	2134	ND
30	5	DC	.044	.022	.052	2015	.179	54.13	264	372	1774	ND
31	1	DC	1.10	.057	.474	4252	.29	53.03	204	935	2200	ND
31	2	DC	2.27	.106	.81	5203	.33	52.05	263	1976	1189	ND
31	3	DC	.11	.07	.06	2092	.17	54.66	195	32	822	ND
31	4	DC	.22	ND	.08	1541	.153	53.12	167	ND	916	ND
32	1	P	.028	.002	.01	1986	.281	54.58	174	ND	4959	ND
32	2	P	.39	.019	.016	1942	.278	55.65	63	ND	5308	ND
32	3	P	.57	.002	.029	1889	.26	54.36	183	185	5090	ND
32	4	P	51	.019	.023	1018	.16	54.86	186	80	4395	ND
32	5	P	.07	.02	.016	1494	.166	55.22	164	ND	4606	ND
46	1	DC	.80	.007	.338	776	.304	53.16	64	655	2312	ND
46	2	DC	.93	.035	.167	9047	.618	55.17	90	1086	1386	ND
46	3	DC	ND	.002	.017	5626	.606	54.87	68	158	2785	ND
46	4	DC	ND	ND	.027	1050	.354	55.05	77	ND	3867	ND
46	5	DC	ND	.008	.005	1637	.391	55.94	147	46	3864	ND
46	6	DC	ND	.010	.017	4059	.959	55.76	220	ND	1712	ND
45	1	P	.0004	.001	.02	1295	.158	54.78	64	ND	3601	254
45	2	P	ND	ND	.008	240	.079	54.85	217	108	2821	ND
45	3	P	ND	ND	.015	481	.127	54.69	71	16	3774	ND
45	4	P	ND	ND	.009	221	.089	54.57	74	71	2458	ND
45	5	P	ND	ND	.021	52	.022	55.49	26	12	1820	ND
44	1	P	.007	.002	.008	2116	.21	54.38	61	ND	3864	118
44	2	P	ND	ND	.009	4731	.19	53.96	ND	ND	2982	ND
44	3	P	.003	ND	.02	3800	.16	55.12	69	216	4634	218
44	4	P	ND	.001	.01	2978	.27	54.9	95	198	4180	170
44	5	P	ND	ND	ND	3500	.23	54.8	116	76	5059	ND

Appendix 4.2 continued.

Sample No	crystals analysed	Type	SiO_2	TiO_2	Al_2O_3	Fe ppm	MgO%	CaO%	Na ppm	K ppm	Mn ppm	Sr ppm
64	1	DC	ND	.012	.005	491	.399	54.79	70	132	5459	ND
64	2	DC	ND	.008	.002	866	.152	55.89	74	ND	3540	ND
64	3	DC	ND	.006	.015	766	.147	55.57	124	ND	3395	ND
64	4	DC	ND	.008	.020	1333	.214	55.51	61	ND	3927	ND
64	5	DC	ND	.003	.003	981	.186	55.68	ND	ND	3530	ND
64	6	DC	ND	.014	.007	611	.132	54.95	48	ND	2687	ND
63	1	P	.035	ND	.019	77	.035	55.95	67	50	1694	ND
63	2	P	ND	ND	.003	364	.088	55.83	74	ND	2479	ND
63	3	P	ND	.001	.007	84	.059	55.58	64	ND	1809	ND
102	1	DC	.075	.010	.042	4318	1.22	54.78	117	ND	2351	ND
102	2	DC	ND	.008	.017	1998	1.02	54.25	70	ND	1807	ND
102	3	DC	ND	ND	.005	2040	.77	54.91	89	ND	1845	ND
102	4	DC	ND	ND	.024	693	.22	55.95	ND	ND	4291	ND
102	5	DC	.018	.003	.019	589	.26	55.06	ND	25	3848	ND
101	1	DC	1.37	.060	.593	5067	.672	50.21	216	1431	1621	ND
101	2	DC	.402	.012	.195	2024	.376	52.55	220	779	2060	ND
101	3	DC	ND	.002	.020	1753	.291	55.29	140	ND	84	1656
101	4	DC	.083	ND	.028	3082	.526	52.27	217	28	1853	ND
101	5	DC	ND	ND	.017	103	.552	54.71	99	ND	114	ND
99	1	P	ND	ND	.015	5451	.612	55.39	58	30	1141	61
99	2	P	.05	ND	.052	3904	.38	54.36	23	ND	986	ND
99	3	P	.019	ND	.022	2006	.35	54.77	10	83	2336	ND
99	4	P	ND	ND	.016	3071	.45	54.54	144	ND	1408	ND
95	5	P	ND	ND	.021	3598	.51	54.76	176	ND	1044	ND

ND = not detected

Appendix 7.1 Location of samples from the Viking, Cardium and Belly River Formations

Sample No	Formation	Location
1	Viking	14-30-31-28-W4 (1866.5 m)
2	"	14-30-31-28-W4 (1869 m)
3	"	16-6-32-5-W5 (2390 m)
4	"	13-26-32-4-W5 (2374 m)
5	"	13-26-32-4-W5 (2366 m)
6	"	13-26-32-4-W5 (2363.2 m)
7	"	6-22-32-3-W5 (2244.3 m)
8	"	6-22-32-3-W5 (2244 m)
9	"	6-22-32-3-W5 (2242.5 m)
10	"	6-18-32-w-W5 (2187 m)
11	"	6-18-32-2-W5 (2186 m)
12	"	6-18-32-2-W5 (2181 m)
13	"	6-18-32-2-W5 (2180 m)
14	"	6-18-32-2-W5 (2178 m)
15	"	6-18-32-2-W5 (2175.7 m)
16	"	6-33-33-3-W5 (2226 m)
17	"	6-33-33-3-W5 (2220.7 m)
18	"	10-23-33-2-W5 (6611')
19	"	10-23-33-2-W5 (6607')
20	"	10-23-33-2-W5 (6597')
21	"	10-23-33-2-W5 (6595')
22	"	12-23-34-8-W5 (8238')
23	"	5-28-34-6-W5 (2715 m)
24	"	5-28-34-6-W5 (2714 m)
25	"	5-28-34-6-W5 (2712.5 m)
26	"	6-5-34-27-W4 (5741')
27	"	6-5-34-27-W4 (5730')
28	"	6-5-34-27-W4 (5724')
29	"	6-5-34-27-W4 (5717')
30	"	-34-27-W4 (3689.5')
31	"	16-9-35-6-W5 (8730')
32	"	16-9-35-6-W5 (8716.5')
33	"	16-9-35-6-W5 (8701')
34	"	14-11-35-4-W5 (2221.8 m)
35	"	14-11-35-4-W5 (2219 m)
36	"	14-11-35-4-W5 (2218 m)
37	"	14-11-35-4-W5 (2216.6 m)
38	"	6-6-35-2-W5 (2047 m)
39	"	6-6-35-2-W5 (2046 m)
40	"	6-6-35-2-W5 (2043.5 m)
41	"	6-6-35-2-W5 (2038 m)
42	"	14-10-35-28-W4 (1791 m)
43	"	14-10-35-28-W4 (1789 m)
44	"	10-13-35-26-W4 (5075')
45	"	10-13-35-26-W4 (5000')
46	"	16-12-36-3-W5 (6492')
47	"	16-12-36-3-25 (6481')
48	"	16-12-36-3-W5 (6477')
49	"	16-12-36-3-W5 (6469')
50	"	14-7-36-27-W4 (1682.5 m)

Appendix 7.1 continued

Sample No	Formation	Location
51	Viking	16-25-36-26-W4 (5187')
52	"	16-25-36-26-W4 (5179')
53	"	10-11-37-8-W5 (2795 m)
54	"	10-11-37-8-W5 (2791.5 m)
55	"	10-11-37-8-W5 (2789 m)
56	"	10-11-37-8-W5 (2787.5 m)
57	"	7-14-37-6-W5 (2382')
58	"	7-14-37-6-W5 (2378.5 m)
59	"	2-6-37-27-W4 (5462')
60	"	16-16-37-25-W4 (5031')
61	"	16-16-37-25-W4 (5025')
62	"	16-16-37-25-W4 (5015')
63	"	8-5-38-3-W5 (1688 m)
64	"	7-28-38-2-W5 (6271')
65	"	8-27-38-28-W4 (1708 m)
66	"	16-2-38-26-W4 (1512 m)
67	"	5-22-38-25-W4 (4691')
68	"	12-23-39-8-W5 (8230')
69	"	12-23-39-8-W5 (7331')
70	"	6-1-39-7-W5 (2403 m)
71	"	5-22-38-25-W4 (4731')
72	"	5-22-38-25-W4 (4715')
73	"	4-21-39-27-W4 (5201')
74	"	4-5-39-26-W4 (5151')
75	"	6-1-39-7-W5 (2392.3 m)
76	"	4-5-39-26-W4 (5169')
77	"	6-15-40-15-W5 (6984')
78	"	10-29-40-8-W5 (2129.5 m)
79	"	6-36-40-7-W5 (2324 m)
80	"	6-15-40-5-W5 (6981')
81	"	10-29-40-8-W5 (2128.5 m)
82	"	6-15-40-5-W5 (6976')
83	"	6-2-40-3-W5 (6249')
84	"	4-12-40-1-W5 (5487')
85	"	4-12-40-1-W5 (5485')
86	"	4-12-40-1-W5 (5482')
87	"	4-27-40-25-W4 (4874.3')
88	"	5-6-41-6-W5 (2319 m)
89	"	5-6-41-6-W5 (2301.8 m)
90	"	5-6-41-6-W5 (2293.9 m)
91	"	10-10-41-3-W5 (6321')
92	"	4-9-41-3-W5 (6306')
93	"	1-14-41-25-W4 (4585')
94	"	1-14-41-25-W4 (4581')
95	"	11-24-42-6-W5 (6963')
96	"	11-24-42-6-W5 (6957')
97	"	11-1-44-9-W5 (7386')
98	"	7-12-45-8-W5 (6698')
99	"	14-31-45-3-W5 (1791 m)
100	"	14-31-45-3-W5 (1781.65 m)

Appendix 7.1 continued

Sample No	Formation	Location
101	Viking	14-31-45-3-W5 (1778.9 m)
102	"	14-31-45-3-W5 (1777 m)
103	"	14-31-45-3-Wt (1769.5 m)
104	"	14-31-45-3-W5 (1741 m)
105	"	14-31-45-3-W5 (1734 m)
106	"	14-1-46-4-W5 (1735.6 m)
107	"	6-12-46-2-W5 (1727.3 m)
108	"	14-1-46-4-W5 (1727.3 m)
109	"	14-1-46-4-W5 (1716.8 m)
110	"	6-12-46-4-W5 (1710 m)
111	"	8-13-46-4-W5 (1700 m)
112	"	11-27-46-3-W5 (5413')
113	"	11-27-46-3-W5 (5403')
114	"	16-18-46-3-W5 (1737 m)
115	"	16-18-46-3-WS (1731.5 m)
116	Cardium	16-15-31-1-W5 (1814 m)
117	"	15-23-32-6-W5 (2353.5 m)
118	"	10-9-32-2-W5 (6109')
119	"	10-9-32-2-W5 (6105')
120	"	10-20-32-2-W5 (6095')
121	"	10-3-32-2-W5 (6080')
122	"	7-28-32-28-W4 (3959')
123	"	7-28-32-28-W4 (3938')
124	"	11-36-33-6-W5 (7939')
125	"	16-15-33-4-W5 (6876')
126	"	16-29-33-3-W5 (6540')
127	"	16-29-33-3-W5 (6538')
128	"	16-16-33-3-W5 (6435')
129	"	16-16-33-3-W5 (6328')
130	"	10-23-33-3-W5 (6324')
131	"	10-23-33-3-W5 (6321')
132	"	14-28-33-3-W5 (1968 m)
133	"	14-28-33-3-W5 (1934.3 m)
134	"	34-5-W5 (2108 m)
135	"	8-25-34-5-W5 (1854.5 m)
136	"	4-25-36-6-W5 (7215')
137	"	10-5-36-7-W5 (2201.7 m)
138	"	12-29-38-7-W5 (2201.7 m)
139	"	5-14-38-7-W5 (2135 m)
140	"	5-14-38-7-W5 (2133 m)
141	"	5-14-38-7-W5 (2132.5 m)
142	"	6-10-38-5-W5 (6300')
143	"	6-10-38-5-W5 (6293')
144	"	8-9-39-9-W5 (8190')
145	"	8-9-39-9-W5 (8185')
146	"	8-9-39-9-W5 (8181')
147	"	8-9-39-9-W5 (8177')
148	"	16-2-39-5-W5 (1858 m)
149	"	6-9-40-7-W5 (6748')
150	"	6-9-40-7-W5 (6744')
151	"	6-9-40-7-W5 (6741')
152	"	6-15-40-5-W5 (5986')

Appendix 7.1 continued

Sample No	Formation	Location
153	Cardium	6-15-40-5-W5 (5978')
154	"	6-2-40-5-W5 (5931')
155	"	6-2-40-5-W5 (5921')
156	"	6-2-40-5-W5 (5908')
157	"	6-30-40-4-W5 (5898')
158	"	16-7-40-4-W5 (5373')
159	"	16-7-40-4-W5 (1783 m)
160	"	16-7-40-4-W5 (1781.5 m)
161	"	12-24-41-9-W5 (2144 m)
162	"	10-21-41-5-W5 (5844')
163	"	12-3-43-8-W5 (6361')
164	"	12-3-43-8-W5 (6343')
165	"	12-3-43-8-W5 (6337')
166	"	12-3-43-8-W5 (6329')
167	"	11-1-44-9-W5 (6339')
168	"	11-1-44-9-W5 (6350')
169	"	10-18-44-8-W5 (6028')
170	"	10-18-44-8-W5 (6014')
171	"	10-18-44-8-W5 (6008')
172	"	10-18-44-8-W5 (6006')
173	"	6-24-44-6-W5 (5640')
174	"	6-20-45-5-W5 (5259')
175	"	6-20-45-5-W5 (5256')
176	"	5-11-45-2-W5 (4580')
177	"	6-9-46-9-W5 (5921')
178	"	6-9-46-9-W5 (5911')
179	"	10-3-46-9-W5 (5667')
180	"	6-28-46-9-W5 (5651')
181	"	6-28-46-9-W5 (5649')
182	"	4-17-46-8-W5 (5841')
183	"	8-8-46-7-W5 (5371')
184	"	8-8-46-7-W5 (5353')
185	"	8-8-46-7-W5 (5348')
186	"	16-23-46-28-W4 (3895')
187	"	16-23-46-28-W4 (3891')
188	"	2-4-46-27-W4 (3978')
189	Belly River	7-28-32-28-W4 (3973')
190	"	7-28-32-28-W4 (3958')
191	"	7-28-32-28-W4 (3947')
192	"	7-28-32-28-W4 (3944')
193	"	7-28-32-28-W4 (3988')
194	"	7-34-32-27-W4 (3549')
195	"	7-34-32-27-W4 (3548')
196	"	7-34-32-27-W4 (3535')
197	"	7-34-32-27-W4 (3538')
198	"	7-34-32-27-W4 (3526')
199	"	7-34-32-27-W4 (3522')
200	"	11-19-32-25-W4 (3430')
201	"	11-19-32-25-W4 (3428.3')
202	"	11-19-32-25-W4 (3420')
203	"	11-19-32-25-W4 (3420')
204	"	11-19-32-25-W4 (3407')
205	"	10-24-33-29-W4 (1258.4 m)

Appendix 7.1 continued

Sample No	Formation	Location
206	Belly River	10-24-33-29-W4 (1258.2 m)
207	"	10-24-33-29-W4 (1258 m)
208	"	7-26-33-29-W4 (1254 m)
209	"	7-26-33-29-W4 (1251.1 m)
210	"	10-24-33-29-W4 (1249 m)
211	"	7-26-33-27-W4 (3588')
212	"	7-6-33-27-W4 (3582')
213	"	7-26-33-27-W4 (3566')
214	"	7-26-33-27-W4 (3553')
215	"	6-35-34-1-W5 (1250 m)
216	"	6-35-34-1-W5 (1243.6 m)
217	"	7-8-34-28-W4 (1233.5 m)
218	"	7-8-34-28-W4 (1221 m)
219	"	7-8-34-28-W4 (1219 m)
220	"	6-9-34-27-W4 (3677')
221	"	6-9-34-27-W4 (3673')
222	"	6-9-34-27-W4 (3670')
223	"	6-9-34-27-W4 (3660')
224	"	6-9-35-26-W4 (3589')
225	"	6-9-35-26-W4 (3573')
226	"	6-9-35-26-W4 (3570')
227	"	5-23-36-1-W5 (1175 m)
228	"	5-23-36-1-W5 (1171.3 m)
229	"	5-23-36-1-W5 (1169.4 m)
230	"	5-23-36-1-W5 (1164')
231	"	38-2-W5 (6261')
232	"	7-21-39-1-W5 (3932')
233	"	7-21-39-1-W5 (3905')
234	"	7-21-39-1-W5 (3887')
235	"	7-21-39-1-W5 (3880')
236	"	7-21-39-1-W5 (3523')
237	"	7-21-39-1-W5 (3500')
238	"	3-36-40-9-W5 (5711')
239	"	3-36-40-9-W5 (5707')
240	"	3-36-40-9-W5 (5704')
241	"	3-36-40-9-W5 (5666')
242	"	3-36-40-9-W5 (5660')
243	"	10-29-40-8-W5 (1719 m)
244	"	10-29-40-8-W5 (1713 m)
245	"	10-29-40-8-W5 (1713 m)
246	"	10-29-40-8-W5 (1710.5 m)
247	"	2-7-41-8-W5 (1688 m)
248	"	2-7-41-8-W5 (1682.8 m)
249	"	2-7-41-8-W5 (1679 m)
250	"	2-5-41-7-W5 (1570 m)
251	"	7-5-41-7-W5 (1562 m)
252	"	7-5-41-7-W5 (1557 m)
253	"	7-5-41-7-W5 (1554 m)
254	"	6-30-42-7-W5 (5239')
255	"	6-30-42-7-25 (5233')
256	"	6-30-42-7-W5 (5215')
257	"	6-30-42-7-W5 (5199')
258	"	11-30-43-12-W5 (5188')
259	"	11-3-43-7-W5 (4923')
260	"	11-3-43-7-W5 (4911')

Appendix 7.1 continued

Sample No	Formation	Location
261	Belly River	11-3-43-7-W5 (4908')
262	"	11-3-43-7-W5 (4904')
263	"	11-3-43-7-W5 (4895')
264	"	11-3-43-7-W5 (4891')
265	"	4-20-43-2-W5 (3635')
266	"	4-20-43-2-W5 (3614')
267	"	4-20-43-2-W5 (3612')
268	"	4-20-43-2-W5 (3590')
269	"	6-26-45-7-W5 (4410')
270	"	6-26-45-7-W5 (4394')
271	"	6-26-45-7-W5 (4387')
272	"	6-26-45-7-W5 (4378')
273	"	6-26-45-7-W5 (4364')
274	"	6-26-45-7-W5 (4342')
275	"	6-26-45-7-W5 (4333')
276	"	6-26-45-7-W5 (4322')
277	"	6-26-45-7-W5 ( )
278	"	12-20-46-6-W5 (1244 m)
279	"	12-20-46-6-W5 (1241 m)
280	"	12-20-46-6-W5 (1238.5 m)
281	"	12-36-46-2-W5 (989 m)
282	"	12-36-46-2-W5 (984 m)
283	"	12-36-46-2-W5 (979.5 m)
284	"	12-36-46-2-W5 (976 m)
285	"	10-11-46-26-W4 (2508')
286	"	10-11-46-26-W4 (2503')
287	"	10-11-46-26-W4 (2486')
288	"	10-11-46-26-W4 (2465')
289	"	10-11-46-26-W4 (2433')

Appendix 7.2 Average mineralogical composition of the Viking Formation (Vol %)

Sample No	Quartz	Chert	Feldspars	Rock Fragments	Micas	Opaque	Matrix	Ca Cement
2	70	11	2	-	1	3	5	8
3	12	56	-	4	-	-	-	28
6	48	24	5	1	4	3	7	8
7	50	36	7	2	1	4	-	-
8	30	44	4	2	-	-	-	-
13	44	30	6	7	-	2	-	-
14	42	50	5	3	-	-	-	-
15	21	69	3	3	-	-	-	4
17	52	27	4	2	2	2	4	7
20	52	34	4	3	1	6	-	-
21	52	45	-	3	-	-	-	-
23	45	32	5	4	1	1	-	7
24	43	38	4	3	2	2	-	-
25	46	33	3	12	-	6	-	-
29	11	67	-	7	-	-	-	15
32	33	46	1	9	-	-	-	-
33	27	54	4	3	-	-	-	12
37	48	38	2	3	-	1	-	8
39	48	22	2	5	3	6	6	8
42	50	27	2	4	2	2	4	9
45	45	28	1	5	2	8	5	6
48	65	11	2	1	3	-	-	18
49	15	30	-	3	-	2	-	-
51	66	20	3	4	4	3	-	-
55	20	70	3	3	-	4	-	-
56	19	62	5	2	-	-	-	12
58	59	19	3	2	1	7	-	9
59	40	6	1	1	6	12	26	8
60	46	20	3	3	3	8	12	5
63	40	12	2	---	3	8	35	-
64	72	14	2	--	1	5	36	-
65	7	50	-	12	-	-	-	31
66	12	47	-	5	-	6	-	12
67	36	33	9	4	-	-	-	10
68	51	14	3	1	5	8	18	-
72	26	42	-	8	-	-	-	9
73	32	43	-	4	-	-	-	4
74	-	80	-	2	-	-	-	18
75	14	79	1	6	-	-	-	-
76	50	37	-	5	-	2	-	6
79	71	18	2	4	2	3	-	-
80	30	36	5	3	1	4	21	-
81	67	4	1	2	4	4	-	18
82	38	45	8	3	-	-	-	6
84	40	34	-	12	1	-	-	-
85	18	74	-	8	-	-	-	-
86	20	67	1	7	-	-	-	5
87	22	62	-	6	-	-	-	4
90	18	64	-	3	-	7	-	-
90	40	33	2	5	-	4	-	-
92	16	53	-	4	-	-	-	7
93	59	40	-	3	-	8	-	-
94	23	53	-	6	-	2	-	16
95	50	46	-	3	1	-	-	-
96	22	54	2	4	-	6	8	4

Appendix 7.2 continued

98	57	14	-	3	1	4	21	-
100	72	16	1	3	1	7	-	-
102	71	18	-	4	-	-	-	-
106	47	28	-	2	1	2	-	2
107	50	26	4	3	1	5	-	5
108	70	18	-	3	-	2	-	-
110	66	16	3	5	-	-	-	-
111	72	16	1	4	-	2	-	-
112	72	18	3	3	1	3	-	-
113	45	35	5	5	2	4	-	4
114	63	20	3	3	-	3	-	-
115	34	43	-	3	-	4	-	4
Average	41.2	37.2	2.1	4	0.9	2.8	3.1	5

ppendix 7.3 Average mineralogical composition of the Cardium Formation (Vol %)

ample No	Quartz	Chert	Feldspar	Rock Fragments	Micas	Opaques	Matrix	Cement
16	42	35	-	1	-	-	22	-
17	8	65	-	5	-	-	-	22
19	16	50	1	4	-	-	21	8
20	60	14	1	-	2	4	19	-
21	15	63	2	-	-	-	-	-
22	16	42	6	5	1	-	-	8
23	20	46	6	6	1	2	-	1
24	55	30	2	4	1	8	-	8
25	55	18	-	-	2	5	20	-
26	17	51	-	7	-	-	-	25
27	7	54	-	4	-	-	-	35
28	29	32	-	4	-	-	-	11
31	61	18	2	-	2	3	14	-
32	21	51	2	5	-	2	16	3
34	51	23	2	-	2	4	18	-
36	8	46	-	7	-	3	-	24
37	66	18	1	-	3	4	8	-
38	84	8	2	-	4	2	-	-
39	71	16	2	-	3	2	6	-
41	6	3	-	5	-	-	-	84
43	57	15	-	-	2	8	18	-
45	64	17	1	-	3	5	7	3
49	41	8	2	-	2	5	-	40
51	61	9	-	-	1	3	4	20
53	77	10	-	-	-	8	5	-
56	42	2	-	-	-	4	52	-
57	4	54	-	2	-	5	-	35
58	56	8	-	2	2	4	5	23
60	9	-	-	2	-	-	-	34
61	56	12	-	2	5	6	5	-
62	59	14	-	-	1	4	12	-
63	74	11	-	-	-	7	6	2
65	4	67	-	5	-	-	-	24
66	7	56	-	5	-	-	-	28
70	84	7	-	-	2	3	4	-
72	75	10	1	-	1	4	5	4
73	5	78	-	2	-	-	-	15
75	14	74	-	2	-	3	7	-
77	76	9	1	-	2	3	5	4
79	54	6	1	-	1	4	-	34
80	54	15	2	-	3	4	20	-
81	7	70	-	3	-	2	5	13
82	63	18	1	1	3	5	3	5
83	75	9	2	-	3	-	7	4
85	14	66	-	-	-	8	12	-
Average	41.1	29.5	0.9	1.8	1.2	3	7.3	11.5

Appendix 7.4 Average mineralogical composition of the Belly River Formation (Vol %)

Sample No	Quartz	Chert	Feldspars	Rock Fragments	Micas	Opaques	Matrix	Cement
192	22	37	6	7	1	2	-	18
193	23	39	4	7	-	2	-	-
196	33	39	7	2	3	4	-	7
199	32	36	6	3	2	1	-	18
200	32	29	6	8	1	2	-	22
202	46	23	7	3	4	3	-	14
207	22	32	3	6	1	2	-	14
208	20	36	-	9	1	2	-	4
210	19	31	7	3	-	2	-	15
214	18	33	6	5	2	3	-	33
215	30	32	5	6	4	3	-	16
217	25	35	8	5	5	2	-	15
219	18	34	5	5	1	1	-	22
221	25	36	7	6	2	6	-	17
223	19	36	10	6	1	2	-	19
225	26	31	6	7	4	4	-	10
227	30	35	5	5	1	5	-	16
229	33	37	4	4	-	4	-	14
235	28	32	10	5	4	3	-	15
237	26	36	6	8	1	2	-	21
241	28	43	6	7	2	4	-	10
242	25	50	3	7	1	1	-	5
243	36	48	5	6	3	2	-	-
246	27	35	6	6	1	3	-	18
249	30	36	4	7	-	6	-	9
251	31	40	7	7	3	7	-	-
256	34	37	6	6	-	5	-	8
257	30	36	4	8	3	8	-	9
258	14	49	6	6	3	4	-	4
259	26	34	8	8	4	6	-	9
260	28	36	6	8	2	2	-	18
269	38	44	5	5	3	3	-	-
276	28	35	7	8	3	1	-	10
277	30	36	10	7	2	4	--	7
279	25	21	5	5	2	2	-	20
280	28	32	7	6	2	3	-	25
282	27	40	6	7	5	2	-	3
283	29	35	5	5	3	3	-	2
288	16	18	5	5	1	6	-	41
Average	27.1	35.8	5.8	5.9	2.1	3.2	-	13